

STUDY OF ADVANCED COMPOSITE STRUCTURAL DESIGN CONCEPTS FOR AN ARROW WING SUPERSONIC CRUISE CONFIGURATION

Task III Final Report
Boeing Commercial Airplane Company
Preliminary Design Department

January 1978

(NASA-CR-145192) STUDY OF ADVANCED
COMPOSITE STRUCTURAL DESIGN CONCEPTS FOR AN
ARROW WING SUPERSONIC CRUISE CONFIGURATION,
TASK 3 Final Report (Boeing Commercial
Airplane Co., Seattle) 381 p HC A17/MF A01 G3/05 11905

8-20112

Unclas
11905

Prepared under contract NAS1-12287

for

Langley Research Center
NATIONAL AERONAUTICS AND SPACE ADMINISTRATION
Hampton, Virginia 23665



1 Report No NASA CR-145192		2. Government Accession No		3 Recipient's Catalog No	
4 Title and Subtitle STUDY OF ADVANCED COMPOSITE STRUCTURAL DESIGN CONCEPTS FOR AN ARROW WING SUPERSONIC TRANSPORT CONFIGURATION				5 Report Date January 1978	
				6 Performing Organization Code D6-42438-4	
7. Author(s) Preliminary Design Department				8 Performing Organization Report No	
				10 Work Unit No.	
9. Performing Organization Name and Address Boeing Commercial Airplane Company P.O. Box 3707 Seattle, Washington 98124				11 Contract or Grant No. NAS1-12287	
				13. Type of Report and Period Covered Task III Final Report	
12. Sponsoring Agency Name and Address National Aeronautics and Space Administration Langley Research Center Hampton, Virginia 23665				14 Sponsoring Agency Code	
15. Supplementary Notes Contract Monitors: James C. Robinson and E. Carson Yates, Jr. NASA Langley Research Center, Hampton, Virginia					
16 Abstract A structural design study was conducted to assess the relative merits of structural concepts using advanced composite materials for an advanced supersonic aircraft cruising at Mach 2.7. The configuration and structural arrangement developed during Task I and II of the study, previously reported in NASA CR-132576, was used as the baseline configuration. Allowable stresses and strains were established for boron and advanced graphite fibers based on projected fiber properties available in the next decade. Structural concepts were designed and analyzed using graphite polyimide and boron polyimide, applied to stiffened panels and conventional sandwich panels. The conventional sandwich panels were selected as the structural concept to be used on the wing structure. The upper and lower surface panels of the Task I arrow wing were redesigned using high-strength graphite polyimide sandwich panels over the titanium spars and ribs. The ATLAS computer system was used as the basis for stress analysis and resizing the surface panels using the loads from the Task II study, without adjustment for change in aeroelastic deformation. The flutter analysis indicated a decrease in the flutter speed compared to the baseline titanium wing design. The flutter speed was increased to that of the titanium wing, with a weight penalty less than that of the metallic airplane.					
17. Key Words (Suggested by Author(s)) Arrow Wing, Supersonic Cruise SCAR Technology NASA SCAT 15-F Advanced Composites				18. Distribution Statement Unclassified - Unlimited	
19. Security Classif. (of this report) Unclassified		20. Security Classif. (of this page) Unclassified		21. No of Pages 383	
				22 Price* \$13.00	

CONTENTS

	Page
INTRODUCTION	I-1
1 MATERIAL PROPERTIES	1
2 ALLOWABLES	25
3 CONCEPT DESIGN AND MATERIAL SELECTION	49
4 PANEL DESIGN	95
5 THEORETICAL-TO-ACTUAL MASS FACTORS	139
6 COMPOSITE ANALYSIS AND DESIGN	157
7 REVISION OF MATHEMATICAL MODEL	188
8 FLUTTER ANALYSIS	261
9 FINAL WEIGHT ANALYSIS	323
10 AERODYNAMIC HEATING ANALYSIS	338

INTRODUCTION

This document presents a detailed account of Task III of a study conducted by the Boeing Commercial Airplane Company as a part of the NASA Supersonic Cruise Aircraft Research program. The principal overall objectives of the study were to assess the relative merits of various concepts and materials suitable for an advanced supersonic aircraft cruising at Mach 2.7, to select the structural approaches best suited for the Mach 2.7 environment, and to provide construction details and structural mass estimates based on in-depth structural design studies of representative wing and fuselage structures. Earlier work in Tasks I and II of this study comprised the following activities: (1) detailed analysis and refinement of the aircraft configuration; (2) evaluation of alternate structural arrangements and selection of an arrangement for detailed analysis and design studies; (3) evaluation and selection of materials and concepts representative of a 1975 technology level; (4) detailed structural analysis and design and structural mass analysis utilizing the 1975 materials and concepts. In Task III the detailed structural analysis and the design and mass analysis have been repeated with advanced concepts and materials that are expected to be available in the 1986 time period.

The airplane configuration on which the structural analysis was conducted is an arrow-wing concept representative of a 1975 technology level. It was derived from a configuration presented by NASA (see reference I-1), and is similar to the Model 969-336C that was studied during the National SST Program (ref. I-2). A detailed multidisciplinary analysis of the configuration was conducted during Task I of the study, and further modifications and refinements were introduced. The resulting configuration, designated as Model 969-512B is shown in figure-1. Geometric data and other characteristics are listed in table-1. The wing structure that was selected for detailed analysis and design in Task II consisted of a multispar internal structure with aluminum brazed titanium sandwich panels for the wing surfaces, except for a machined skin concept on the lower surface of the main wing box. The fuselage structure consisted of skin stringer construction. Ti-6Al-4V alloy was used as the primary structural material throughout.

A single basic finite element model of the structure was developed for aeroelastic loads, stress and flutter analyses, containing approximately 2000 nodes, 4200 elements and 8500 active degrees of freedom. Analyses were performed by an integrated structural analysis and design system interfaced with loads and flutter analysis systems. The elements in the wing covers were resized using an automated resizing module in the integrated system, with convergence, measured in terms of total mass change, occurring in three cycles. Nine flutter analyses were conducted to evaluate a series of stiffness changes to remedy a flutter deficiency in the strength design. Stiffness changes were based on engineering judgment and experience from the National SST Program.

The resulting configuration has a maximum taxi gross mass of 340 200 kg (750 000 lbm) and a payload of 22 200 kg (49 000 lbm), representing 234 passengers in tourist accommodations, and a cruise Mach number of 2.7. The structure, stability and control characteristics, and systems meet the appropriate requirements of Federal Aviation Regulations, Part 25, and the Tentative Airworthiness Requirements for Supersonic Transports.

A detailed account of the work performed in Tasks I and II is presented in reference I-1; for a more condensed summary see reference I-3.

The configuration and structural arrangement developed for the titanium structure were used without modification in the subsequent investigation discussed in this report. Allowable stresses and strains, based on estimated fiber properties to be available in the next decade, were established for advanced composite materials using boron and graphite fibers. Stiffened panel and conventional sandwich panel concepts were designed and analyzed, using graphite/polyimide and boron/polyimide materials, and the conventional sandwich panel was selected as the structural concept to be used in the modified wing structure.

Upper and lower surface panels of the arrow wing structure were then redesigned, using high strength graphite/polyimide sandwich panels, retaining the titanium spars and ribs that had been designed in the prior study. The ATLAS integrated analysis and design system was used for stress analysis and automated resizing of surface panels, using the design loads that were developed in the prior study of the metallic structure.

For the present study properties of candidate advance composite materials were estimated for a 1986 time period, based on assumptions regarding development work to be accomplished in the intervening time period. Estimated material properties were then used in structural concept design studies, and in concept and material evaluation and selection. Following material and concept selection, a finite element model of the complete structure was defined retaining the structural arrangement and finite element geometry from the prior study of the metallic structure.

Since supersonic cruise aircraft tend to be large and flexible, aeroelasticity is a major design consideration, and realistic aeroelastic considerations based on analysis of finite element structural models and sophisticated aerodynamic loading analysis are required, even in a preliminary design study of such a vehicle. Strong interaction of the various technical disciplines in aeroelastic analysis requires the use of computer-aided design methods to organize and expedite the aeroelastic and structural resizing cycle. Computer-aided design methods are also required to handle the large number of material parameters that must be accommodated in designing a composite structure.

Flutter analysis of the hybrid structure showed a significant decrease in flutter speed relative to the baseline strength designed titanium wing structure. The flutter speed was increased to that of the final titanium design by selective increase in thickness of wing panel laminates and by substituting a graphite/polyimide material with properties intermediate between high strength and high modulus materials. The final mass of the hybrid wing structure was significantly less than that of the titanium wing with equal flutter speed.

The following sections of the report present a detailed account of design and analytical work, resizing of the wing shell to satisfy strength and flutter criteria, and evaluation of the reduction in structural wing mass relative to the all titanium wing. Recommendations are also presented relating to further research and development work that will be needed to achieve the anticipated benefits from application of advanced composite materials in primary structure of large supersonic cruise aircraft.

Table I.—Configuration Characteristics, Model 969-512B

Geometry		Wing	Wing vert. stabilizer	Vertical stabilizer	Horizontal stabilizer
Area	m ² (sq ft)	915 (9,848)*	26.7 (287)/side	41.7 (449)	55.7 (600) exposed
Aspect ratio, AR		1.78	0.493	0.848	1.32
Taper ratio, λ			0.135	0.24	0.247
Sweep at LE	Rad (deg)	1.29/1.23/1.05 (74/70.5/60)	1.30 (74.5)	0.89 (51)	.94 54
Incidence	Rad (deg)	—	—	—	-0.26/0.52 + 0.26/0.44 (-15/30 + 15/25)
Dihedral	Rad (deg)	—	—	—	0
Root t/c	%	—	3	3	3
Tip t/c	%	—	3	3	3
Root chord	m (in.)	47.8 (1881.1)	13.0 (510)	11.30 (445)	10.52 (414)
Tip chord	m (in.)	5.18 (204)	1.75 (69)	2.72 (107)	2.59 (102)
MAC	m (in.)	30.1 (1187)	8.79 (346)	7.90 (311)	7.34 (289)
Span	m (in.)	40.4 (1590)	3.63 (143)	—	8.59 (338)
Tail arm	m (in.)	—	17.70 (697)	24.82 (977)	26.97 (1062)
Tail vol coeff, v		—	0.013	0.028	0.0545

* Reference area Total wing area ABCDEFGH = 1045 m² (11 244 sq ft)

Gross mass* 340 200 kg (750 000 lbm)

Body	Length, m (in.)	Max dia, m (in.)	Accommodation	
	92.4 (3640)	3.87 (152.2)	234 pass	4/5 AB
Powerplants	Number	Type	Airflow	Inlet
	4	ATAT-1	287 kg/sec (633 lbm/sec)	Axisym
Landing gear wheels	Nose	Main	Loc % MAC	
	2—86 x 41 cm (34 x 16 in.)	24—103 x 36 cm (40.7 x 14 in.)	57.7 (pivot)	
Fuel capacity, kg (lbm)	Wing	Body	Total	
	143 970 (317 400)	32 660 (72 000)	176 450 (389 000)	
cg limits	Takeoff	Cruise	Landing	
% MAC	Fwd		49.7	
	Aft	55.5	53.0	

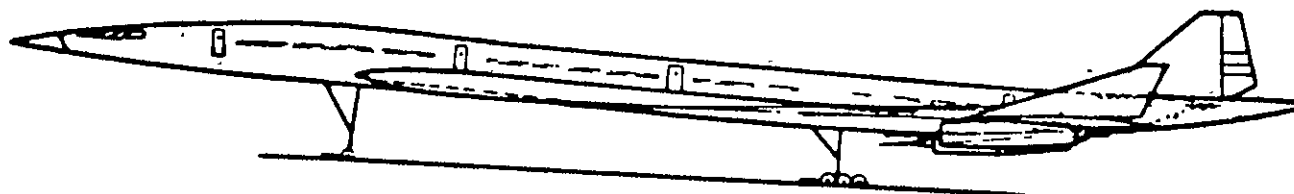
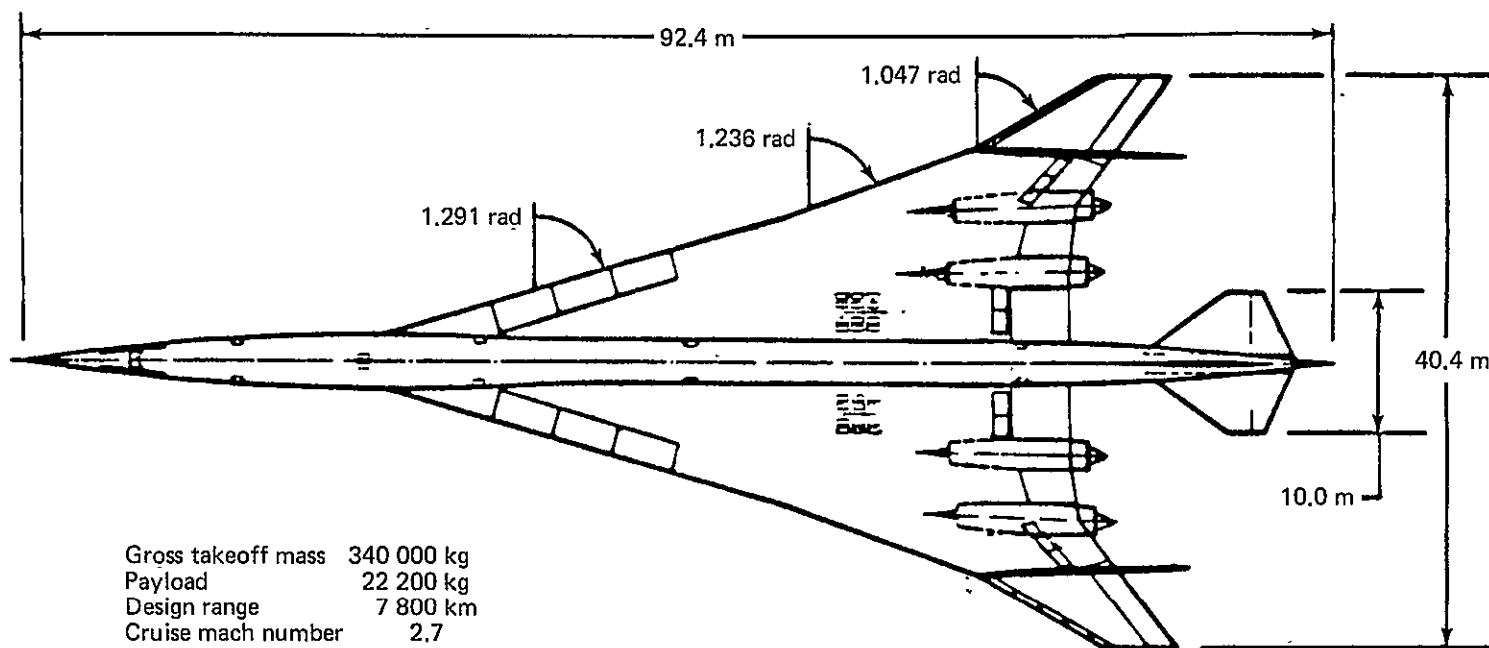


Figure 1.—Configuration for Structural Analysis, Model 969-512B

REFERENCES

- I-1 Boeing Staff: *Study of Structural Design Concepts for an Arrow Wing Supersonic Transport Configuration*. NASA CR 132576-1 and -2, 1976.
- I-2 Boeing Staff: *Mach 2.7 Fixed Wing SST Model 969-336C (SCAT 15F)*. D6A11666-1, The Boeing Company, 1969.
- I-3 Turner, M. J.; and Grande, D. L.: *Study of Metallic Structural Design Concepts for an Arrow Wing Supersonic Cruise Configuration*. NASA CR-2743, 1976.

SECTION 1

MATERIAL PROPERTIES

by

C. L. HENDRICKS

CONTENTS

Page

INTRODUCTION	6
LITERATURE SEARCH	6
1975 COMPOSITE PROPERTIES	8
1986 COMPOSITE PROPERTIES	10
RECOMMENDED IMPROVEMENTS IN DATA BASE	11
REFERENCES	13

TABLES

No.		Page
1-1	Basic Graphite/Polyimide Laminate Unidirectional [0] Properties	14
1-2	Basic Graphite/Polyimide Unidirectional Laminate [90] Properties	15
1-3	Basic Graphite/Polyimide Laminate [± 45] _S Properties	16
1-4	Normalized Graphite/Polyimide Laminate [0] Properties Normalized to 60% Fiber Volume	17
1-5	Normalized Graphite/Polyimide Laminate [90] Properties Normalized to 60% Fiber Volume	18
1-6	Normalized Graphite/Polyimide Laminate [± 45] _S Properties Normalized to 60% Fiber Volume	19
1-7	“B” Allowables, Graphite/Polyimide Laminate Normalized to 60% Fiber Volume, 1975	20
1-8	“B” Allowables, Graphite/Polyimide Laminate Normalized to 60% Fiber Volume, 1986	21
1-9	“B” Allowables, Boron/Polyimide Laminate Normalized to 50% Fiber Volume, 1986	22

FIGURES

No.		Page
1-1	Temperature Dependence of Material Properties for Advanced Composite Wing Cover Panels	23
1-2	Strength and Moduli of Various Materials	24

SYMBOLS

E_c	Modulus of elasticity in compression
E_t	Modulus of elasticity in tension
F_{cu}	Ultimate compressive stress
F_{tu}	Ultimate tensile stress
RT	Room temperature
H/M	High modulus
H/S	High strength

INTRODUCTION

The incorporation of high-strength low density fibers into a compatible matrix presents a composite material that offers the potential for a major breakthrough in airframe design. The most common composite materials that have been studied and put into limited use are boron-epoxy and graphite-epoxy. These materials are limited to a maximum service temperature of 450K (350°F) continuous and 489K (420°F) for intermittent service. For higher temperatures than that, the matrix material must be either metallic such as aluminum, or a high temperature organic material such as polyimide (PI). Either of these materials is suitable for operation at Mach 2.7 involving temperatures of 559K (490°F).

Figure 1-1 presents a comparison of the ultimate tension stress of several composite laminates with titanium for temperatures up to 506K (450°F). Figure 1-2 compares the ultimate tension stress and the Young's modulus of representative metals and composite materials.

The use of advanced composites on a supersonic cruise aircraft assumes that the earliest flight of the airplane will be about 1990, and the engineering freeze on the design will be about four years preceding that time; thus, 1986 is the year in which the engineering properties for the composite material would have to be known to be of use on such a program. This date is also consistent from the standpoint that it will require about that amount of time to develop the material systems and the necessary manufacturing techniques and mechanical properties to utilize the material.

The objective of this subtask is to project the allowables for the advanced composite materials to values that would be available in 1986 for application to the structure of a supersonic aircraft. In selecting the fibers to be considered, it has been noted that both the boron and graphite fibers are currently available and under development. The graphite technology seems to be advancing much more rapidly than the boron technology, however, as reflected in the reduction in price and increase in production volume. The dramatic increase in the use of the graphite fibers seems to be associated with athletic equipment such as golf club shafts, bows, tennis rackets and the like. Boron, on the other hand, does not seem to be enjoying this popularity in the common market, and thus has not attained that level of funding in research and development. Because of this, major emphasis was placed on graphite/polyimide properties. Boron/polyimide data were also compiled. Boron/aluminum data acquisition effort was limited since a significant amount of work on this material was already completed in Task II.

The steps used to obtain projected composite properties included research of past and current program efforts, compilation of applicable data, estimation of 1975 allowables and projection of estimated 1986 allowables.

LITERATURE SEARCH

A literature search was conducted to determine the state-of-development of high temperature stable advanced composites. The state-of-the-art to date provides limited design data for composites exposed to long time simulated arrow wing service environment. The level and objectives of current programs and future efforts may provide this vital information.

The data base for estimation of composite mechanical properties is taken from the following sources:

- *Development of Design Data for Graphite Reinforced Epoxy and Polyimide Composites.*

This report, reference 1-1, presents basic design data for HM-S and HT-S/polyimide composites at room temperature and 588K (600°F).

- *Time-Temperature-Stress Capabilities of Composite Materials for Advanced Supersonic Technology Applications.*

This report, reference 1-2, presents work currently being conducted to determine the effects of supersonic airplane environments upon composite properties. Composite exposure time to 1 000 hours at 506K (450°F) has been reached. Limited design data was taken from this work.

- *Develop Fabrication/Processing Techniques for High Temperature Advanced Composites for Use in Aircraft Structures.*

The composite design data in this report, reference 1-3, were the most complete of the various applicable sources. A comparison of coupon and sandwich beam test properties contained in this report provided a correlation for other programs which conducted only coupon tests. Elevated temperature tests were performed at 560K (550°F).

- *Development and Fabrication of a Graphite/Polyimide Box Beam.*

The data from this program were compiled in reference 1-4 with that derived from other sources. It evaluated and used Gemon polyimide matrix.

- *Resin/Graphite Fiber Composites.*

This report, reference 1-5, was used to illustrate the kind of research in polyimide resins that could produce high quality, thermally stable composite systems applicable to supersonic transport primary structure.

- *Effects of Thermal and Environmental Exposure on the Mechanical Properties of Graphite/Polyimide Composites.*

This report, reference 1-6, contains long-time elevated-temperature exposure data on graphite/polyimide composites which indicates some degradation at service temperatures. However, the resin matrix used in the tested composites is not one of the more thermally stable polyimide systems. A major part of the data is presented as interlaminar shear not directly translated to other design properties.

- *Effect of 450°F and 600°F Exposures on the Mechanical Properties of Polyimide/Glass-Fiber Honeycomb Sandwiches and Laminated Beams.*

This report, reference 1-7, contains data on long-time elevated-temperature exposure of glass/polyimide structure. Data to 4000 hours at 506K (450°F) with reduced pressure (simulating flight altitude) shows no significant degradation of mechanical properties. This data was used for rationale to assume that polyimide composites are subject to only minor degradation at 506K (450°F) when combined with reduced atmospheric pressure and covered with a protective or decorative coating.

- *Elevated Temperature Laminates.*

The data in this report, reference 1-8, includes exposure of glass/polyimide laminates to elevated temperatures for up to 30 000 hours. Degradation of mechanical properties at 506K (450°F) had stabilized at 2-3000 hours even when exposed to continuous atmospheric pressure and no protection. Aging at this temperature was discontinued at 5000 hours. Test results after exposure to 477K (400°F) indicated no significant degradation between 10 000 and 30 000 hours.

- *Development of Engineering Data on the Mechanical and Physical Properties of Advanced Composite Materials.*

The data in this report, reference 1-9, covered boron/aluminum, AVCO 5505 boron/epoxy, and graphite/epoxy composites. It was used as a base of comparison from epoxy to polyimide composites design data.

- *Crack Propagation in Fiber Reinforced Plastic Composites. Fundamental Aspects of Fiber Reinforced Plastic Composites.*

This report, reference 1-10, was used to illustrate the kind of resin modification which can be successful in elimination of micro cracking in tension stressed advanced composite systems.

1975 COMPOSITE PROPERTIES

The data published in the reports listed previously are organized and compiled according to the test laminate orientations [0], [90], and [± 45] (tables 1-1, 1-2, and 1-3). Much of the data was subject to variables such as sandwich beam versus coupon test methods, differences in composite fiber fractions, resin systems, test temperatures and exposure times.

Each mechanical property value was normalized to represent a 60% fiber volume for graphite and a 50% fiber volume for boron. These normalized test values were determined by multiplying the graphite test values by the ratio:

$$\frac{60 \text{ volume percent fiber}}{\text{fiber volume percent of specimen}}$$

and by multiplying the boron composite test values by the ratio:

$$\frac{50 \text{ volume percent fiber}}{\text{fiber volume percent of specimen}}$$

The normalized test coupon values were subsequently factored to sandwich beam values. These factors (from ref. 1-3) are listed below:

<u>Laminated Orientation</u>	<u>Factor</u>
[0] Tension, Strength	1.21
Modulus	NF*
[0] Compression, Strength	1.74
Modulus	NF
[90] Tension, Strength	3.90
Modulus	2.0
[90] Compression, Strength	NF
Modulus	NF

*NF = not factored

The [± 45] laminate tension and compression properties were assumed equal to values for epoxy as published in the *Air Force Advanced Composites Design Guide* because the polyimide data generated in the various reports were inferior to that for epoxy. This was done on the assumption that a good quality dense polyimide matrix composite should perform at least as well as a good quality epoxy matrix composite.

Normalized and factored numbers (tables 1-4, 1-5, and 1-6) were averaged and used to derive the 1975 "B" allowables for graphite/polyimide allowables (table 1-7). It should be noted that the data in reference 1-5 contained significantly lower values when compared to the other data sources and was not included when computing the average value.

The allowables were calculated using an assumed 30 specimen population and 8% coefficient of variation which results in a K factor of 1.777. An illustration of the method of calculating "B" allowables is as follows:

$$\text{"B" Allowable} = \bar{X} - K_B S$$

where

\bar{X} = calculated average value

K_B = one-sided tolerance limit factor for normal distribution and sample size
at $P = 0.90$

S = standard deviation

$S = (C_V) (\bar{X})$
where C_V = coefficient of variation

Example:

HT-S 0° Tension Ultimate Strength (UTS) average = 200 KSI (see table 1-4)

$K_B = 1.777$ (30 specimen population – minimum allowed for “B” allowable calculation)

$C_V = 0.08$ (assumed value)

$S_B = (0.08) (200 \text{ KSI}) = 16 \text{ KSI}$

“B” allowable = $200 \text{ KSI} - (1.777) (16 \text{ KSI})$

= 172 KSI (see table 1-7)

1986 COMPOSITE PROPERTIES

Properties of the composite materials are projected to 1986 based on assumptions on the amount of development work that will likely be accomplished in the intervening time period. These assumptions have been arrived at through conversations and communications with the manufacturers who are currently involved in research in the advanced composite field. The allowables presented in table 1-8 for graphite/polyimide are based on these assumptions and have been adjusted to represent a 60% fiber volume. The allowables in table 1-9 for the boron/polyimide are adjusted in a similar manner to represent a 50% fiber volume.

GRAPHITE/POLYIMIDE

Polyimide resins have, for the past several years, undergone development to improve processing characteristics and thermal stability. The various programs currently being funded and future work on this material can be expected to yield a moderate degree of success to achieve these objectives and result in a dense polyimide matrix capable of performance under the supersonic environmental conditions.

The manufacturers of graphite fibers are continuing to develop fibers with improved properties. They currently have in the laboratory high strength and high modulus fibers that can be expected to be available on the market by the 1986 time period. These fibers range from a high strength version having a 4136 MN/m^2 (600 ksi) strength to a high modulus version having a Young's modulus of 620 GN/m^2 (90×10^6 psi).

The coefficient of variation for graphite composites, typically in the range of 12%, is expected to drop to a value no more than 8% through improved quality control in the manufacture of the fiber and the processing of the composite.

BORON/POLYIMIDE

The development of superior polyimide resin matrices for boron composites can be expected by 1986 through continuing programs as discussed previously for graphite/polyimide composites.

Research directed to improve boron filament properties have not been successful. The basic process with boron deposition on tungsten wire core has reached the upper limits of optimization. Attempts at depositing Boron silicon on graphite cores are not expected to result in higher fiber mechanical properties.

Continued close quality control of fiber production, and of the processing and prestressing of fiber tapes can be expected to reduce the coefficient of variation to the range of 8%.

BORSIC/ALUMINUM

No improvements in basic borsic fiber are expected for 1986 composite technology. The elastic allowables developed in Task II are used for Task III design considerations. "B" allowable fiber strains for borsic aluminum are assumed to be identical to "B" allowable strains used for boron/polyimide composites.

There are not allowables shown in the tables for borsic/aluminum since the material properties and allowables were developed during the Task II studies. These allowables and material properties can be found in Section 14 of reference 1-11.

RECOMMENDED IMPROVEMENTS IN DATA BASE

The survey of high temperature stable advanced composite systems programs indicated major areas which lack sufficient technical information to accurately predict performance of these materials in a commercial SST environment.

Time-temperature-stress relationships simulating future supersonic transport requirements for more than 5000 hours are non-existent for composite materials. Many of the polyimide systems used are not sufficiently thermally stable, or process with difficulty in the manufacture of high quality, uniform, reproducible composites; much of the data generated in past programs emphasized inter-laminar shear and/or flexure properties for materials evaluation. This data is not directly translatable to other design properties. The test programs which have generated design data used a combination of test coupons and sandwich beam methods which require factors for correlation between the test methods and test programs.

One of the basic problems associated with advanced composites utilizing organic matrices is localized cracking of the matrix produced by externally applied tensile loads. Matrix cracking results primarily from a combination of resin brittleness, fiber-to-fiber contact or proximity and tensile stress components acting perpendicular to the fibers. This problem was recognized several years ago in fiberglass/epoxy systems (ref. 1-10). Attempts to eliminate micro cracking have been successful through blending of low percentages ($\leq 10\%$) of elastomeric polymers into the matrix. The addition of elastomers is thought to greatly increase the fracture surface work in the matrix preventing the initiation of micro cracks. This same kind of modification appears feasible and practical for polyimide matrix composites by 1986.

The technical personnel of Narmco, a major supplier of prepreg tapes, have stated that they also foresee the application of high temperature stable elastomers to polyimide or similar resin matrices to eliminate the micro cracking problem.

It should be noted that the ten most significant reports, used as the basis for projection of composite properties to 1986, required the application of several basic assumptions discussed previously to reduce the data to usable design information. Reference 1-2 was the only effort whose objectives closely matched the data requirements to obtain advanced composites design information for the arrow wing supersonic cruise vehicle.

Improvements in the data base should be directed toward (1) continued research on polyimide systems with improved thermal stability and processing characteristics, (2) improvement in graphite fiber properties similar to that being attempted by Union Carbide under contract to the Air Force, (3) research to eliminate tension strain micro cracking problems, through addition of elastomeric polymer to the matrix, (4) continuation of composite aging studies using time-temperature-stress combination effects, (5) standardization of composite test methods which reflect actual load parameters, and (6) establishment of design allowables applicable in design of supersonic cruise aircraft.

REFERENCES

- 1-1 Scheck, W. G.: *Development of Design Data for Graphite Reinforced Epoxy and Polyimide Composites*. NASA CR 120413, General Dynamics Convair Aerospace.
- 1-2 Haskins, J. F.; Kerr, J. R.; and Stein, B. A.: *Time-Temperature-Stress Capabilities of Composite Materials for Advanced Supersonic Technology Applications*. Proceedings of the SCAR Conference, NASA CP-001, 1976.
- 1-3 E. B. Birchfield and R. Kollmansberger: *Develop Fabrication/Processing Techniques for High Temperature Advanced Composites for Use in Aircraft Structures*. AFML TR-72-91, McDonnell Aircraft Company, 1972.
- 1-4 Nadler, M. A.; and Darms, F. J.: *Development and Fabrication of a Graphite/Polyimide Box Beam*. NASA CR 123959, North American Rockwell Space Division, 1972.
- 1-5 Cavano, P. J.: *Resin/Graphite Fiber Composites*. NASA CR 121275, TRW Incorporated, 1974.
- 1-6 Hanson, M. P.; and Serafini, T. T.: *Effects of Thermal and Environmental Exposure on the Mechanical Properties of Graphite/Polyimide Composites*. NASA TN D-6604, 1971.
- 1-7 Stein, B. A.; and Pride, Richard A.: *Effect of 450°F and 600°F Exposures on the Mechanical Properties of Polyimide/Glass-Fiber Honeycomb Sandwiches and Laminated Beams*. Journal of Aircraft, Vol. V., No. 1, January-February 1968.
- 1-8 Elton, J.: *Elevated Temperature Laminates*. Document No. D6A-10737-1, The Boeing Company, 1971.
- 1-9 Hofer, Jr., K. E.; Rao, N.; and Larson, D.: *Development of Engineering Data on the Mechanical and Physical Properties of Advanced Composite Materials*. AFML TR-72-205, 1974.
- 1-10 McGarry, Frederick J.: *Crack Propagation in Fiber Reinforced Plastic Composites. Fundamental Aspects of Fiber Reinforced Plastic Composites*. R. T. Schwartz and H. S. Schwartz, eds., Inter Science Publishers, 1968
- 1-11 Boeing Staff: *Study of Structural Design Concepts for an Arrow Wing Supersonic Transport Configuration*. NASA CR 132576-1 and -2, 1976.

Table 1-1.—Basic Graphite/Polyimide Laminate Unidirectional [0] Properties

Fiber	Resin	Test temp °F	Exposure temp. °F	Exposure time, hr	Test specimen	F _{tu} , ksi	E _{tr} , 10 ⁶ lb/in. ²	Strain, μ in./in.	F _{cu} , ksi	E _c , 10 ⁶ lb/in. ²	Strain, μ in./in.	Poisson's ratio	Thermal expansion μ in./in./°F	Source
Polyimide ↓ Polyimide ↓ Epoxy ↓ Epoxy ↓ Polyimide ↓ Polyimide	Mod II	Skybond 703	RT	RT	0	SW beam	213.0	23.2	8692	178.0	22.0	9034		Ref. 1-3
			550	550	0.5	↓	169.0	23.6	7429					
			550	550	100.0	SW beam	162.0	20.7	7867					
			RT	RT	0	Coupon	176.0	17.7	9370					
			550	550	0.5					102.0	19.1	6237		
			550	550	100.0					64.0	22.5	2838		
	Mod II	Skybond 703	550	550	100.0					50.0	20.0	2658		Ref. 1-3
	HT-S	Skybond 710	RT	RT	0.7		163.0	22.7	6741	102.0	19.7	5316		Ref. 1-1
			600	600	0.5		162.0	21.6	6900	54.5	19.6	5394		
			600	600	100.0		165.0							
			600	600	200.0		154.0							
	HT-S		600	600	400.0		150.0							
	HM-S		RT	RT	0		131.0	26.0	5380	51.1	27.3	2950		
			600	600	0		129.0	25.6	4532	37.2				
			RT	600	200.0		129.0	23.7	8180	46.1				
	HM-S		600	600	200.0		123.0	28.6	4875	37.0				Ref. 1-1
	HT-S		RT	RT	0		176.0							Ref. 1-2
			450	450	500.0		113.0							
			450	450	1000.0		172.0							
			RT	RT	0		191.0							
			550	550	200.0		189.0							
			550	550	500.0		178.0							
	HT-S	Skybond 710	550	550	1000.0		167.0							Ref. 1-2
	Mod II	Gemonl	RT	RT	0		170.0	19.3		138.0	17.3		0.37	Ref. 1-4
		Gemonl	500	500	0.5		154.0			57.0	17.5		0.51	Ref. 1-4
	Mod II	5206	RT	RT	0		161.0	22.5	6920	141.0	19.6	7610		Ref. 1-9
	HM-S	3002M	RT	RT	0		98.0	26.9	3360	100.0	24.6	4300		Ref. 1-9
		PMR-15	RT	RT	0		78.8	23.9	3300	147.0			0.29	Ref. 1-5
			500	500	0.5					133.0				
	HM-S	PMR-15	500	550	500.0	Coupon				130.0			-0.6 -0.3	Ref. 1-5

Table 1-2.—Basic Graphite/Polyimide Unidirectional Laminate [90] Properties

Fiber	Resin	Test temp, °F	Exposure temp, °F	Exposure time, hr	Test specimen	F _{tu} ' ksi	E _t ' 10 ⁶ lb/in. ²	Strain, μ in./in.	F _{cu} ' ksi	E _c ' 10 ⁶ lb/in. ²	Strain μ in./in.	Thermal expansion μ in./in.°F	Source
Polyimide ↓ Polyimide Epoxy Epoxy	Mod II	Skybond 703	RT	RT	0	SW beam	9.89	2.02	4535	18.99	1.16	11 536	Ref. 1-3
			550	550	0.5	↓ SW beam	4.34	1.15	5000				
			550	550	100.0	↓ SW beam	4.34	1.20	4708				
			RT	RT	0	↓ Coupon	2.53	0.99	1880				
			550	550	0.5					21.2	0.68	18 850	
			550	550	100.0					10.2	0.84	14 630	
	Mod II	Skybond 703	550	550						9.83	0.82	17 810	Ref. 1-3
	HT-S	Skybond 710	RT	RT	0		2.32	1.37	2859	12.4	1.22	2 285	Ref. 1-1
	HT-S		600	600	0.5		1.72	1.17	2625	11.4	0.99	2 500	
	HM-S		RT	RT	0		1.77	1.44	2420	8.94	2.02		
	Mod II	Skybond 710	600	600	0.5		1.70	1.44	2680	7.35	1.02	1 695	Ref. 1-1
	Mod II	Gemonl	RT	RT	0		2.39	1.32					Ref. 1-4
	Mod II	Gemonl	500	500	0.5		0.95	0.6					Ref. 1-4
	HM-S	PMR-15	RT	RT	0		7.0	0.86	7200				Ref. 1-5
	Mod II	5206	RT	RT	0		5.2	1.28	4050	24.7	1.71	20 340	Ref. 1-9
	HM-S	3002M	RT	RT	0	Coupon	2.3	0.98	2260	21.4	1.25	19 670	Ref. 1-9

ORIGINAL PAGE IS
OF POOR QUALITY

Table 1-3. Basic Graphite/Polyimide Laminate $[\pm 45]_S$ Properties

Fiber	Resin	Test temp., °F	Exposure temp., °F	Exposure time, hr.	Test specimen	F_{tu}' ksi	E_t' 10^6 lb/in ²	Strain μ in./in.	F_{cu}' ksi	E_c' 10^6 lb/in ²	Strain μ in./in.	Poisson's Ratio	Source
HT-S	Skybond 710	RT	RT	0	Coupon	16.2	2.6	10 500	28.5	4.63	11 900		Ref. 1-1
HT-S	↓	600	600	0.5	↓	10.8	1.7	15 700	20.5	2.19	11 900		Ref. 1-1
HM-S	↓	RT	RT	0	↓	10.7	2.0	7 880	15.1	3.77	9 670		Ref. 1-1
HM-S	Skybond 710	600	600	0.5	↓	8.3	1.7	12 800	11.6	2.47	13 712		Ref. 1-1
Mod II	Gemonl	RT	RT	0	↓	17.9	2.96					0.80	Ref. 1-4
Mod II	Gemonl	500	500	0.5	Coupon	17.2	2.30					0.76	Ref. 1-4

Note: Tensile test specimens had a 64.8% volume fraction. Compression test specimens had a 61.1% volume fraction.

Table 1-4.—Normalized Graphite/Polyimide Laminate [0] Properties Normalized to 60% Fiber Volume

	Fiber	Resin	Test temp., °F	Exposure temp., °F	Exposure time, hr	Test specimen	F_{tu} ksi	E_t 10^6 lb/in ²	Strain μ in./in.	F_{cu} ksi	E_c 10^6 lb/in ²	Strain μ in./in.	Poisson's ratio	No. of specimens	Source
High strength	Mod II	Skybond 703	RT	RT	0	SW beam	213.0	23.2	8692	178.0	22.0	9034		10	Ref. 1-3
	Mod II	Skybond 703	↓	↓	0	Coupon	176.0	17.7	9370	102.0	19.1	6237		10	Ref. 1-3
	HT-S	Skybond 710			0	↓	144.0	19.9	7190	98.0	18.8	5210		6	Ref. 1-1
	HT-S	Skybond 710			0		165.0	17.2	9590				0.37	7	Ref. 1-2
	Mod II	Gémonl			0		175.0	19.7	8880					3	Ref. 1-4
	HT-S	PMR-15	RT	RT	0	Coupon	140.0 ^a	20.8	6730					3	Ref. 1-5
	Above strength values (F_{tu} and F_{cu}) corrected by multiplication to sandwich beam 1.21 tension, 1.74 compression														
							213.0 174.0 200.0 211.0 170.0 ^a			178.0 170.0					Ref. 1-3 Ref. 1-1 Ref. 1-2 Ref. 1-4 Ref. 1-5
	Average						200.0	19.7	9850	174.0	20.0	8700			
	"B" allowables (see text for method of calculation)						172.0	19.7	8430	149.0	20.0	7450			
High modulus	HM-S	Skybond 710					173.0	25.2	6860	147.0	27.3 24.6				Ref. 1-1 Ref. 1-5
	Average						173.0	25.2	6860	147.0	26.0	5650			
	"B" allowable (see text for method of calculation)						148.0	25.2	5870	126.0	20.0	4850			

^aNot used for averaging.

Table 1-5.—Normalized Graphite/Polyimide Laminate [90] Properties Normalized to 60% Fiber Volume

	Fiber	Resin	Test temp., °F	Exposure temp., °F	Exposure time, hr	Test specimen	F_{tu} ksi	E_t 10 ⁶ lb/in ²	Strain, μ in./in.	F_{cu} ksi	E_c 10 ⁶ lb/in ²	Strain, μ in./in.	No. of specimen	Source
High strength	Mod II	703	RT	RT	0	SW beam	9.89	2.02	4535	18.99	1.16	11 536	10	Ref. 1-3
	Mod II	703	↓	↓	0	Coupon	2.53	0.99	1880	21.20	0.68	18 850	10	Ref. 1-3
	HT-S	710	↓	↓	0	↓	2.32	1.37	2859	12.4	1.22	2 285	6	Ref. 1-1
	HT-S	710	↓	↓	0	↓	3.18	0.75	4240				6	Ref. 1-2
	Mod II	Gemonl	RT	RT	0	Coupon	2.39	1.32	1810	15.79	1.70	9 290	3	Ref. 1-4
	Above data (F_{tu} , E_t , F_{cu} , and E_c) corrected to sandwich beam (3.90) tension strength, (2.0) tension modulus, (1.0) compression strength, (1.0) compression modulus													
	Mod II	703					9.89	2.02		18.99	1.16			Ref. 1-3
	HT-S	710					9.04	2.74		12.4	1.22			Ref. 1-1
	HT-S	710					12.40	1.50						Ref. 1-2
	Mod II	Gemonl					9.32	2.64		15.79	1.70			Ref. 1-4
High modulus	Average						10.2	2.22		17.09	1.19			Ref. 1-3
	"B" allowable (see text for method of calculation)						8.75	2.22	3940	14.66	1.19	12 320		
	HM-S	710	RT	RT	0	Coupon	1.77	1.44	2420	8.94	2.02	4 430		Ref. 1-1
	HM-S	PMR-15	RT	RT	0	Coupon	7.0 ^a	0.86 ^a	7200 ^a					Ref. 1-5
	Above data (F_{tu} , E_t , F_{cu} , and E_c) corrected to sandwich beam (3.90), tension strength, (2.0) tension modulus, (1.0) compression strength, (1.0) compression modulus													
	Corrected data values						6.90	2.88		8.94	2.02			Ref. 1-1
	"B" allowable (see text for method of calculation)						5.92	2.88	2055	7.66	2.02	3 790		

^aData not used for "B" allowableORIGINAL PAGE IS
OF POOR QUALITY

Table 1-6. Normalized Graphite/Polyimide Laminate $[\pm 45]_S$ Properties Normalized to 60% Fiber Volume

	Fiber	Resin	Test temp., °F	Exposure temp., °F	Exposure time, hr	F_{tu} , ksi	E_t , 10^6 in./lb ²	Strain, μ in./in.	F_{cu} , ksi	E_c , 10^6 lb/in ²	Strain, μ in./in.	Source
High strength	HT-S	710	RT	RT	0	15.0	2.18	6 880	28.0	4.55	6 150	Ref. 1-1
	Mod II	Gemonl	RT	RT	0	22.6	3.73	6 060				Ref. 1-4
	HT-S	Epoxy	RT	RT	0	30.0	2.34	5 000	38.0	2.34	4 300	AFDG
	Average HT-S				0	30.0 ^b	2.75	5 000 ^a	38.0 ^b	3.44	4 300 ^a	
	"B" allowable HT-S				0	25.7	2.75	2 500 ^a	32.6	3.44	3 000 ^a	
High modulus	HM-S	710	RT	RT	0	11.5	2.14	8 000 ^a	16.2	4.03	10 000 ^a	Ref. 1-1
	↓	Epoxy	RT	RT	0	21.0	2.38	14 500	27.0 ^a	2.38 ^a		AFDG
	Average				0	21.0	3.80 ^a	13 000 ^a	27.0 ^a	3.80 ^a	15 000 ^a	
	"B" allowable HM-S				0	18.0	3.80 ^a	10 000 ^a	23.2	3.80 ^a	11 000 ^a	

^aEstimated

^bBased on Air Force Design Guide data, polyimide data inferior

ORIGINAL PA
OF POOR QUL

Table 1-7.—"B" Allowables, Graphite/Polyimide Laminate Normalized to 60% Fiber Volume, 1975

Fiber Orientation	Fiber type	Test temp, °F	F_{tu} , ksi	E_t , 10^6 lb/in. ²	Strain, μ in./in.	F_{cu} , ksi	E_c , 10^6 lb/in. ²	Strain, μ in./in.	Poisson's ratio	Thermal cond. $\frac{\text{Btu in.}}{\text{hr ft}^2 \text{ } ^\circ\text{F}}$	Thermal expansion μ in./in.°F	Absorptivity
[0]	High strength	RT	172.0	19.7	8 730	172.0	20.0	8 600	0.31	160	-0.17	0.85
[0]	↓	450	155.0	19.7	7 900	155.0	20.0	7 800	0.31			
[90]		RT	8.75	2.22	4 000	14.7	1.19	12 400		16	9.45	
[90]		450	6.5	1.9	3 400	13.0	1.0	13 000				
[±45]	↓	RT	25.7	2.75	12 000 ^a	32.6	3.44	13 000 ^a	0.80			
[±45]	High strength	450	17.5	1.8	12 000 ^a	19.8	1.7	14 000 ^a	0.84			
[0]	High modulus	RT	148.0	25.2	5 900	126.0	26.0	4 800	0.29	370	-0.4	
[0]	↓	450	133.0	25.2	5 300	113.0	26.0	4 300	0.29			
[90]		RT	5.92	2.88	2 100	16.0	2.02	8 800 ^a		20	17.0	
[90]		450	5.0	2.7	1 900	14.5	1.6	10 000 ^a				
[±45]	↓	RT	18.0	3.80 ^a	5 800 ^a	23.2	3.80	7 600 ^a	0.79			
[±45]	High modulus	450	14.0	3.2	5 200 ^a	18.0	3.2	6 400 ^a	0.83			0.85

^aEstimatedORIGINAL PAGE IS
OF POOR QUALITY

ORIGINAL PAGE IS
OF POOR QUALITY

Table 1-8.—"B" Allowables, Graphite/Polyimide Laminate Normalized to 60% Fiber Volume, 1986

Fiber Orientation	Fiber	Test temp., °F	F_{tu} ksi	E_t 10^6 lb/in^2	Strain, $\mu \text{ in./in.}$	F_{cu} ksi	E_c 10^6 lb/in^2	Strain, $\mu \text{ in./in.}$	Poisson's ratio	Thermal cond, $\frac{\text{Btu in.}}{\text{hr ft}^2 \text{ °F}}$	Thermal expansion, $\mu \text{ in./in. °F}$	Absorptivity
[0]	T600 ^a	RT	295.0	20.0	14 750	290.0	20.0	14 500	0.31	160	-0.17	0.85 ↓ 0.85
[0]	T600 ^a	450	265.0	20.0	13 250	260.0	20.0	13 000 ^b	0.31			
[90]	T600 ^a	RT	8.8	2.0	5 000	23.0	1.8	15 000		16	9.45	
[90]	T600 ^a	450	6.5	1.9	3 900	21.0	1.7	15 500				
[±45] _S	T600 ^a	RT	44.0	2.8	19 000	56.0	2.8	25 000	0.80			
[±45] _S	T600 ^a	450	30.0	1.8	19 000	34.0	1.8	23 000	0.84			
[0]	T90 ^c	RT	148.0	40.0	3 700	126.0	40.0	3 150	0.29	370	-0.40	
[0]	T90 ^c	450	133.0	40.0	3 305	113.0	40.0	2 825	0.29			
[90]	T90 ^c	RT	7.0	2.0	4 000	18.0	1.8	12 000		20	17.0	
[90]	T90 ^c	450	5.0	1.9	3 100	16.5	1.7	12 400				
[±45] _S	T90 ^c	RT	18.0	3.8	7 500	23.0	3.8	10 000	0.79			
[±45] _S	T90 ^c	450	14.0	3.2	6 500	18.0	3.2	8 500	0.83			

^a $\rho_{T600} = 0.056 \text{ lb/in}^3$

^bEstimated

^c $\rho_{T90} = 0.058 \text{ lb/in}^3$

Table 1-9.—"B" Allowables, Boron/Polyimide Laminate^a
Normalized to 50% Fiber Volume, 1986

Fiber Orientation	Test temp, °F	F _{tu} , ksi	E _t , 10 ⁶ lb/in. ²	Strain, μ in./in.	F _{cu} , ksi	E _c , 10 ⁶ lb/in. ²	Strain, μ in./in.	Poisson's ratio	Thermal cond. $\frac{\text{Btu in.}}{\text{hr ft}^2 \text{ } ^\circ\text{F}}$	Thermal expansion μ in./in. $^\circ\text{F}$
[0]	RT	195.0	32.0	6100	350	32.0	11 000	0.21	16	2.3
[0]	450	175.0	30.0	5900	315	30.0	10 500	0.21	16	3.0
[90]	RT	7.8	2.8	3500	38	3.6	14 000		8	10.6
[90]	450	7.0	2.5	3600	34	3.0	15 000		8	19.6
[±45]	RT	22.0	2.5	9500	35	2.5	16 000	0.85		
[±45]	450	20.0	2.3	9500	32	2.3	15 500	0.91		

^a $\rho = 0.0725 \text{ lb/in}^3$

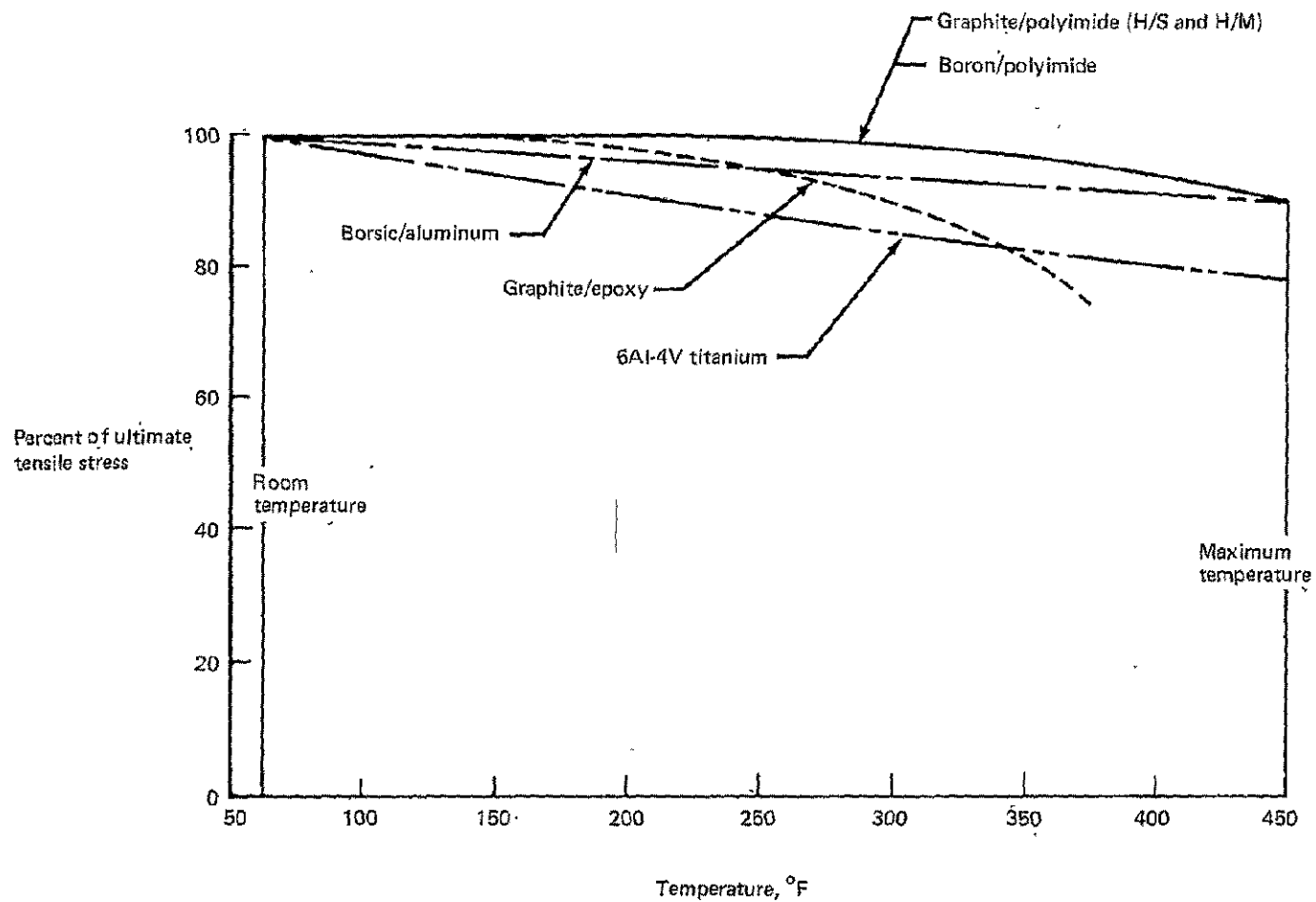


Figure 1-1.—Temperature Dependence of Material Properties for Advanced Composite Wing Cover Panels

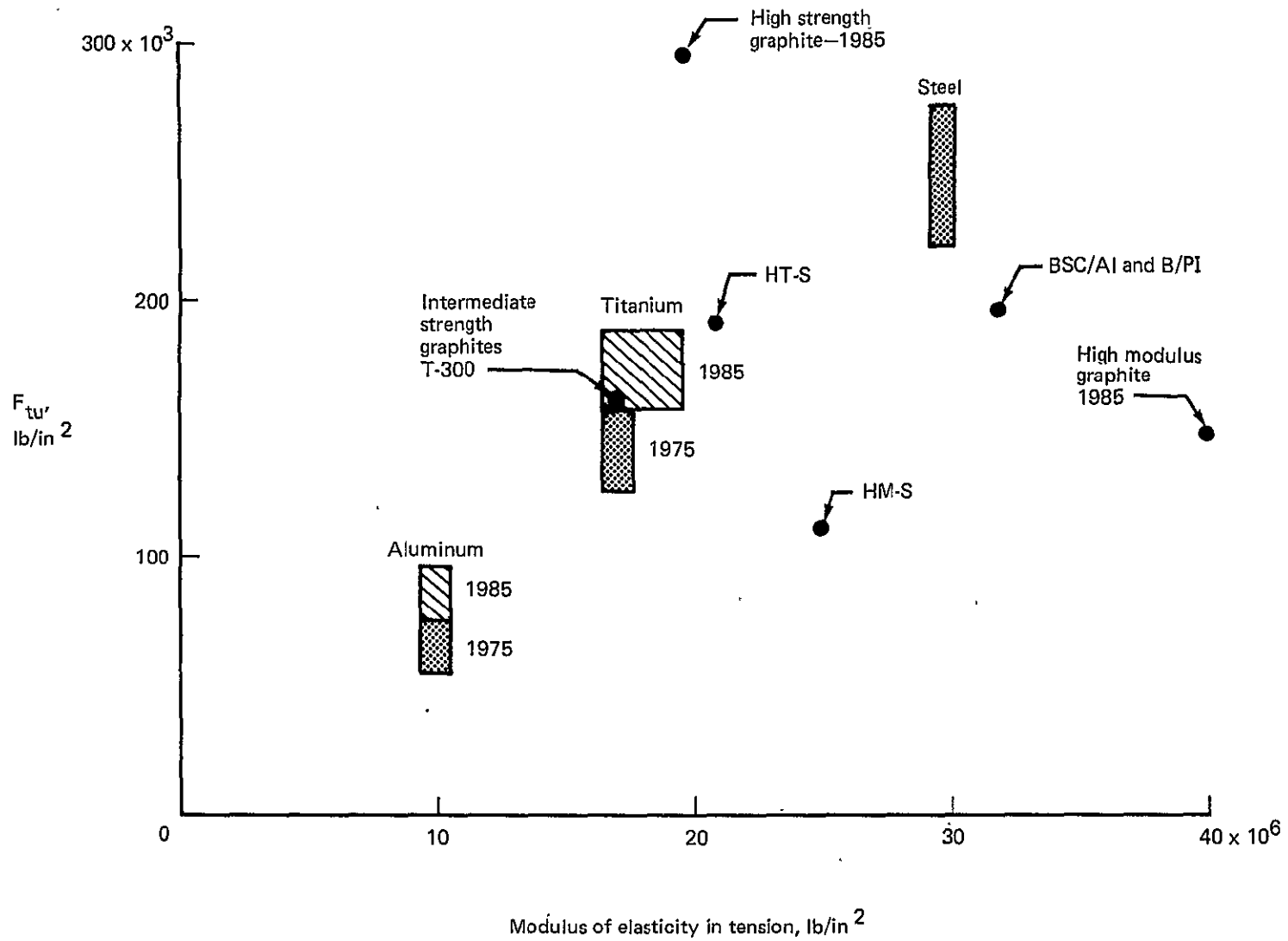


Figure 1-2.—Strength and Moduli of Various Materials

SECTION 2

ALLOWABLES

by

V. D. BESS

F. D. FLOOD

CONTENTS

Page

INTRODUCTION	30
STRESS-STRAIN RELATIONSHIPS	30
THERMAL EFFECTS	35
MATERIAL ALLOWABLES	35
REFERENCES	36

TABLES

No.		Page
2-1	High Strength Graphite/Polyimide Mechanical Properties	37
2-2	High Modulus Graphite/Polyimide Mechanical Properties	38
2-3	Boron/Polyimide Mechanical Properties	39
2-4	5.7-Mil Borsic/Aluminum Mechanical Properties	40

FIGURES

No.		Page
2-1	Graphite/Polyimide Stress-Strain, Tension and Compression, [0] Orientation	41
2-2	Graphite/Polyimide Stress-Strain, Tension, [90] Orientation	42
2-3	Graphite/Polyimide Stress-Strain, Compression, [90] Orientation	43
2-4	Graphite/Polyimide Stress-Strain, Tension and Compression, [90] Orientation	44
2-5	Graphite/Polyimide Stress-Strain, Tension, [± 45] Orientation	45
2-6	Graphite/Polyimide Stress-Strain, Compression, [± 45] Orientation	46
2-7	Graphite/Polyimide Stress-Strain, Tension and Compression, [± 45] Orientation . . .	47

SYMBOLS

CLT	Classical lamination theory
E	Modulus of elasticity
E_s	Secant modulus
G	Modulus of rigidity (shear)
N	Load per inch of edge length
t	Skin thickness
γ	Shear strain
ϵ	Axial strain
μ	Poisson's ratio
σ	Axial stress
τ	Shear stress
Subscripts	
L	Longitudinal
T	Transverse

INTRODUCTION

In the next decade development of polyimide matrix systems is expected to permit design and fabrication of advanced composite material systems that are truly fiber critical. The problem that must be addressed is that of increasing the matrix strain capability to equal or exceed that of the fiber. Strains of this magnitude must not induce micro-cracks, and the matrix modulus must be sufficiently large to develop acceptable fiber strengths in compressive loading. Research toward achieving these goals for epoxy matrices is reported in references 1-10 and 2-1. In the development of allowables reported below it is assumed that the composite material system is fiber critical.

When developing elastic property values for use with the ATLAS system it was a requisite that the values be constant throughout the total range of loading at any given temperature. Thus, for example, a modulus of elasticity for tensile loads should equal that for compressive loads. The approach used to establish elastic and mechanical properties is outlined below using the high-strength graphite/polyimide room temperature (R.T.) values for illustrative purposes. In the discussion that follows, a unidirectional laminate loaded parallel to the fibers is identified as a [0] laminate. A unidirectional laminate loaded transverse to the fibers is identified as a [90] laminate.

STRESS-STRAIN RELATIONSHIPS

Figure 2-1 is a plot of the tensile and compressive stress-strain curves for a [0] laminate. Both the tension and compression curves are linear to the "B" allowable stresses and exhibit the same modulus of elasticity. The allowable tensile fiber strain from the load-free state is 0.01475 in./in. while that in compression is 0.0145 in./in. These critical data are as taken from table 1-8.

Figure 2-2 is a plot of the tensile stress-strain curve for a [90] laminate. The basic data is from a current-technology, matrix-critical system. As noted previously, development of the polyimide matrix system anticipates vast improvement in the matrix strain capability. Since no major reduction in the modulus can be sustained without loss of fiber compressive strength, it has been assumed that the matrix improvement would be realized as plastic strain beyond the current matrix allowable tensile strain. This plastic strain terminates at the critical tensile fiber strain (fig. 2-1).

Figure 2-3 is a plot of the compressive stress-strain curve for a [90] laminate. Since the allowable fiber compressive strain is less than the allowable matrix compressive strain, the fiber strain will be critical in a $[0_i/\pm 45_j/90_k]$ laminate.

The secant moduli at the critical fiber strains are shown on figures 2-2 and 2-3. The tensile and compressive moduli are unequal. These moduli are averaged to get a single value to use for either tensile or compressive loads. This average modulus is plotted in figure 2-4 along with replots of figures 2-2 and 2-3 to illustrate the effect of the foregoing procedure. While the changes in allowable stresses, strains and moduli illustrated in figure 2-4 appear quite large, it should be emphasized that the contributions of the fibers to the strength and stiffness of a fiber critical laminate is much greater than that of the matrix, and therefore, these altered matrix properties are inconsequential in predicting the strength and stiffness of a $[0_i/\pm 45_j/90_k]$ laminate.

Figures 2-5 and 2-6 are plots of the tensile and compressive stress-strain curves, respectively, for a $[\pm 45]_S$ laminate loaded along the 0° axis. In each case, the allowable strain of the $[\pm 45]_S$ laminate exceeds the allowable fiber strain (fig. 2-1). The secant moduli were calculated at the critical fiber strain as shown. The average of these secant moduli is plotted on figure 2-7 along with the original curves from figures 2-5 and 2-6. The deviation from the original curves is slight and is acceptable for evaluating any laminate which incorporates this $[\pm 45]_S$ laminate as a subset. These data will be used later to establish the inplane shear modulus of a unidirectional laminate.

Section 1 identified values for Poisson's ratios for a $[0]$ laminate and a $[\pm 45]_S$ laminate. The Poisson's ratio for a $[90]$ laminate (which as noted above is the Poisson's ratio for a unidirectional laminate loaded transversely) may be calculated from classical lamination theory (CLT), (ref. 2-2) as

$$\mu_T = \frac{E_T}{E_L} \mu_L \quad (2-1)$$

where the T denotes $[90]$ - and L denotes $[0]$ - values.

The data presented in section 1 did not identify shear properties of the various laminates because of the difficulties typically encountered in both rail shear and picture-frame shear testing. Properly tested, buckle-free torque tube test data was not apparently available. Thus, the shear properties were calculated using CLT as discussed below. The technique parallels that employed in reduction of sandwich cross-beam test data.

From figure 2-7

$$E_x = E_y = 2.58 \text{ Msi}$$

From table 1-8

$$\mu_{xy} = \mu_{yx} = 0.80$$

Since the $[\pm 45]$ laminate is orthotropic with respect to the X-Y axes, the reduced stiffnesses are given in terms of the engineering constants as (ref. 2-2).

$$Q_{11} = \frac{E_x}{1 - \mu_{xy} \mu_{yx}} = \frac{2.58 \times 10^6}{1 - (.8)^2} = 7.1667 \times 10^6 \text{ psi}$$

$$Q_{22} = \frac{E_y}{1 - \mu_{xy} \mu_{yx}} = \frac{2.58 \times 10^6}{1 - (.8)^2} = 7.1667 \times 10^6 \text{ psi}$$

$$Q_{12} = \mu_{yx} Q_{11} = 0.8 (7.1667 \times 10^6) = 5.7333 \times 10^6 \text{ psi}$$

$$Q_{66} = G_{xy}$$

$Q_{16} = Q_{26} = 0$, as a consequence of orthotropy

The reduced stiffnesses relate the strains to the stresses as

$$\begin{Bmatrix} \sigma_x \\ \sigma_y \\ \tau_{xy} \end{Bmatrix} = \begin{bmatrix} Q_{11} & Q_{12} & Q_{16} \\ & Q_{22} & Q_{26} \\ \text{(Sym)} & & Q_{66} \end{bmatrix} \begin{Bmatrix} \epsilon_x \\ \epsilon_y \\ \gamma_{xy} \end{Bmatrix} = 10^6 \begin{bmatrix} 7.1667 & 5.7333 & 0 \\ & 7.1667 & 0 \\ \text{(Sym)} & & Q_{66} \end{bmatrix} \begin{Bmatrix} \epsilon_x \\ \epsilon_y \\ \gamma_{xy} \end{Bmatrix} \quad (2-2)$$

The strain-stress relations are derived from $[Q]^{-1}$ as

$$\begin{Bmatrix} \epsilon_x \\ \epsilon_y \\ \gamma_{xy} \end{Bmatrix} = 10^{-6} \begin{bmatrix} 0.38758 & -0.31006 & 0 \\ & 0.38758 & 0 \\ \text{(Sym)} & & Q_{66}^{-1} \end{bmatrix} \begin{Bmatrix} \sigma_x \\ \sigma_y \\ \tau_{xy} \end{Bmatrix} \quad (2-3)$$

For the specified loading

$$\begin{Bmatrix} \sigma_x \\ \sigma_y \\ \tau_{xy} \end{Bmatrix} = \begin{Bmatrix} N/t \\ -N/t \\ 0 \end{Bmatrix} \quad (2-4)$$

The strains for the specified loadings are

$$\begin{Bmatrix} \epsilon_x \\ \epsilon_y \\ \gamma_{xy} \end{Bmatrix} = 10^{-6} \begin{bmatrix} 0.38758 & -0.31006 & 0 \\ & 0.38758 & 0 \\ & & Q_{66}^{-1} \end{bmatrix} \begin{Bmatrix} N/t \\ -N/t \\ 0 \end{Bmatrix} = \begin{Bmatrix} 0.69764 \times 10^{-6} & N/t \\ -0.69764 \times 10^{-6} & N/t \\ 0 & \end{Bmatrix} \quad (2-5)$$

The strains are now transformed to the 1-2 axis system which is coincident with the fibers in the $[\pm 45]_S$ laminate.

$$\begin{Bmatrix} \epsilon_1 \\ \epsilon_2 \\ \frac{1}{2}\gamma_{12} \end{Bmatrix} = \begin{bmatrix} \cos^2 45^\circ & \sin^2 45^\circ & 2\sin 45^\circ \cos 45^\circ \\ \sin^2 45^\circ & \cos^2 45^\circ & -2\sin 45^\circ \cos 45^\circ \\ -\sin 45^\circ \cos 45^\circ & \sin 45^\circ \cos 45^\circ & \cos^2 45^\circ - \sin^2 45^\circ \end{bmatrix} \begin{Bmatrix} \epsilon_x \\ \epsilon_y \\ \frac{1}{2}\gamma_{xy} \end{Bmatrix} \quad (2-6)$$

$$\begin{Bmatrix} \epsilon_1 \\ \epsilon_2 \\ \frac{1}{2}\gamma_{12} \end{Bmatrix} = \begin{bmatrix} \frac{1}{2} & \frac{1}{2} & 1 \\ \frac{1}{2} & \frac{1}{2} & -1 \\ -\frac{1}{2} & \frac{1}{2} & 0 \end{bmatrix} \begin{Bmatrix} 0.69764 \times 10^{-6} \text{ N/t} \\ -0.69764 \times 10^{-6} \text{ N/t} \\ 0 \end{Bmatrix} = \begin{Bmatrix} 0 \\ 0 \\ -0.69764 \times 10^{-6} \text{ N/t} \end{Bmatrix} \quad (2-7)$$

The stresses (loading) may be similarly transformed

$$\begin{Bmatrix} \sigma_1 \\ \sigma_2 \\ \tau_{12} \end{Bmatrix} = \begin{bmatrix} \frac{1}{2} & \frac{1}{2} & 1 \\ \frac{1}{2} & \frac{1}{2} & -1 \\ -\frac{1}{2} & \frac{1}{2} & 0 \end{bmatrix} \begin{Bmatrix} \text{N/t} \\ -\text{N/t} \\ 0 \end{Bmatrix} = \begin{Bmatrix} 0 \\ 0 \\ \text{N/t} \end{Bmatrix} \quad (2-8)$$

It may be seen from the transformed stress that the specified loading is applied shear only in the 1-2 axis system. This is a loading wherein the matrix only carries the shear load and is considered equivalent to a shear loading on a unidirectional laminate. The shear modulus is given by

$$G_{12} = \frac{\tau_{12}}{\gamma_{12}} = \frac{-\text{N/t}}{2(-0.69764 \times 10^{-6} \text{ N/t})} = 0.717 \text{ Msi} \quad (2-9)$$

As a check, CLT was used to obtain the strain-stress relations for a $[\pm 45]_S$ laminate using the following properties for an unidirectional laminate

$$E_1 = 20. \text{ Msi}$$

$$E_2 = 1.13 \text{ Msi}$$

$$G_{12} = 0.717 \text{ Msi}$$

$$\mu_{12} = 0.31$$

The apparent elastic properties of the $[\pm 45]_S$ laminate in the X-Y (0° - 90°) axis system are

$$E_x = E_y = 2.54 \text{ Msi (vs } 2.58 \text{ Msi from figure 2-7)}$$

$$\mu_{xy} = \mu_{yx} = 0.77 \text{ (vs } 0.80 \text{ from section 1)}$$

$$G_{xy} = 5.14 \text{ Msi (not reported in section 1)}$$

These values are in excellent agreement with the reported values of section 1. The basic laminate elastic properties noted above will be used in conjunction with CLT to determine the elastic characteristics of the $[0_i/\pm 45_j/90_k]_S$ laminates evaluated.

The procedure to determine the inplane shear strength of a unidirectional laminate is shown below. It is assumed that the inplane shear strength of a unidirectional laminate equals that of a $[0/90]_S$ laminate. The stress-strain relations for a $[0/90]_S$ laminate are

$$\begin{Bmatrix} \sigma_x \\ \sigma_y \\ \tau_{xy} \end{Bmatrix} = 10^6 \begin{bmatrix} 10.6226 & 0.35191 & 0 \\ & 10.6226 & 0 \\ \text{(Sym)} & & 0.717 \end{bmatrix} \begin{Bmatrix} \epsilon_x \\ \epsilon_y \\ \gamma_{xy} \end{Bmatrix} \quad (2-10)$$

The strain-stress relations are

$$\begin{Bmatrix} \epsilon_x \\ \epsilon_y \\ \gamma_{xy} \end{Bmatrix} = 10^{-6} \begin{bmatrix} 0.094242 & -0.0031221 & 0 \\ & 0.094242 & 0 \\ \text{(Sym)} & & 1.3947 \end{bmatrix} \begin{Bmatrix} \sigma_x \\ \sigma_y \\ \tau_{xy} \end{Bmatrix} \quad (2-11)$$

For a shear stress only the strains are

$$\begin{Bmatrix} \epsilon_x \\ \epsilon_y \\ \gamma_{xy} \end{Bmatrix} = \begin{Bmatrix} 0 \\ 0 \\ 1.3947 \times 10^{-6} \tau_{xy} \end{Bmatrix} \quad (2-12)$$

Transforming these strains to a 1-2 axis system at $\pm 45^\circ$ from the X-Y axis gives.

$$\begin{Bmatrix} \epsilon_1 \\ \epsilon_2 \\ \frac{1}{2}\gamma_{12} \end{Bmatrix} = \begin{bmatrix} \frac{1}{2} & \frac{1}{2} & 1 \\ \frac{1}{2} & \frac{1}{2} & -1 \\ -\frac{1}{2} & \frac{1}{2} & 0 \end{bmatrix} \begin{Bmatrix} 0 \\ 0 \\ 1.3947 \times 10^{-6} \tau_{xy}/2 \end{Bmatrix} = \begin{Bmatrix} 1.3947 \times 10^{-6} \tau_{xy}/2 \\ 1.3947 \times 10^{-6} \tau_{xy}/2 \\ 0 \end{Bmatrix} \quad (2-13)$$

In a $[0_i/\pm 45_j/90_k]_S$ fiber critical laminate, the critical compressive fiber strain is 0.0145 in./in. Thus, the matrix shear strength may be defined by substituting this value for ϵ_2 . The shear strength is then given by

$$\tau_{xy \text{ allow.}} = \frac{-14500 \times 10^{-6}}{(-1.3947 \times 10^{-6})/2} = 20800 \text{ psi} \quad (2-14)$$

Interlaminar shear strengths are assumed equal to the shear strength of a unidirectional laminate.

THERMAL EFFECTS

Coefficients of thermal expansion were given for [0] and [90] laminates at room temperature. In checking the data source, it was discovered that the given values were an average over a temperature range greater than room temperature to 450°F. Therefore, the same values are used at room temperature and 450°F.

Thermal conductivities are shown in section 1 for [0] and [90] laminates. These values were obtained from tests on graphite/epoxy at 450°F. Since the fibers are the main contributors to the conductivity, the values for the [0] laminates should be quite close. The [90] laminate conductivities will be dependent upon the assumption that the conductivity of epoxy is approximately that of polyimide.

While some tentative values for other thermophysical properties are tabulated in section 1 and the section 2 tables, these values are subject to revision by our thermal analyst (see section 10).

MATERIAL ALLOWABLES

Tables 2-1 through 2-4 list the unidirectional laminate properties for the candidate advanced composite material systems. As noted above, all [0; \pm 45;90]_k laminates evaluated will have properties based on the unidirectional laminate properties with the specific properties based on classical lamination theory.

REFERENCES

- 2-1 Mazzio, V. F.; Mehan, R. L.; and Mullin, J. V.: *Basic Failure Mechanics in Advanced Composites*. NASA CR-134525, 1973.
- 2-2 Jones, R. M.: *Mechanics of Composite Materials*. McGraw-Hill, 1975.

Table 2-1. - Estimated Mechanical Properties of High Strength Graphite/Polyimide Available in 1986.

$$V_f = 0.60$$

			Room temperature	450 °F
Design strengths "B" values	Longitudinal tensile ultimate, ksi	F_L^{tu}	295	265
	Transverse tensile ultimate, ksi	F_T^{tu}	16.7	13.7
	Longitudinal compression ultimate, ksi	F_L^{cu}	290	260
	Transverse compression ultimate, ksi	F_T^{cu}	16.4	13.4
	Inplane shear ultimate, ksi	F_{LT}^{su}	20.8	12.0
	Interlaminar shear ultimate, ksi	F_{isu}	20.8	12.0
	Ultimate longitudinal tensile strain, μ in./in.	ϵ_L^{tu}	14 750	13 250
	Ultimate longitudinal compressive strain, μ in./in.	ϵ_L^{cu}	14 500	13 000
Elastic properties (typ)	Longitudinal tension modulus, 10^6 lb/in ²	E_L^t	20.0	
	Transverse tension modulus, 10^6 lb/in ²	E_T^t	1.13	1.03
	Longitudinal compression modulus, 10^6 lb/in ²	E_L^c	20.0	20.0
	Transverse compression modulus, 10^6 lb/in ²	E_T^c	1.13	1.03
	Inplane shear modulus, 10^6 lb/in ²	G_{LT}	0.717	0.462
	Longitudinal Poisson's ratio	μ_{LT}	0.31	0.31
	Transverse Poisson's ratio	μ_{TL}	0.018	0.016
Physical constants (typ)	Density, lb/in ³	ρ	0.056	0.056
	Longitudinal coefficient of thermal expansion, μ in./in./°F	α_L	-0.17	-0.17
	Transverse coefficient of thermal expansion, μ in./in./°F	α_T	17.0	17.0
	Longitudinal thermal conductivity, $\frac{\text{Btu in.}}{\text{hr ft}^2 \text{ °F}}$	K_T	160	—
	Transverse thermal conductivity, $\frac{\text{Btu in.}}{\text{hr ft}^2 \text{ °F}}$	K_T	16	—
	Absorptivity	α	0.85	—
	Emissivity	ϵ		

Table 2-2. - Estimated Mechanical Properties of High Modulus Graphite/Polyimide Available in 1986.

$V_f = 0.60$

			Room temperature	450 °F
Design strengths "B" values	Longitudinal tensile ultimate, ksi	F_L^{tu}	148	133
	Transverse tensile ultimate, ksi	F_T^{tu}	6.7	5.3
	Longitudinal compression ultimate, ksi	F_L^{cu}	126	113
	Transverse compression ultimate, ksi	F_T^{cu}	5.7	4.5
	Inplane shear ultimate, ksi	F_{LT}^{su}	6.2	4.6
	Interlaminar shear ultimate, ksi	F_{isu}	6.2	4.6
	Ultimate longitudinal tensile strain, μ in./in.	ϵ_L^{tu}	3700	3325
	Ultimate longitudinal compressive strain, μ in./in.	ϵ_L^{cu}	3150	2825
Elastic properties (typ)	Longitudinal tension modulus, 10^6 lb/in ²	E_L^t	40.0	40.0
	Transverse tension modulus, 10^6 lb/in ²	E_T^t	1.8	1.6
	Longitudinal compression modulus, 10^6 lb/in ²	E_L^c	40.0	40.0
	Transverse compression modulus, 10^6 lb/in ²	E_T^c	1.8	1.6
	Inplane shear modulus, 10^6 lb/in ²	G_{LT}	0.98	0.82
	Longitudinal Poisson's ratio	μ_{LT}	0.29	0.29
	Transverse Poisson's ratio	μ_{TL}	0.013	0.012
Physical constants (typ)	Density, lb/in ³	ρ	0.058	0.058
	Longitudinal coefficient of thermal expansion, μ in./in./°F	α_L	-0.4	-0.4
	Transverse coefficient of thermal expansion, μ in./in./°F	α_T	17.0	17.0
	Longitudinal thermal conductivity, $\frac{\text{Btu in.}}{\text{hr ft}^2 \text{ } ^\circ\text{F}}$	K_L	370	—
	Transverse thermal conductivity, $\frac{\text{Btu in.}}{\text{hr ft}^2 \text{ } ^\circ\text{F}}$	K_T	20	—
	Absorptivity	α	0.85	—
	Emissivity	ϵ		

Table 2-3. - Estimated Mechanical Properties of Boron/Polyimide
Available in 1986.

$$V_f = 0.50$$

			Room temperature	450 °F
Design strengths "B" values	Longitudinal tensile ultimate, ksi	F_L^{tu}	195	175
	Transverse tensile ultimate, ksi	F_T^{tu}	14.6	13.0
	Longitudinal compression ultimate, ksi	F_L^{cu}	350	315
	Transverse compression ultimate, ksi	F_T^{cu}	26.4	23.1
	Inplane shear ultimate, ksi	F_{LT}^{su}	8.3	7.1
	Interlaminar shear ultimate, ksi	F^{isu}	8.3	7.1
	Ultimate longitudinal tensile strain, μ in./in.	ϵ_L^{tu}	6 100	5,900
	Ultimate longitudinal compressive strain, μ in./in.	ϵ_L^{cu}	11 000	10 500
Elastic properties (typ)	Longitudinal tension modulus, 10^6 lb/in ²	E_L^t	32.0	30.0
	Transverse tension modulus, 10^6 lb/in ²	E_T^t	2.4	2.2
	Longitudinal compression modulus, 10^6 lb/in ²	E_L^c	32.0	30.0
	Transverse compression modulus, 10^6 lb/in ²	E_T^c	2.4	2.2
	Inplane shear modulus, 10^6 lb/in ²	G_{LT}	0.68	0.60
	Longitudinal Poisson's ratio	μ_{LT}	0.21	0.21
	Transverse Poisson's ratio	μ_{TL}	0.016	0.015
Physical constants (typ)	Density, lb/in ³	ρ	0.0725	0.0725
	Longitudinal coefficient of thermal expansion, μ in./in./°F	α_L	2.6	2.6
	Transverse coefficient of thermal expansion, μ in./in./°F	α_T	15.1	15.1
	Longitudinal thermal conductivity, $\frac{\text{Btu in.}}{\text{hr ft}^2 \text{°F}}$	K_L	16	—
	Transverse thermal conductivity, $\frac{\text{Btu in.}}{\text{hr ft}^2 \text{°F}}$	K_T	8	—
	Absorptivity	α	0.85	—
	Emissivity	ϵ		

Table 2-4. - Estimated Mechanical Properties of 5.7 Mil Borsic/Aluminum
Available in 1986.

$V_f = 0.50$

			Room temperature	450°F
Design strengths "B" values	Longitudinal tensile ultimate, ksi	F_L^{tu}	195	180
	Transverse tensile ultimate, ksi	F_T^{tu}	17.3	15.0
	Longitudinal compression ultimate, ksi	F_L^{cu}	352	320
	Transverse compression ultimate, ksi	F_T^{cu}	31.1	26.8
	Inplane shear ultimate, ksi	F_{LT}^{su}	8.1	6.8
	Interlaminar shear ultimate, ksi	F^{isu}	8.1	6.8
	Ultimate longitudinal tensile strain, μ in./in.	ϵ_L^{tu}	6 100	5 900
	Ultimate longitudinal compressive strain, μ in./in.	ϵ_L^{cu}	11 000	10 500
Elastic properties (typ)	Longitudinal tension modulus, 10^6 lb/in ²	E_L^t	32.0	30.5
	Transverse tension modulus, 10^6 lb/in ²	E_T^t	2.83	2.55
	Longitudinal compression modulus, 10^6 lb/in ²	E_L^c	32.0	30.5
	Transverse compression modulus, 10^6 lb/in ²	E_T^c	2.83	2.55
	Inplane shear modulus, 10^6 lb/in ²	G_{LT}	0.67	0.58
	Longitudinal Poisson's ratio	μ_{LT}	0.30	0.30
	Transverse Poisson's ratio	μ_{TL}	0.027	0.025
Physical constants (typ)	Density, lb/in ³	ρ	0.098	0.098
	Longitudinal coefficient of thermal expansion, μ in./in./°F	α_L	3.2	3.2
	Transverse coefficient of thermal expansion, μ in./in./°F	α_T	10.6	10.6
	Longitudinal thermal conductivity, $\frac{\text{Btu in.}}{\text{hr ft}^2 \text{ } ^\circ\text{F}}$	K_L	600	—
	Transverse thermal conductivity, $\frac{\text{Btu in.}}{\text{hr ft}^2 \text{ } ^\circ\text{F}}$	K_T	440	—
	Absorptivity	α	—	—
	Emissivity	ϵ	—	—

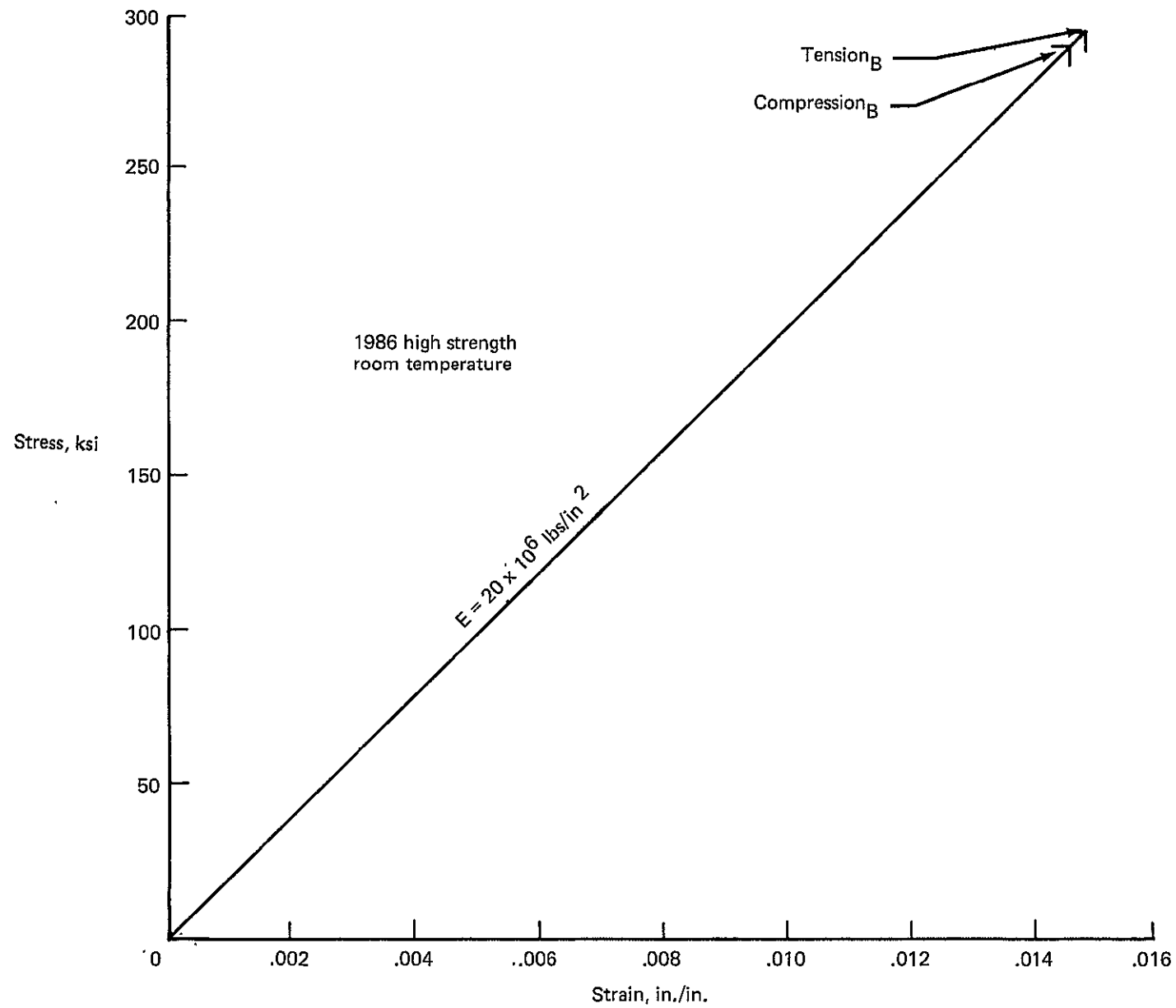


Figure 2-1.— Graphite/Polyimide Stress-Strain, Tension and Compression, [0] Orientation

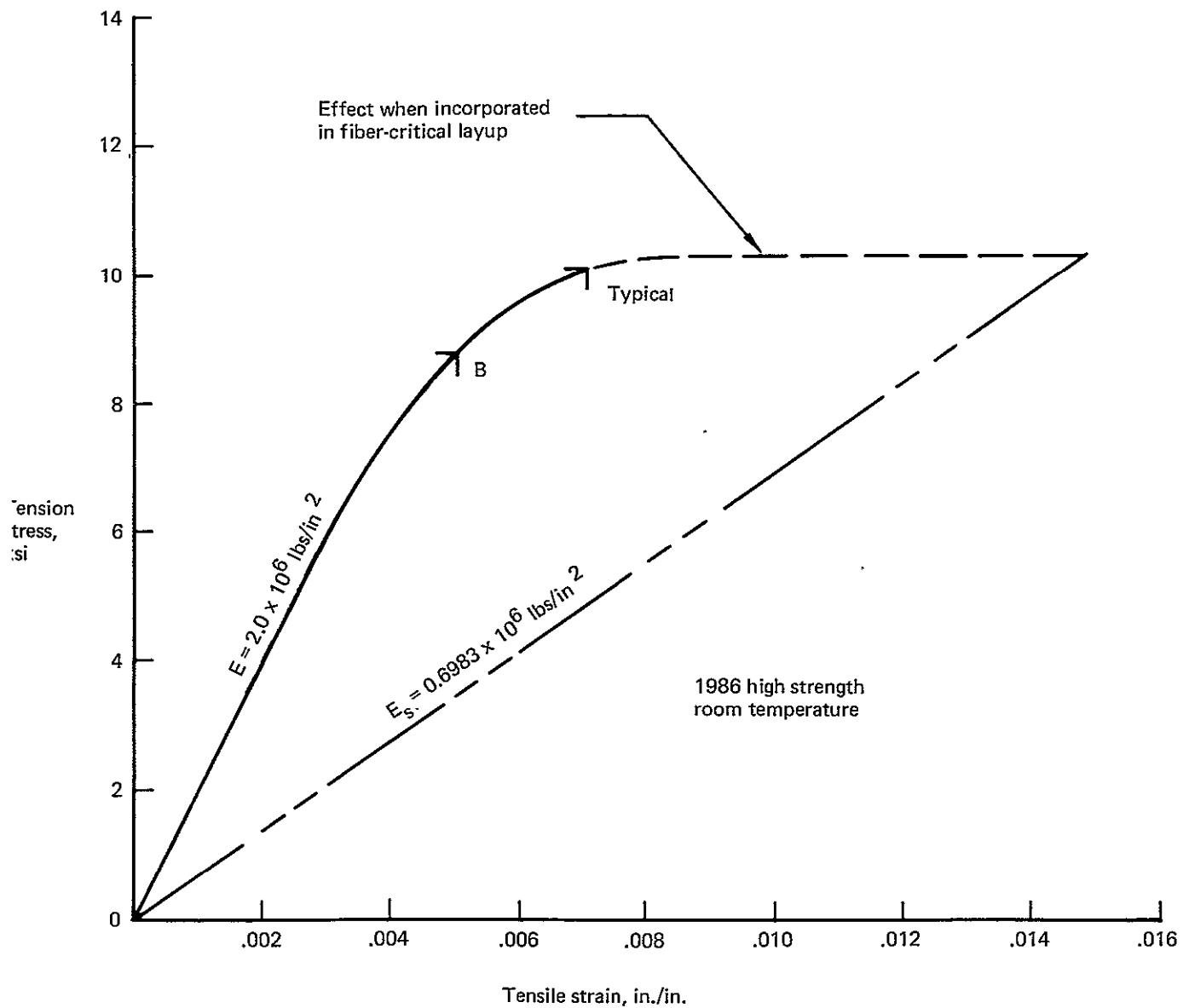


Figure 2-2.—Graphite/Polyimide Stress-Strain, Tension, [90] Orientation

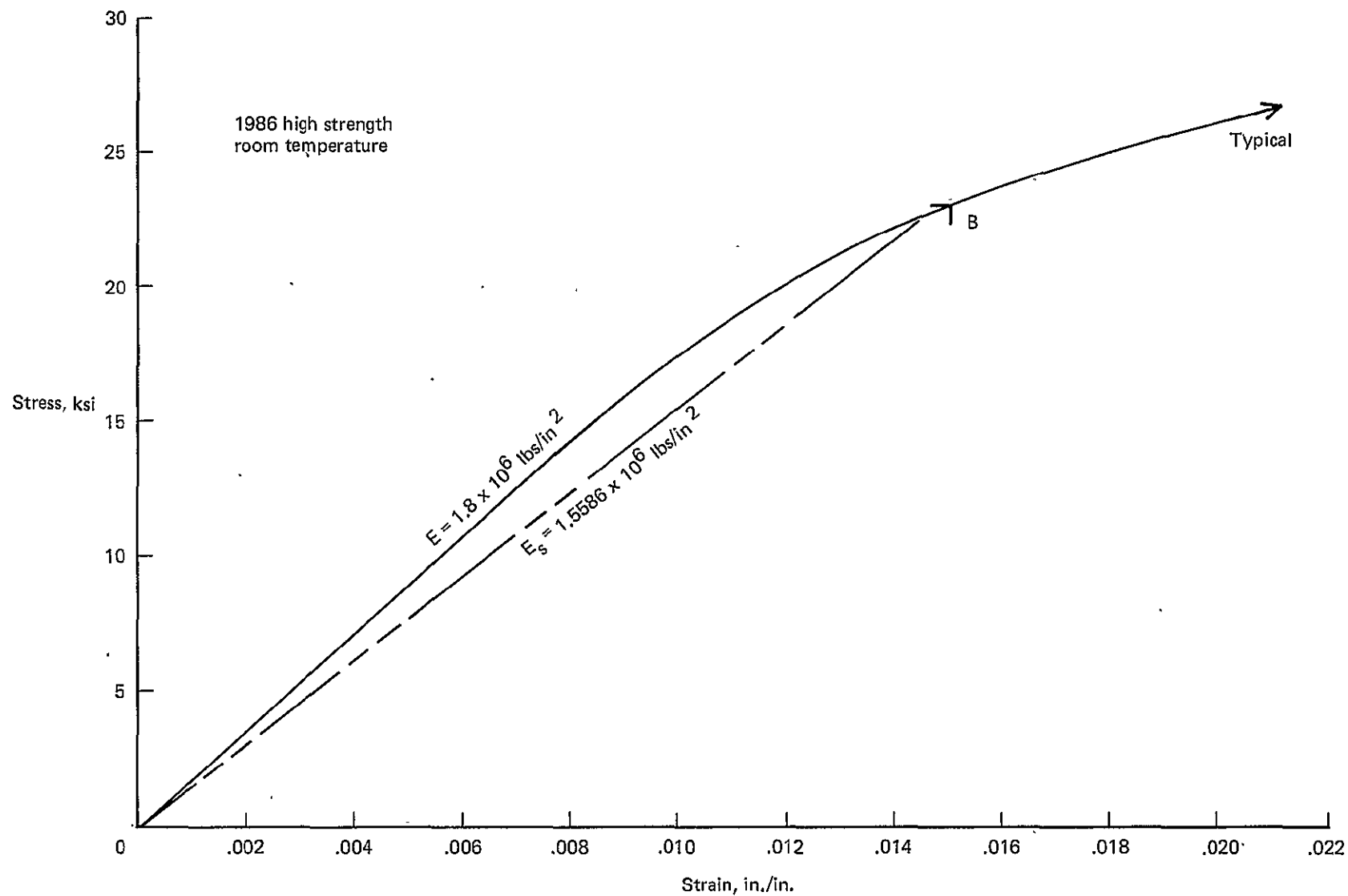


Figure 2-3.—Graphite/Polyimide Stress-Strain, Compression, [90] Orientation

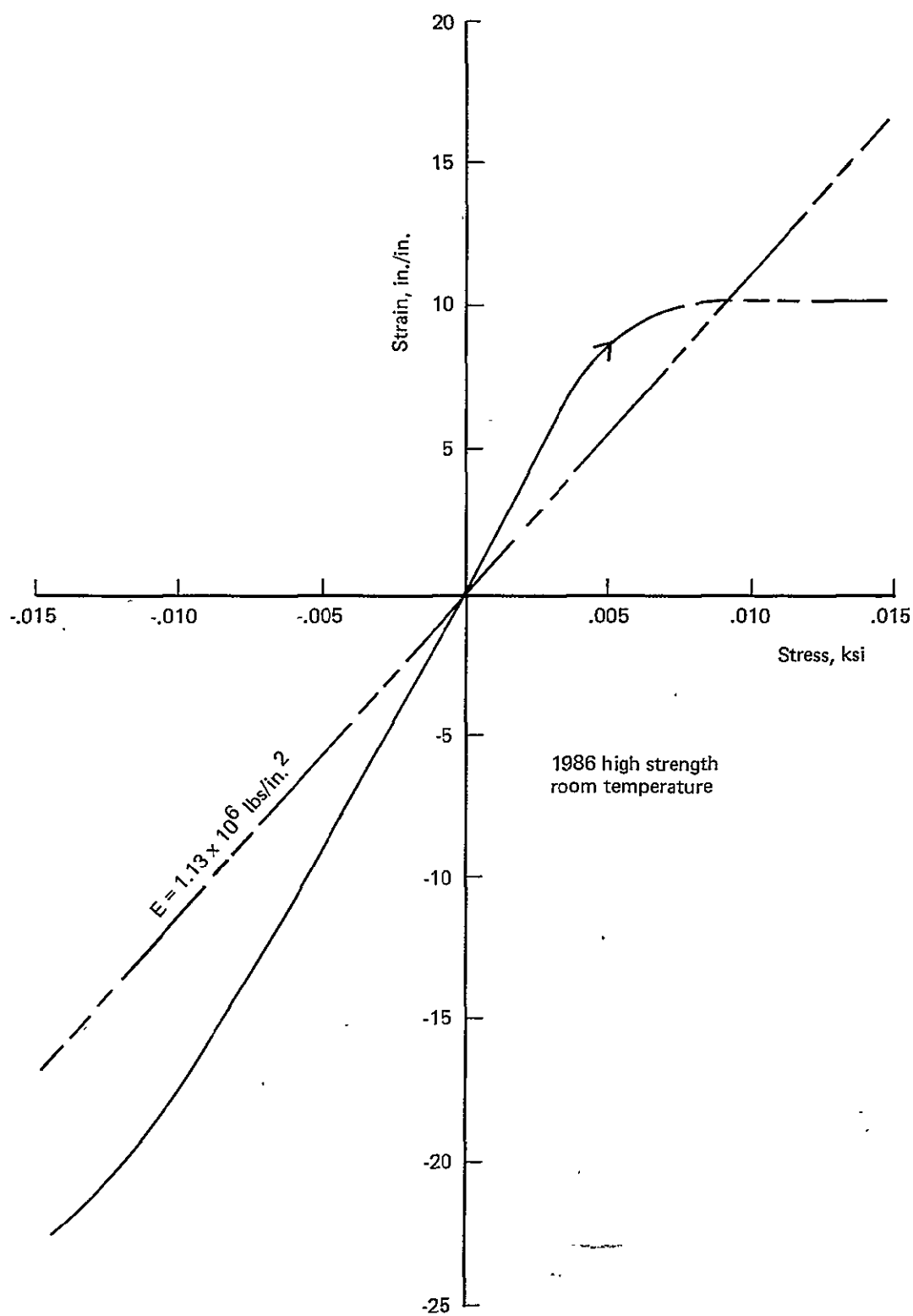


Figure 2-4.—Graphite/Polyimide Stress-Strain, Tension and Compression, [90] Orientation

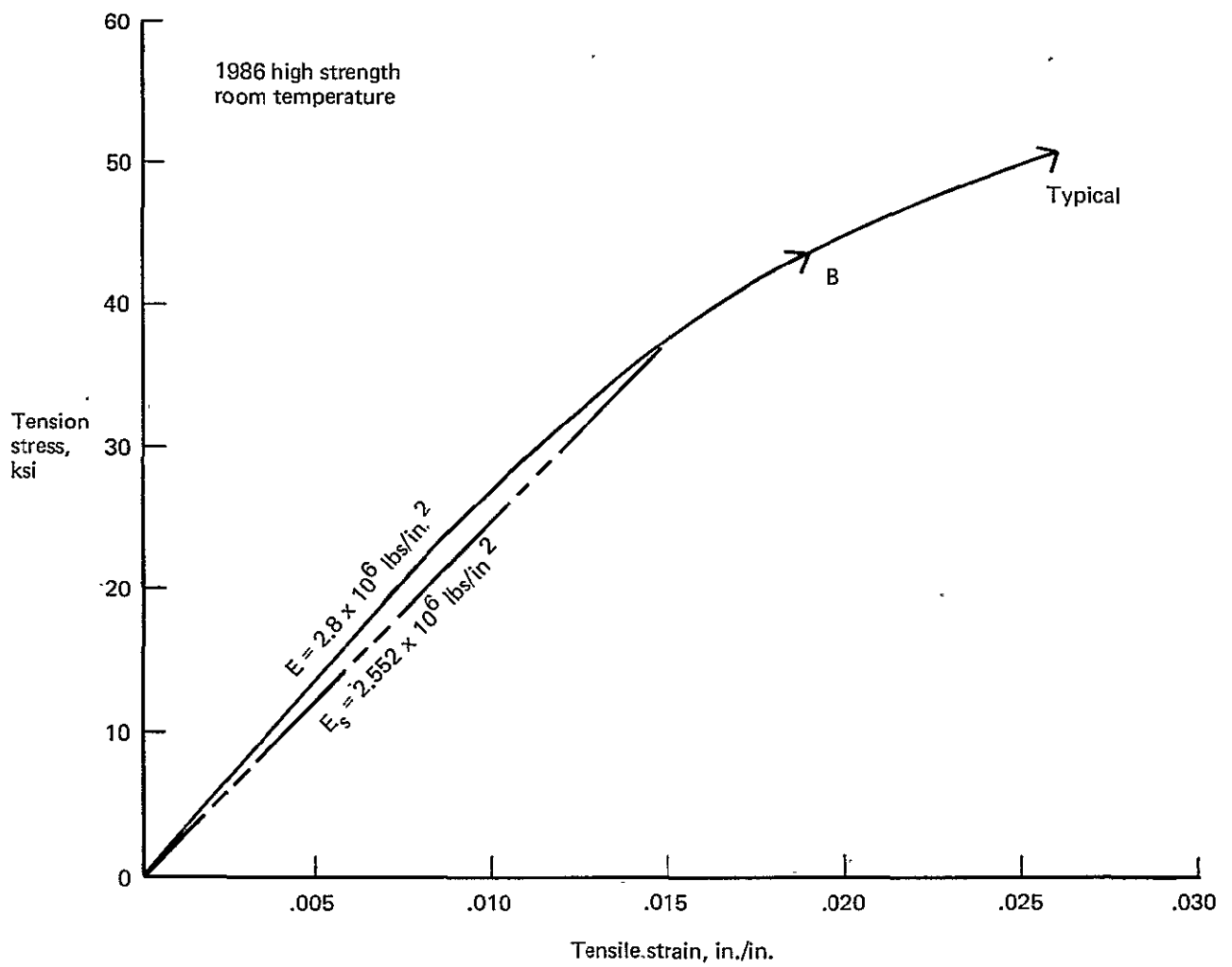


Figure 2.5.—Graphite/Polyimide Stress-Strain, Tension $[\pm 45]_S$ Orientation

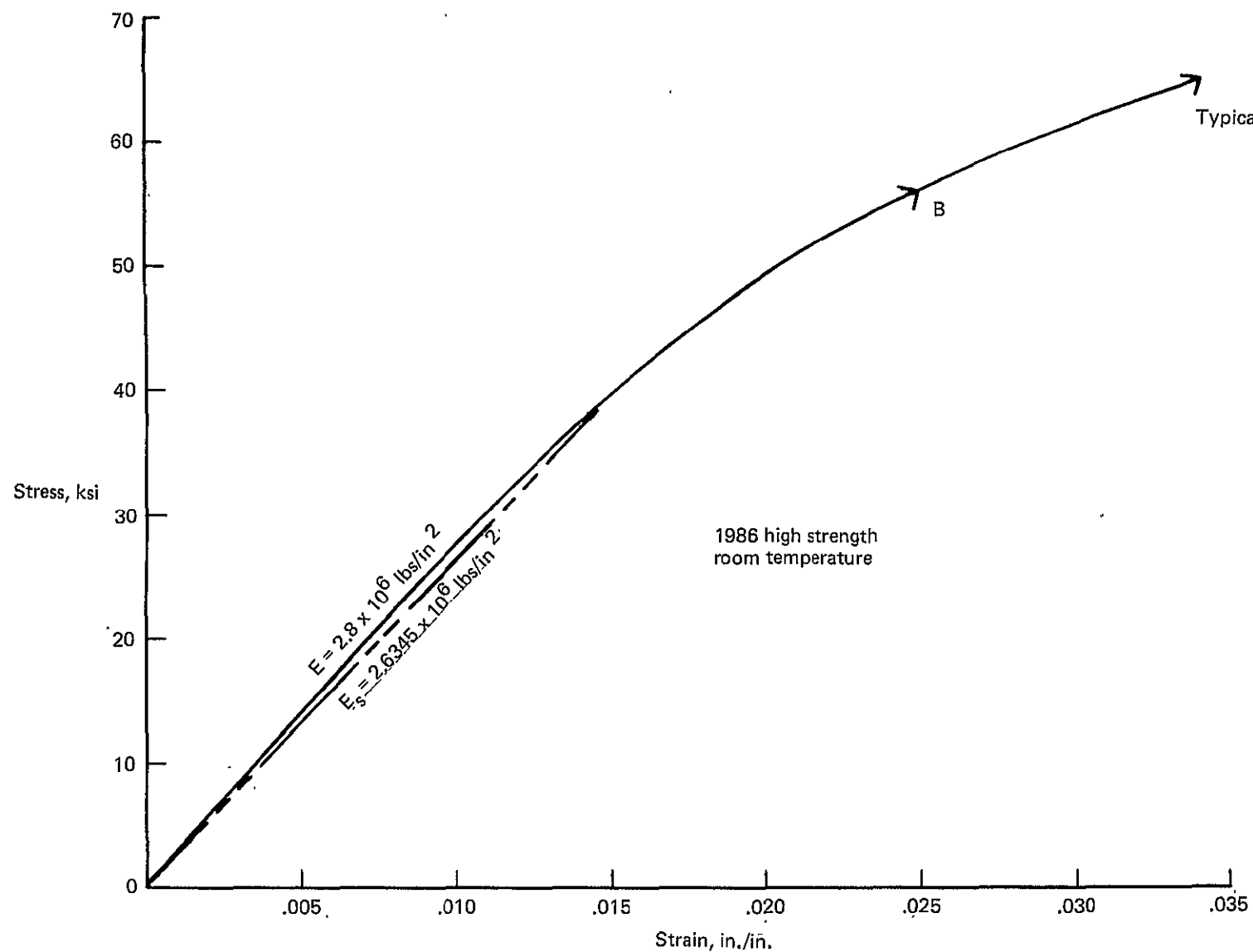


Figure 2-6.—Graphite/Polyimide Stress-Strain, Compression, $[\pm 45]_S$ Orientation

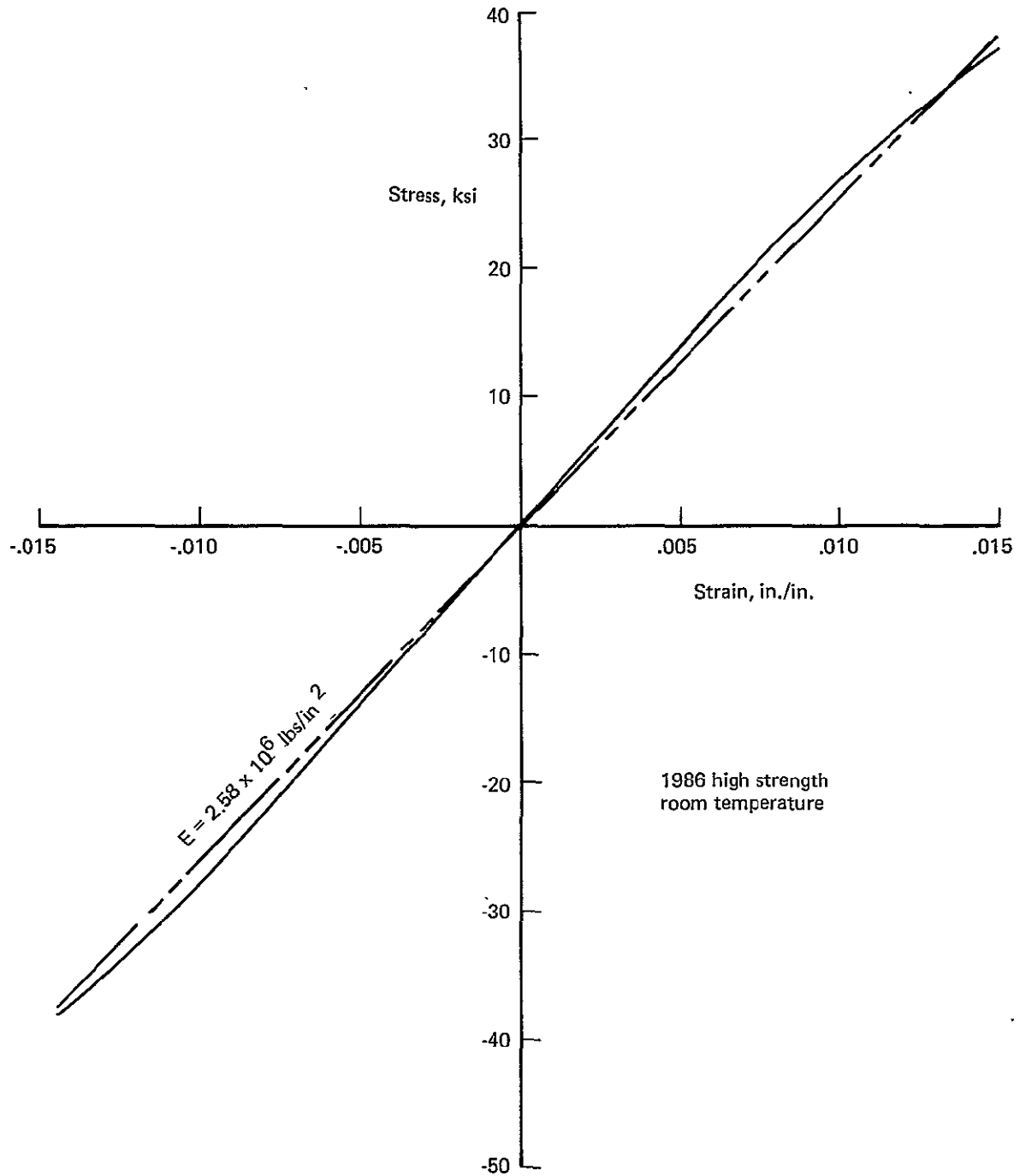


Figure 2-7.—Graphite/Polyimide Stress-Strain, Tension and Compression, $[\pm 45]$ Orientation

SECTION 3

CONCEPT DESIGN AND MATERIAL SELECTION

by

V. D. BESS

PRECEDING PAGE BLANK NOT FILMED

CONTENTS

	Page
INTRODUCTION	54
CONCEPT SELECTION	54
MATERIAL SELECTION	55
REFERENCES	59

TABLES

No.		Page
3-1	Control Point Loads	60
3-2	Specific Mechanical Properties, [0]	61
3-3	Specific Mechanical Properties, [± 45] _S Layups	62
3-4	Mechanical Properties and Specific Mechanical Properties, Room Temperature	63
3-5	Mechanical Properties and Specific Mechanical Properties, 450°F	64

FIGURES

No.		Page
3-1	Wing and Body Control Points	65
3-2	Borsic/Aluminum Concept Comparison	66
3-3	Borsic/Aluminum Skin Reinforced Titanium Stiffeners	67
3-4	Borsic/Aluminum Skin, Thin Titanium Core, Reinforced Titanium Stiffeners	69
3-5	Borsic/Aluminum Skin, Titanium Core	71
3-6	Graphite/PPQ Skin, Titanium Core	73
3-7	Baseline, Integrally Machined and Welded Titanium Skin and Stiffeners	75
3-8	Weight Comparison, Advanced Structural Concepts, Wing Lower Surface	77
3-9	Wing Skin Panel, Al Braze Titanium Honeycomb	78
3-10	Weight Comparison, Advanced Structural Concepts, Wing Upper Surface	79
3-11	Borsic/Aluminum Skin, Reinforced Titanium Stiffeners, 17.75 Inch Frame Spacing	81
3-12	Borsic/Aluminum Skin, Titanium Core, Reinforced Titanium Stiffeners, 17.75 Inch Frame Spacing	83
3-13	Borsic/Aluminum Skin, Titanium Core, 35.5 Inch Frame Spacing	85
3-14	Graphite/PPQ Skin, Titanium Core, 35.5 Inch Frame Spacing	87
3-15	Baseline, Titanium Skin and Stiffeners, 17.25 Inch Frame Spacing	89
3-16	Weight Comparison, Advanced Structural Concepts, Body	91
3-17	Minimum Gage Considerations	92
3-18	Panel Weights for Spanwise Compression Loading	93
3-19	Panel Weights for Chordwise Loading	94
3-20	Panel Weights for Shear Loading	95

SYMBOLS

E	Modulus of elasticity
E_c	Modulus of elasticity in compression
E_t	Modulus of elasticity in tension
F_{cu}	Ultimate compressive stress
F_{su}	Ultimate stress in pure shear
F_{tu}	Ultimate tensile stress
G	Modulus of rigidity (shear)
N	Load per inch of edge length, applied at the neutral axis of sandwich
t	Skin thickness or face thickness
ρ	Weight density
L	Longitudinal
T	Transverse

INTRODUCTION

The titanium arrow-wing structure that was developed during the Task II effort, reference 3-1, was redesigned to utilize composite material in the wing surfaces to assess the potential impact of advanced composites on the strength and flutter characteristics. Because of limited budget, it was decided to retain the titanium substructure as designed in Task II, initially, and to develop a new design for the external wing shell utilizing advanced composite materials. After resizing the surfaces, internal members would be appropriately resized in subsequent cycles of analysis of a more detailed study.

Composite concepts were studied at two different times during the arrow wing contract. During Task II three concepts (sheet-stiffener, stiffened thin honeycomb sandwich, and conventional sandwich panels) were used in exploratory design studies in fuselage and skin panels. The material combinations considered in these studies were: titanium stiffeners reinforced with borsic/aluminum, borsic/aluminum composite skins, sandwich panels composed of borsic/aluminum surfaces and titanium honeycomb core, and sandwich panels with graphite/PPQ surfaces and titanium honeycomb core. These concepts were used in the design of wing and fuselage panels for comparison with baseline titanium designs, and the most efficient concepts were identified.

Early in Task III, the material selection task was reopened and expanded to include consideration of polyimide resin, since significant progress had been made in solving the manufacturing problems associated with this organic matrix material. Only the conventional sandwich concept was considered at this stage, since that concept had been shown to be most efficient for all of the materials considered. The following sections describe these activities in greater detail.

CONCEPT SELECTION

Three advanced composite concepts were studied in Section 14 of reference 3-1. These consisted of skin stiffener, stiffened thin sandwich, and conventional sandwich designs. Initially, each concept was studied for application to a body panel at point 5, and upper and lower wing panels at point 269, as shown in figure 3-1. The study was limited to these two locations so that each concept could be developed in sufficient detail to establish feasibility for practical component design. This initial comparison was based on the design of full-panels for each application. Each concept was designed using borsic/aluminum, and the conventional sandwich was also designed using the graphite/PPQ material for the face sheets. A unit weight comparison of the three concepts using borsic/aluminum is presented in figure 3-2. This shows that the conventional sandwich panel is lightest in weight. It should be noted that three of the wing surface panels have been evaluated with two different shear allowables since the preliminary published data contained inconsistent low values. Following consultation with NASA personnel, unpublished test data, providing justification for the higher theoretical allowables, were obtained, as explained in Section 2. These panels were designed for the loads presented in table 3-1.

The three types of skin panels designed for the wing lower surface are shown in figures 3-3, 3-4, 3-5 and 3-6. The baseline concept is the integrally machined and welded titanium skin and stiffener design shown in figure 3-7. Comparative weights of these designs are presented in figure 3-8, showing that

the graphite/PPQ conventional sandwich is lightest and the borsic/aluminum conventional sandwich is next lightest of the three designs.

Skin panel designs for the wing upper surface are also shown in figures 3-3, 3-4, 3-5 and 3-6. The baseline concept for comparison is the conventional aluminum brazed titanium honeycomb sandwich design presented in figure 3-9. The weight comparison of these designs is presented in figure 3-10, showing that graphite/PPQ conventional sandwich has a significant weight advantage over the others.

Fuselage skin panel designs are presented in figures 3-11, 3-12, 3-13, and 3-14. The baseline panel design is the titanium skin and stiffener panel with 17.25 in. frame spacing, shown in figure 3-15. Comparative weights of these designs are presented in figure 3-16, showing that the conventional graphite/PPQ sandwich is lightest with the conventional borsic/aluminum sandwich second. Based on these comparisons, it is clear that the graphite/PPQ conventional sandwich is the lightest design concept for all locations considered. This concept was recommended for further consideration.

MATERIAL SELECTION

Initially, interest centered on borsic-aluminum since this material showed great promise of maintaining significant strength at the temperatures at which the arrow wing supersonic cruise aircraft operates. Consequently, borsic/aluminum was selected for evaluation on the first set of three concepts: skin-stringer, stiffened thin sandwich, and conventional sandwich.

Subsequently, however, interest in the organic matrix increased because of the much greater ease of fabrication, and the lower thermal conductivity. Fuel heating is a critical design consideration for supersonic cruise since the fuel is used as a heat sink for the environmental control system and other heat sources within the airplane. Because of this requirement, and the high conductance of aluminum brazed material, insulation is required for aluminum brazed titanium honeycomb sandwich panels. The use of aluminum matrix material for wing panel face sheets would provide a further increase in thermal conductance of the panels. The organic materials have lower conductivity and, therefore, will alleviate the thermal problem. There has been only limited development work on high temperature polymers, with the polyimide resins getting the greatest emphasis currently, and there is considerable promise that polyimide development problems will be overcome. The development risk is offset by the attractive characteristics of relatively low cost, low density, high shear strength, and moderate manufacturing complexity, compared to the metal matrix composites.

The four materials selected for evaluation were:

- High strength graphite/polyimide
- High modulus graphite/polyimide
- Boron/polyimide, and
- Borsic/aluminum

Design allowable strength, and typical elastic and physical properties, shown in Section 1, were projected through ten years of additional development. The material properties resulting from this projection were submitted to and approved by NASA Langley Research Center. Based on these

data, specific strengths and stiffnesses were compared, as shown in tables 3-2 and 3-3. The high strength graphite/polyimide and the boron/polyimide were selected for further study on this basis.

Tables 3-4 and 3-5 show the comparison of the specific properties for the selected candidates at room temperature and at 450°F, indicating generally that graphite has higher specific strength while boron has higher specific stiffnesses. These materials were next used in the design of skins for honeycomb panels to provide a broader basis for engineering evaluation.

The following ground rules were adopted for this study:

- (1) Layups were designed to be fiber-critical
- (2) All laminates were designed as balanced, symmetrical layups.

Ground rule (1) is consistent with expected improvements in properties of matrix materials to be achieved prior to 1986. Ground rule (2) was adopted to avoid unsymmetrical deformations due to curing and to the application of external loads. Minimum gage criteria were established to provide acceptable practical durability from operational considerations.

The minimum gages selected for the Task II titanium honeycomb skins were as follows:

	Wing Upper Surface	Wing Lower Surface
Inner Skin	.010	.010
Outer Skin	.015	.020

These values were based upon experience and stemmed from consideration of:

Walking loads, material handling, hail damage, runway debris, practical fabrication limits, and lightning strike.

It was recognized that the advanced composites are more susceptible to damage from impact and in general less forgiving than the conventional metals. Because of this, a somewhat arbitrary decision was made to use minimum gages such that the local moment of inertia of each skin would be four times that of the titanium equivalent. Since

$$I = \frac{b t^3}{12}$$

it follows that

$$4 (t_{\text{titanium}})^3 = (t_{\text{adv. composite}})^3$$

$$\frac{t_{\text{adv. composite}}}{t_{\text{titanium}}} = \sqrt[3]{4} = 1.5874 \approx 1.6$$

The resulting minimum gages for the advanced composites were:

	Wing Upper Surface	Wing Lower Surface
Inner Skin	.016	.016
Outer Skin	.024	.032

A second procedure for estimating minimum gages is as follows: The ply thicknesses expected to be available by 1986 for these materials are:

Boron/Polyimide
 5.2 mil, 7.0 mil and thicker
 H.S. graphite/polyimide
 2 mil, 3 mil, 4 mil and thicker

In order to comply with the indicated ground rules, the following layups were established for minimum gage areas:

Boron/Polyimide
[0/±45/90]_S
 7 plies x .0052 = .0364

This resulted in the following:

	Wing Upper Surface	Wing Lower Surface
Inner Skin	.0364	.0364
Outer Skin	.0364	.0364

Graphite/Polyimide
[0/±45/90]_S
 8 plies x .002, .003 and .004 = .016, .024 and .032

This resulted in the following:

	Wing Upper Surface	Wing Lower Surface
Inner Skin	.016	.016
Outer Skin	.024	.032

A comparison was then made of the skin weights per square foot for the titanium, boron/polyimide and H.S. graphite/polyimide. Weight densities of 0.16 lb/in³, .0725 lb/in³ and .056 lb/in³, respectively, were used.

The resulting weights are presented in figure 3-17 and show the H.S. graphite/polyimide to be significantly lighter.

A review of the wing structure that was resized during Task II using titanium showed that approximately 50% of the area was minimum gage. The resized area lies generally between the rear spar and the leading edge spar and between the side of body and the wing mounted fin. The control surfaces and the fixed leading edge structure were minimum gage.

Using H.S. graphite, and with the anticipated change in loads, it is estimated that 30-35% of the resize portion will be minimum gage. Using boron/polyimide it is estimated that 70% of this area would be minimum gage.

For structure designed by tension loads it is obvious, from a comparison of specific tensile strengths, that the H.S. graphite will be the lightest. This is true even after restricting the allowable strain to that of titanium.

In areas where loads require less than minimum gage it is again apparent that H.S. graphite will be the lightest.

A final parametric comparison was made to establish which of the materials would result in the lightest cover panels to resist spanwise compression, chordwise compression and shear loads considering typical layups and ply orientations. Figure 3-18 compares the weight of boron and graphite layups designed to carry the indicated spanwise compression loads. From this figure, it can be seen that the high strength graphite results in lighter panels across the complete loads range. Figure 3-19 presents similar data for the range of chordwise compression loads, with a similar conclusion. Figure 3-20 is a similar presentation for shear loads. The graphite layups again are significantly lighter than the boron layups.

Based on these data and analyses, the high strength graphite fibers are selected for use in the conventional sandwich structural panels.

REFERENCES

- 3-1 Boeing Staff: *Study of Structural Design Concepts for an Arrow Wing Supersonic Transport Configuration*. NASA Langley Research Center, CR 132576-1 and -2, 1976.

Table 3-1.— Control Point Loads

Body: control point 5 (lower body skin panel)

Design condition	
N_x	(11.92 kips/in.)
Pressure	(10.78 lb/in ²)
Temperature	(450° F)

Wing: control point 269

Component	Design condition	
Upper panel	N_x	-10.9 kips/in.
	N_y	- 1.48 kips/in.
	N_{xy}	6.32 kips/in.
	Temperature	250° F
Lower panel	N_x	11.82 kips/in.
	N_y	2.04 kips/in.
	N_{xy}	6.89 kips/in.
	Temperature	Room temperature

Table 3-2.—Specific Mechanical Properties

	F_{tu}/ρ in $\times 10^3$		F_{cu}/ρ in $\times 10^3$		F_{su}/ρ in $\times 10^3$	E_t/ρ in $\times 10^6$		E_c/ρ in $\times 10^6$		G/ρ in $\times 10^6$
	L	T	L	T	LT	L	T	L	T	LT
High strength graphite, $\rho = 0.056 \text{ lbs/in}^3$	5268	298	5179	293	371	357	20	357	20	13
High modulus graphite, $\rho = 0.058 \text{ lbs/in}^3$	2552	116	2172	98	107	690	31	690	31	17.0
Boron/polyimide, $\rho = 0.0725 \text{ lbs/in}^3$	2690	201	4828	364	114	441	33	441	33	9.0
Borsic/aluminum, $\rho = 0.098 \text{ lbs/in}^3$	1990	177	3592	317	83	327	29	327	29	7.0

Table 3-3.—Specific Mechanical Properties [$\pm 45^\circ$] S Layups

Material	F_{tu}/ρ in. x 10^3	F_{cu}/ρ in. x 10^3	F_{su}/ρ in. x 10^3	E/ρ in. x 10^6	G/ρ in. x 10^6
High strength graphite, $\rho = 0.056 \text{ lbs/in}^3$	679	670	2643	46	91
High modulus graphite, $\rho = 0.058 \text{ lbs/in}^3$	222	190	1109	60	176
Boron/polyimide, $\rho = 0.0725 \text{ lbs/in}^3$	210	379	1407	34	116
Borsic aluminum, $\rho = 0.098 \text{ lbs/in}^3$	149	269	1031	24	85

Table 3-4.—Mechanical Properties and Specific Mechanical Properties, Room Temperature

[0]

Material	F_{tu} F_{tu}/ρ		F_{cu} F_{cu}/ρ		F_{su} F_{su}/ρ	E E/ρ		G G/ρ
	L	T	L	T	LT	L	T	LT
	ksi in. x 10 ³	ksi in. x 10 ³	ksi in. x 10 ³	ksi in. x 10 ³	ksi in. x 10 ³	10 ⁶ psi in. x 10 ⁶	10 ⁶ psi in. x 10 ⁶	10 ⁶ psi in. x 10 ⁶
High strength graphite	295.0 5268	16.7 298	290.0 5179	16.4 293	20.8 371	20.0 357	1.1 20	0.72 13
Boron/polyimide	195.0 2690	14.6 201	350.0 4828	26.4 364	8.3 114	32.0 441	2.4 33	0.68 9

[±45]

Material	F_{tu} F_{tu}/ρ	F_{cu} F_{cu}/ρ	F_{su} F_{su}/ρ	E E/ρ	G G/ρ
	ksi in. x 10 ³	ksi in. x 10 ³	ksi in. x 10 ³	10 ⁶ psi in. x 10 ⁶	10 ⁶ psi in. x 10 ⁶
High strength graphite	38.0 679	37.4 670	148.0 2643	2.6 46	5.1 91
Boron/polyimide	15.2 210	27.5 379	102.0 1407	2.5 34	8.4 116

ORIGINAL PAGE IS
OF POOR QUALITY

Table 3-5.—Mechanical Properties and Specific Mechanical Properties, 450° F

[0]

Material	F_{tu} F_{tu}/ρ		F_{cu} F_{cu}/ρ		F_{su} F_{su}/ρ	E E/ρ		G G/ρ
	L	T	L	T	LT	L	T	G
	ksi in. x 10 ³	ksi in. x 10 ³	ksi in. x 10 ³	ksi in. x 10 ³	ksi in. x 10 ³	10 ⁶ psi in. x 10 ⁶	10 ⁶ psi in. x 10 ⁶	10 ⁶ psi in. x 10 ⁶
High strength graphite	265.0 4732	13.7 245	260.0 4643	13.4 239	12.0 214	20.0 357	1.0 18	0.46 8.25
Boron/polyimide	175.0 2414	13.0 179	315.0 4345	23.1 319	7.1 98	30.0 414	2.2 30	0.6 8.28

[±45]

Material	F_{tu} F_{tu}/ρ	F_{cu} F_{cu}/ρ	F_{su} F_{su}/ρ	E E/ρ	G G/ρ
	ksi in. x 10 ³	ksi in. x 10 ³	ksi in. x 10 ³	10 ⁶ psi in. x 10 ⁶	10 ⁶ psi in. x 10 ⁶
High strength graphite	22.5 402	22.1 395	132.6 2368	1.7 30	5.1 91
Boron/polyimide	13.6 188	24.1 332	92.0 1269	2.3 32	7.8 108

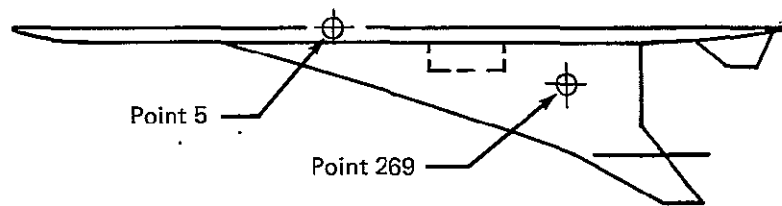
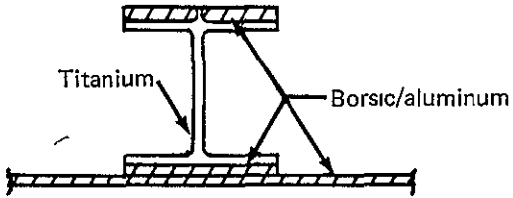
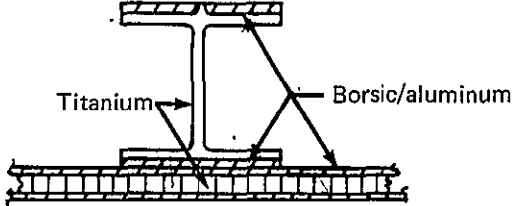
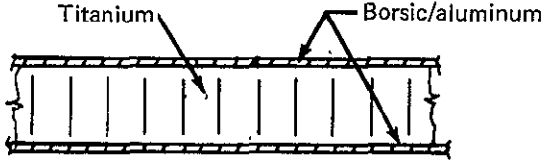


Figure 3-1.—Wing and Body Control Points

ORIGINAL PAGE IS
OF POOR QUALITY

Structural concept	Unit weight, lb/ft ²		
	Body	Wing upper surface	Wing lower surface
	4.34 (Includes 0.036 braze)	4.29 (Includes 0.020 braze)	4.24 3.46 ^a (Includes 0.017 braze)
	4.29 (Includes 0.104 core 0.219 braze)	3.95 3.37 ^a (Includes 0.143 core 0.176 braze)	4.40 (Includes 0.056 core 0.124 braze)
	3.61 (Includes 0.681 core 0.348 braze)	3.61 (Includes 0.519 core 0.248 braze)	4.01 3.42 ^a (Includes 0.384 core 0.202 braze)

Note: Indicated weights do not include thermal insulation.

^aHigh shear allowable derived from NASA-LRC tests.

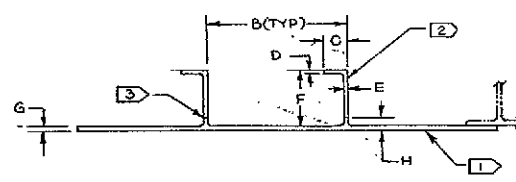
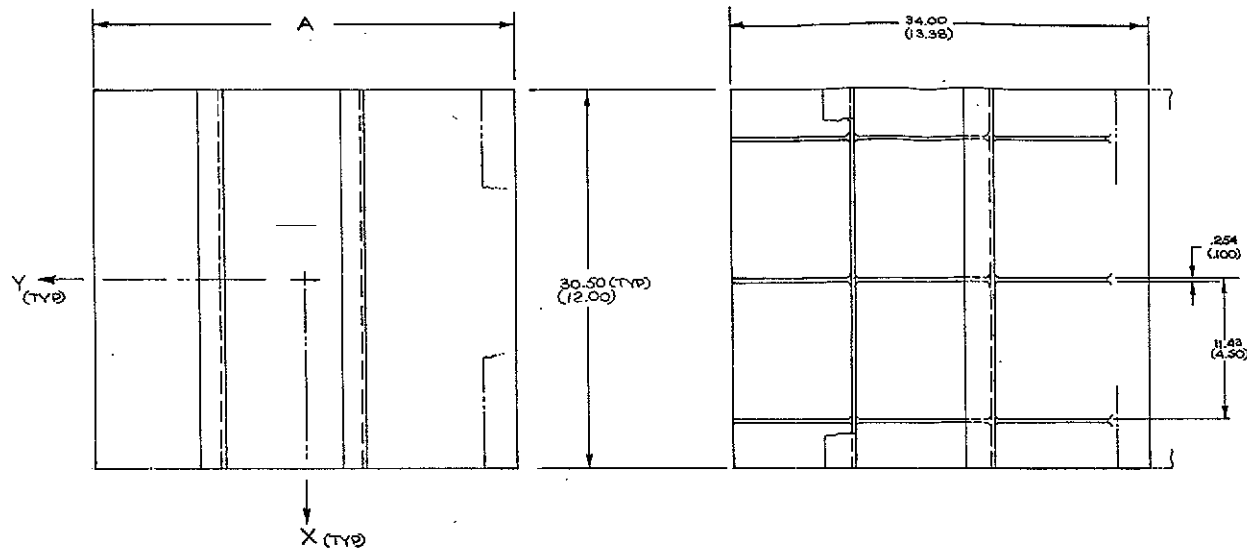
Figure 3-2.—Borsic/Aluminum Concept Comparison

FOLDOUT FRAME

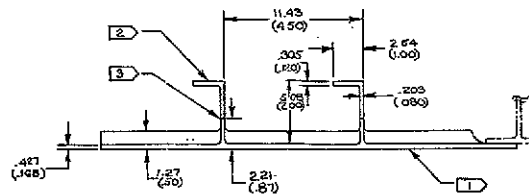
PRECEDING PAGE BLANK NOT FRAMED

FOLDOUT FRAME

2



PT 269 LWR SURF
PT 431 UPR+ LWR SURF



PT. 269 UPR SURF

POINT	A	B	C	D	E	F	G	H	
249									UPPER PANEL
269	34.00 (13.38)	11.43 (4.50)	1.91 (.75)	1.25 (.50)	1.78 (.70)	2.45 (.96)	3.17 (1.25)	2.25 (.88)	UPPER PANEL
431	33.03 (15.97)	10.35 (4.07)	2.54 (1.00)	4.57 (1.80)	3.03 (1.20)	5.08 (2.00)	5.46 (2.15)	1.423 (.560)	UPPER PANEL
									LOWER PANEL

- 3 WELD PER BAC 5547 CLASS A
- 2 MACHINED FROM GAL-4V EXTR PER BMS 7-44 CLASS B
- 1 GAL-4V COND I

SEE AJS-100 FOR PANEL POINT LOCATIONS
BASIC DIMENSIONS - CM
() DIMENSIONS - IN.

REF. WING DRAWING AWS 108

Figure 3-7.—Baseline, Integrally Machined and Welded Titanium Skin and Stiffeners

Structural arrangement

(a) Figure 3-5—Bsc/Al skin
Ti core
(2 to 17 ply skin assembly)

(b) Figure 3-5—Bsc/Al skin
Ti core
(2 to 14 ply skin assembly)

(c) Figure 3-6—graphite/PPQ skin
Ti core
(2 to 19 ply skin assembly)

(d) Figure 3-7—baseline
integrally machined and
welded Ti skin and stiffener

(e) Figure 3-3—Bsc/Al skin
reinforced Ti stiffener
(21 ply skin assembly)

(f) Figure 3-3—Bsc/Al skin
reinforced Ti stiffener
(29 ply skin assembly)

(g) Figure 3-4—Bsc/Al skin
thin Ti core—reinforced Ti stiffener
(2 to 15 ply skin assembly)
(a) High shear allowable
(b) Adhesive bonding
(c) Skin reinforcement

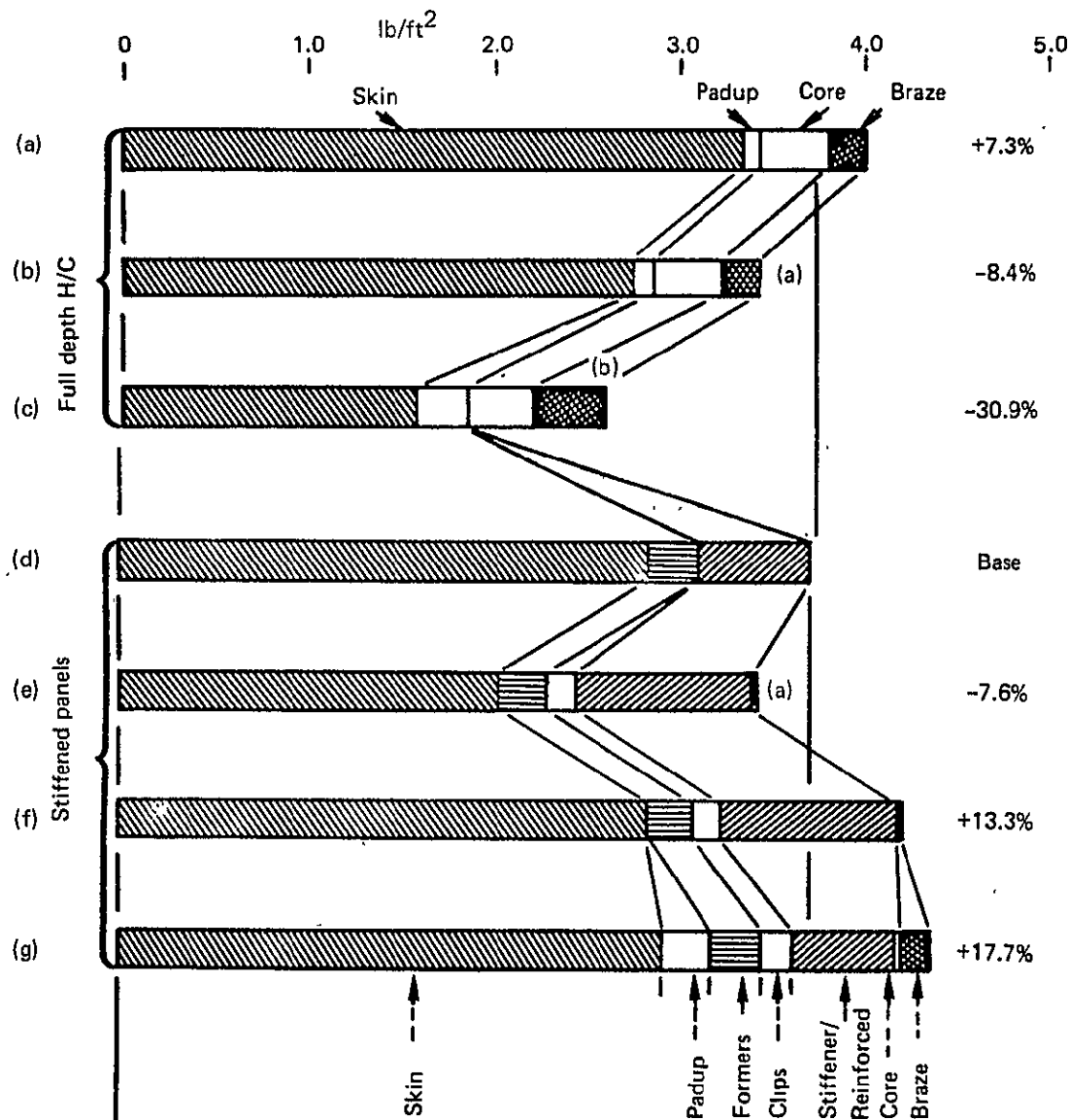
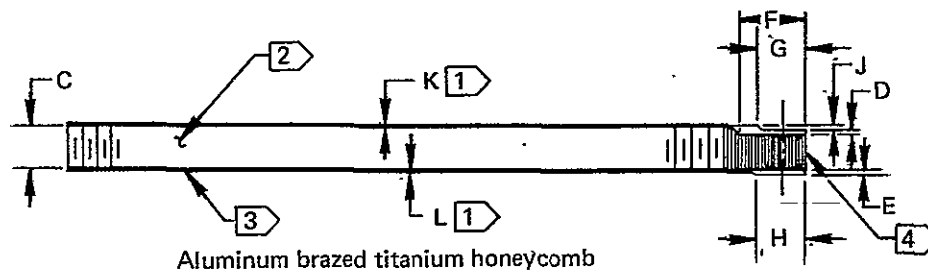
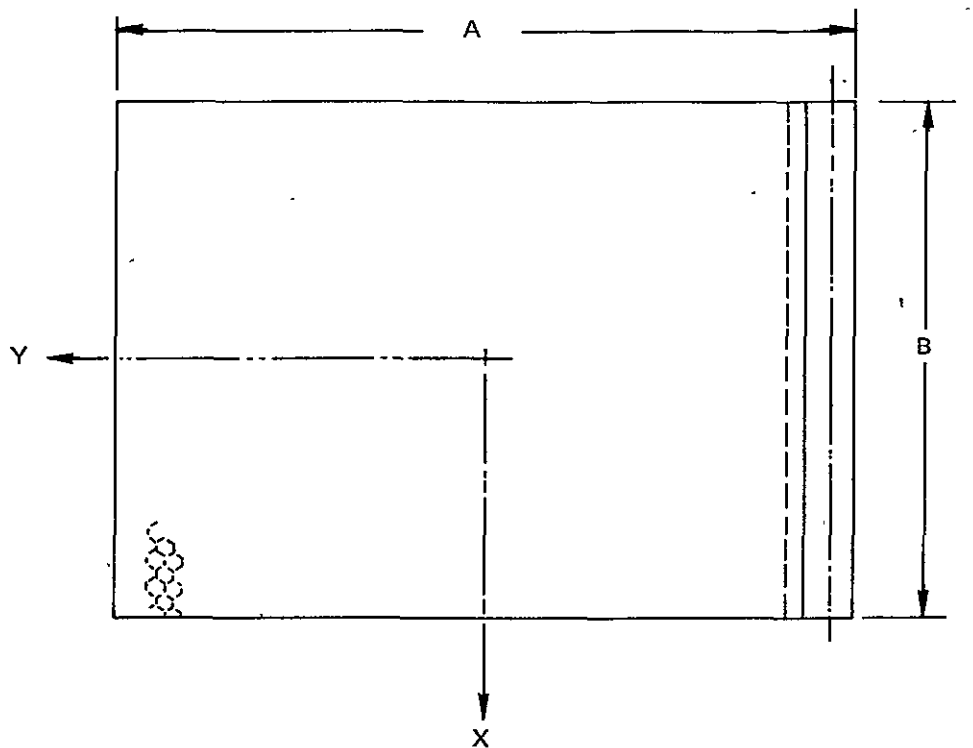


Figure 3-6.—Weight Comparison, Advanced Structural Concepts, Wing Lower Surface

REPRODUCING PAGE BLANK NOT FILLED



Basic dimensions—cm

() dimensions—in.

4 464.9 kg/m³ (29 lb/ft³) SS2-60 core Ti-6Al-4V

3 Braze

2 78.50 kg/m³ (4.9 lb/ft³)—SCA-20 core Ti-3Al-2.5V

1 Ti-6Al-4V Cond I

Point	A	B	C	D	E	F	G	H	J	K	L	
249	44.0 (17.32)	30.5 (12.00)	2.54 (1.00)	0.153 (0.060)	0.153 (0.060)	3.80 (1.50)	2.62 (1.03)	3.05 (1.20)	0.228 (0.090)	0.038 (0.015)	0.025 (0.010)	Upr Surf
										0.051 (0.020)	0.025 (0.010)	Lwr Surf
269	34.00 (13.38)	30.50 (12.00)	2.54 (1.00)	0.221 (0.087)	0.221 (0.087)	4.32 (1.70)	3.05 (1.20)	3.05 (1.20)	0.305 (0.120)	0.221 (0.087)	0.221 (0.087)	Upr Surf
										0.152 (0.060)	0.152 (0.060)	Lwr Surf
431	39.03 (15.37)	30.50 (12.00)	2.54 (1.00)	0.246 (0.097)	0.246 (0.097)	4.32 (1.70)	3.05 (1.20)	3.05 (1.20)	0.305 (0.120)	0.246 (0.097)	0.246 (0.097)	Upr Surf
										0.224 (0.088)	0.224 (0.088)	Lwr Surf

Figure 3-9.—Wing Skin Panel, Al Brazed Titanium Honeycomb

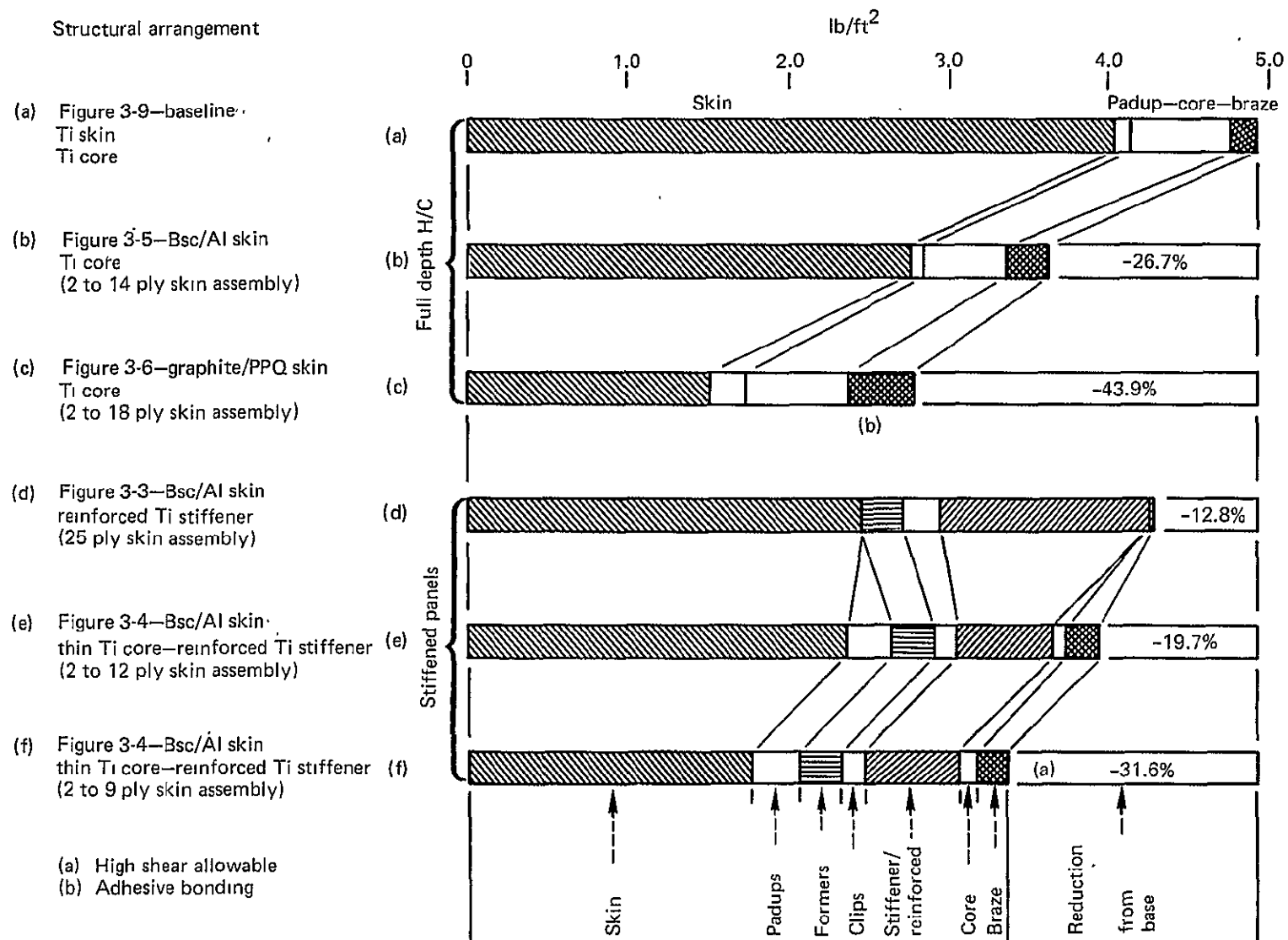


Figure 3-10.—Weight Comparison, Advanced Structural Concepts, Wing Upper Surface

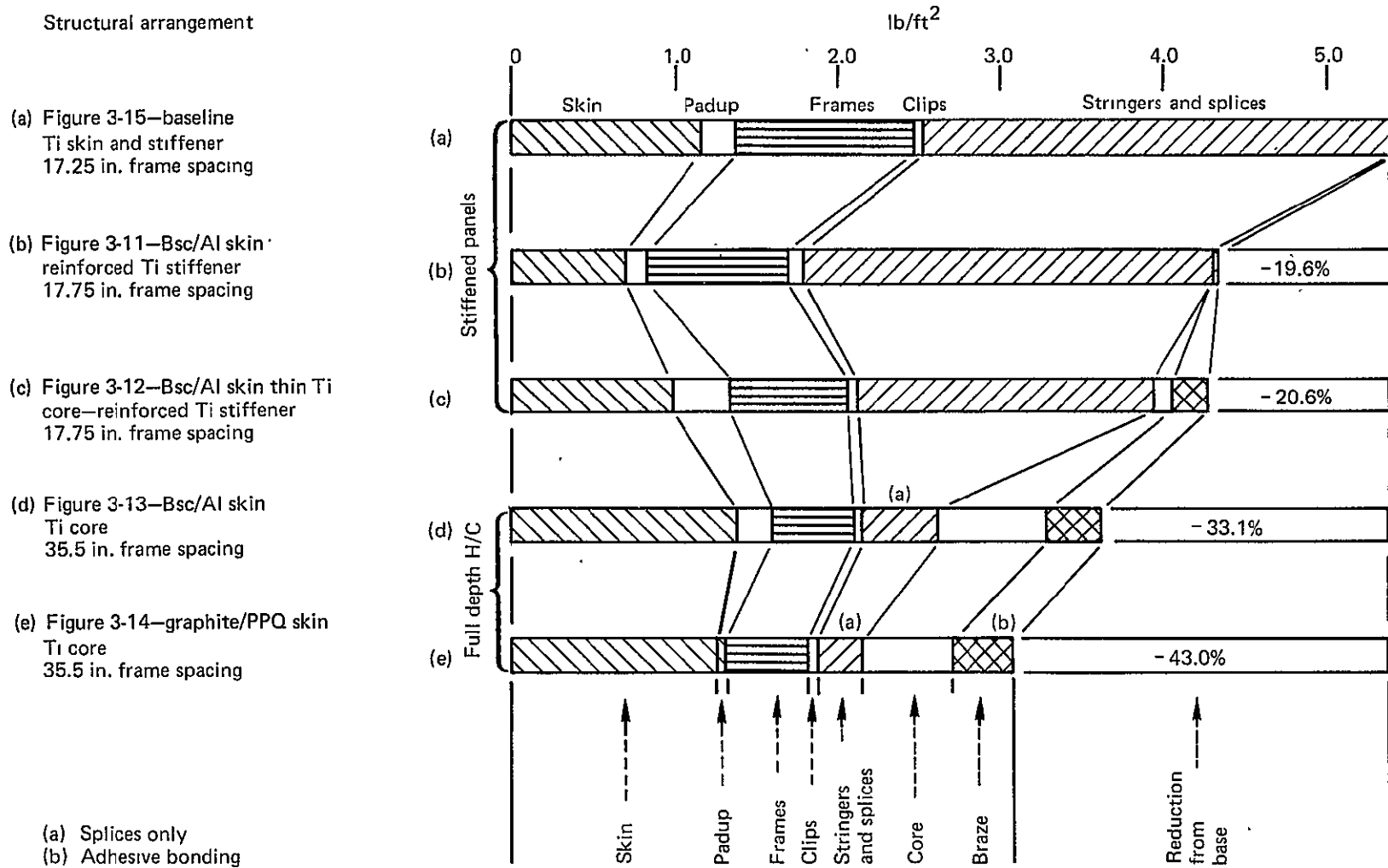


Figure 3-16.—Weight Comparison, Advanced Structural Concepts, Body

Material	Upper surface			Lower surface		
	Skin gage		Weight, lb/ft ²	Skin gage		Weight, lb/ft ²
	Inner	Outer		Inner	Outer	
Titanium	0.010	0.015	0.576	0.010	0.020	0.691
H/S graphite/polyimide, (0/±45/90) _S	0.016	0.024	0.323	0.016	0.032	0.387
Boron/polyimide, (0/±45/90) _S	0.0364	0.0364	0.76	0.0364	0.0364	0.76

Based on:

Minimum gage of tapes available by 1986

Graphite/polyimide 2 mil/ply

Boron/polyimide 5.2 mil/ply

Minimum gage for practical considerations

Graphite/polyimide

3 mil/ply upper-surface outer skins

4 mil/ply lower surface outer skins

Figure 3-17.—Minimum Gage Considerations

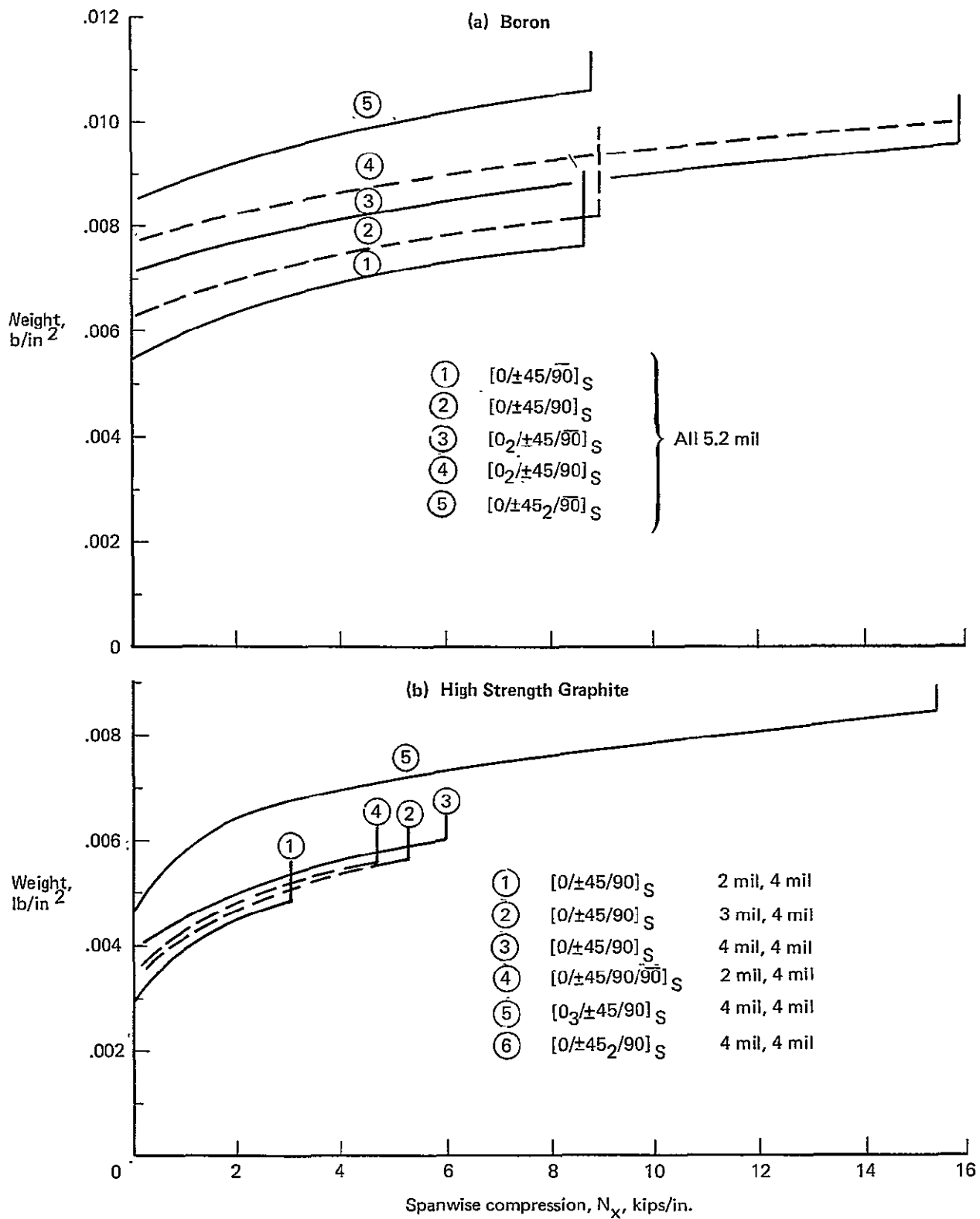


Figure 3-18.—Panel Weights for Spanwise Compression Loading

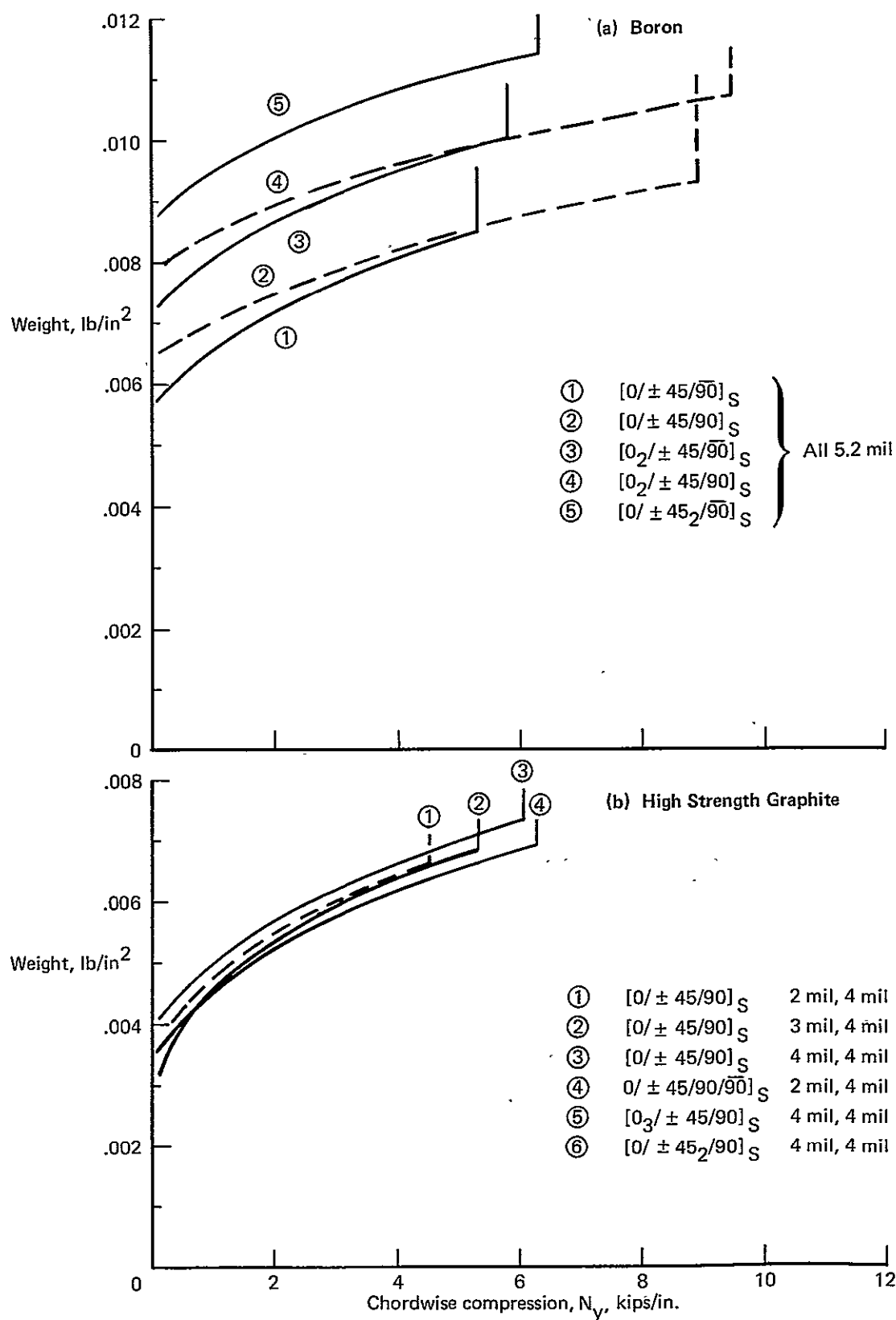


Figure 3-19.—Panel Weights for Chordwise Loading

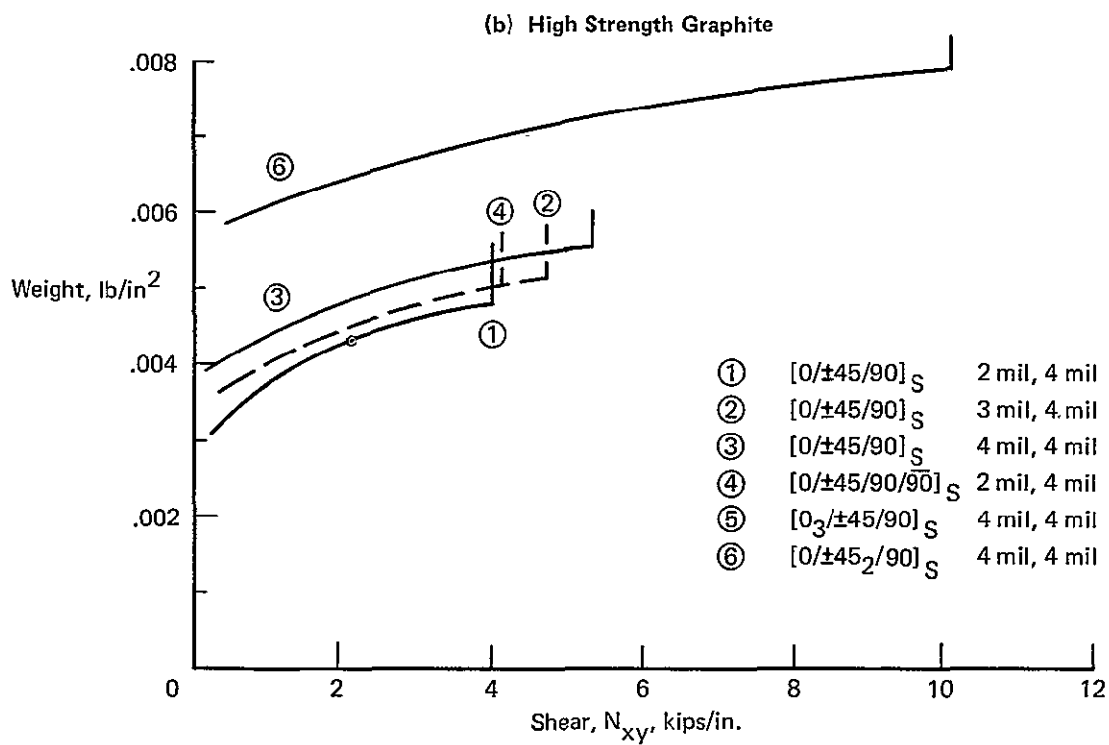
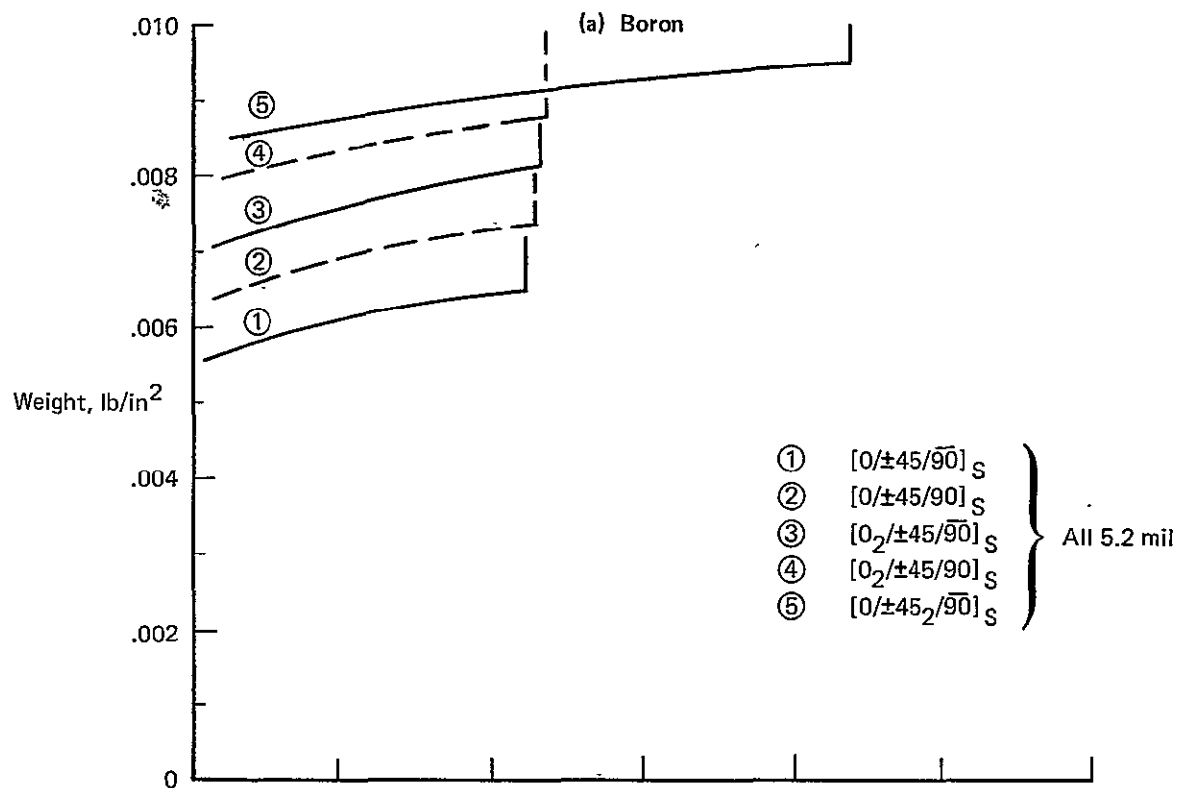


Figure 3-20.—Panel Weights for Shear Loading

SECTION 4

~~REPRODUCING PAGE BLANK NOT PERMITTED~~

PANEL DESIGN

by

C. L. ABELL

~~REPRODUCING PAGE BLANK NOT PERMITTED~~

CONTENTS

Page

WING PANEL DESIGN OBJECTIVES	101
PANEL SELECTION	101
PANEL LOADS	101
COMPOSITE WING PANEL DESIGN	102
ALUMINUM BRAZED TITANIUM WING PANEL DESIGN	105
REFERENCES	107

FIGURES

No.		Page
4-1	Design for Nonoptimum Factors, Panel Locations	108
4-2	Lower Wing Panel, Light Gage Bonded Graphite/Polyimide Sandwich, Model 969-512B	109
4-3	Lower Wing Panel, Medium Gage Bonded Graphite/Polyimide Sandwich, Model 969-512B	111
4-4	Lower Wing Panel, Heavy Gage Bonded Graphite/Polyimide Sandwich, Model 969-512B	113
4-5	Upper Wing Panel, Medium Gage Bonded Graphite/Polyimide Sandwich, Model 969-512B	115
4-6	Upper Wing Panel, Heavy Gage Bonded Graphite/Polyimide Sandwich, Model 969-512B	117
4-7	Composite Skin Layup Diagram, Minimum Gage, Lower Wing Panel	119
4-8	Composite Skin Layup Diagram, Medium Gage, Lower Wing Panel	120
4-9	Composite Skin Layup Diagram, Heavy Gage, Lower Wing Panel	121
4-10	Composite Skin Layup Diagram, Medium Gage, Upper Wing Panel	122
4-11	Composite Skin Layup Diagram, Heavy Gage, Upper Wing Panel	123
4-12	Lower Wing Panel, Light Gage Brazed-Titanium Sandwich, Model 969-512B	125
4-13	Lower Wing Panel, Medium Gage Brazed-Titanium Sandwich, Model 969-512B	127
4-14	Lower Wing Panel, Heavy Gage Brazed-Titanium Sandwich, Model 969-512B	129
4-15	Upper Wing Panel, Medium Gage Brazed-Titanium Sandwich, Model 969-512B	131
4-16	Upper Wing Panel, Heavy Gage Brazed-Titanium Sandwich, Model 969-512B	133

SYMBOLS

N_x	Stress resultant in the x direction
N_y	Stress resultant in the y direction
N_{xy}	Shear Stress resultant

WING PANEL DESIGN OBJECTIVES

There were two primary objectives to be achieved in the panel design effort: to evaluate and identify problem areas; and to design in detail the panel edges and joint. To evaluate and identify problem areas, it was necessary to develop and display a rational detail design approach using the selected 1986 high strength graphite/polyimide composite in the bonded honeycomb sandwich wing panels. Detail designs relating the panel edge and joint features to the basic panel requirements were necessary to support the development of theoretical-to-actual factors for weight calculations.

It was also necessary to develop and display aluminum brazed titanium honeycomb sandwich panel designs, equivalent in their response to strength and environmental requirements, to relate the composite design to the titanium data base. A more detailed discussion of the development of theoretical-to-actual factors may be found in Section 5.

PANEL SELECTION

Five specific primary wing panels were selected on model 969-512B for the presentation of the detail designs. The 969-512B configuration was developed in the preceding study, as described in reference 4-1. Panel locations were selected to cover a representative load range. They include a lower surface minimum gage panel, upper and lower surface intermediate gage panels and upper and lower surface heavy gage panels. Figure 4-1 shows the locations of the representative panels.

It should be noted that the structural arrangement for Model 969-512B was developed with titanium as the baseline structural material. It does not necessarily follow that it is as near to optimum if composite materials were used. Additional improvement in the areas of weight and producibility should be attainable. However, reconfiguration of the structural arrangement to further exploit the composite materials is considered beyond the scope of this study and should be the subject of future work.

PANEL LOADS

The loads for the wing panel design effort were taken directly from the final Task II analysis in reference 4-1 with no adjustment for differences in static aeroelastic deformation between the Task II titanium aircraft and the Task III composite aircraft. In Task II there were specified spar loads and panel loads. This effort used the panel loads with the assumption that a difference in spar area to panel area ratio would not cause a significant change in the panel loads or effect the theoretical-to-actual factor.

Each wing panel covered an area represented by four to seven "cover plates" in the math model. Twenty-five load cases were evaluated for their criticality with regard to combined stresses, buckling interaction, and critical joint stress resultants. Critical N_x , N_y , and N_{xy} loads were identified for each "cover plate." Both sets of panels were designed to these loads.

COMPOSITE WING PANEL DESIGN

Figures 4-2, 4-3, 4-4, 4-5, and 4-6 show the detail design for the five representative composite panels. The detail shown is limited to the basic panels and their interfaces at joints and supports. Details are omitted with regard to corners, concentrated load points and access provisions because they depend on the detail design of the inner structure and systems which is a subject outside the scope of this effort. However, the aluminum-brazed titanium panels were given the same treatment in this respect and can be related to the titanium data base which does include all the nonoptimum features.

The graphite/polyimide honeycomb panels were analyzed according to procedures outlined in Section 6 of this report.

COMPOSITE SKINS

The basic inner and outer skins are fiber critical laminates, made of 1986 high strength graphite/polyimide unidirectional tapes having orientations of $[0]$, $[\pm 45]$ and $[90]$. These tapes have a volume fraction of .6 and are laid up in an order that is symmetrical about the centerline of each skin thickness. The tapes are .004 in. thick in most areas, however, .002 in. thick tapes are used in the upper and lower panel inner skins in the minimum gage and low load areas. Also, .003 in. thick tapes are used in the upper panel outer skins in minimum gage and low load areas.

The skins are bonded to the core using a polyimide adhesive. The adhesive formulation is based upon improved addition reaction polyimide resins which have thermal and processing characteristics superior to present systems. The weight of the adhesive is assumed to be .085 lb/ft² per bond line in the skin to core application.

The load in each "cover plate" was considered in arriving at layups that were practical for each wing panel. Skins were tapered to meet changing load requirements by adding or terminating lamina symmetrically in each skin. Terminations were staggered to minimize step heights.

Figures 4-7, 4-8, 4-9, 4-10 and 4-11 show the layup order of the five representative panels in more detail. No reflection of contour, pad up or thickness relationships is intended. The titanium interleaves exist only at joints and supports and are indicated to show only relative location with respect to the basic composite laminae. For panel edge design details see figures 4-2, 4-3, 4-4, 4-5 and 4-6.

The external lamina for each skin was consistently oriented in the spanwise direction $[0]$. The orientations of the remaining laminae were alternated as far as possible to reduce the chances of suffering damage to all the laminae of a given orientation in the event of a surface scratch.

COMPOSITE CORE

The honeycomb core used consists of 1986 high strength graphite fiber reinforcement in a polyimide matrix. The fiber orientation is tailored for different applications of shear and tension-compression to optimize design. Shear applications will rely on $[\pm 45]$ fiber orientation. Tension-compression applications will utilize $[0]$ and $[90]$ oriented fiber. A density of 3.5 lb/ft³ was selected for the basic center core for all panels. For a discussion of core allowables see Section 2. A discussion of panel thickness follows.

During the process of selecting the structural concept and the material to be used (discussed in more detail in Section 3) an evaluation of buckling strength versus core thickness was made. Although each specific layup was different, the general conclusions reached were: (1) 1 in. core was required to prevent shear buckling at ultimate allowable shear stress. (2) 1.5 in. core was required to prevent spanwise buckling at ultimate allowable spanwise compression stress. (3) 2.0 in. core was required to prevent chordwise buckling at ultimate allowable chordwise compression stress.

The majority of the wing upper surface is designed by high spanwise compression, medium shear and low chordwise compression loading.

Significant chordwise compression strains exist near the body on the wing lower surface and on both wing surfaces near the wing ribs. Large portions of the wing lower surface skins are established by combined tension and shear stresses but the core thickness is still established by the wing down bending conditions which are basically comp-comp-shear. A cursory examination of the wing upper surface was made utilizing the internal load distributions resulting from Task II. Core thicknesses over 1.5 in. would add more core weight than it would save skin weight. Core thickness less than 1.5 in. would add more skin weight than it would save core weight. The complications involved in changing core thicknesses are many and varied and result in weight penalties.

The allowable chordwise (and spanwise) strain in the covers was reduced to be compatible with the titanium ribs and spars. A 1.5 in. core was required to prevent buckling at this chordwise strain.

For these reasons, 1.5 in. core was selected for the entire wing primary structure. It is possible, though only at the expense of very many manhours, to save a small percentage of the core weight by further optimizing, but it would not be a significant amount.

JOINTS AND SUPPORTS

All load conditions were reviewed in consideration of the joint design requirements. Critical joint loads were not necessarily found to be the same as the critical panel loads. Fastener sizes and spacing were picked to meet the criteria for loads, fail safety and fuel containment. In the minimum gage area, 3/16 in. diameter fasteners were adequate. In the remaining areas, one and sometimes two rows of 1/4 in. diameter fasteners were required.

In the region of the fasteners, titanium interleaves were used to increase the bearing strength and to bridge the load between fasteners. The widths of these interleaves are varied in increments to achieve the effect of a taper. The joints were analyzed for ultimate load utilizing only the titanium interleaves for bearing. Fail safety analysis considered the interleaves plus the composite for bearing.

Also in the region of the fasteners in the spanwise joints, the unidirectional laminae having [0] orientation were replaced with [± 45] woven graphite/polyimide fabric to reduce the stress concentration at fastener holes.

The skin thicknesses at the panel edges are made up of the basic panel laminae plus the sum of the titanium interleaves plus the polyimide adhesive required to bond the interleaves to the composite laminae. The relative location of the interleaves to the specific laminae is shown in figures 4-7, 4-8, 4-9, 4-10, and 4-11. The locations were specifically picked to provide more uniform load distribution to the interleaves with a minimum of interlaminar shear. The adhesive in this application is .0035 in.

thick and weighs $.03 \text{ lb/ft}^2$ per bond line. In addition to the above, the inner skin pad up includes an integral shim made of $[\pm 45]$ woven graphite/polyimide fabric to account for panel thickness tolerance. The shim includes a machining allowance of 0.03 in. over and above the nominal height. The shim is ground down to achieve a constant panel thickness which will facilitate matching the panel to the inner structure and adjacent panels at installation.

The panel edge core is similar to the center core, but is more dense in order to react the bolt clamp up forces. Core having a density of 7 lb/ft^3 is used with $3/16$ in. diameter bolts and core having a density of 14 lb/ft^3 is used with $1/4$ in. diameter bolts.

The core splice locations are such that all the skin eccentricities occur in the dense core region. The polyimide core splice adhesive is a formulation very similar to the structural adhesive used in the laminated and sandwich areas. Handling and processing is comparable to present systems. The average core splice bond line thickness is assumed to be .10 in. with a density of 30 lb/ft^3 . High temperature stable potting material used to seal the edges of the honeycomb sandwich core is a polyimide based structural foam with a formulation very similar to the bonding and core splice adhesive. For weight estimating purposes, an average thickness of .1 in. and a density of 44 lb/ft^3 was assumed.

OTHER DESIGN CONSIDERATIONS

Lightning

No attempt was made to solve the problems of lightning protection, but an attempt was made to include a weight penalty representative of a realistic solution.

The joint concept selected for this program employs titanium splice plates which will act as a grid work of bus bars on both wing surfaces running spanwise at 35 in. spacing and connected together at the leading edge spar, the wing ribs and the body.

Lightning strikes and discharges on metal airplanes generally occur at the airplane extremities and utilize the structure in between as a conductive path.

Similar behavior would be expected for an "all composite" airplane but unique problems should be anticipated for structure utilizing various mixtures of metal and nonmetal materials.

Weights needed for adequate protection of this airplane will probably range from nearly zero to $.1 \text{ lb/ft}^2$ depending on location. The lightning strike protection system is designed to conduct a 200 000 amp discharge. It is assumed to weigh $.05 \text{ lb/ft}^2$ and is incorporated as an integral part of the structure or applied to the exterior surface in operations subsequent to fabrication.

Exterior Finish

The high temperature stable conductive and/or decorative paint used on the exterior of the composite structure is assumed to be formulated from a polyimide or other stable resin base and conductive graphite powder. The estimated weight is 0.027 lb/ft^2 .

Producibility

Consideration was given to producibility in arriving at the designs shown in figures 4-2 through 4-6. The skins are each balanced symmetrical laminates. This should reduce the tendency for warpage. An integral shim with excess machining allowance is included on the inner skin at joints and supports to account for panel thickness tolerances. The drawings were reviewed by manufacturing with the conclusion that the panels could be produced using current manufacturing technology.

ALUMINUM-BRAZED TITANIUM WING PANEL DESIGN

Figures 4-12 to 4-16 show the detail design for the five representative aluminum-brazed titanium panels. The scope of the detail shown is the same as that shown for the equivalent composite panels. In general, the design technology is like the 2707-300 SST because that detail design effort is the source of the data base for aluminum-brazed titanium wing panel theoretical-to-actual factors.

The titanium honeycomb panels were analyzed according to procedures outlined in Section 4 of reference 4-1.

TITANIUM SKINS

The titanium inner and outer skins are chem-milled Ti-6Al-4V sheet. As discussed under panel loads, the loads in each "cover plate" were considered in arriving at the basic skin thicknesses. The skins are tapered where the loads vary within a panel.

The skins are aluminum brazed to the core. The total braze alloy thickness per panel as .016 in.

TITANIUM CORE

The basic core used in the panel center consists of composition 2, SC4-20NM honeycomb core with a density of 4.9 lb/ft³. The core depth is 1.00 in. These values are the same as for the 2707-300 SST data base design.

JOINTS AND SUPPORTS

The same design conditions were applied to the titanium panel joint and support features as were used for the composite panels resulting in the same fastener sizes and spacing. The thickness of the external splice straps is the same also, since it is a function of the countersunk bolt heads. The skins are chem-milled leaving a padded up strip at all joints and supports to account for the flush external splice strap recess and to achieve adequate bearing strength and to distribute the bolt crushing forces to the core.

The core in the region of the fasteners is more dense in order to withstand the crushing loads due to bolt clamp up forces. Composition 3 SS2-30NM honeycomb core with a density of 14.1 lb/ft³, is used with 3/16 in. diameter fasteners in minimum gage panels. Composition 3, SS2-60NM honeycomb core with a density of 28.1 lb/ft³ is used with 1/4 in. diameter fasteners in medium and heavy gage panels.

The joints between the center and edge core are spotwelded and are located so that all of the local eccentricities are in the region of the dense core.

The exposed edges of the panels at joints are given two coats of primer to inhibit corrosion.

OTHER DESIGN CONSIDERATIONS

Lightning

Again no attempt was made to solve the various problems of lightning protection. However, because the aluminum brazed wing panels are all metal and are supported on titanium inner structure, no weight penalty for lightning protection has been included.

Exterior Finish

No provision for an exterior finish has been made.

Producibility

The detail design shown is consistent with the technology developed on the 2707-300 SST program during which hardware was produced. Fit up tolerances to achieve a good braze are very exacting. To facilitate fit up, only one step height was allowed on the inner surface of the outer skin within any one panel. This is a compromise with optimum pad up requirements for the sake of producibility.

REFERENCE

- 4-1 Boeing Staff: *Study of Structural Design Concepts for an Arrow Wing Supersonic Transport Configuration*. NASA Langley Research Center, CR 132576-1 and -2, 1976.

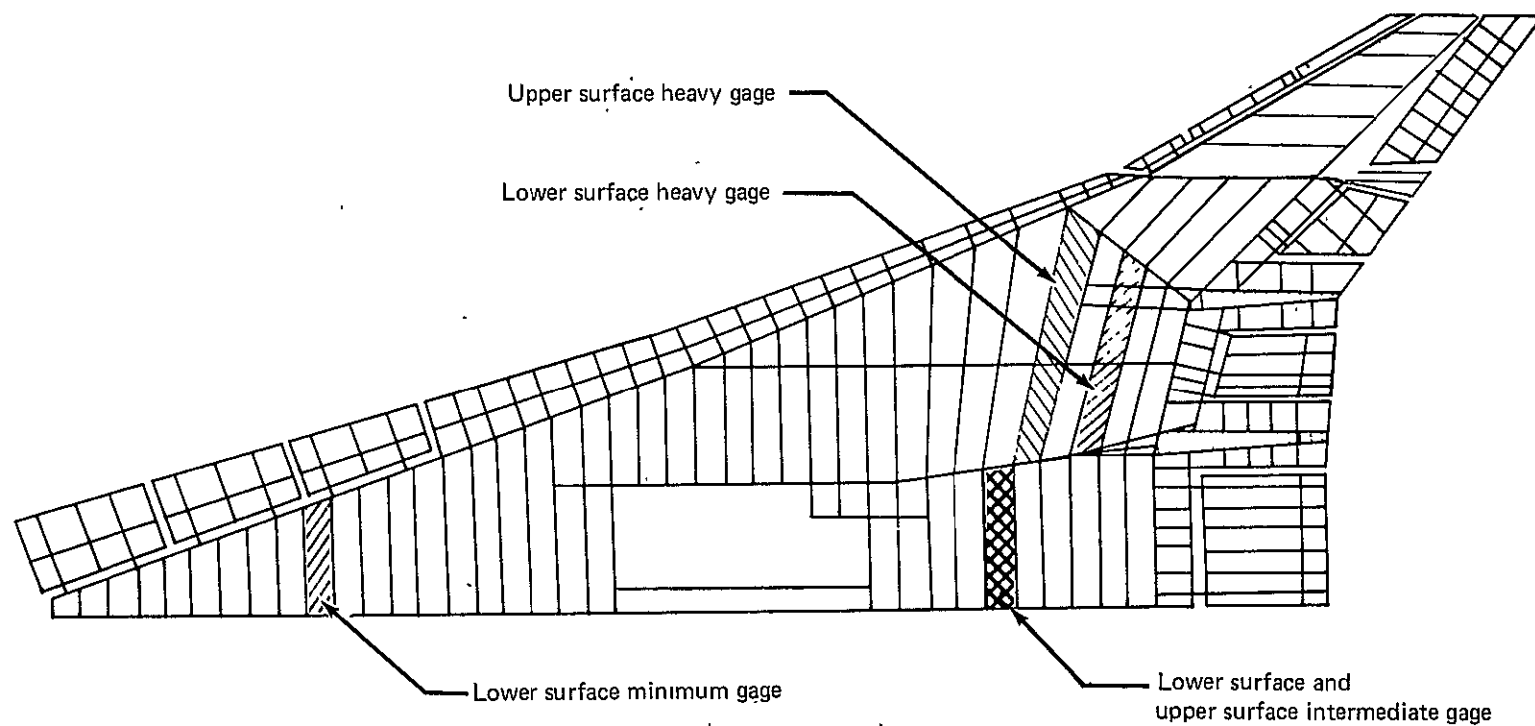
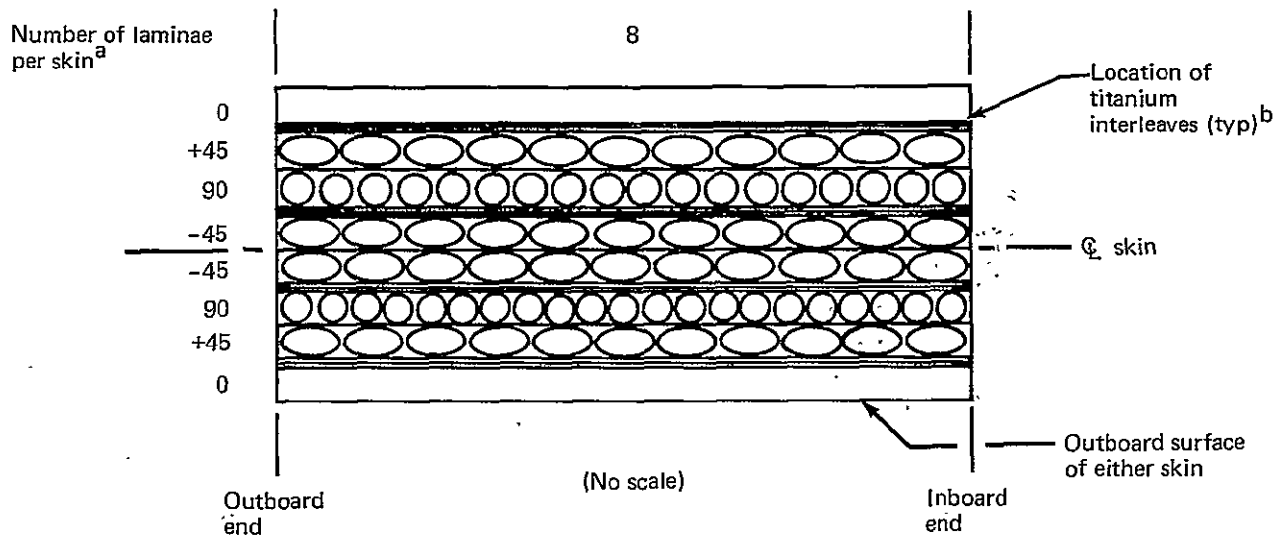


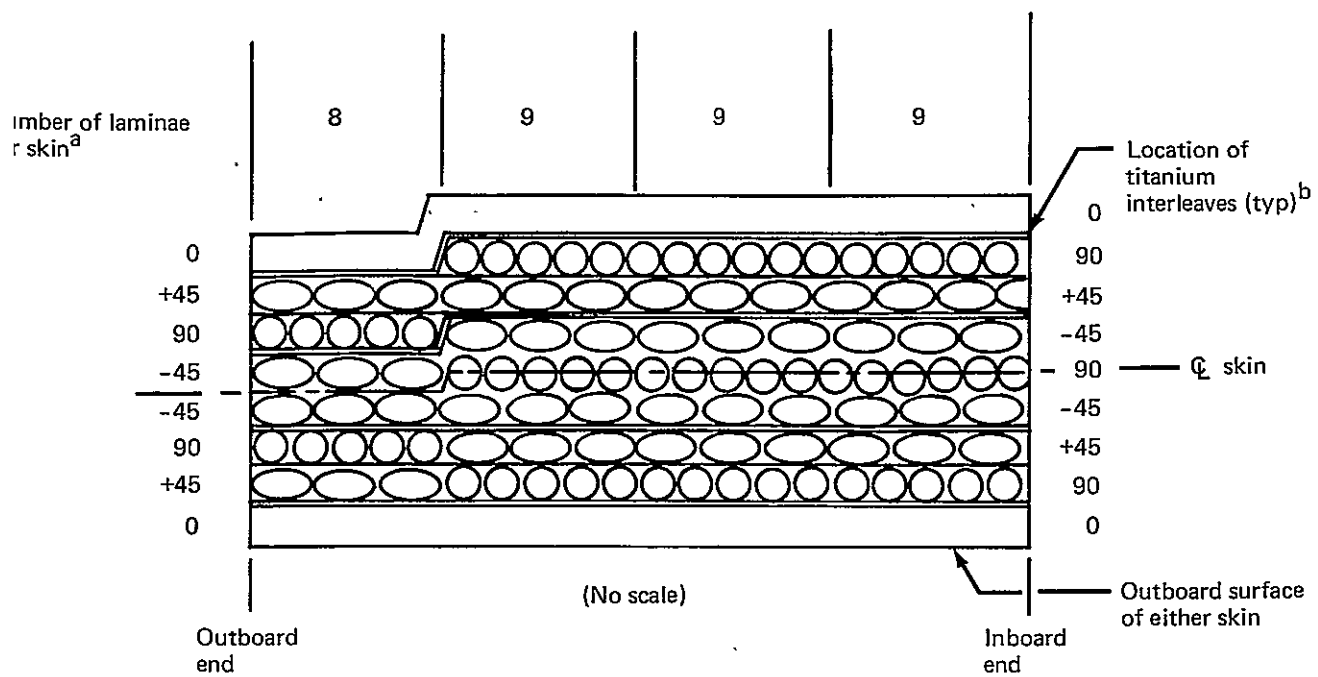
Figure 4-1.—Design for Nonoptimum Factors, Panel Locations



^aUnidirectional 1986 high strength graphite/polyimide tape (Outer skin: 4 mil; inner skin: 2 mil).

^bOuter skin: $\sum T_i = 4 \times 0.008 = 0.032$ all four edges
 Inner skin: $\sum T_i = 4 \times 0.004 = 0.016$ all four edges.

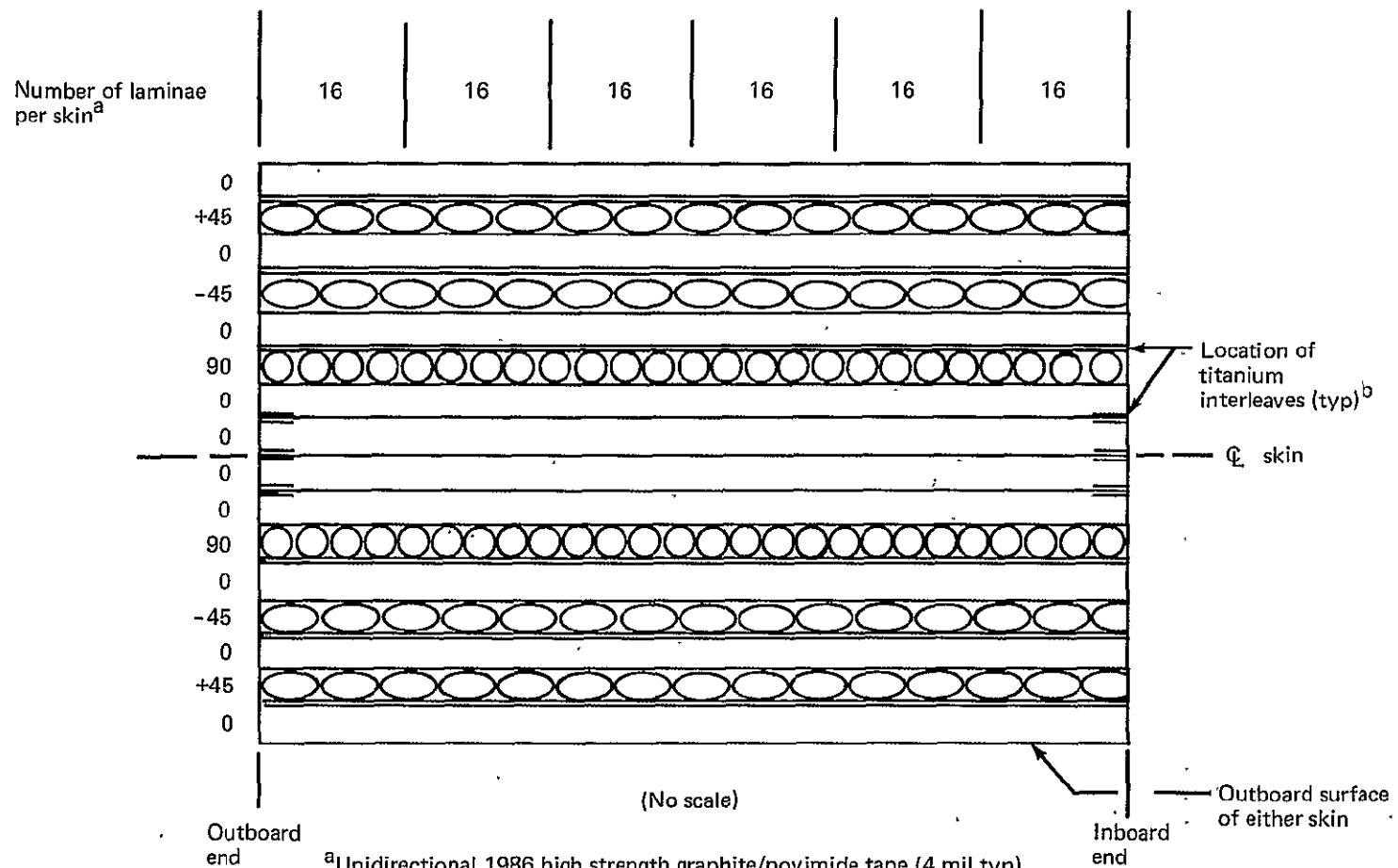
Figure 4-7.—Composite Skin Layup Diagram, Minimum Gage, Lower Wing Panel



^aUnidirectional 1986 high strength graphite/polyimide tape (outer skin: 4 mil; inner skin: 2 mil).

^bOuter skin: $\sum Ti = 4 \times 0.010 = 0.040$ all four edges
Inner skin: $\sum Ti = 4 \times 0.005 = 0.020$ all four edges.

Figure 4-8.—Composite Skin Layup Diagram, Medium Gage, Lower Wing Panel

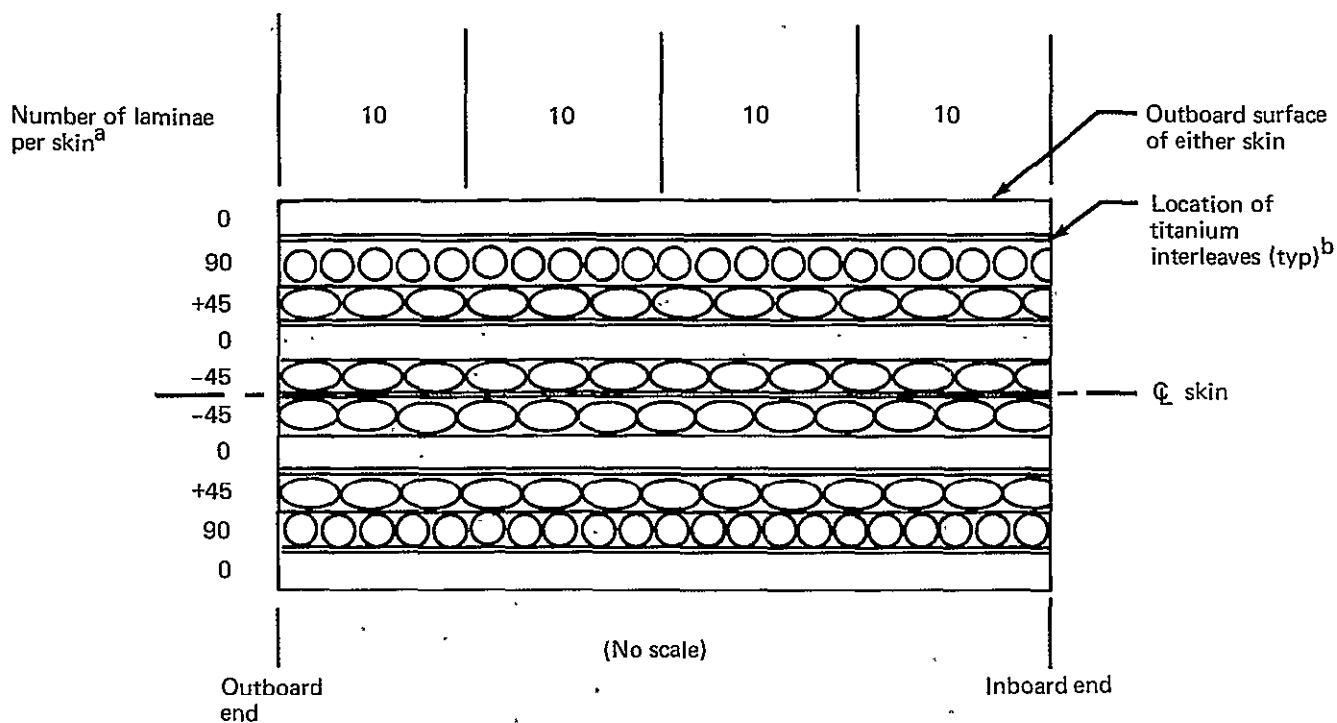


^aUnidirectional 1986 high strength graphite/polyimide tape (4 mil typ)

^bOuter and inner skin: $\sum T_i = 9 \times 0.007 = 0.063$ inboard and outboard edges

Outer and inner skin: $\sum T_i = 6 \times 0.007 = 0.042$ spanwise edges

Figure 4-9.—Composite Skin Layup Diagram, Heavy Gage, Lower Wing Panel

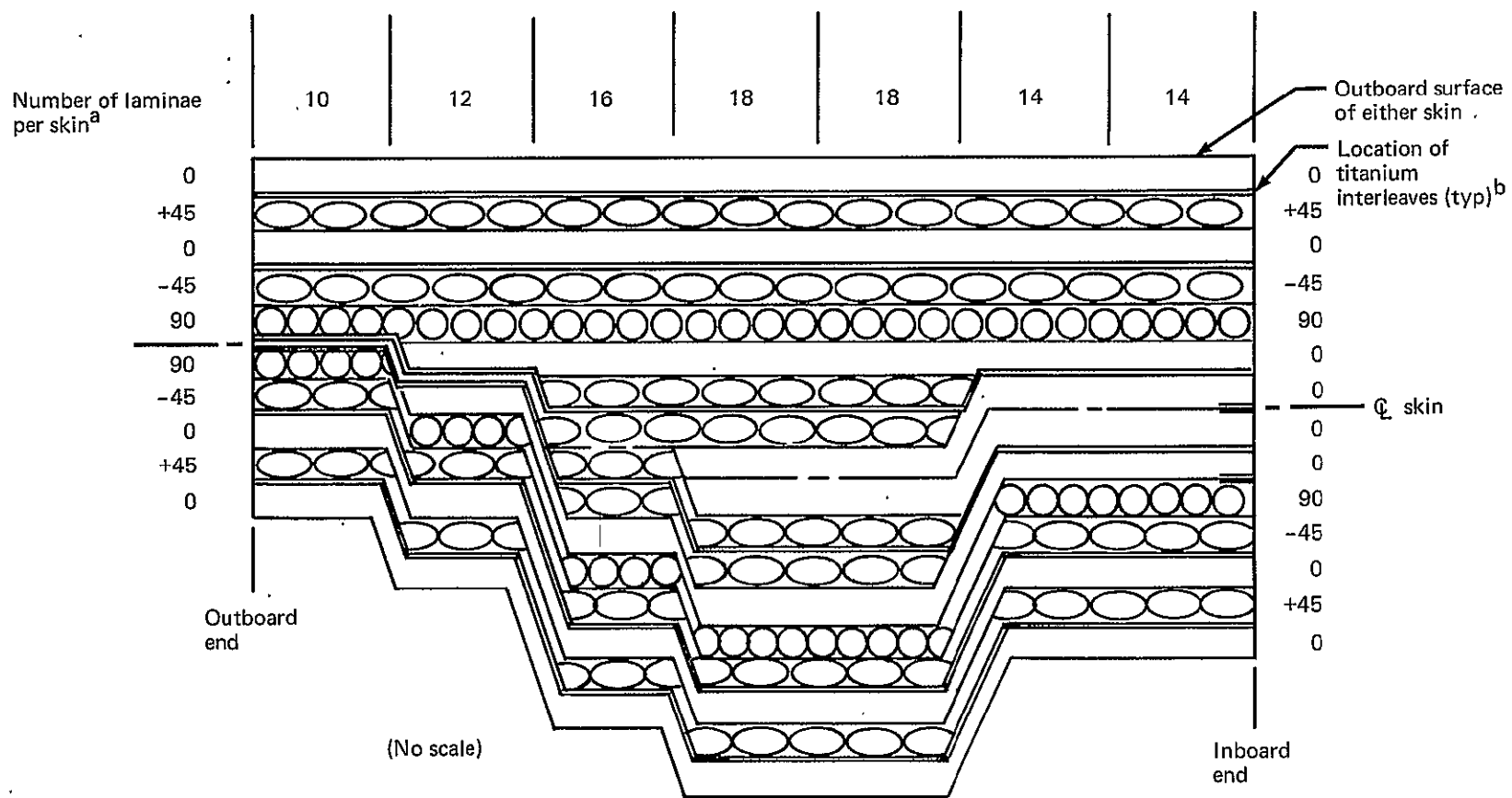


^aUnidirectional 1986 high strength graphite/polyimide tape (4 mil typ).

^bOuter skin: $\sum Ti = 5 \times 0.011 = 0.055$ all four edges

Inner skin: $\sum Ti = 5 \times 0.005 = 0.025$ all four edges.

Figure 4-10.—Composite Skin Layup Diagram, Medium Gage, Upper Wing Panel



^aUnidirectional 1986 high strength graphite/polyimide tape (4 mil typ)

^bOuter and inner skin: $\sum Ti = 9 \times 0.007 = 0.063$ inboard edge
Outer and inner skin: $\sum Ti = 6 \times 0.007 = 0.042$ outboard and spanwise edges

Figure 4-11.—Composite Skin Layup Diagram, Heavy Gage, Upper Wing Panel

SECTION 5

~~PRECEDING PAGE BLANK NOT FILLED~~

THEORETICAL-TO-ACTUAL MASS FACTORS

by

M. D. HALVORSEN

CONTENTS

	Page
INTRODUCTION	139
SKIN THEORETICAL-TO-ACTUAL CONVERSION FACTORS	140
HONEYCOMB CORE	143
CORE TO SKIN ADHESIVE	143
CORE EDGING (SPLICE AND SEALING)	143
LIGHTNING PROTECTION AND SURFACE FINISH	143
SPAR AND RIB MASS INCREMENT	143
PANEL MASS COMPARISON (TITANIUM VERSUS GRAPHITE/POLYIMIDE)	144
REFERENCES	145

TABLES

No.		Page
5-1	Titanium Honeycomb Panel Mass Summary	146
5-2	Graphite/Polyimide Honeycomb Panel Mass Summary	147
5-3	Theoretical-To-Actual Mass Increment Derivation Honeycomb Panel Skin	148
5-4	ATLAS Input Data to Support Mass Calculations	149
5-5	Mass Comparison, Titanium and Graphite/Polyimide Upper Surface Honeycomb Panels.	149

FIGURES

No.		Page
5-1	Theoretical-to-Actual Mass Increment, Titanium Honeycomb Panel Skin, National SST Data	150
5-2	Skin Spanwise Edge Design	151
5-3	Skin Edge Padup Mass Increment, Titanium Honeycomb Panels	152
5-4	Skin Edge Padup Mass Increment, Graphite/Polyimide Honeycomb Panels	153
5-5	Theoretical-to-Actual Mass Increment, Titanium Honeycomb Panel Skin	154
5-6	Theoretical-to-Actual Mass Increment, Graphite/Polyimide Honeycomb Panel Skin	155

INTRODUCTION

The ATLAS finite element structural analysis provides the theoretical size and mass of modeled structural members. On the arrow wing, those members modeled in the wing box structure include the covers, spar and rib chords and spar and rib webs.

Calculation of total wing structural mass requires the inclusion of a number of additional features in the structural box and wing elements external to the box, e.g., leading edge, trailing edge, control surfaces, etc. This section discusses the development of the additional structural features in the wing box and related conversion factors. Total wing mass analysis is discussed in Section 9.

Items in the wing box for which additional mass must be calculated include the following:

- Skin padup, door reinforcement, skin tolerance etc.
- Honeycomb core
- Core to skin adhesive
- Core edging (splice and sealing)
- Lightning protection and surface finish
- Spar and rib web stiffeners
- Spar and rib padup, web tolerance, hole reinforcement, etc.

Structural sizing from the ATLAS analysis defines the theoretical structure required for the strength to carry design loads. The increments discussed above account for additional elements of the structure that are required to satisfy design criteria not covered by theoretical analysis.

Prior to the development of the theoretical-to-actual mass factor for the graphite/polyimide construction, it was found necessary to first revise the theoretical-to-actual conversion factors used for the titanium construction (ref. 5-1). These revised titanium factors were used to change the wing mass reported in reference 5-1 as noted in Section 9. Five titanium honeycomb panels and five graphite/polyimide honeycomb panels were designed as described in Section 4. Evaluation of the components of these panels provided the data to generate the graphite/polyimide theoretical-to-actual conversion factors and to revise the titanium factors (see tables 5-1 and 5-2).

SKIN THEORETICAL-TO-ACTUAL CONVERSION FACTORS

The five titanium and five graphite/polyimide panels discussed in Section 4 were all designed with production type edge attachments. None of the panels, however, included wing lower surface access doors or provisions for fitting attachments, nor were such items as corner construction fully developed for the ten panels. These additional features add mass and increase the theoretical-to-actual factors.

The skin spanwise edge padup for the titanium honeycomb panels can be accounted for in three different ways in finite element structural analysis. First, the spanwise edge padup can be included in the cover material, which then becomes a part of the effective skin thickness. The chordwise skin padup, corner treatment, door cutout reinforcement, fuel system provisions, material tolerance, etc., are accounted for in the theoretical-to-actual factor. This first case is shown by curves [1] in figure 5-1, where the theoretical-to-actual increment is plotted versus the effective theoretical skin thickness based on data from the National SST program. The second alternate is to consider the spanwise padup as a part of the spar chord area. The skin thickness in the structural model is then equal to the theoretical thickness, t . The third alternate is to include the spanwise skin padup as a part of the theoretical-to-actual mass increment. This alternate is applicable to lightly loaded areas of the wing, where the minimum spar chord areas are dictated by minimum gage design constraints.

Figure 5-2 identifies the components of a typical panel and splice. Tables 5-1 and 5-2 list the data used in developing the theoretical-to-actual mass increments. The following paragraphs describe the development of these data.

Table 5-1 gives a detailed mass buildup of each of the five titanium wing skin panels that were designed for the arrow wing study. Figure 5-3 shows the skin edge padup increment, ratioed to the skin mass, as a function of skin thickness. Separate sets of curves labeled [2], [3], and [4] are shown for chordwise edge padup, spanwise edge padup and total edge padup, respectively.

Mass data for the five graphite/polyimide panels that were designed for the present study are presented in table 5-2 and figure 5-4. Curve [5] in figure 5-4 shows the mass increment for spanwise titanium interleaves along the graphite/polyimide panel edges, as a function of skin thickness, t . Curve [6] shows the remainder of the edge padup, which includes the spanwise graphite/polyimide padup, chordwise graphite/polyimide padup and chordwise titanium interleaves. Curve [7] represents the total edge padup increment.

Principal steps in the derivation of theoretical-to-actual mass increment for the titanium and graphite/polyimide skin panels are shown in table 5-3. Selected skin thicknesses for either titanium or graphite/polyimide, covering the range of interest, are listed at the top of the table. Corresponding values of \bar{t}/t , obtained from the five titanium panel designs discussed in Section 4, are listed in line (1) where t is the basic skin thickness and \bar{t} is the effective theoretical skin thickness including the spanwise edge padups. These \bar{t}/t values can be obtained by adding 1.000 to the values from curves [3] in figure 5-3. The corresponding \bar{t} 's for the t 's listed at the top of table 5-3 are obtained by forming product $(t) \times (\bar{t}/t)$ as given in line (2).

The original theoretical-to-actual increment for the skin of titanium honeycomb panels was developed during the study reported in reference 5-1 by collecting data on calculated panel masses from the

National SST program. These data were used to prepare the graph shown in figure 5-1. In that presentation spanwise edge padup is included as a part of effective theoretical skin mass (thickness denoted by \bar{t}), and the remaining padup is represented as a function of t . If we define

$$\begin{aligned}w_x &= \text{mass increment for spanwise padup} \\w_y &= \text{total mass increment} \\w_t &= \text{mass of basic skin (thickness } t) \\w_{\bar{t}} &= w_t + w_x\end{aligned}$$

then the incremental mass plot 1 in figure 5-1 shows the variable

$$P_1 = (w_y - w_x)/w_{\bar{t}} \quad (5-1)$$

versus \bar{t}

Values for P_1 are listed on line (3) of table 5-3 for the \bar{t} values listed on line (2).

In the more highly loaded portion of the titanium arrow wing the spanwise skin edge padup was considered as effective structural material included as a part of the spar chord, while the National SST Program considered this material as part of the skin t . In this second case the variable

$$P_2 = (w_y - w_x)/w_t \quad (5-2)$$

is treated as a function of t . Since

$$P_2 = \left(\frac{w_y - w_x}{w_{\bar{t}}} \right) \left(\frac{w_{\bar{t}}}{w_t} \right)$$

and

$$w_{\bar{t}}/w_t = \bar{t}/t$$

it follows that

$$P_2 = \left(\frac{w_y - w_x}{w_{\bar{t}}} \right) \left(\frac{\bar{t}}{t} \right)$$

or

$$P_2 = P_1 (\bar{t}/t) \quad (5-3)$$

In the third case which is applicable to the more lightly loaded forward portion of the titanium arrow wing the spanwise skin padup becomes a part of the theoretical-to-actual mass increment. Then the variable

$$P_3 = w_y/w_t \quad (5-4)$$

is also treated as a function of t .

Since

$$w_x/w_y = (\bar{t} - t)/t = \bar{t}/t - 1$$

then

$$P_3 = P_1 (\bar{t}/t) + \bar{t}/t - 1 \quad (5-5)$$

P_2 and P_3 , based on data from the national SST program and the five titanium panel designs, are tabulated in lines (4) and (5) of table 5-3. P_2 and P_3 are also represented, as functions of t , by curves [8] and [9], respectively in figure 5-5. Thus far the development of the theoretical-to-actual mass increment for the skin of the titanium honeycomb panels has been presented. The remainder of the tabulation in table 5-3 gives the steps in the development of the theoretical-to-actual mass increment for the skin of the graphite/polyimide honeycomb panels.

Values of P_4 in line (6), representing total edge padup for titanium panels, are taken from curve [4] in figure 5-3. Values in line (7) for the edge padup increment, P_4 , for graphite/polyimide panels were calculated from the five advanced composite panel designs discussed in Section 4 and plotted as curve [7] of figure 5-4. In deriving values of the theoretical-to-actual increment, P_3 , listed in line (8), it has been assumed that the ratio P'_3/P'_4 for graphite panels is equal to the ratio P_3/P_4 for titanium panels. These values of P'_3 , applicable to light gage regions of the wing, include spanwise titanium interleaves as incremental mass. Values of the mass increment for spanwise interleaves, P'_5 , from curve [5] in figure 5-4, are listed in line (9). Finally, values of the theoretical-to-actual increment P'_2 , omitting the contribution of spanwise interleaves (considered as spar chord area), are listed in line (10). Data from lines (8) and (10) have been used in plotting curves [10] and [11], respectively, in figure 5-6.

The computation of the actual honeycomb skin mass in ATLAS requires the input of a mass factor, rather than a mass increment. These theoretical-to-actual mass factors for the skin are obtained by adding unity to the incremental values from figures 5-5 and 5-6.

Table 5-4 gives a summary of additional data required for the complete wing structure. The chart also shows a comparison of the theoretical-to-actual factors for both the titanium and composite honeycomb wing panel construction. The following paragraphs discuss the basis for significant additional items that are included in the analysis.

HONEYCOMB CORE

Density of the basic 1.5 in. polyimide honeycomb core is 3.5 lbm/ft^3 , and the mass per unit area is $.4375 \text{ lbm/ft}^2$. This basic core mass must be multiplied by a factor of 1.2 on the upper wing surface and 1.25 on the lower wing surface to account for the dense core required around panel edges and around access doors on the lower surface.

CORE TO SKIN ADHESIVE

The core to skin adhesive for the graphite/polyimide panels is .015 in. thick and its area density is $.170 \text{ lbm/ft}^2$. The adhesive is uniform in thickness, regardless of the core density.

CORE EDGING (SPlice AND SEALING)

The mass of splice adhesive between dense core and basic core and the mass of the panel edge seal are functions of the panel perimeter-to-area ratio as well as the thickness and density of the material. In this case, however, masses of both core splice adhesive and the panel edge seal are treated as functions of panel area. This is based on an average panel perimeter-to-area ratio, resulting in a core splice adhesive mass of $.025 \text{ lbm/ft}^2$ on the upper surface and $.030 \text{ lbm/ft}^2$ on the lower surface. The factor for the lower surface is greater, due to the dense core splice around access doors in the lower surface. The area density of panel edge seal is estimated to be $.046 \text{ lbm/ft}^2$ for an average panel geometry.

LIGHTNING PROTECTION AND SURFACE FINISH

The average lightning strike protective coating is .002 in. thick and its area density is $.050 \text{ lbm/ft}^2$. The surface finish is a high temperature stable conductive coating and decorative paint, with area density of $.027 \text{ lbm/ft}^2$.

SPAR AND RIB MASS INCREMENT

The sizing and mass of the basic chords and webs for the spars and ribs are calculated by the ATLAS design module. Some of the webs are of sine wave construction while the remainder are flat with stiffeners. The developed lengths of the sine wave webs were accounted for by altering the material density. The stiffeners for the flat webs were not modeled or sized within the program but the mass was accounted for by introduction of a factor within the program. For flat webs the stiffener mass was accounted for by multiplying the web mass by a factor of 1.5. This factor was further increased to account for additional increments to spar and rib mass. The final theoretical-to-actual mass conversion factors for the flat webs were:

$$\text{Mass Factor for Flat Spar Webs} = (1.5) (1.15) = 1.725$$

$$\text{Mass Factor for Flat Rib Webs} = (1.5) (1.18) = 1.770$$

The sine wave webs and chords for the spars and ribs were also multiplied by the following theoretical-to-actual conversion factors:

$$\text{Factor for Sine Wave Spar Webs} = 1.15$$

$$\text{Factor for Sine Wave Rib Webs} = 1.18$$

$$\text{Factor for Spar Chords} = 1.15$$

$$\text{Factor for Rib Chords} = 1.18$$

These are the factors, derived for the National SST Program, that were used in reference 5-1 for the titanium wing substructure.

**PANEL MASS COMPARISON
(TITANIUM VERSUS GRAPHITE/POLYIMIDE)**

An example of a detailed mass comparison of titanium and graphite/polyimide medium gage honeycomb panels, designed to the same criteria, is shown in table 5-5. The overall mass advantage for the composite panel is 30.7%; the basic skin shows a relative advantage of 60.7%. The theoretical-to-actual increment for the composite skin is 12.4% greater than the titanium increment, while the remainder of the incremental masses such as core, adhesive, finish, etc. show no relative advantage for either panel. The theoretical-to-actual conversion increment as a percent of the basic skin mass generated by ATLAS structural analysis is 86% (46% of panel mass) for the titanium panel, and 227% (69% of panel mass) for the composite panel.

REFERENCES

- 5-1 Boeing Staff: *Study of Structural Design Concepts for an Arrow Wing Supersonic Transport Configuration*. NASA CR 132576-1 and -2, 1976.

Table 5-1.—Titanium Honeycomb Panel Mass Summary

	Lower surface			Upper surface	
	Light gage	Medium gage	Heavy gage	Medium gage	Heavy gage
Average t (outer + inner skin) (in.)	.030	.083	.120	.084	.134
Basic skin mass (lbm)	22.68	76.42	154.34	77.85	271.96
Chordwise skin edge padup (lbm)	1.46	3.25	5.36	2.77	5.81
Chordwise skin edge padup/ basic skin	.065	.042	.035	.035	.021
Spanwise skin edge padup (lbm)	5.45	14.88	14.85	10.88	19.57
Spanwise skin edge padup/ basic skin	.240	.195	.096	.140	.072
Total skin edge padup (lbm)	6.91	18.13	20.21	13.65	25.38
Total skin edge padup/ basic skin	.305	.237	.131	.175	.093
Basic core (lbm)	13.40	16.43	22.79	16.43	35.87
Center core (lbm)	11.66	13.80	18.51	13.89	30.72
Edge core (lbm)	4.51	13.23	22.28	12.82	26.19
Center core + edge core/ basic core	1.207	1.645	1.790	1.626	1.587
Basic braze (lbm)	7.37	9.04	12.54	9.04	19.73
Center braze (lbm)	6.42	7.59	10.18	7.64	16.90
Edge braze (lbm)	2.52	3.77	6.26	3.67	7.46
Center braze + edge braze/ basic braze	1.213	1.257	1.311	1.251	1.235
Edge finish (lbm)	.02	.03	.06	.03	.05
Edge finish mass/panel area (lbm/ft ²)	.001	.001	.001	.001	.001
Total panel mass (lbm)	54.72	132.97	231.84	129.55	378.66
Panel area (ft ²)	32.81	40.23	55.82	40.23	87.84
Panel mass/panel area (lbm/ft ²)	1.67	3.31	4.15	3.22	4.31

Table 5-2.—Graphite/Polyimide Honeycomb Panel Mass Summary

	Lower surface			Upper surface	
	Light gage	Medium gage	Heavy gage	Medium gage	Heavy gage
Average t (outer + inner skin) (in.)	.048	.053	.128	.080	.117
Basic skin mass (lbm)	12.70	17.28	57.62	25.95	82.86
Spanwise Ti interleaves (lbm)	2.31	3.97	10.56	4.05	12.74
Spanwise Ti interleaves/ basic skin	.182	.230	.183	.156	.154
Spanwise skin edge padup less spanwise Ti interleaves (lbm)	3.30	5.56	14.14	7.70	17.74
Spanwise skin edge padup less spanwise Ti interleaves/ basic skin	.260	.322	.246	.297	.214
Total skin edge padup (lbm)	5.61	9.53	24.70	11.75	30.48
Total skin edge padup/ basic skin	.442	.552	.429	.453	.368
Basic core (lbm)	14.36	17.60	24.42	17.60	38.43
Center core (lbm)	12.36	14.77	19.57	14.72	32.52
Edge core (lbm)	8.78	10.47	17.95	10.67	22.84
Center core + edge core/ basic core	1.124	1.434	1.536	1.443	1.441
Core to skin adhesive (lbm)	5.58	6.84	9.49	6.84	14.93
Core splice adhesive (lbm)	.84	1.00	1.50	.99	1.95
Splice adhesive mass/panel area (lbm/ft ²)	.0256	.0249	.0269	.0246	.0222
Panel edge seal (lbm)	1.67	1.84	2.56	1.84	3.40
Edge seal mass/panel area (lbm/ft ²)	.0509	.0457	.0459	.0457	.0387
Lightning strike protective coating (lbm)	1.64	2.01	2.79	2.01	4.39
Surface finish (lbm)	.89	1.09	1.51	1.09	2.37
Total panel mass (lbm)	45.07	64.83	137.69	75.86	195.74
Panel area (ft ²)	32.81	40.23	55.82	40.23	87.84
Panel mass/panel area (lbm/ft ²)	1.37	1.61	2.47	1.89	2.23

Table 5-3.—Theoretical-To-Actual Mass Increment Derivation Honeycomb Panel Skin

t, skin thickness	$\frac{LWR}{.030}$	$\frac{UPR}{.030}$	$\frac{LWR}{.060}$	$\frac{UPR}{.060}$	$\frac{LWR}{.090}$	$\frac{UPR}{.090}$	$\frac{LWR}{.120}$	$\frac{UPR}{.120}$	$\frac{LWR}{.150}$	$\frac{UPR}{.150}$	$\frac{LWR}{.180}$	$\frac{UPR}{.180}$
(1) \bar{t}/t , for Ti panel designs from [3] + 1 in figure 5-3	1.336	1.286	1.214	1.183	1.140	1.118	1.096	1.092	1.075	1.064	1.073	1.062
(2) $t = (t) (\bar{t}/t)$.040	.039	.073	.071	.103	.101	.131	.130	.161	.160	.193	.191
(3) P_1 , defined by equation (5-1), from [1] in figure 5-1	.533	.418	.362	.282	.252	.187	.187	.129	.154	.102	.150	.100
(4) P_2 , defined by equation (5-3)	.712	.538	.439	.334	.287	.209	.205	.140	.166	.109	.161	.106
(5) P_3 , defined by equation (5-5)	1.048	.824	.653	.517	.427	.327	.301	.222	.241	.173	.234	.168
(6) P_4 , Ti edge padup factor, from [4] in figure 5-3	.400	.341	.261	.220	.179	.147	.131	.105	.108	.086	.104	.085
(7) P'_4 , Gr/Pi total edge padup factor, from [7] in figure 5-4	.568	.568	.486	.486	.430	.430	.403	.403	.400	.400	.400	.400
* (8) $P'_3 = (P'_4) (P_3/P_4)$, GR/Pi theoretical-to-actual factor	1.488	1.375	1.210	1.113	1.023	.937	.923	.842	.892	.812	.882	.802
(9) P'_5 , mass factor for spanwise Ti interleaves from [5] in figure 5-4	.220	.220	.195	.195	.175	.175	.160	.160	.160	.160	.160	.160
(10) $P'_2 = P'_3 - P'_5$	1.268	1.155	1.015	.918	.848	.762	.763	.682	.732	.652	.722	.642

*These values have been adjusted to a smooth curve

Table 5-4. ATLAS Input Data to Support Mass Calculations

	Titanium H/C panels from study reported in ref. 5-1	Composite H/C panels from present study
Basic skin t	Input t which is resized by ATLAS analysis	Input t which is resized by ATLAS analysis
Factor for skin	Values from fig. 5-5 plus 1.0	Values from fig. 5-6 plus 1.0
Basic H/C core	1 in. thick, 5.0 lbm/ft ³ .4167 lbm/ft ²	1.5 in. thick, 3.5 lbm/ft ³ .4375 lbm/ft ²
Factor for edge core	Upper surface 1.25 Lower surface 1.30	Upper surface 1.20 Lower surface 1.25
Basic core to skin braze or adhesive	Alum. braze/surface .2246 lbm/ft ²	Polyimide adhesive/surface .170 lbm/ft ²
Factor for edge core braze or adhesive	Upper surface 1.25 Lower surface 1.30	Upper surface 1.00 Lower surface 1.00
Core splice adhesive		Upper surface .025 lbm/ft ² Lower surface .030 lbm/ft ²
Panel edge seal		.046 lbm/ft ²
Lightning strike protective coating		.050 lbm/ft ²
Surface finish		.027 lbm/ft ²
Basic spar structure	Input structure which is resized by ATLAS analysis	Input structure which is resized by ATLAS analysis
Factor for spar (incl. stiff.)	Flat spar webs 1.725 Sine wave spar webs and chords 1.15	Flat spar webs 1.725 Sine wave spar webs and chords 1.15
Basic rib structure	Input structure which is resized by ATLAS analysis	Input structure which is resized by ATLAS analysis
Factor for rib (incl. stiff.)	Flat rib webs 1.77 Sine wave rib webs and chords 1.18	Flat rib webs 1.77 Sine wave rib webs and chords 1.18

Table 5-5.—Mass Comparison, Titanium and Graphite/Polyimide Upper Surface Honeycomb Panels

	Titanium panel	Mass reduction	Graphite/polyimide panel
Basic skin gage	.0713 in.		.080 in.
Skin mass	66.1 lbm	-60.7%	26.0 lbm
Incremental skin mass	18.6 lbm	+12.4%	20.9 lbm
Core, adhesive finish, etc.	38.1 lbm		38.2 lbm
Total panel mass	122.8 lbm	-30.7%	85.1 lbm
Mass increment as % of basic skin	85.8%		227.3%

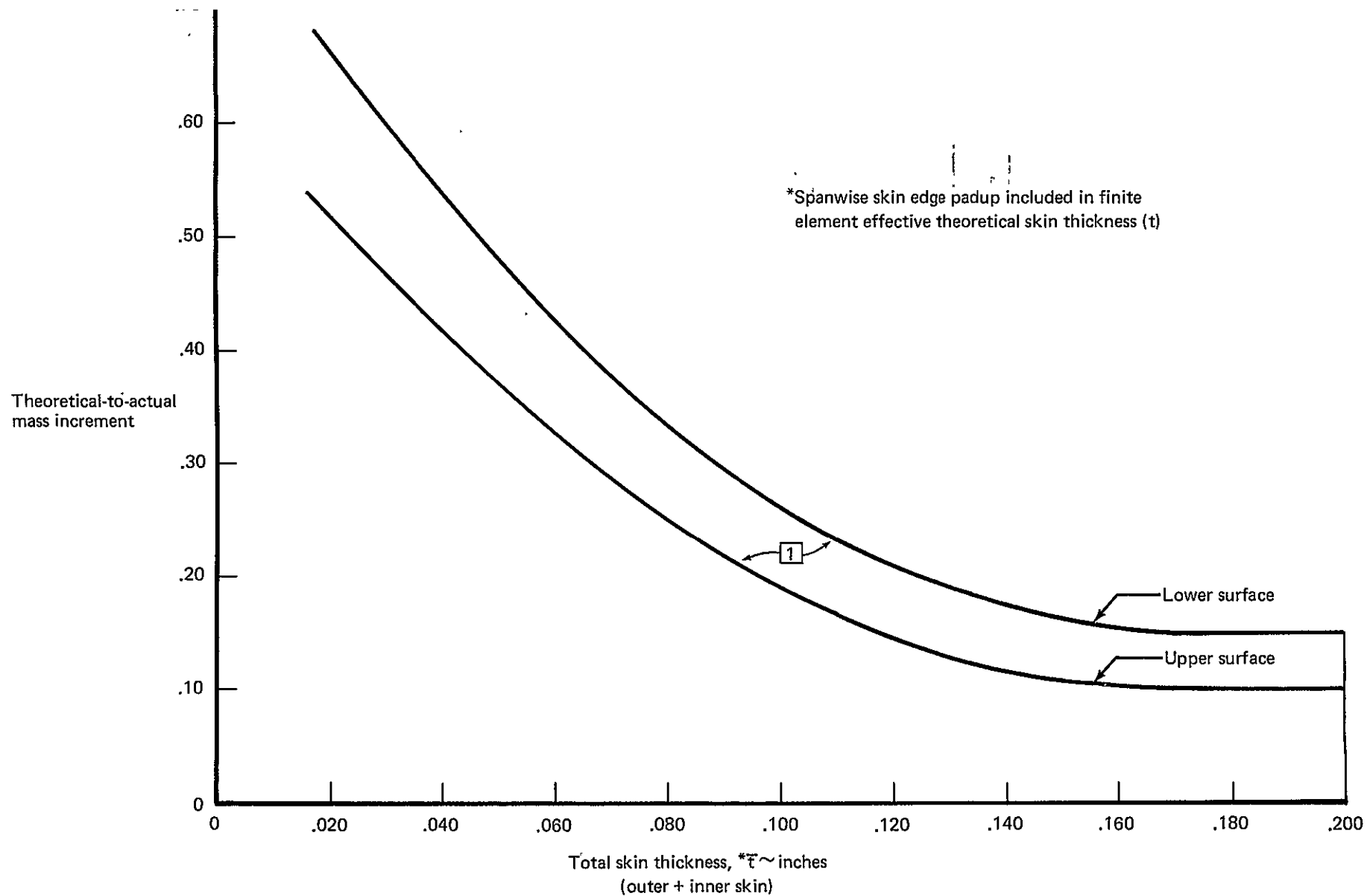


Figure 5-1.—Theoretical-To-Actual Mass Increment, Titanium Honeycomb Panel Skin, National SST Data

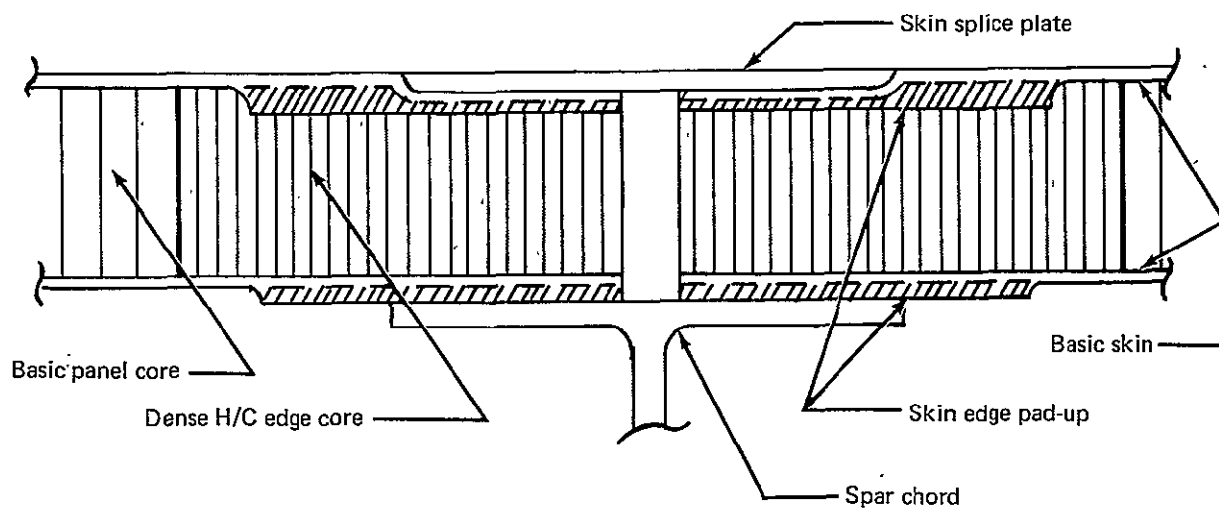


Figure 5-2.—Skin Spanwise Edge Design

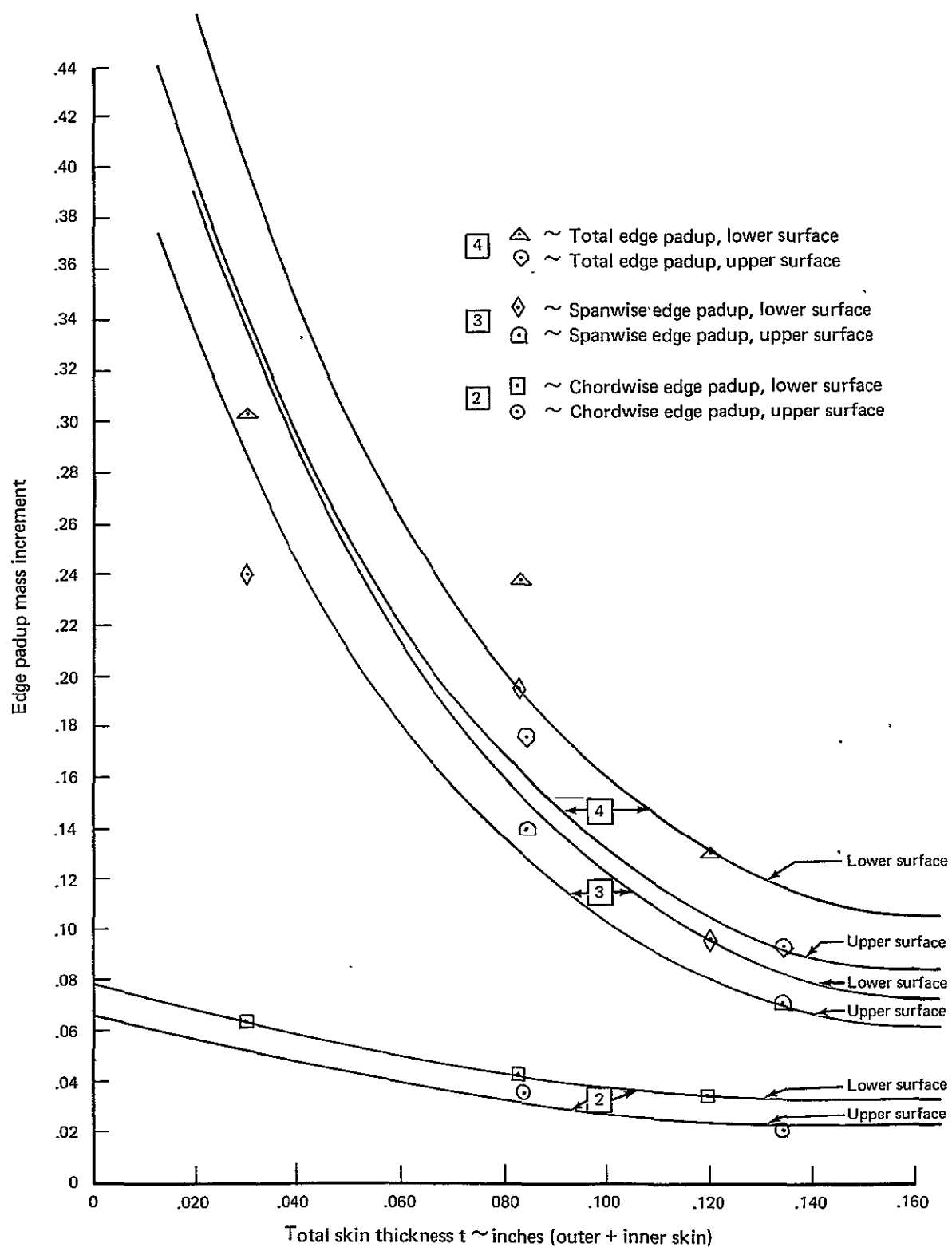


Figure 5-3.—Skin Edge Padup Mass Increment, Titanium Honeycomb Panels

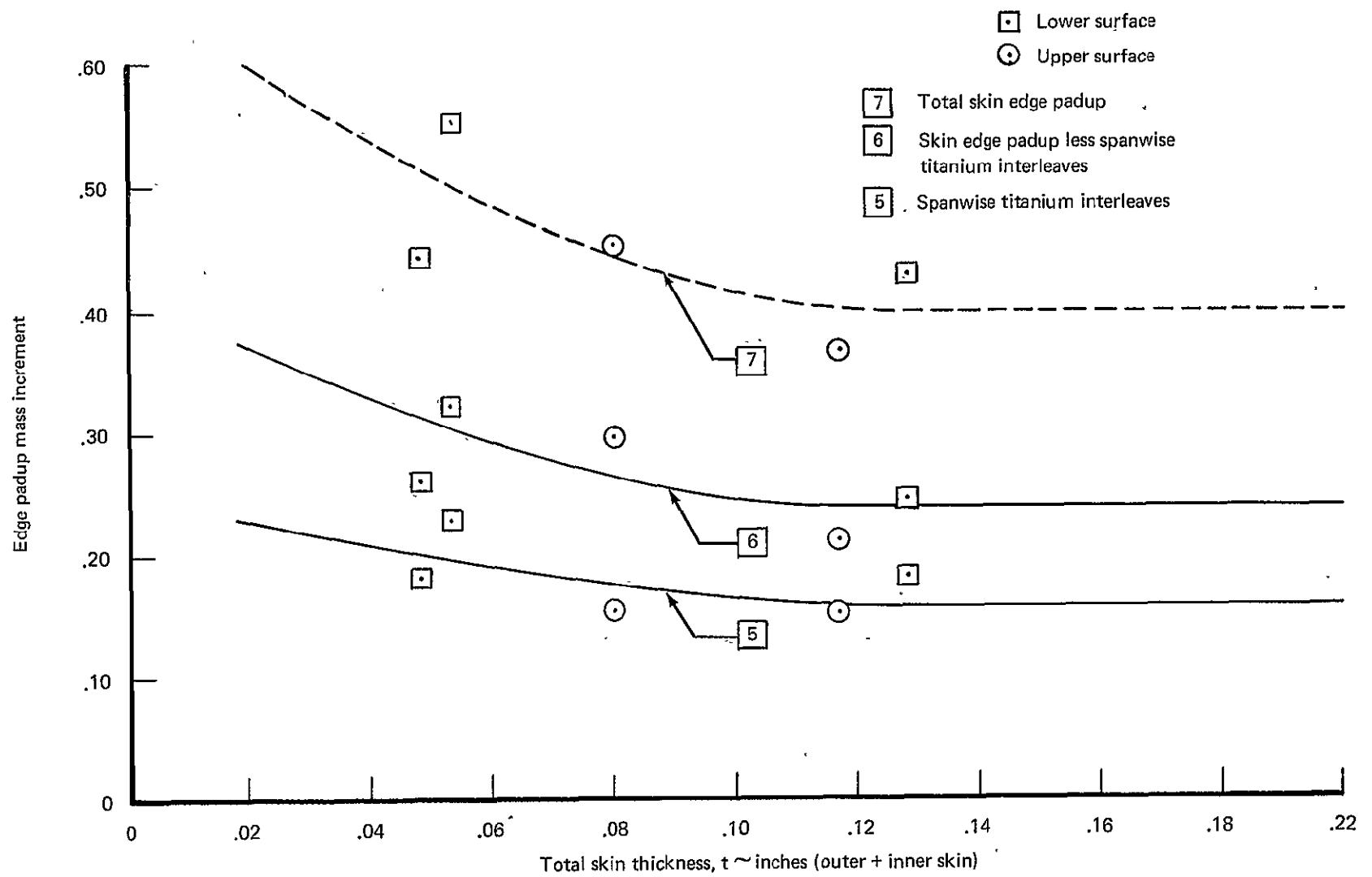


Figure 5-4.—Skin Edge Padup Mass Increment, Graphite/Polyimide Honeycomb Panels

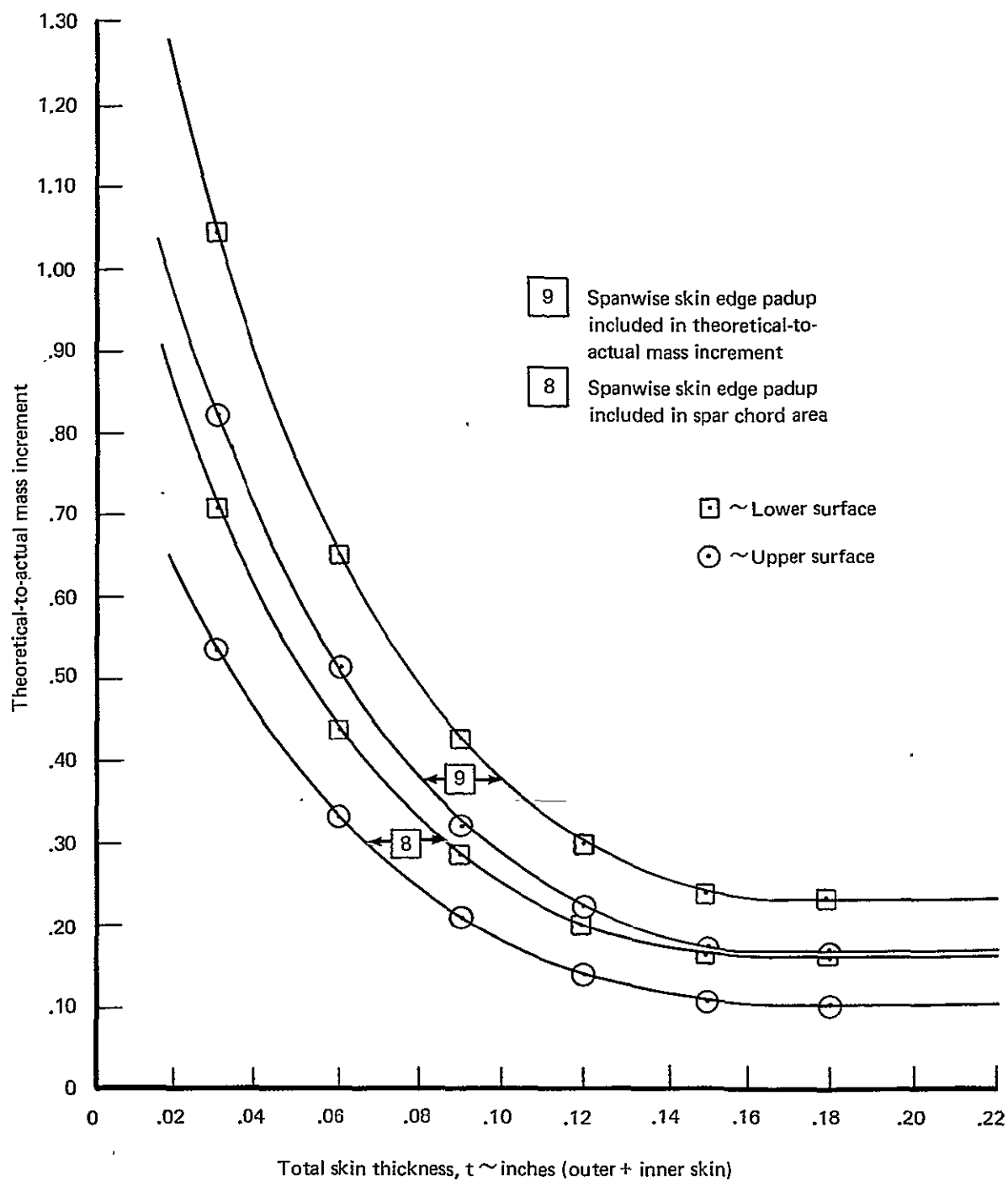


Figure 5-5.—Theoretical-To-Actual Mass Increment, Titanium Honeycomb Panel Skin

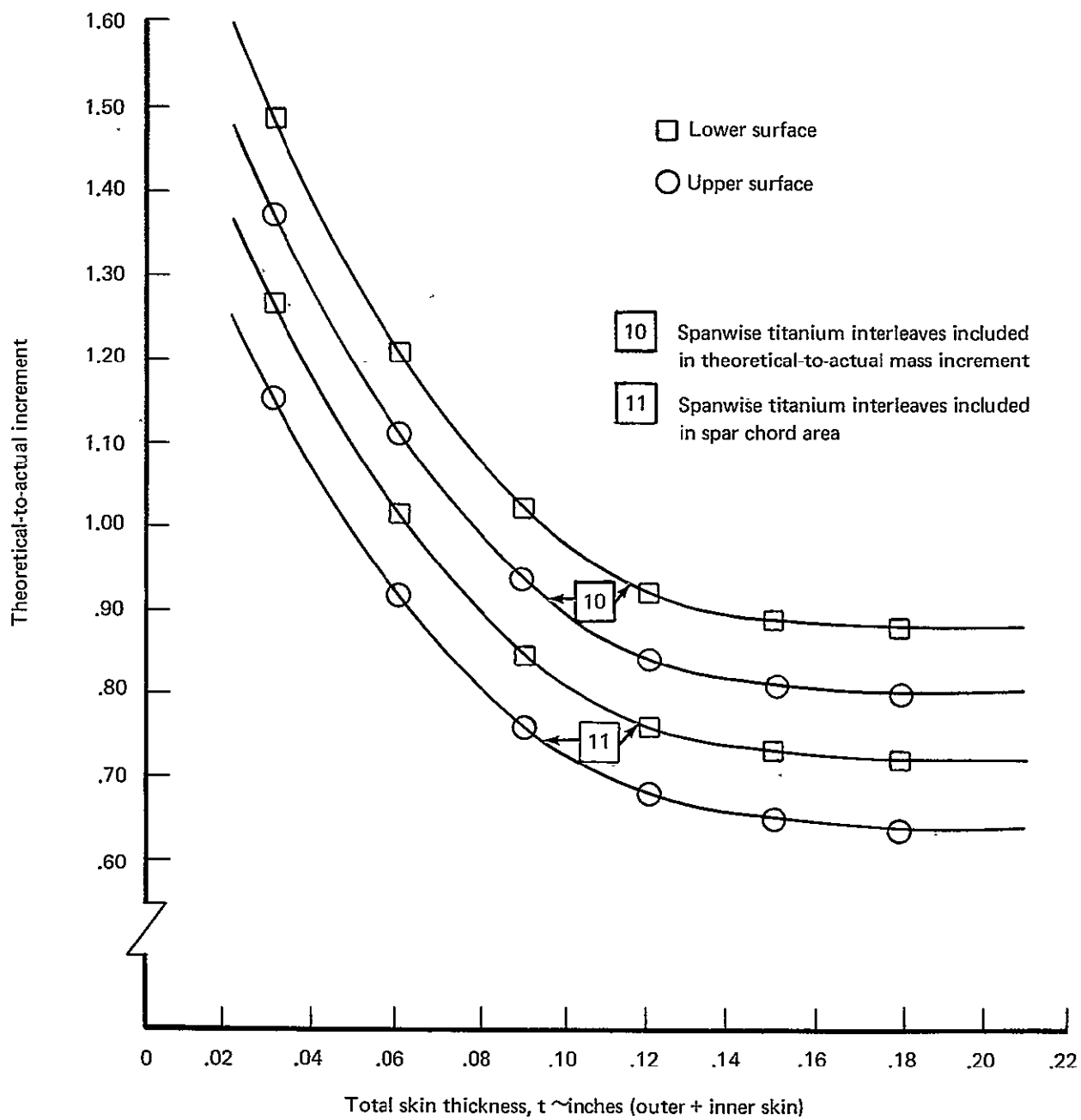


Figure 5-6.—Theoretical-To-Actual Mass Increment, Graphite/Polyimide Honeycomb Panel Skin

SECTION 6

~~RECORDING PAGE BLANK NOT FILMED~~

COMPOSITE ANALYSIS AND DESIGN

by

F. D. Flood

CONTENTS

	Page
INTRODUCTION	162
COMPOSITE ANALYSIS IN ATLAS	162
STRENGTH OPTIMIZATION IN ATLAS	163
INITIAL SIZING PROCEDURES	165
ALLOWABLES FOR STRUCTURAL RESIZING	171
REFERENCE	176

TABLES

No.		Page
6-1	Allowable Buckling Stress Versus Core Thickness, Graphite/Polyimide, [0/±45/90]S	177
6-2	Allowable Buckling Stress Versus Core Thickness, Graphite/Polyimide, [0/±45/90/90]S	178
6-3	Allowable Buckling Stress Versus Core Thickness, Graphite/Polyimide, [0 ₃ /±45/90]S	178
6-4	Allowable Buckling Stress Versus Core Thickness, Graphite/Polyimide, [0 ₄ /±45/90]S	179
6-5	Allowable Buckling Stress Versus Core Thickness, Graphite/Polyimide, [0 ₂ /±45/90]S	179
6-6	Allowable Buckling Stress Versus Core Thickness, Graphite/Polyimide, [0 ₂ /±45 ₂ /90]S	180
6-7	Allowable Buckling Stress Versus Core Thickness, Graphite/Polyimide, [0/±45 ₂ /90]S	180
6-8	Allowable Buckling Stress Versus Core Thickness, Graphite/Polyimide, [0 ₃ /±45 ₂ /90]S	181
6-9	Allowable Buckling Stress Versus Core Thickness, Graphite/Polyimide, [0 ₄ /±45 ₂ /90]S	181
6-10	Allowable Buckling Stress Versus Core Thickness, Graphite/Polyimide, [0 ₅ /±45/90]S	182
6-11	Core Thickness Required to Develop Buckling Allowables Equal to Material Strength .	182

FIGURES

No.		Page
6-1	Stiffness CPLATE Element	183
6-2	Stiffness CCOVER Element	184
6-3	ATLAS Composite Design Subsets (Illustrative Only)	185
6-4	Initial Buckling of Flat Rectangular Panels	186

SYMBOLS

E_c	Young's Modulus in compression
E_k	Subset of elements (region)
F	Allowable axial stress
F_c	Allowable compressive stress
F_s	Allowable inplane shear stress
G	Modulus of rigidity (shear)
R	Maximum stress ratio
T_{ik}	Allowable matrix
a	Spanwise dimension of a panel
b	Chordwise dimension of a panel
d	Distance between centroids of sandwich panel face sheets
t	Face sheet thickness
σ	Vector of stresses
μ	Poisson's ratio

Subscripts

x	spanwise
y	chordwise
xy	diagonal

INTRODUCTION

This section discusses the advanced composite analysis and design capability within the ATLAS system. This capability was used to resize the honeycomb sandwich panels constructed of high strength graphite/polyimide. This section defines the procedures used for initial sizing prior to the automated resize activity described in Section 7. The choice of the maximum-strain failure criterion for the automated strength resize is discussed. The method of reducing the allowable strains such that the panels will be stable under combined biaxial compression and shear load for the strength-only resize is outlined. The subsequent panel stability evaluation indicated that buckling of the strength-sized panels was of very limited extent and required a negligible weight increase to preclude buckling altogether.

The design guidelines that were used in the automated strength sizing are discussed at length. The results of each of the automated resize cycles are shown in detail in Section 7.

COMPOSITE ANALYSIS IN ATLAS

To perform the advanced composite analysis and automated design, two special-purpose elements were added to the ATLAS system (ref. 6-1). The CPLATE element shown in figure 6-1 is used to model advanced composite laminates. The CCOVER element shown in figure 6-2 is a macro-element derived from the CPLATE element. The CCOVER element models the advanced composite laminates of the wing upper and lower surface panels simultaneously within a single element.

Each composite material (identified by a reference code) is defined by:

- 1) ply (layer) thickness
- 2) material area density defining the mass of a unit area of the ply (layer)
- 3) the following material properties for each applicable temperature
 - a) Young's moduli associated with the two orthogonal principal directions of the material
 - b) major Poisson's ratio in the plane determined by the above principal directions
 - c) shear modulus in the plane determined by the above principal directions
 - d) thermal strain for above temperature relative to 70°F for each of the two principal directions
 - e) allowable ultimate and yield (limit) tensile stresses for the two principal directions

- f) allowable ultimate and yield (limit) compressive stresses for the two principal directions
- g) allowable ultimate and yield (limit) shear stress in the plane determined by the principal directions

STRENGTH OPTIMIZATION IN ATLAS

The advanced composite optimization in ATLAS is of the "math programming" type. It operates solely on the CPLATE and CCOVER elements. The lamina thicknesses are minimized on the basis of user-defined specifications. The structure is considered to be divided into a number of regions. Each region constitutes an optimization problem which is considered independently of the others. A region may be defined as anything from a single element to all the elements composing the entire structure. The optimization of structure thus involves the solution of the problems (regions) that represent the entire structure. The remainder of this discussion of strength optimization in ATLAS will address only a single optimization problem (region).

A single optimization problem may be defined in the following manner (see figure 6-3). Given a subset of elements E_K (region) and an associated subset E_{KS} (design set), laminate strains for the design load cases and an initial set of lamina thicknesses upon which the strains are based; determine the set of lamina thicknesses having least weight for all composite elements in E_K based on the results of optimization of all elements in E_{KS} assuming regionally constant results.

The optimization procedure requires the repeated evaluation of stresses or strains as the design variables (lamina thicknesses) change. The lamina stresses or strains are based on the assumption that total laminate load remains constant and strain compatibility exists for all laminae. It is further assumed that all elements in E_K have the same number of laminae, identical lamina orientations and that the lamina thicknesses can be regarded as real variables.

This composite optimization satisfies strength constraints for which two optional failure criteria are considered. The maximum strain failure criterion involves the comparison of applied strain components to allowable strain components. This criteria is performed for each lamina for each design load case. The most critical margin of safety is used to update the sizing. The alternative to the maximum strain criterion is the Tsai-Hill failure criterion. This may be defined as

$$\vec{\sigma}_{ik} T_{ik} \vec{\sigma}_{ik} \leq 1.0 \quad (6-1)$$

where σ_{ik} is the vector of stresses for lamina i of the laminate k . The allowables matrix T_{ik} is defined as

$$T_{ik} = \begin{bmatrix} \frac{1}{F_{x_{ik}}^2} & \frac{-1}{2F_{x_{ik}}^2} & 0 \\ \frac{-1}{2F_{x_{ik}}^2} & \frac{1}{F_{y_{ik}}^2} & 0 \\ 0 & 0 & \frac{1}{F_{xy_{ik}}^2} \end{bmatrix} \quad (6-2)$$

where

$$\begin{aligned} F_{x_{ik}} &= \text{allowable axial stress in the x-direction} \\ F_{y_{ik}} &= \text{allowable axial stress in the y-direction} \\ F_{xy_{ik}} &= \text{allowable shear stress} \end{aligned}$$

The x- and y-directions are the two orthogonal principal directions of the orthotropic lamina i in the laminate k . Tensile or compressive allowable stress is selected to agree with the sign of the corresponding applied stress. To use the Tsai-Hill criterion as the basis for resizing, certain requirements must be satisfied regarding the allowable stresses. The allowables matrix cited above must be positive definite. If it were not, it would be possible to have stress fields for which the expression would remain negative for any lamina thickness. The determinant of the matrix T_{ik} is given by

$$\det T_{ik} = \frac{1}{F_{xy_{ik}}^2} \left[\frac{1}{F_{x_{ik}}^2} \left(\frac{1}{F_{y_{ik}}^2} - \frac{1}{4F_{x_{ik}}^2} \right) \right] \quad (6-3)$$

It may be seen that T_{ik} is not positive definite when $F_{y_{ik}} > 2F_{x_{ik}}$. Thus it is required that the layer allowable axial stress always is associated with the x-direction within the lamina.

Each optimization problem is solved iteratively. Each cycle in this iteration involves a screening or definition phase and a solution phase. The screening phase searches subset E_{ks} to establish the critical element and load case for each lamina of the laminate. This screening is performed with the objective of establishing the strength constraints to be used during the optimization or solution phase. This procedure consequently requires all elements in subset E_k to have the same number of laminae in corresponding laminates. Subsets containing CCOVER elements are treated as two independent problems (i.e., upper and lower CPLATES). The solution phase involves the optimization for minimum weight with constraints as defined above. In a given cycle after the optimization is completed the screening is repeated. If the same element and load case is critical for each lamina, the solution is complete. Otherwise, another optimization is performed subject to the newly defined constraints. This iteration is continued until the constraint definitions have stabilized or for a maximum of ten times for each problem.

The optimization is based on the method of feasible directions. Weight is the merit function which is to be minimized subject to the defined constraints. The method of feasible directions (Zoutendyk's method) establishes a direction along which a small step can be taken without violating the constraints. In this method, this direction is defined by solving a linear programming problem in which the decrease in the merit function (weight) is maximized subject to the constraints which insure that the direction is feasible.

Prior to initiating optimization the design variables (lamina thicknesses) are scaled so that the largest constraint value is equal to zero. This same normalization is performed after the optimization is complete.

The optimization is considered to have converged if in three consecutive iterations the relative and absolute change in the value of the merit function is less than 0.001. As noted above, the maximum number of iterations is ten.

The user may define constraints that equate the thicknesses for different laminae. This results in an optimization problem with fewer design variables but the same number of constraints.

After the optimization problem has been solved for the values of the design variables, when the latter are regarded as real variables, each value is then transformed to an integer number of layers (plies) to describe the corresponding actual laminate. Since the primary purpose of the ATLAS Composite Design module in this application is to establish theoretical structural weight, the real-to-integer transformation is based on an arithmetic averaging concept. For example 6.3 layers would be rounded to six layers. This obviously does not insure positive margins throughout the structure, but is expected to yield a more realistic theoretical weight estimate for the total structure considered.

INITIAL SIZING PROCEDURES

The initial sizing of most of the elements of the advanced composite model for analysis and design via ATLAS is described in detail in Section 7. Not described in Section 7, however, is the core thickness of the honeycomb sandwich wing panels. These paragraphs will outline the manual analysis procedures used to evaluate core thickness requirements to develop the laminate strengths in spanwise or chordwise compression or shear. Similar results are shown for a number of laminates from which a core thickness was selected.

Abbreviated analysis procedures were established for general instability analyses of the advanced composite honeycomb sandwich panels by assuming the core was rigid. Panels sized by these abbreviated procedures were "spot-checked" with analyses using the more complex formulae that account for the core properties. Spanwise (0°) and chordwise compression allowables checked out within two percent (unconservative), while the shear allowables differed by about eight percent (conservative). Shear and compression intracell buckling were checked for 1/4 in. cell size with minimum skin gage. All local instability allowables exceeded the material strength for the $[0+45/90/-45]_S$ laminate with 2 mil ply thicknesses. The $[0/\pm 45/90]_S$ laminate was shown to be appreciably weaker in chordwise compressive intracell buckling for which the laminate material strength was not developed.

The abbreviated formulae for panel general instability are given below. The allowable spanwise compressive stress (F_{cx}) is given by

$$F_{cx} = K E_x \left(\frac{t_e}{b\alpha^{1/4}} \right)^2 \quad (6-4)$$

where

$$K = \text{a function of } \frac{a}{b\alpha^{1/4}}$$

$$a = \text{spanwise dimension of panel}$$

$$b = \text{chordwise dimension of panel}$$

$$\alpha = \frac{E_x}{E_y}$$

$$t_e = \frac{2\sqrt{t_1 t_2}}{t_1 + t_2} d\sqrt{3} \quad \text{for unequal face sheet thicknesses}$$

$$t_e = d\sqrt{3} \quad \text{for equal face sheet thicknesses}$$

For unequal face gages the allowable spanwise compressive stress is given by

$$F_{cx} = K E_x \frac{12 t_1 t_2}{(t_1 + t_2)} \left(\frac{d}{b \alpha^{1/4}} \right)^2 \quad (6-5)$$

For equal face gages the allowable spanwise compressive stress is given by

$$F_{cx} = 3 K E_x \left(\frac{d}{b \alpha^{1/4}} \right)^2 \quad (6-6)$$

The abbreviated formula for the chordwise compressive allowable stress, F_{cy} , is

$$F_{cy} = \frac{\pi^2}{12\lambda} E_y \left(\frac{t_e}{b} \right)^2 c_f \quad (6-7)$$

where

$$\lambda = 1 - \mu_x \mu_y$$

$$c_f = \text{end fixity factor provided the panel by the spars}$$

For unequal face sheet thicknesses, the allowable chordwise compressive stress is given by

$$F_{cy} = \pi^2 \frac{E_y}{\lambda} \frac{t_1 t_2}{(t_1 + t_2)} \left(\frac{d}{b} \right)^2 c_f \quad (6-8)$$

For equal face sheet thicknesses, the allowable chordwise compressive stress is given by

$$F_{cy} = \frac{\pi^2}{4} \frac{E_y}{\lambda} \left(\frac{d}{b} \right)^2 c_f \quad (6-9)$$

The abbreviated formula for the allowable inplane shear stress F_{xy} , is given by

$$F_{xy} = K_s \frac{\pi^2}{12\lambda} E \left(\frac{t_e}{b} \right)^2 \quad (6-10)$$

where

$$E = 2(1 + \mu_e) G$$

$$\mu_e = (\mu_x \mu_y)^{1/2}$$

$$\lambda = 1 - \mu_x \mu_y$$

$$K_s = \text{a function of } a/b$$

For unequal face sheet thicknesses, the allowable shear stress is given by

$$F_{xy} = 2 K_s \pi^2 \frac{G}{1 - \mu_e} \frac{t_1 t_2}{(t_1 + t_2)} \left(\frac{d}{b} \right)^2 \quad (6-11)$$

For equal face sheet thicknesses, the allowable shear stress is given by

$$F_{xy} = \frac{K_S \pi^2}{2} \frac{G}{1 - \mu_e} \left(\frac{d}{b} \right)^2 \quad (6-12)$$

The more complex formulae for panel general instability which account for the core properties are given below. The allowable spanwise compressive stress is given by

$$F_{cx} = \frac{3 E_x \left(\frac{2h K_c}{t_1 + t_2} \right)}{\left[\frac{b \alpha^{1/4}}{d k^{1/2}} \frac{t_1 + t_2}{2 \sqrt{t_1 t_2}} \right]^2 \left(\frac{2h K_c}{t_1 + t_2} \right) + E_x} \quad (6-13)$$

where

$$h = c + t_1 + t_2 = d + \frac{1}{2} (t_1 + t_2)$$

$$K_c = \frac{1}{6} (G_{yz} + G_{xz})$$

$$k = K \frac{\pi^2}{12 (1 - \mu_x \mu_y)}$$

The formula for the chordwise compressive allowable stress which accounts for the core properties is

$$F_{cy} = \frac{3 E_y \left(\frac{2h K_c}{t_1 + t_2} \right)}{\left[\frac{b}{d \sqrt{k}} \frac{t_1 + t_2}{2 \sqrt{t_1 t_2}} \right]^2 \left(\frac{2h K_c}{t_1 + t_2} \right) + E_y} \quad (6-14)$$

where

$$h = c + t_1 + t_2 = d + \frac{1}{2} (t_1 + t_2)$$

$$K_c = \frac{1}{6} (G_{yz})$$

$$k = \frac{\pi^2 c_f}{12 (1 - \mu_x \mu_y)} \left(\frac{b}{a} \right)^2$$

$$c_f = \text{the end fixity factor provided the panels by the spars}$$

The formula for the allowable inplane shear stress accounting for the core properties is

$$F_S = \frac{G/2}{\frac{1}{6} \left(\frac{b}{d \sqrt{k_s}} \frac{t_1 + t_2}{2 \sqrt{t_1 t_2}} \right)^2 + \left(\frac{G}{\frac{2h K_{cs}}{t_1 + t_2}} \right)} \quad (6-15)$$

where

$$K_{CS} = \frac{1}{2} (G_{yz} + G_{xz})$$

$$k_S = K_S \frac{\pi^2}{12(1 - \mu_x \mu_y)}$$

$$K_S = \text{a function of } a/b$$

It should be noted from Section 3 that the 1986 high-strength graphite/polyimide will be available in 2-, 3- and 4-mil thickness tapes. Also that 0.016 in. and 0.032 in. (0.024 in.) were selected as minimum gage for the inner and outer face sheet gages, respectively, for the lower (upper) surface. The inner and outer face sheets will be further constrained to exhibit the same stress-strain relations. For the subsequent calculations, the component laminates are assumed to have the properties shown below:

Property	Laminate		
	0°	90°	±45°
Compressive Strength, F_c (ksi)	290	16.4	37.4
Poisson's Ratio, μ	0.31	0.018	0.80
Young's Modulus, E_c (msi)	20.0	1.13	2.58
Shear Strength, F_S (ksi)	20.8	20.8	148.0
Modulus of Rigidity, G (msi)	0.717	0.717	5.1

In addition, the laminate density is taken as 0.056 lb/in³ and that of the core as 0.00203 lb/in³

Considering first the spanwise compressive allowable, consider equation 6-5 and 6-6. Since the value of the corrected aspect ratio is much larger than unity, the value of K is taken as the asymptotic value 3.62. Additionally, the loaded width b is the spar spacing, 35 in. Substituting these values first in equation 6-5 and 6-6 yields

$$F_{cx} = 35\,500 \frac{t_1 t_2}{(t_1 + t_2)^2} \frac{E_x}{10^6} \frac{d^2}{\sqrt{\alpha}} \quad (6-16)$$

for unequal face sheet thicknesses and

$$F_{cx} = 8860 \frac{E_x}{10^6} \frac{d^2}{\sqrt{\alpha}} \quad (6-17)$$

for equal face sheet thicknesses.

Considering next the chordwise compressive allowable, recall equations 6-8 and 6-9. Again the chordwise dimension of the panel is 35 in. and an end fixity factor of 2 is assumed. Substituting gives

$$F_{cy} = 16\,110 \left(\frac{t_1 t_2}{t_1 + t_2} \right)^2 \frac{d^2}{\lambda} \frac{E_y}{10^6} \quad (6-18)$$

for unequal face sheet thicknesses and

$$F_{cy} = 4030 \frac{d^2}{\lambda} \frac{E_y}{10^6} \quad (6-19)$$

for equal face sheet thicknesses.

Now consider the inplane allowable shear stress from equations 6-11 and 6-12. For large panel aspect ratio, the buckling factor K_S equals 5.34. Substituting this and the value of 35 in. for b gives

$$F_{xy} = 86\,000 \left(\frac{t_1 t_2}{t_1 + t_2} \right)^2 (1 - \mu_e) \frac{G}{10^6} \frac{d^2}{\lambda} \quad (6-20)$$

for unequal face sheet thicknesses and

$$F_{xy} = 21\,500 (1 + \mu_e) \frac{G}{10^6} \frac{d^2}{\lambda} \quad (6-21)$$

for equal face sheet thicknesses.

Consider now a sandwich panel with the face sheets constructed of $[0/\pm 45/90]_S$ laminates. The inner face sheet has 8 plies of 0.002 in. thickness, and the outer has 16 plies of 0.002 in. thick material. Thus,

$$\begin{aligned} T_1 &= 8(.002) = 0.016 \text{ in.} \\ T_2 &= 16(.002) = 0.032 \text{ in.} \\ t &= 24(.002) = 0.048 \text{ in.} \\ d &= c + \frac{1}{2}(0.016 + 0.032) = c + 0.024 \end{aligned} \quad (6-22)$$

where

$$\begin{aligned} T_1 &= \text{the inner face sheet thickness} \\ T_2 &= \text{the outer face sheet thickness} \\ d &= \text{distance between face sheet centroids} \\ c &= \text{core height} \end{aligned}$$

Using the property values from above we obtain the following average values for the laminate

$$\begin{aligned}
 F_{cx} &= \frac{1}{4}(290 + 16.4 + 74.8) = F_{cy} = 95.3 \text{ ksi} \\
 E_x &= \frac{1}{4}(20 + 1.13 + 5.16) = E_y = 6.57 \text{ msi} \\
 F_S &= \frac{1}{2}(20.8 + 148) = 84.4 \text{ ksi} \\
 G &= \frac{1}{2}(0.717 + 5.1) = 2.91 \text{ msi} \\
 \mu_x &= \frac{.31(1.13) + .018(20) + .80(2.58)^2}{1.13 + 20. + 2.58(2)} = \mu_y = 0.184 \quad (6-23) \\
 \alpha &= E_x/E_y = 95.3/95.3 = 1 \\
 \mu_e &= (\mu_x \mu_y)^{1/2} = 0.184 \\
 \lambda &= 1 - \mu_x \mu_y = 1 - (0.184)^2 = 0.966
 \end{aligned}$$

$$\frac{t_1 t_2}{(t_1 + t_2)^2} = \frac{.016(.032)}{(.016 + .032)^2} = 2/9$$

Substituting the above values in equations 6-16, 6-18 and 6-20 gives

$$\begin{aligned}
 F_{cx} &= 35\,500(2/9)6.57d^2 = 51\,800d^2 \\
 F_{cy} &= 16\,110(2/9)6.57(1/.966d^2) = 24\,400d^2 \\
 F_{xy} &= 86\,000(2/9)\frac{1.184}{6.966}(2.91)d^2 = 68\,200d^2
 \end{aligned} \quad (6-24)$$

The allowable spanwise and chordwise compressive stresses and the allowable shear stress for the above panel are given in table 6-1 for a range of core thicknesses. Tables 6-1 through 6-10 show allowable stresses for a range of core thicknesses for other laminates (face sheets) of interest. Finally, table 6-11 shows a summary of the core thicknesses required to develop each of the allowable stresses for the laminates shown. Due to the limited scope of the study, only a single core thickness was selected although this parameter is known to effect optimum theoretical weight significantly. A core thickness of 1.50 in. was chosen since it develops the allowable spanwise compressive stress up to the material strength for all panels except those with thick face sheets and a preponderance of spanwise-oriented plies. It is more than sufficient to develop the allowable inplane shear strength. A core of nearly 2.00 in. thickness would be required to develop the chordwise compressive allowable stresses up to the material strength. Chordwise compression loads are small except near the side-of-body, near the landing trunnions and other such points with localized loads being introduced. The possible addition of some face sheet material over a very limited portion of the wing seemed advantageous compared to the relatively large increase in core thickness throughout the wing primary structure.

ALLOWABLES FOR STRUCTURAL RESIZING

Prior to performing the automated strength resizing, it was necessary to select a failure criterion and the associated material allowables. For 1976 advanced composites with their attendant matrix micro-cracking problems, the Tsai-Hill failure criterion correlates with test data better than other failure criteria (ref. 2-2). Since it was hypothesized that the 1986 high strength graphite/polyimide would permit design and fabrication of laminates that are truly fiber critical, an empirical data base with which to evaluate the various failure criteria was effectively lost. This, and the ease with which the maximum strain criterion can be physically interpreted, led to the choice of the latter as the failure criterion.

The titanium wing panels of Task II were replaced with high strength graphite/polyimide sandwich panels. However, since this phase of the contract was limited in scope, the spars and ribs in the wing primary structure remained of titanium structure as defined in Task II. However, it was assumed that the titanium alloy used in 1986 would, through development, have higher allowable stresses (strains) with no change in the elastic properties. The specific assumptions made for the titanium allowable properties are shown below:

Temperature °F	Modulus msi	Allowable Stress* ksi	Allowable Strain* μm/m
RT	16.4	164.0	10 000
250	15.5	139.5	9 000
450	14.6	116.8	8 000

*Uniaxial Tension or Compression

The high strength graphite/polyimide properties are shown in table 2-1. The values for 250°F while not shown are identical to those at room temperature. It should be noted that the allowable strains for the high strength graphite/polyimide are significantly larger than those for the titanium alloy. To retain strain compatibility with the titanium spar and rib chords, the strains of the high strength graphite/polyimide have been limited to the allowable titanium strain. The mathematical model of the structure specifies a different material for the 0°, ±45° and 90° laminae on the upper surface and the lower. Thus, different strain limitations may be imposed on these laminae.

The 0° and 90° laminae allowable tensile strains were reduced to the allowable titanium tensile strain for the appropriate temperature. The allowable compressive strain for the 0° lamina (spanwise) was also reduced to these same strain limits. This, then, for uniaxial spanwise loading defines the maximum stress ratios as

$$\begin{aligned}
 R_{\text{spanwise}} &= \frac{F_{\text{applied}}}{F_{\text{allowable}}} = \frac{200 \text{ ksi}}{290 \text{ ksi}} = 0.69 \text{ @ Room Temperature} \\
 &= \frac{180 \text{ ksi}}{290 \text{ ksi}} = 0.621 \text{ @ 250°F} \\
 &= \frac{160 \text{ ksi}}{260 \text{ ksi}} = 0.615 \text{ @ 450°F}
 \end{aligned}$$

The interaction relationship used for buckling failure under combined biaxial compression and shear is shown in figure 6-4. This is used solely to establish the allowable strains. From figure 6-4 it can be seen that if $R_x = 0.69$, then R_y (chordwise) is limited to 0.767 in the absence of any shear loading. In the Initial Sizing Procedures paragraph above, a core thickness of 1.5 inches was selected. This core thickness develops only about 67% of the material allowable as an allowable buckling stress for chordwise compression loads. Thus for a chordwise-oriented ply, the allowable stress for the above biaxial compressive loading ($R_x = 0.69$ and $R_y = 0.767$) is

$$F_{cy} = 0.767 (0.67) 290 = 149 \text{ ksi}$$

The decision was made to reduce the above chordwise compressive stress from 149 ksi to 134 ksi to permit some allowance for shear loading in conjunction with the biaxial compression. Thus, the maximum chordwise compressive stress ratio becomes

$$R_{y_{\max}} = \frac{134}{0.67 (290)} = 0.69$$

For spanwise compression and shear loading only the maximum shear stress ratio R_{xy} would be 0.55. For chordwise compression and shear loading only, the maximum shear stress ratio would be 0.76. With these conflicting values, a maximum diagonal stress of 200 ksi was selected which gives

$$R_{xy_{\max}} = \frac{200 \text{ ksi}}{290 \text{ ksi}} = 0.69$$

Thus for room temperature, the allowable stress ratios are

$$\begin{aligned} R_{x_{\max}} &= 0.69 \\ R_{y_{\max}} &= 0.69 \\ R_{xy_{\max}} &= 0.69 \end{aligned}$$

Procedures similar to those above were followed with the 250°F properties to give

$$\begin{aligned} R_{x_{\max}} &= 0.621 \\ R_{y_{\max}} &= 0.739 \\ R_{xy_{\max}} &= 0.721 \end{aligned}$$

And, similarly for 450°F

$$\begin{aligned} R_{x_{\max}} &= 0.615 \\ R_{y_{\max}} &= 0.744 \\ R_{xy_{\max}} &= 0.719 \end{aligned}$$

For room temperature the preceding values redefined in terms of allowable strains in the individual lamina axes for the various laminae becomes

Lamina	Allowable Strain, in./in.		
	Tension	Compression	Shear
0°—longitudinal	0.01	-0.01	±0.029
0°—transverse	0.01475	-0.0145	±0.029
±45°—longitudinal	0.01475	-0.01	±0.029
±45°—transverse	0.01475	-0.0145	±0.029
90°—longitudinal	0.01	-0.0067	±0.029
90°—transverse	0.01475	-0.0145	±0.029

For 250°F, the allowable strains in the individual lamina axes for the various laminae are

Lamina	Allowable Strain, in./in.		
	Tension	Compression	Shear
0°—longitudinal	0.009	-0.009	±0.029
0°—transverse	0.01475	-0.0145	±0.029
±45°—longitudinal	0.01475	-0.01045	±0.029
±45°—transverse	0.01475	-0.0145	±0.029
90°—longitudinal	0.009	-0.0072	±0.029
90°—transverse	0.01475	-0.0145	±0.029

For 450°F, the allowable strains in the individual lamina axes for the various laminae are

Lamina	Allowable Strain, in./in.		
	Tension	Compression	Shear
0°—longitudinal	0.008	-0.008	±0.026
0°—transverse	0.0133	-0.013	±0.026
±45°—longitudinal	0.01325	-0.00935	±0.026
±45°—transverse	0.0133	-0.013	±0.026
90°—longitudinal	0.008	-0.0065	±0.026
90°—transverse	0.0133	-0.013	±0.026

It should be noted that all laminates will be designed having a minimum of one lamina in each orientation.

For the ATLAS composite design module, the various laminate allowable strains had to be specified as allowable stresses. The reduced stiffnesses which transform strains to stresses in the individual lamina 1-2 coordinate axis system are given in terms of engineering constants by

$$\begin{aligned}
Q_{11} &= E_1 / (1 - \mu_{12} \mu_{21}) \\
Q_{12} &= \mu_{12} E_2 / (1 - \mu_{12} \mu_{21}) = \mu_{21} E_1 / (1 - \mu_{12} \mu_{21}) \\
Q_{22} &= E_2 / (1 - \mu_{12} \mu_{21}) \\
Q_{66} &= G_{12}
\end{aligned} \tag{6-26}$$

Thus for an individual lamina, the strain-stress relations are

$$\begin{Bmatrix} \sigma_1 \\ \sigma_2 \\ \tau_{12} \end{Bmatrix} = \begin{bmatrix} Q_{11} & Q_{12} & 0 \\ & Q_{22} & 0 \\ \text{(sym)} & & Q_{66} \end{bmatrix} \begin{Bmatrix} \epsilon_1 \\ \epsilon_2 \\ \gamma_{12} \end{Bmatrix} = \begin{bmatrix} \frac{E_1}{1 - \mu_{12} \mu_{21}} & \frac{\mu_{12} E_2}{1 - \mu_{12} \mu_{21}} & 0 \\ & \frac{E_2}{1 - \mu_{12} \mu_{21}} & 0 \\ \text{(sym)} & & G_{12} \end{bmatrix} \begin{Bmatrix} \epsilon_1 \\ \epsilon_2 \\ \gamma_{12} \end{Bmatrix} \tag{6-27}$$

For high strength graphite/polyimide at room temperature:

$$\begin{aligned}
E_1 &= 20\,000 \text{ ksi} \\
E_2 &= 1130 \text{ ksi} \\
G_{12} &= 717 \text{ ksi} \\
\mu_{12} &= 0.31
\end{aligned} \tag{6-28}$$

From the reciprocal relation

$$\frac{\mu_{12}}{E_1} = \frac{\mu_{21}}{E_2} \tag{6-29}$$

it follows that

$$\mu_{21} = \frac{E_2}{E_1} \mu_{12} = \frac{1130}{20\,000} (0.31) = 0.0175 \tag{6-30}$$

Substituting these values in equation 6-27 gives

$$\begin{Bmatrix} \sigma_1 \\ \sigma_2 \\ \tau_{12} \end{Bmatrix} = \begin{bmatrix} \frac{20\,000}{1 - 0.31(0.0175)} & \frac{0.31(1130)}{1 - 0.31(0.0175)} & 0 \\ & \frac{1130}{1 - 0.31(0.0175)} & 0 \\ \text{(sym)} & & 717 \end{bmatrix} \begin{Bmatrix} \epsilon_1 \\ \epsilon_2 \\ \gamma_{12} \end{Bmatrix} = \begin{bmatrix} 20\,100 & 352 & 0 \\ & 1136 & 0 \\ \text{(sym)} & & 717 \end{bmatrix} \begin{Bmatrix} \epsilon_1 \\ \epsilon_2 \\ \gamma_{12} \end{Bmatrix} \tag{6-31}$$

Now substituting the allowable strains for room temperature in equation 6-31 provides the corresponding allowable stresses along the individual lamina axes.

Lamina	Allowable Stress, ksi		
	Tension	Compression	Shear
0°—longitudinal	206.0	-206.0	±20.8
0°—transverse	20.3	- 19.99	±20.8
±45°—longitudinal	302.0	-206.00	±20.8
±45°—transverse	21.9	- 19.99	±20.8
90°—longitudinal	206.0	-139.80	±20.8
90°—transverse	20.3	- 18.83	±20.8

Similarly for 250°F, the allowable stresses for the various laminae along the individual lamina axes are

Lamina	Allowable Stress, ksi		
	Tension	Compression	Shear
0°—longitudinal	186.10	-186.00	±20.8
0°—transverse	19.92	- 19.64	±20.8
±45°—longitudinal	302.00	-215.00	±20.8
±45°—transverse	21.90	- 20.20	±20.8
90°—longitudinal	186.10	-149.80	±20.8
90°—transverse	19.92	- 19.01	±20.8

For 450°F, the allowable stresses for the various laminae along the individual lamina axes are

Lamina	Allowable Stress, ksi		
	Tension	Compression	Shear
0°—longitudinal	164.30	-164.30	±12.01
0°—transverse	16.33	- 16.02	±12.01
±45°—longitudinal	269.00	-191.30	±12.01
±45°—transverse	18.02	- 16.46	±12.01
90°—longitudinal	164.30	-134.20	±12.01
90°—transverse	16.33	- 15.54	±12.01

The above allowables have been shown through use in the strength resizing to have adequately accomplished their purpose. That is, to provide allowance for panel stability under combined loading during strength resizing which had no explicit panel stability analysis. This is discussed further in Section 7.

REFERENCE

- 6-1 Robinson, James C.; Yates, E. Carson, Jr.; Turner, M. Jonathan; and Grande, Donald L.: *"Application of an Advanced Computerized Structural Design System to an Arrow-Wing Supersonic Cruise Aircraft."* AIAA Paper 75-1038, August 1975.

Table 6-1.—Allowable Buckling Stress Versus Core Thickness,
Graphite/Polymide, $[0/\pm 45/90]_S$

$F_{cx} = 95.3$ ksi
 $F_{cy} = 95.3$ ksi
 $F_s = 84.4$ ksi

Minimum gage

$t_1 = 0.016$ in. $t_2 = 0.032$ in. $\bar{t} = 0.048$ in.

c, in.	d, in.	$F_{x'}$ ksi	$F_{y'}$ ksi	$F_{xy'}$ ksi
0.25	0.274	3.887	1.828	5.120
0.50	0.574	14.216	6.687	18.726
0.75	0.774	31.016	14.590	40.858
1.0884	1.1124	64.066	30.136	84.4
1.3327	1.3567	95.3	44.827	
1.9542	1.9782		95.3	

$t_1 = 0.024$ in. $t_2 = 0.032$ in. $\bar{t} = 0.056$ in.

c, in.	d, in.	$F_{x'}$ ksi	$F_{y'}$ ksi	$F_{xy'}$ ksi
0.25	0.278	4.321	2.033	5.693
0.50	0.528	15.588	7.333	20.534
0.75	0.778	33.844	15.921	44.583
1.042	1.070	64.017	30.114	84.4
1.2775	1.3055	95.3	44.829	
1.875	1.903		95.3	

$t_1 = t_2 = 0.032$ in. $\bar{t} = 0.064$ in. —

c, in.	d, in.	$F_{x'}$ ksi	$F_{y'}$ ksi	$F_{xy'}$ ksi
0.25	0.282	4.631	2.179	6.102
0.50	0.532	16.484	7.753	21.716
0.75	0.782	35.617	16.752	46.92
1.017	1.049	64.091	30.145	84.4
1.247	1.279	95.3	44.814	
1.833	1.865		95.3	

Table 6-2.—Allowable Buckling Stress Versus Core Thickness,
Graphite/Polyimide, $[0/\pm 45/90]_S$

$t_1 = 0.018$ in.
 $t_2 = 0.036$ in.
 $\bar{t} = 0.054$ in.

$F_{cx} = 86.5$ ksi
 $F_{cy} = 116.9$ ksi
 $F_s = 77.3$ ksi

c, in.	d, in.	$F_{x'}$ ksi	$F_{y'}$ ksi	$F_{xy'}$ ksi
0.25	0.277	4.192	2.274	5.253
0.50	0.527	15.175	8.230	19.014
0.75	0.777	32.988	17.890	41.333
1.036	1.063	61.74	33.483	77.3
1.2312	1.2582	86.5	46.909	
1.500	1.527		69.094	
1.600	1.627		78.439	
1.700	1.727		88.379	
1.8	1.827		98.910	
1.959	1.986		116.9	

Table 6-3.—Allowable Buckling Stress Versus Core Thickness,
Graphite/Polyimide, $[0_3/\pm 45/90]_S$

4 mil plies
 $t_1 = t_2 = 0.048$ in.
 $\bar{t} = 0.096$ in.

$F_{cx} = 160.2$ ksi
 $F_{cy} = 69.0$ ksi
 $F_s = 63.2$ ksi

c, in.	d, in.	$F_{x'}$ ksi	$F_{y'}$ ksi	$F_{xy'}$ ksi
0.25	0.298	5.708	1.73	4.77
0.50	0.548	19.3	5.85	16.1
0.75	0.798	40.9	12.4	34.2
1.0363	1.0843	75.57	22.9	63.2
1.2	1.248	100.1	30.3	
1.3	1.348	116.8	35.4	
1.4	1.448	134.8	40.9	
1.5	1.548	154	46.7	
1.5307	1.5787	160.2	48.562	
1.8338	1.8818		69.0	

Table 6-4.—Allowable Buckling Stress Versus Core Thickness,
Graphite/Polyimide, $[0_4/\pm 45/90]_S$

4 mil inner ply
4 mil outer ply
 $t_1 = t_2 = 0.056$ in.
 $\bar{t} = 0.112$ in.

$F_{cx} = 178.7$ ksi
 $F_{cy} = 61.5$ ksi
 $F_s = 57.1$ ksi

c, in.	d, in.	$F_{x'}$ ksi	$F_{y'}$ ksi	$F_{xy'}$ ksi
0.25	0.306	6.0	1.62	4.49
0.50	0.556	19.82	5.35	14.81
0.75	0.806	41.65	11.24	31.13
1.0356	1.0916	76.39	20.62	<u>57.1</u>
1.2	1.256	101.13	27.3	
1.4	1.456	135.91	36.7	
1.5	1.556	155.2	41.9	
1.6136	1.6696	<u>178.7</u>	48.2	
1.829	1.885		<u>61.5</u>	

Table 6-5.—Allowable Buckling Stress Versus Core Thickness,
Graphite/Polyimide, $[0_2/\pm 45/90]_S$

4 mil inner ply
4 mil outer ply
 $t_1 = t_2 = 0.040$ in.
 $\bar{t} = 0.080$ in.

$F_{cx} = 134.2$ ksi
 $F_{cy} = 79.5$ ksi
 $F_s = 71.7$ ksi

c, in.	d, in.	$F_{x'}$ ksi	$F_{y'}$ ksi	$F_{xy'}$ ksi
0.25	0.29	5.31	1.9	5.2
0.50	0.54	18.4	6.57	18.1
0.75	0.79	39.4	14.1	38.8
1.0341	1.0741	72.85	26.0	<u>71.7</u>
1.2	1.24	97.1	34.7	
1.4178	1.4578	<u>134.2</u>	47.9	
1.5	1.54		53.5	
1.8578	1.8778		<u>79.5</u>	

Table 6-6.—Allowable Buckling Stress Versus Core Thickness,
Graphite/Polyimide, $[0_2/\pm 45_2/90]_S$

4 mil inner ply
4 mil outer ply
 $t_1 = t_2 = 0.056$ in.
 $\bar{t} = 0.112$ in.

$F_{cx} = 106.6$ ksi
 $F_{cy} = 67.5$ ksi
 $F_s = 93.5$ ksi

c, in.	d, in.	$F_{x'}$ ksi	$F_{y'}$ ksi	$F_{xy'}$ ksi
0.25	0.306	4.9	1.85	8.4
0.50	0.556	16.0	6.1	27.7
0.75	0.806	33.7	12.8	58.3
0.965	1.021	54.0	20.6	<u>93.5</u>
1.20	1.256	81.77	31.2	
1.378	1.434	<u>106.6</u>	40.6	
1.50	1.556		47.8	
1.792	1.848		<u>67.5</u>	

Table 6-7.—Allowable Buckling Stress Versus Core Thickness,
Graphite/Polyimide, $[0/\pm 45_2/90]_S$

$t_1 = t_2 = 0.048$ in.
 $\bar{t} = 0.096$ in.

$F_{cx} = 76.0$ ksi
 $F_{cy} = 76.0$ ksi
 $F_s = 105.6$ ksi

c, in.	d, in.	$F_{x'}$ ksi	$F_{y'}$ ksi	$F_{xy'}$ ksi
0.25	0.298	4.125	2.040	5.410
0.50	0.548	13.950	6.897	18.295
0.75	0.798	29.581	14.625	38.795
1.0	1.048	51.020	25.225	66.911
1.23	1.278	<u>75.87</u>	37.512	99.503
1.27	1.318		39.897	<u>105.829</u>
1.50	1.548		55.036	
1.75	1.798		74.248	
1.77	1.818		<u>75.909</u>	

*Table 6-8.—Allowable Buckling Stress Versus Core Thickness,
Graphite/Polyimide, $[0_3/\pm 45_2/90]_S$*

All 4 mil plies
 $t_1 = t_2 = 0.064$ in.
 $\bar{t} = 0.128$ in.

$F_{cx} = 129.5$ ksi
 $F_{cy} = 61.1$ ksi
 $F_s = 84.4$ ksi

c, in.	d, in.	$F_{x'}$ ksi	$F_{y'}$ ksi	$F_{xy'}$ ksi
0.25	0.314	5.36	1.74	7.7
0.50	0.564	17.3	5.6	24.8
0.75	0.814	36.0	11.7	51.7
0.976	1.040	58.8	19.1	<u>84.4</u>
1.2	1.264	86.9	28.2	
1.479	1.543	<u>129.5</u>	42.0	
1.50	1.564		43.2	
1.797	1.861		<u>61.1</u>	

*Table 6-9.—Allowable Buckling Stress Versus Core Thickness,
Graphite/Polyimide, $[0_4/\pm 45_2/90]_S$*

$t_1 = t_2 = 0.072$ in.
 $\bar{t} = 0.144$ in.

$F_{cx} = 147.3$ ksi
 $F_{cy} = 56.1$ ksi
 $F_s = 77.3$ ksi

c, in.	d, in.	$F_{x'}$ ksi	$F_{y'}$ ksi	$F_{xy'}$ ksi
0.25	0.322	5.765	1.659	7.105
0.5	0.572	13.191	5.236	22.419
0.75	0.822	37.567	10.814	46.300
0.99	1.062	62.706	18.050	<u>77.283</u>
1.00	1.072	63.892	18.391	
1.25	1.322	97.168	27.970	
1.5	1.572	137.393	39.549	
1.56	1.632	<u>148.081</u>	42.625	
1.75	1.822		53.128	
1.80	1.872		<u>56.084</u>	

Table 6-10.—Allowable Buckling Stress Versus Core Thickness,
Graphite/Polyimide, $[0_5/\pm 45/90]_S$

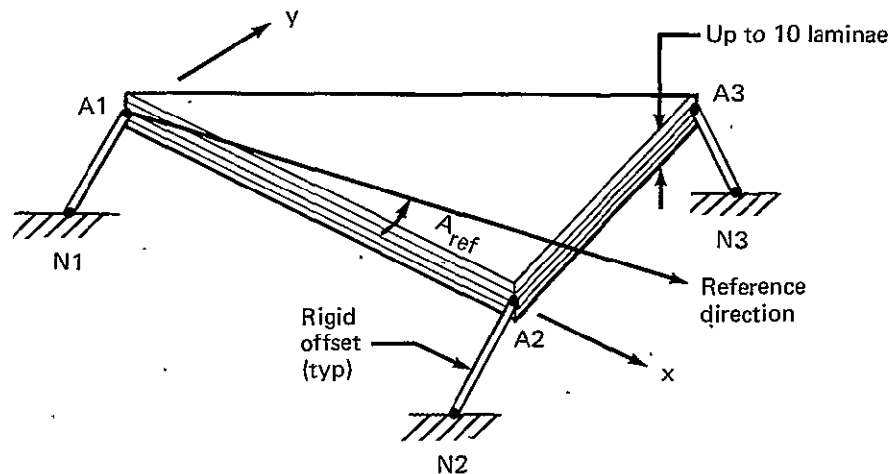
All 4 mil plies
 $t_1 = t_2 = 0.064$
 $\bar{t} = 0.128$

$F_{cx} = 192.65$ ksi
 $F_{cy} = 55.85$ ksi
 $F_s = 52.6$ ksi

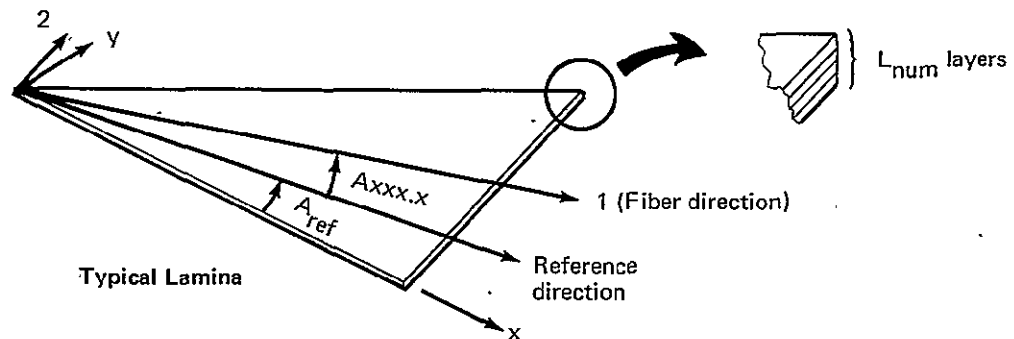
c, in.	d, in.	$F_{x'}$ ksi	$F_{y'}$ ksi	$F_{xy'}$ ksi
0.25	0.314	6.25		
0.50	0.564	20.2		
0.75	0.814	42.0		
1.095	1.159	85.2		52.6
1.25	1.314	109.5		
1.50	1.564	155.1	38.4	
1.743	1.807	192.65		
1.886	1.950		55.85	

Table 6-11.—Core Thickness Required to Develop Buckling Allowables
Equal to Material Strength

See table	Thickness of core required to develop allowables, in.			Layup	t_1 , in.	t_2 , in.
	$F_{cx'}$	$F_{cy'}$	$F_{s'}$			
6-1	1.33	1.95	1.09	$[0/\pm 45/90]_S$	0.016	0.032
6-1	1.28	1.88	1.04	$[0/\pm 45/90]_S$	0.024	0.032
6-1	1.25	1.83	1.02	$[0/\pm 45/90]_S$	0.032	0.032
6-2	1.23	1.96	1.04	$[0/\pm 45/90/\bar{90}]_S$	0.018	0.036
6-3	1.53	1.83	1.04	$[0_3/\pm 45/90]_S$	0.048	0.048
6-4	1.61	1.83	1.04	$[0_4/\pm 45/90]_S$	0.056	0.056
6-5	1.42	1.84	1.03	$[0_2/\pm 45/90]_S$	0.040	0.040
6-6	1.38	1.79	0.97	$[0_2/\pm 45_2/90]_S$	0.056	0.056
6-7	1.23	1.77	1.27	$[0/\pm 45_2/90]_S$	0.048	0.048
6-8	1.48	1.80	0.98	$[0_3/\pm 45_2/90]_S$	0.064	0.064
6-9	1.56	1.80	0.99	$[0_4/\pm 45_2/90]_S$	0.072	0.072
6-10	1.74	1.89	1.10	$[0_5/\pm 45/90]_S$	0.064	0.064

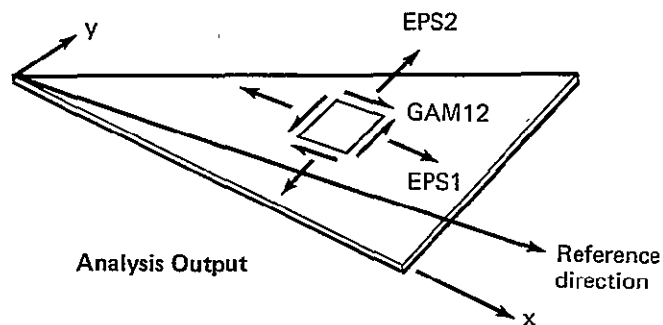


Triangular or quadrilateral laminated membrane plate element composed of up to 10 orthotropic laminae. The triangular CPLATE is a constant strain element. The quadrilateral CPLATE stiffness is generated from four constant strain triangles which intersect at a fifth internal node. This internal node is reduced by a static condensation. If warped, the quadrilateral CPLATE is equilibrated by transverse forces. The element may be offset from its structural nodes as shown above. A_{ref} defines the reference direction for the element.



The CPLATE is composed of 1 to 10 laminae, each of which is defined by four properties as shown below:

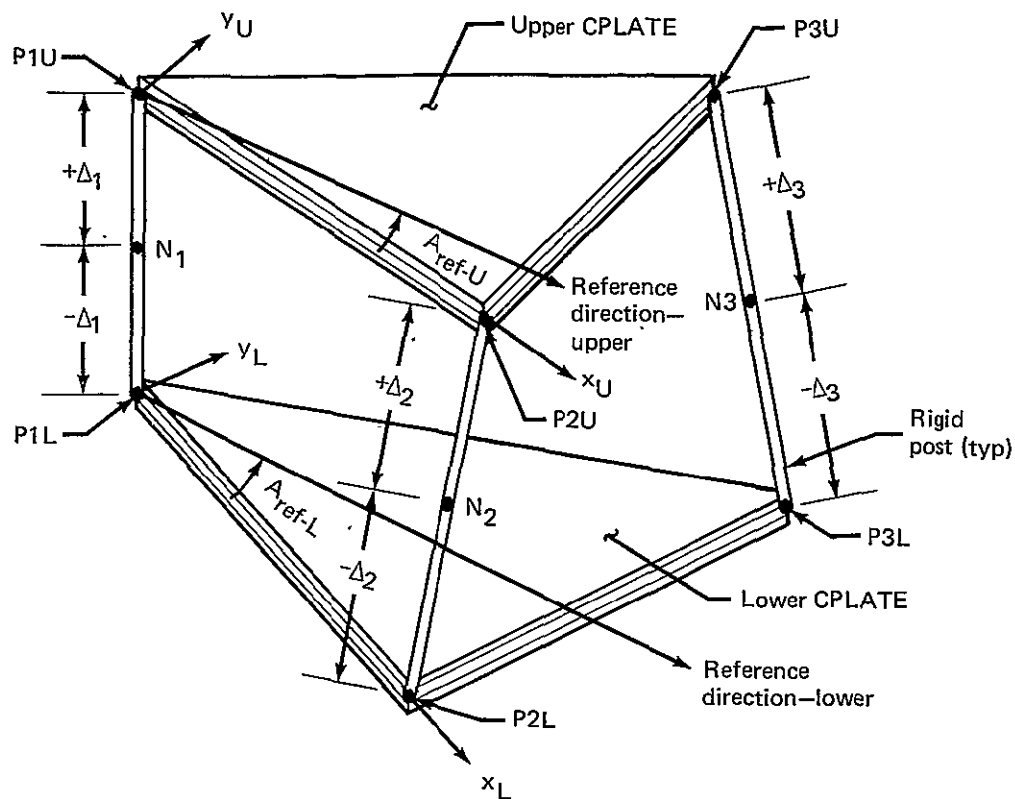
- ▼ $A_{xxx.x}$ — Defines the lamina fiber direction relative to the element reference direction
- ▼ T_{xxx} — Defines the lamina temperature difference relative to the element reference temperature
- ▼ L_{num} — Defines the number of layers (plies) of composite material within the lamina
- ▼ C_{code} — Identifies the composite material of the lamina



The CPLATE analysis output shown in the above diagram is defined below:

- ▼ EPS1 — Lamina axial strain parallel to reference direction
- ▼ EPS2 — Lamina axial strain perpendicular to reference direction
- ▼ GAM12 — Lamina shear strain

Figure 6-1.—Stiffness CPLATE Element



CCOVER element is composed of two triangular or quadrilateral ATLAS CPLATE elements separated by rigid posts. Each CPLATE is as described in figure 6-1. One of the CPLATES may have zero properties. Mid-surface nodes (N1, N2, N3) are required. Addition of the respective Δ_z coordinates to the input nodal Z coordinates defines the upper CPLATE corners, whereas subtraction defines the lower CPLATE corners. The directions of the rigid posts are defined by the nodal Z-axes which need not be parallel.

Figure 6-2.—Stiffness CCOVER Element

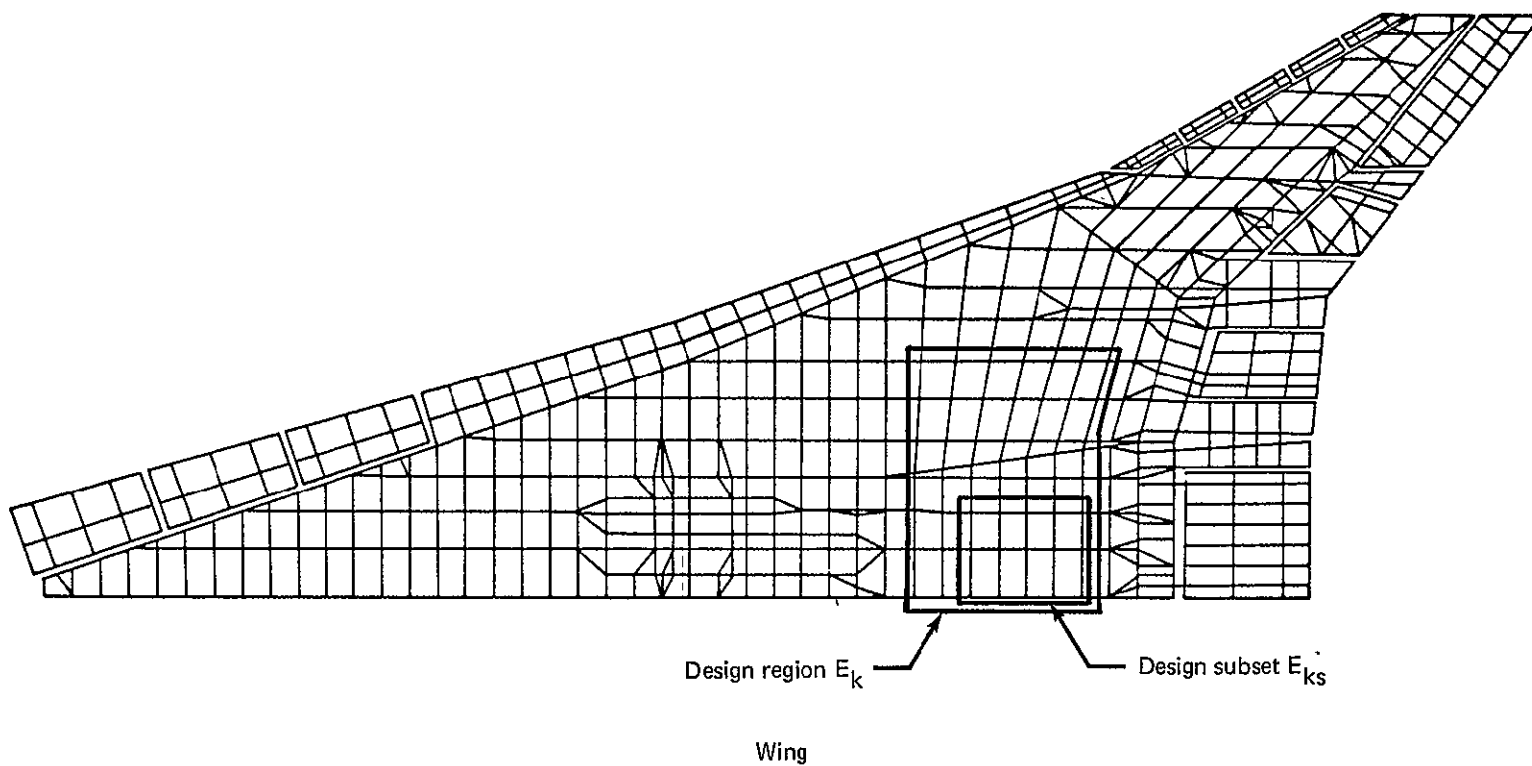


Figure 6-3.—ATLAS Composite Design Subsets (Illustrative Only)

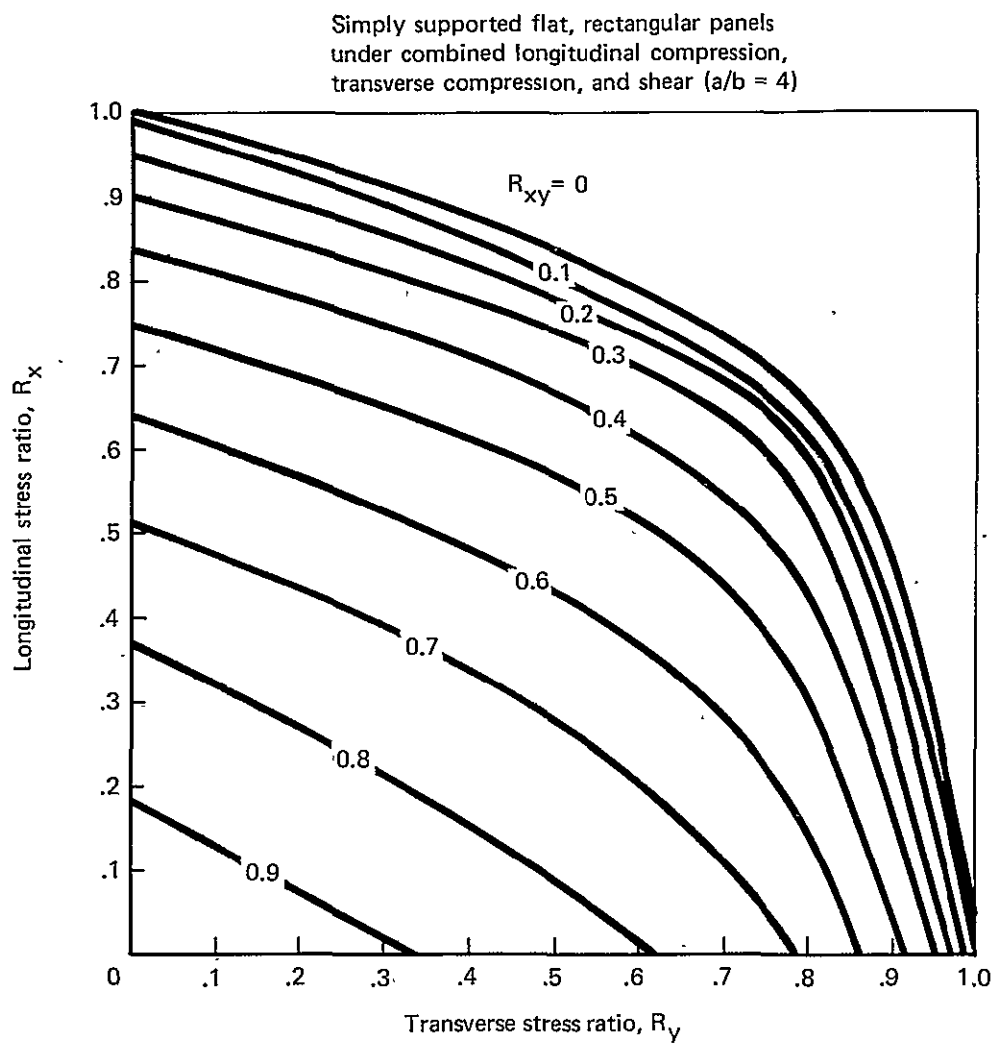


Figure 6-4.—Initial Buckling of Flat Rectangular Panels

SECTION 7

REVISION OF MATHEMATICAL MODEL

by

F. D. FLOOD

CONTENTS

	Page
INTRODUCTION	192
MAIN WING BOX	192
WING TIP	193
WING MOUNTED FIN	193
LEADING AND TRAILING EDGES	194
FUSELAGE	194
STRENGTH RESIZING	195
PANEL STABILITY EVALUATION	197
REFERENCES	198

TABLES

No.		Page
7-1	Material Designations and Number of Plies/Lamina to Initiate Model Preliminary Sizing	199
7-2	Comparison of Titanium and Composite Fuselage, Station 1180.25	200
7-3	Comparison of Titanium and Composite Fuselage, Station 1775.26	201
7-4	Comparison of Titanium and Composite Fuselage, Station 2160.26	202
7-5	Comparison of Titanium and Composite Fuselage, Station 2930.26	203
7-6	Comparison of Titanium and Composite Fuselage, Station 3070.24	204
7-7	Summary, Comparison of Metal and Composite Fuselage Structure	205
7-8	Fuselage Stiffness Ratios	207

FIGURES

No.		Page
7-1	Zones Used for Resize	208
7-2	Fuselage Stiffness Factor Distribution	209
7-3	Average Stiffness Factors	210
7-4	Sizing of Elements, First Strength Resize	211
7-5	Sizing of Elements, Second Strength Resize	225
7-6	Sizing of Elements, Third Strength Resize	239
7-7	Theoretical Wing Weight, Wing Box Primary Structure, ATLAS Resizing	253
7-8	Upper Surface Panels Checked for Stability After Resize Cycle 1	254
7-9	Lower Surface Panels Checked for Stability After Resize Cycle 1	255
7-10	Layup Changes Required for Stability After Resize Cycle 1 (Upper Surface)	256
7-11	Layup Changes Required for Stability After Resize Cycle 1 (Lower Surface)	257
7-12	Upper Surface Panel Stability Checks After Resize Cycle 2	258
7-13	Lower Surface Panel Stability Checks After Resize Cycle 2	259

SYMBOLS

E	Modulus of elasticity
G	Modulus of rigidity (shear)
H/C	Honeycomb
K	Stiffness factor
t	Thickness
\bar{t}	Equivalent thickness
μ	Poisson ratio
ρ	Density
V_A	Design maneuvering speed
V_f	Design speed for deflected flaps

INTRODUCTION

The mathematical model used as the basis for the design of composite wing panels is the mathematical model resulting from the Task I and II configuration and analysis cycles, from reference 7-2. This original airframe concept consisted of all-titanium structure and was developed from the many trade studies and the experience accumulated during the National SST Program and the ensuing DOT funded follow-on program. The internal arrangement is based on the structure designed for the SCAT-15 configuration (ref. 7-2), with the member sizes based on allowables that reflect a current assessment of the available titanium technology.

The definition of the nodes used in the structural mathematical model was unchanged. The wing cover panels were revised to allow analysis and automated resize of advanced composite materials. The initial definition of the cover panels was estimated based on the loads from the reference 7-1 stress analysis. This initial sizing served to minimize the number of iterations necessary for convergence. The titanium internal structure of the wing was left unchanged because of the lack of sufficient budget to convert it to composite material.

Other structure such as the fuselage, empennage, and wing leading and trailing edges was sized by hand for the composite materials. These components were not resized in the subsequent analysis, but were modified to provide the elastic characteristics of a composite structure in terms of the stiffness and vibration modes. The following paragraphs describe in greater detail the revision of the components of the analytical model.

MAIN WING BOX

The cover panels of the main wing box were replaced using sandwich panels made up of graphite/polyimide composite surfaces and honeycomb core. The materials and the associated elastic and mechanical properties are described in Sections 1 and 2. Because of budget limitations, the internal structure consisting of titanium spars and ribs has not been replaced with composite structure. It has been assumed that the surfaces of the sandwich panels are laid up in a balanced symmetrical array of laminae to avoid the problems of anisotropic behavior during manufacture and under load. This results in somewhat conservative panel design as will be seen later.

The titanium panels were first replaced with representative composite panels having the approximate number of laminae necessary to carry the expected loads. A stress analysis was then performed on the finite element model and the panels resized for zero margin of safety at ultimate load, using the ATLAS composite design module.

The wing surface panels of the main wing box were divided into 16 zones for input for preliminary sizing. Each zone was picked to provide a number of panels that have similar layups and which would be subject to spanwise, chordwise and shear load components of similar proportions or which would be critical for constraint conditions such as minimum gage. These zones are shown in figure 7-1. Although zones 10 and 11 on the wing tip are in a region of minimum gage for strength, these zones

will be used for resizing this area for flutter purposes. As shown in the table 7-1, each zone has a ply orientation specified for the inner and outer skins of the upper and lower surface panels for the initial input. These layups were estimated based on the loads on the panels resulting from the reference 7-1 analysis, and were felt to be reasonable estimates of the panel thicknesses and orientation necessary to carry the loads. Also shown in the table is the material designator assigned to the laminae in each zone;

Minimum gage for the wing surfaces as defined in Section 3 are:

	Upper Surface	Lower Surface
	in.	in.
Inner Skin	.016	.016
Outer Skin	.024	.032

The ATLAS design module resizes the panels based only on the allowable material properties since there is no buckling analysis presently included. For this reason, the materials called out for the upper surface are separate from those called out for the lower surface, in order to permit the use of variations in the allowables to provide for the buckling requirement. The sizing of the panels that result from the resizing will be checked manually to determine if the panels are critical for buckling and if so, the allowables will be reduced appropriately to provide for that case.

In each zone, there is an individual material available for the 0° , $\pm 45^\circ$ and 90° laminae to permit selective stiffening for flutter.

WING TIP

The wing tip surface panels are replaced with composite sandwich covers as shown in table 7-1 (zones 10 and 11). The initial thickness was based on the loads in the tip skins, and this represents an estimate of strength requirements, although this area will likely be designed for stiffness due to flutter requirements. The initial sizing is based on the high strength graphite fiber.

As noted above, the wing tip is divided into two zones for the purpose of resizing. Zone 10 extends from the fin to the wing tip and includes the covers of the main wing box, and Zone 11 the region aft of the rear spar to the hinge line as shown in figure 7-1. The material designations are as shown in table 7-1. Each of the laminae (0° , $\pm 45^\circ$ and 90°) are identified separately so that the type of fibers, lamina thickness, or strength of the individual lamina can be changed separately.

WING MOUNTED FIN

The structure of the wing mounted fin was not changed in this analysis except to substitute the equivalent properties of an equivalent quasi-isotropic layup of high strength fibers. Should it be necessary to stiffen the fin for flutter purposes, it may be more efficient to switch to fibers having a higher modulus and a lower strength.

LEADING AND TRAILING EDGES

The leading and trailing edge surfaces are modeled for graphite/polyimide sandwich construction. Since design loads are not available for these surfaces, the advanced composite surfaces will be designed to have the same inplane stiffnesses as the final reference 7-1 titanium structure. The majority of the leading edge panels will be minimum gage. The minimum gage areas are made of [0/±45/90] which results in the following equivalent mechanical properties:

$$E_x = E_y = 7.635 \times 10^6 \text{ lbs/in}^2$$

$$G = 2.926 \times 10^6 \text{ lbs/in}^2$$

$$\mu_x = \mu_y = .304$$

$$\rho = .056 \text{ lbs/in}^3$$

The panel sizes for the leading and trailing edges are based on keeping the Et's the same, i.e.,

$$Et_{T1} = Et_P/I$$

Maintaining this ratio will result in surfaces having about 1.5 times the compressive strength and twice the shear strength as the titanium surfaces.

FUSELAGE

The fuselage for this analysis is based on the titanium fuselage from reference 7-1. This fuselage will be unchanged in-so-far as the internal arrangement is concerned, since the main purpose of modifying the fuselage is to provide the equivalent of a composite fuselage in its dynamic response in the vibration modes. It was also necessary that the strain under static load conditions be properly simulated in the regions where the wing and body share loads. The stringers and beams in the fuselage included area for the effective skin and the lumped stringers. Alternate frames were modeled with the equivalent area for two frames with effective skin, since the frame spacing in the model is 35 in. as compared to 17.5 in. in the airplane. Skins are idealized as "S" plates carrying shear, only.

The section properties of the titanium elements are not altered from those used on the Task II analysis. The change in stiffness was accounted for by altering the elastic properties in the material tables. This was the most economical way to make the appropriate changes in the fuselage elements.

Tables 7-2 through 7-6 present the comparison of the titanium and the composite skin gages, stringer areas and spacings, the appropriate effective moduli, and the t's for five stations along the fuselage. These results are summarized on table 7-7.

One of the basic considerations in modifying the fuselage skins for composite is the change in the structural concept and the effect that this has on the stiffness distribution around the cross section of the fuselage. The skin-stringer fuselage is generally designed by tension in the crown and by compression in the belly, resulting in fully effective skin panels for the compression in the belly, thereby lowering the effective stiffness. A typical comparison of the ratio of the Et in the crown and the belly for skin-stringer and sandwich is presented in table 7-8.

Another aspect of this consideration is the variation of the crown and belly stiffness distribution as a function of load factor. Because of the effect of buckling, as the load factor increases, the compression side of the skin-stringer fuselage becomes less effective. Generally the criteria for the National SST Prototype provided for no skin buckling up to a load factor of 1.1 for aerodynamic reasons. The sandwich panels, on the other hand, are sized for no buckling up to ultimate load, and therefore will be affected little if any by variations in load factor.

Based on these considerations, it is concluded that the stiffness characteristics of the skin-stringer fuselage is representative of the airplane in unaccelerated flight, but are somewhat high for load factor approaching limit load factor. On the other hand, the stiffness characteristics of the fuselage with sandwich panels is probably representative at all load factors up to limit.

Based on the analysis described earlier, factors are derived that account for the ratio between the modulus of elasticity of titanium and that necessary to maintain the same E_t for the composite fuselage. These K factors are shown in table 7-7, and are presented in figure 7-2. Upon review of these factors and the associated labor and time involved in modifying the input for the mathematical model, it was decided to use a constant factor along the fuselage for these factors as shown in figure 7-3.

STRENGTH RESIZING

The strength resizing was performed considering mechanical loads only. The version of ATLAS that had been checked out for use on the large Arrow Wing mathematical model did not have the thermal loads capability. A significant schedule delay and an undetermined cost for unsuccessful runs would have been incurred had the thermal effects been included in the structural resizing.

Because of the difference in the coefficients of thermal expansion, temperature changes due to environmental conditions and aerodynamic heating will induce stresses in the skins, spar caps and splice plates. Since the critical flight conditions for structural loads are subsonic and transonic, the thermally induced stresses are relatively small compared to the stresses due to airloads. It should be noted, however, that the temperatures due to aerodynamic heating at cruise Mach number will induce local stresses of the order of 20 000 lb/in² and would need to be considered in the detail design of the spar caps and splice plates for a mixed titanium composite structure such as is being considered in this study.

During the strength resizing, some of the variables were constrained to be equal. These equality constraints followed from a prior assumption that each face sheet should be a balanced, symmetric laminate. To be balanced signifies that there is an equal number of +45°- and -45°-plies. To be symmetric implies that commonly oriented plies on opposite sides of the laminate symmetry plane are of equal number. Thus, the +45°-laminae were constrained to be equal in number to the -45°-laminae and each lamina on a given side of the laminate symmetry plane was constrained to be equal to the corresponding lamina on the opposite side of the symmetry plane. Further, with only mechanical loads being considered and with the finite element being used having only inplane (membrane) load-carrying capability, corresponding plies in the inner and outer face sheets of each panel were also constrained to be equal. Although internal pressures act on the wing panels, they are not significant when considered in conjunction with airloads and inertia loads.

For the first strength resize, it was considered technically feasible and financially advantageous to solve each wing panel (upper or lower CPLATE of a CCOVER element) as an individual problem. This certainly results in the most accurate theoretical weight result possible. It does not address the problem of practical layups from a manufacturing viewpoint but rather indicates the target theoretical weight of such a practical layup. The decision to resize each panel resulted in 750 optimization problems to be solved during the first resize. That this was accomplished for about 2/3 of the cost of the preceding stress analysis indicates the efficiency of the ATLAS composite design module. After the first strength resize, it was apparent that the entire strake area (wing forward of wheel well) was minimum gage. This region was excluded from resizing for the second resize.

The detailed results of the first resize are shown in figure 7-4. The zones identified in figure 7-4 correspond to those shown in figure 7-1. All of the final trends of the strength resize are evident in the first resize. This sometimes occurs with an extremely large change in the sizing from that originally specified. This indicates that the original sizing can be considerably different than the final with little effect. The detailed results of the second resize are shown in figure 7-5. For both the first and second resize, the lower bound constraint was solely that at least one layer (ply) must exist in each of the lamina orientations for the $[0/\pm 45/90]$ layup. This lower bound approach was used since the ATLAS lower bound capability was such that lower bounds were imposed after the optimization problem was solved. The lower bounds for the third resize were determined manually since a decision had to be made between identical inner and outer face sheets or face sheets having similar layups with thicknesses in the proportion of the face sheet minimum gages. The decision was based on the lighter weight. Once the minimum gage layups were established, the finite element model was updated using the ATLAS composite design module. The above minimum gage determination for the total laminate is a development capability that should be accomplished in the future.

It is apparent from a review of figures 7-4, 7-5 and 7-6 that the regions outboard and forward of the wheel well and outboard of the wing-mounted fin are sized by the minimum gage constraints. With the exception of the lower surface just inboard of the outboard engine beams, the panels adjacent to the rear spar are predominantly unidirectional laminates oriented parallel to the rear spar. Along the side-of-body on the wing lower surface, the body bending induces chordwise loads that peak inboard of the wheel well where up to six chordwise plies are required. The largest strength requirement for $\pm 45^\circ$ laminae occurs six spars forward of the rear spar midway between the engine beams on the upper surface. Note that the corresponding lower panel does not require these $\pm 45^\circ$ plies. It is also worth noting the relative sizing of these latter lower surface panels and those located immediately aft. These panels were input in two different zones and had different original sizing occurring as a step function across the zone boundary. With two resizes, the relative sizing appears more disparate than the initial sizing. This leads to the conclusion that a preferred approach would be to input a uniform sizing (uniformly varying would require too much input) over the entire wing and let the ATLAS composite design module determine the varying sizing requirements. This approach should result in a more realistic sizing distribution.

Figure 7-7 illustrates the relative theoretical weight for each cycle of resize. The relatively small theoretical weight increment between the first and second resize indicates that for weighing purposes, the resizing has acceptably converged. The relatively larger increment of weight added from the second to the third resize indicates that the minimum gages selected have a significant weight impact.

PANEL STABILITY EVALUATION

After each cycle of strength sizing, the resized wing panels were evaluated regarding instability failure. The Boeing-developed COOPB, Laminated Composite Analysis Program, was used for this purpose. An orthotropic plate buckling analysis for simply supported plates subjected to inplane biaxial compression and shear loads was performed. This analysis includes the effect of core shear stiffnesses.

After the first resize, panels for the stability checks were selected based on 1) the layups of the panels after the strength optimization and 2) an assessment of the loads and change of loads in that region. For example, on the wing upper surface near the rear spar and side-of-body where high spanwise compressive stresses exist, if adjacent panels were several layers different in 0° (spanwise) layers, the lighter panel was selected for a stability check. In this manner a total of 86 upper and lower surface panels were selected and checked. When a panel was found to be unstable for the design loads, additional panels in the immediate region were also evaluated. This resulted in another eighteen panels being checked. The result of this investigation was that nine panels were found which were unstable for the design loads as a consequence of insufficient stiffness. The location of these panels and the critical design load case(s) are shown in figures 7-8 and 7-9. For six of the unstable panels, sufficient stiffness to render them stable for the critical load was achieved by adding one 0.002 in.-thick layer to each of the face sheet laminates. Two 0.002 in.-thick layers per face sheet were required for the other three panels. However, further examination of these latter three panels revealed that the rounding scheme within the ATLAS composite design module for converting the lamina thicknesses from real values to an integer number of plies (layers) had produced thicknesses less than the theoretical optimum in the laminae critical for panel stability. To explain further, a theoretical lamina thickness of 0.0049 in. is sized to two 0.002 in.-thick layers since as noted previously a simple arithmetic rounding scheme is used for the real value-to-integer number conversion. The layup changes required for the unstable strength-sized upper and lower surface panels to become stable are presented in figures 7-10 and 7-11, respectively.

After the second cycle of stress analysis and strength-optimized resize, panel stability was again evaluated using the first cycle results as a guide for selecting panels for evaluation. One upper surface panel near the rear spar at the side of body lacked sufficient stiffness as strength sized to preclude instability failure. Figures 7-12 and 7-13 summarize the panel stability evaluation and results performed after the second strength resize.

The third strength resize enforced the actual minimum gage constraints on the various face sheets as opposed to the single layer minimum constraints in the first and second resize cycles. Thus, each face sheet layup had the same or increased stiffnesses which precluded the necessity for further panel stability evaluation.

REFERENCES

- 7-1 Boeing Staff: *Study of Structural Design Concepts for an Arrow Wing Supersonic Transport Configuration*. NASA CR 132576-1 and -2, 1976.
- 7-2 Boeing Staff: *Mach 2.7 Fixed Wing SST Model 969-336C (SCAT 15F)*. D6A11666-1, The Boeing Company, 1969.

Table 7-1.—Material Designations and Number of Plies/Lamina to Initiate Model Preliminary Sizing

	Zone	Lamina	Material designation and number of plies/lamina			
			Upper surface		Lower surface	
			Outer skin	Inner skin	Inner skin	Outer skin
Main wing box	1a, 1b	0	C07 (3)	C01 (2)	C02 (2)	C14 (4)
		+45, -45	C09 (3)	C03 (2)	C04 (2)	C16 (4)
		90	C11 (3)	C05 (2)	C06 (2)	C18 (4)
	1c, 1d, 1e	0	C07 (3)	C01 (2)		
		+45, -45	C09 (3)	C03 (2)		
		90	C11 (3)	C05 (2)		
	2	0	C07 (3)	C01 (2)	C02 (2)	C14 (4)
		+45, -45	C09 (3)	C03 (2)	C04 (2)	C16 (4)
		90	C11 (3)	C05 (2)	C06 (4)	C18 (8)
	3	0	C07 (3)	C01 (2)	C08 (3)	C14 (4)
		+45, -45	C09 (3)	C03 (2)	C10 (3)	C16 (4)
		90	C11 (3)	C05 (2)	C12 (6)	C18 (8)
Main wing box	4	0	C07 (3)	C07 (3)	C08 (3)	C14 (4)
		+45, -45	C09 (3)	C09 (3)	C10 (3)	C16 (4)
		90	C11 (3)	C11 (3)	C12 (3)	C18 (4)
	5	0	C13 (4)	C13 (4)	C14 (4)	C14 (4)
		+45, -45	C15 (4)	C15 (4)	C16 (4)	C16 (4)
		90	C17 (4)	C17 (4)	C18 (4)	C18 (4)
	6	0	C13 (12)	C13 (12)	C14 (12)	C14 (12)
		+45, -45	C15 (8)	C15 (8)	C16 (8)	C16 (8)
		90	C17 (8)	C17 (8)	C18 (8)	C18 (8)
	7	0	C13 (16)	C13 (16)	C14 (16)	C14 (16)
		+45, -45	C15 (4)	C15 (4)	C16 (4)	C16 (4)
		90	C17 (4)	C17 (4)	C18 (4)	C18 (4)
Main wing box	8	0	C13 (16)	C13 (16)	C14 (16)	C14 (16)
		+45, -45	C15 (8)	C15 (8)	C16 (8)	C16 (8)
		90	C17 (8)	C17 (8)	C18 (8)	C18 (8)
	9a, 9b,	0	C13 (20)	C13 (20)	C14 (20)	C14 (20)
		+45, -45	C15 (4)	C15 (4)	C16 (4)	C16 (4)
		90	C17 (4)	C17 (4)	C18 (4)	C18 (4)
Wing tip	10	0	C19 (4)	C19 (4)	C19 (4)	C19 (4)
		+45, -45	C20 (4)	C20 (4)	C20 (4)	C20 (4)
		90	C21 (4)	C21 (4)	C21 (4)	C21 (4)
	11	0	C22 (4)	C22 (4)	C22 (4)	C22 (4)
		+45, -45	C23 (4)	C23 (4)	C23 (4)	C23 (4)
		90	C24 (4)	C24 (4)	C24 (4)	C24 (4)

Note: Parenthesized values are the number of 0.002-in. plies per lamina.

Table 7-2.—Comparison of Titanium and Composite Fuselage, Station 1180.25

Titanium (ref. resize following first analysis)	Advanced composite honeycomb
<p>Crown</p> <p>Skin gage = 0.030 in.</p> <p>Stringer area = 0.1176 in.² (including padup)</p> <p>Stringer spacing = 5.4 in.</p> <p>$\bar{t} = 0.0518 \text{ in}^2/\text{in.}$</p>	<p>Crown</p> <p>$[0_2/\pm 45/90]_S$</p> <p>4 mil each skin</p> <p>$\bar{t} = 0.080 \text{ in}^2/\text{in.}$</p> <p>$E_{\text{axial}} = 9.26 \times 10^6 \text{ lb/in}^2$</p> <p>$E_{\text{circular}} = 5.48 \times 10^6 \text{ lb/in}^2$</p> <p>$G = 2.91 \times 10^6 \text{ lb/in}^2$</p>
<p>Side</p> <p>Skin gage = 0.030 in.</p> <p>Stringer area = 0.1176 in.²</p> <p>Stringer spacing = 5.0 in.</p> <p>$\bar{t} = 0.0535 \text{ in}^2/\text{in.}$</p>	<p>Side</p> <p>$[0/\pm 45/90]_S$</p> <p>4 mil each skin</p> <p>$\bar{t} = 0.064 \text{ in}^2/\text{in.}$</p> <p>$E_{\text{axial}} = E_{\text{circular}} = 6.57 \times 10^6 \text{ lb/in}^2$</p> <p>$G = 2.91 \times 10^6 \text{ lb/in}^2$</p>
<p>Belly</p> <p>Skin gage = 0.034 in.</p> <p>Stringer area = 0.265 in.²</p> <p>Stringer spacing = 5.4 in.</p> <p>$\bar{t} = 0.083 \text{ in}^2/\text{in.}$</p>	<p>Belly</p> <p>Same as crown</p>
B/C = 1.602	B/C = 1.0

Table 7-3.—Comparison of Titanium and Composite Fuselage, Station 1775.26

Titanium (ref. resize following first analysis)	Advanced composite honeycomb
<p>Crown</p> <p>Skin gage = 0.035 in.</p> <p>Stringer area = 0.17 in²</p> <p>Stringer spacing = 5.0 in.</p> <p>$\bar{t} = 0.069 \text{ in}^2/\text{in.}$</p>	<p>Crown</p> <p>$[0_3/\pm 45/90]_S$</p> <p>4 mil each skin</p> <p>$\bar{t} = 0.096 \text{ in}^2/\text{in.}$</p> <p>$E_{\text{axial}} = 11.05 \times 10^6 \text{ lb/in}^2$</p> <p>$E_{\text{circular}} = 4.76 \times 10^6 \text{ lb/in}^2$</p> <p>$G = 2.18 \times 10^6 \text{ lb/in}^2$</p>
<p>Side</p> <p>Skin gage = 0.030 in.</p> <p>Stringer area = 0.1176 in²</p> <p>Stringer spacing = 5.0 in.</p> <p>$\bar{t} = 0.0535 \text{ in}^2/\text{in.}$</p>	<p>Side</p> <p>$[0/\pm 45/90]_S$</p> <p>4 mil each skin</p> <p>$\bar{t} = 0.064 \text{ in}^2/\text{in.}$</p> <p>$E_{\text{axial}} = E_{\text{circular}} = 6.57 \times 10^6 \text{ lb/in}^2$</p> <p>$G = 2.91 \times 10^6 \text{ lb/in}^2$</p>
<p>Belly</p> <p>Skin gage = 0.050 in.</p> <p>Stringer area = 0.46 in²</p> <p>Stringer spacing = 4.4 in.</p> <p>$\bar{t} = 0.155 \text{ in}^2/\text{in.}$</p>	<p>Belly</p> <p>Same as crown</p>
B/C = 2.246	B/C = 1.0

6-4

Table 7-4.—Comparison of Titanium and Composite Fuselage, Station 2160.26

Titanium (ref. resize following first analysis)	Advanced composite honeycomb
<p>Crown</p> <p>Skin gage = 0.048 in.</p> <p>Stringer area = 0.34 in^2</p> <p>Stringer spacing = 4.7 in.</p> <p>$\bar{t} = 0.12 \text{ in}^2/\text{in.}$</p>	<p>Crown</p> <p>$[0_4/\pm 45/90]_S$</p> <p>4 mil each skin</p> <p>$\bar{t} = 0.112 \text{ in}^2/\text{in.}$</p> <p>$E_{\text{axial}} = 12.33 \times 10^6 \text{ lb/in}^2$</p> <p>$E_{\text{circular}} = 4.24 \times 10^6 \text{ lb/in}^2$</p> <p>$G = 1.97 \times 10^6 \text{ lb/in}^2$</p>
<p>Side</p> <p>Skin gage = 0.035 in.</p> <p>Stringer area = 0.14 in^2</p> <p>Stringer spacing = 5.0 in.</p> <p>$\bar{t} = 0.063 \text{ in}^2/\text{in.}$</p>	<p>Side</p> <p>$[0/\pm 45/90]_S$</p> <p>4 mil each skin</p> <p>$\bar{t} = 0.064 \text{ in}^2/\text{in.}$</p> <p>$E_{\text{axial}} = E_{\text{circular}} = 6.57 \times 10^6 \text{ lb/in}^2$</p> <p>$G = 2.91 \times 10^6 \text{ lb/in}^2$</p>
<p>Belly</p> <p>Skin gage = 0.070 in.</p> <p>Stringer area = 0.56 in^2</p> <p>Stringer spacing = 4.4 in.</p> <p>$\bar{t} = 0.197 \text{ in}^2/\text{in.}$</p>	<p>Belly</p> <p>$[0_5/\pm 45/90]_S$</p> <p>$\bar{t} = 0.128 \text{ in}^2/\text{in.}$</p> <p>$E_{\text{axial}} = 13.29 \times 10^6 \text{ lb/in}^2$</p> <p>$E_{\text{circular}} = 3.85 \times 10^6 \text{ lb/in}^2$</p> <p>$G = 1.813 \times 10^6 \text{ lb/in}^2$</p>
B/C = 1.64	B/C = 1.142

Table 7-5.—Comparison of Titanium and Composite Fuselage, Station 2930.26

Titanium (ref. resize following first analysis)	Advanced composite honeycomb
<p>Crown</p> <p>Skin gage = 0.066 in.</p> <p>Stringer area = 0.53 in^2</p> <p>Stringer spacing = 4.4 in.</p> <p>$\bar{\tau} = 0.186 \text{ in}^2/\text{in.}$</p>	<p>Crown</p> <p>$[0_8/\pm 45/90]_S$</p> <p>4 mil each skin</p> <p>$\bar{\tau} = 0.176 \text{ in}^2/\text{in.}$</p> <p>$E_{\text{axial}} = 15.12 \times 10^6 \text{ lb/ft}^2$</p>
<p>Side of body</p> <p>Skin gage = 0.066 in.</p> <p>$\bar{\tau}_{\text{axial}} = 0.099 \text{ in}^2/\text{in.}$</p>	<p>Side of body</p> <p>Assume: K_G same as side</p> <p>K_E same as belly</p>
<p>Side</p> <p>Skin gage = 0.066 in.</p> <p>Stringer area = 0.45 in^2</p> <p>Stringer spacing = 5.0 in.</p> <p>$\bar{\tau} = 0.156 \text{ in}^2/\text{in.}$</p>	<p>Side</p> <p>$[0_4/\pm 45_2/90]_S$</p> <p>4 mil each skin</p> <p>$\bar{\tau} = .144 \text{ in}^2/\text{in}$</p> <p>$E = 10.16 \times 10^6 \text{ lb/in}^2$</p> <p>$G = 2.67 \times 10^6 \text{ lb/in}^2$</p>
<p>Belly</p> <p>Skin gage = 0.10 in.</p> <p>Stringer area = 0.62 in^2</p> <p>Stringer spacing = 4.6 in.</p> <p>$\bar{\tau}_{\text{axial}} = 0.235 \text{ in}^2/\text{in.}$</p> <p>$\bar{\tau}_{\text{spanwise}} = 0.130 \text{ in}^2/\text{in.}$</p>	<p>Belly</p> <p>$[0_7/\pm 45/90_4]_S$</p> <p>$\bar{\tau} = 0.208 \text{ in}^2/\text{in.}$</p> <p>$E_{\text{axial}} = 11.911 \times 10^6 \text{ lb/in}^2$</p> <p>$E_{\text{spanwise}} = 7.159 \times 10^6 \text{ lb/in}^2$</p>
$B_{\text{axial}}/C = 1.263$	$B_{\text{axial}}/C = 1.182$

Table 7-6.—Comparison of Titanium and Composite Fuselage, Station 3070.24

Titanium (ref. resize following first analysis)	Advanced composite honeycomb
<p>Crown</p> <p>Skin gage = 0.60 in.</p> <p>Stringer area = 0.44 in^2</p> <p>Stringer spacing = 4.4 in.</p> <p>$\bar{t} = 0.16 \text{ in}^2/\text{in.}$</p>	<p>Crown</p> <p>$[0_6/\pm 45/90]_S$</p> <p>4 mil each skin</p> <p>$\bar{t} = 0.144 \text{ in}^2/\text{in.}$</p> <p>$E_{\text{axial}} = 14.03 \times 10^6 \text{ lb/in}^2$</p> <p>$E_{\text{circular}} = 3.55 \times 10^6 \text{ lb/in}^2$</p>
<p>Side of body</p> <p>Skin gage = 0.06 in.</p> <p>$\bar{t} = 0.09 \text{ in}^2/\text{in.}$</p>	
<p>Side</p> <p>Skin gage = 0.06 in.</p> <p>Stringer area = 0.43 in^2</p> <p>Stringer spacing = 5.0 in.</p> <p>$\bar{t} = 0.146 \text{ in}^2/\text{in.}$</p>	<p>Side</p> <p>$[0_5/\pm 45/90]_S$</p> <p>4 mil each skin</p> <p>$\bar{t} = 0.16 \text{ in}^2/\text{in.}$</p> <p>$E_{\text{axial}} = 11.145 \times 10^6 \text{ lb/in}^2$</p> <p>$G = 2.4702 \times 10^6 \text{ lb/in}^2$</p>
<p>Belly</p> <p>Skin gage = 0.10 in.</p> <p>Stringer area = 0.60 in^2</p> <p>Stringer spacing = 4.6 in.</p> <p>$\bar{t} = 0.23 \text{ in}^2/\text{in.}$</p>	<p>Belly</p> <p>Same as crown</p>
B/C = 1.44	B/C = 1.0

Table 7-7.—Summary, Comparison of Metal and Composite Fuselage Structure

Crown							
Station	Titanium			$\frac{E_{tH/C}}{E_{tTi}}$	Advanced composite H/C		
	\bar{t}	E	$E\bar{t}$		\bar{t}	E_{axial}	$E\bar{t}$
1180.25	0.0518	16.4	0.8495	0.872	0.080	9.26	0.7408
1775.26	0.069	16.4	1.1316	0.937	0.096	11.05	1.0608
2160.26	0.120	16.4	1.9680	0.702	0.112	12.33	1.3810
2930.26	0.186	16.4	3.0504	0.872	0.176	15.12	2.6610
3070.24	0.160	16.4	2.6240	0.770	0.144	14.03	2.0200

Belly							
Station	Titanium			$\frac{E_{tH/C}}{E_{tTi}}$	Advanced composite H/C		
	\bar{t}	E	$E\bar{t}$		\bar{t}	E_{axial}	$E\bar{t}$
1180.25	0.083	16.4	1.3612	0.544	0.080	9.26	0.7408
1775.26	0.155	16.4	2.5420	0.417	0.096	11.05	1.0608
2160.26	0.197	16.4	3.2310	0.526	0.128	13.29	1.7011
2930.26	0.235	16.4	3.8540	0.643	0.208	11.91	2.4772
3070.24	0.230	16.4	3.7720	0.536	0.144	14.03	2.0200

Axial Stiffness			
Station	K_{crown}	K_{belly}	K_{avg}
1180.25	0.872	0.544	0.708
1775.26	0.937	0.417	0.677
2160.26	0.702	0.526	0.614
2930.26	0.872	0.643	0.758
3070.24	0.770	0.536	0.653
	avg = 0.8306	avg = 0.5332	avg = 0.682

Table 7-7.—(Concluded)

Side Axial Stiffness

Station	Titanium			$K_{\text{axial side}}$	Advanced composite H/C		
	\bar{t}	E	$E\bar{t}$		\bar{t}	E_{axial}	$E\bar{t}$
1180.25	0.0535	16.4	0.8774	0.4792	0.064	6.570	0.4205
1775.26	0.0535	16.4	0.8774	0.4792	0.064	6.570	0.4205
2160.26	0.0630	16.4	1.0332	0.4070	0.064	6.570	0.4205
2930.26	0.1560	16.4	2.5584	0.5719	0.114	10.160	1.4632
3070.24	0.1460	16.4	2.3944	0.7440	0.160	11.145	1.7832

Side Shear Stiffness

Station	t	G	Gt	$K_{G \text{ side}}$	$t = \bar{t}$	G	Gt
1180.25	0.030	6.2	0.1860	1.0013	0.064	2.91	0.18624
1775.26	0.030	6.2	0.1860	1.0013	0.064	2.91	0.18624
2160.26	0.035	6.2	0.2170	0.8582	0.064	2.91	0.18624
2930.26	0.066	6.2	0.4092	0.9396	0.144	2.67	0.38448
3070.24	0.060	6.2	0.3720	1.0620	0.160	2.47	0.39520
				avg = 0.972			

Table 7-8.—Fuselage Stiffness Ratios

Station	$\bar{E}_{t_{crown}}$	$\bar{E}_{t_{belly}}$	$\frac{\bar{E}_{t_{belly}}}{\bar{E}_{t_{crown}}}$
1180.25	0.8495	1.3612	1.602
1775.26	1.1316	2.5420	2.246
2160.26	1.9680	3.2310	1.642
2930.26	3.0504	3.8540	1.263
3070.24	2.6240	3.7720	1.438
			avg = 1.638

Station	$\bar{E}_{t_{crown}}$	$\bar{E}_{t_{belly}}$	$\frac{\bar{E}_{t_{belly}}}{\bar{E}_{t_{crown}}}$
1180.25	0.7408	0.7408	1.000
1775.26	1.0608	1.0608	1.000
2160.26	1.3810	1.7011	1.233
2930.26	2.6610	2.4772	0.931
3070.24	2.0200	2.0200	1.000
			avg = 1.033

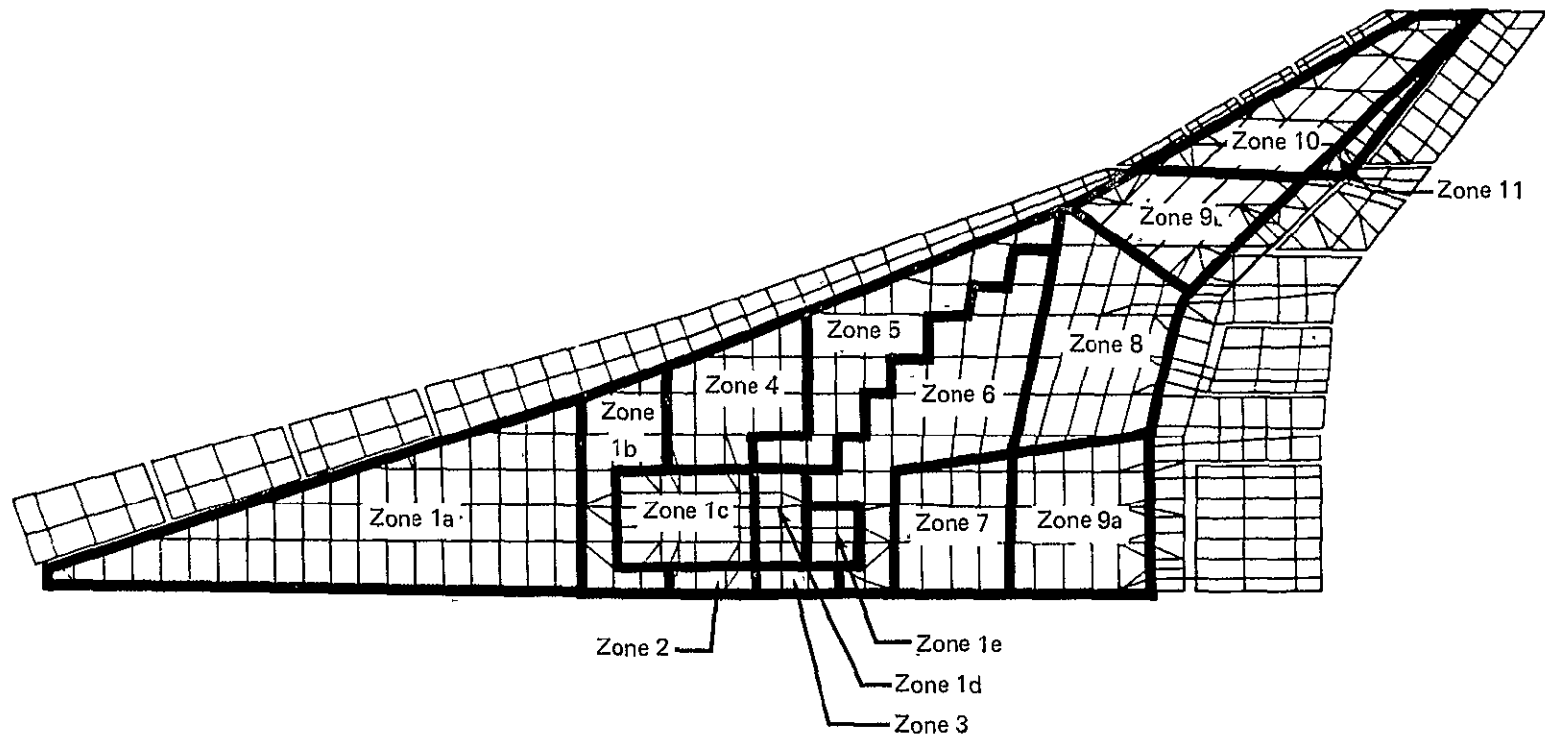


Figure 7-1.—Zones Used for Resize

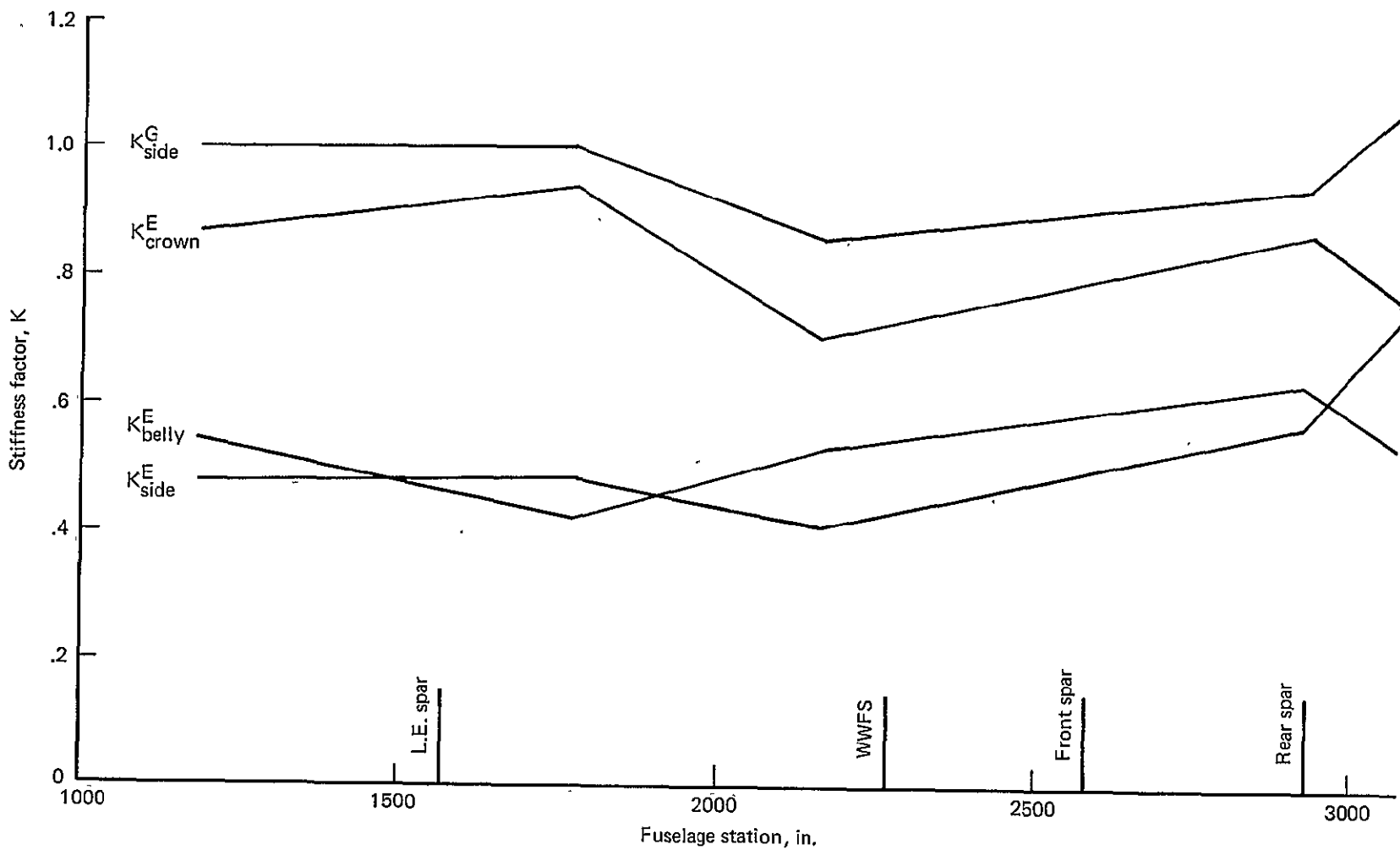


Figure 7-2.—Fuselage Stiffness Factor Distribution

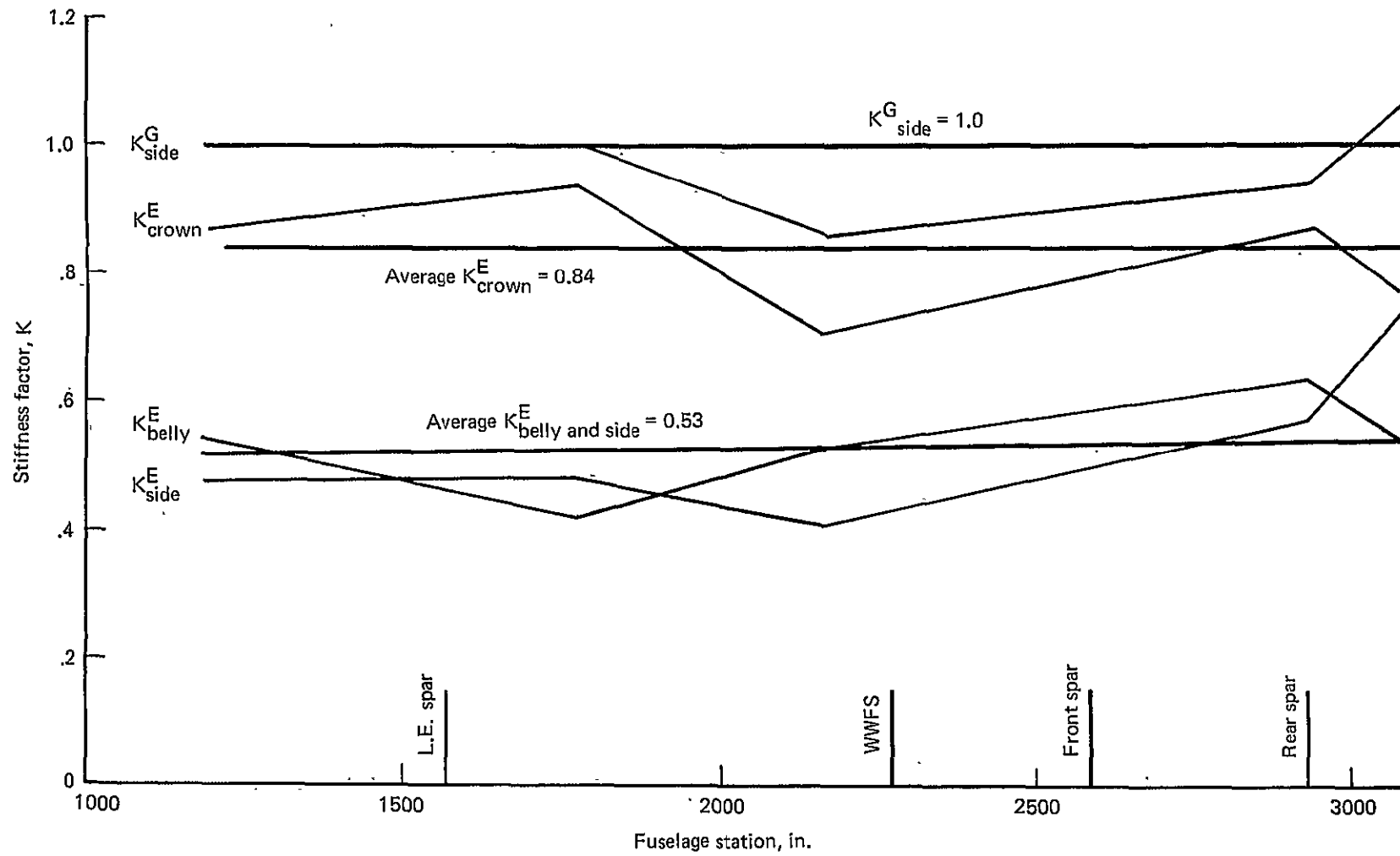


Figure 7-3.—Average Stiffness Factors

NOTE:

1. Sizing values $i/j/k$ define the subscripts in the standard laminate code for a $[0_i/\pm 45_j/90_k]_T$ laminate composed of 0.002-in.-thick plies. The lower (upper) panel sizing is shown without (within) parentheses. If a single set of sizing values is shown for either an upper or lower panel, it applies equally to the sandwich inner and outer face sheets. Otherwise, the two sets of values are shown within a brace with the thinner laminate being the inner face sheet.
2. All face sheets are 1/1/1 except as noted in figures.

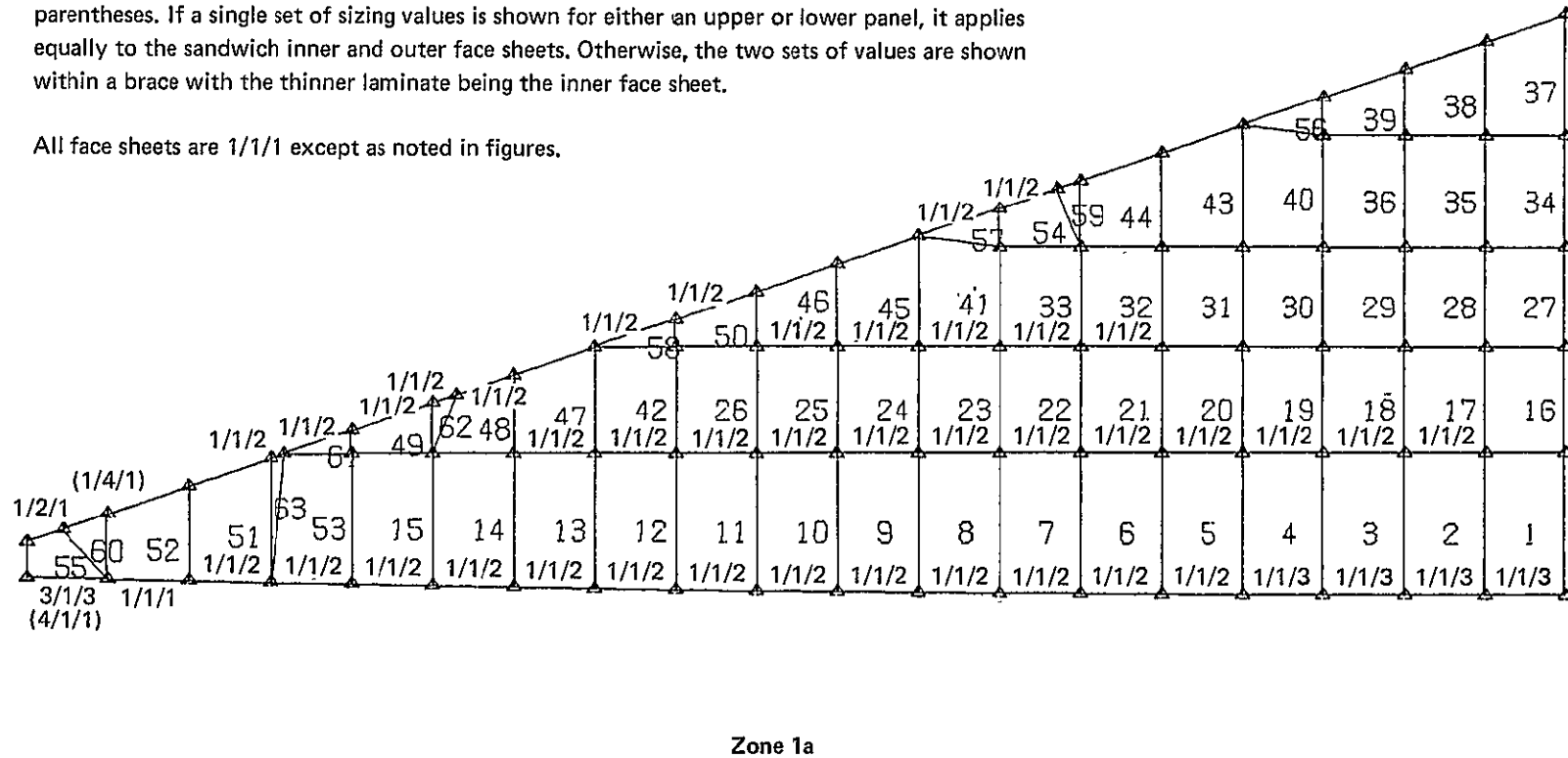
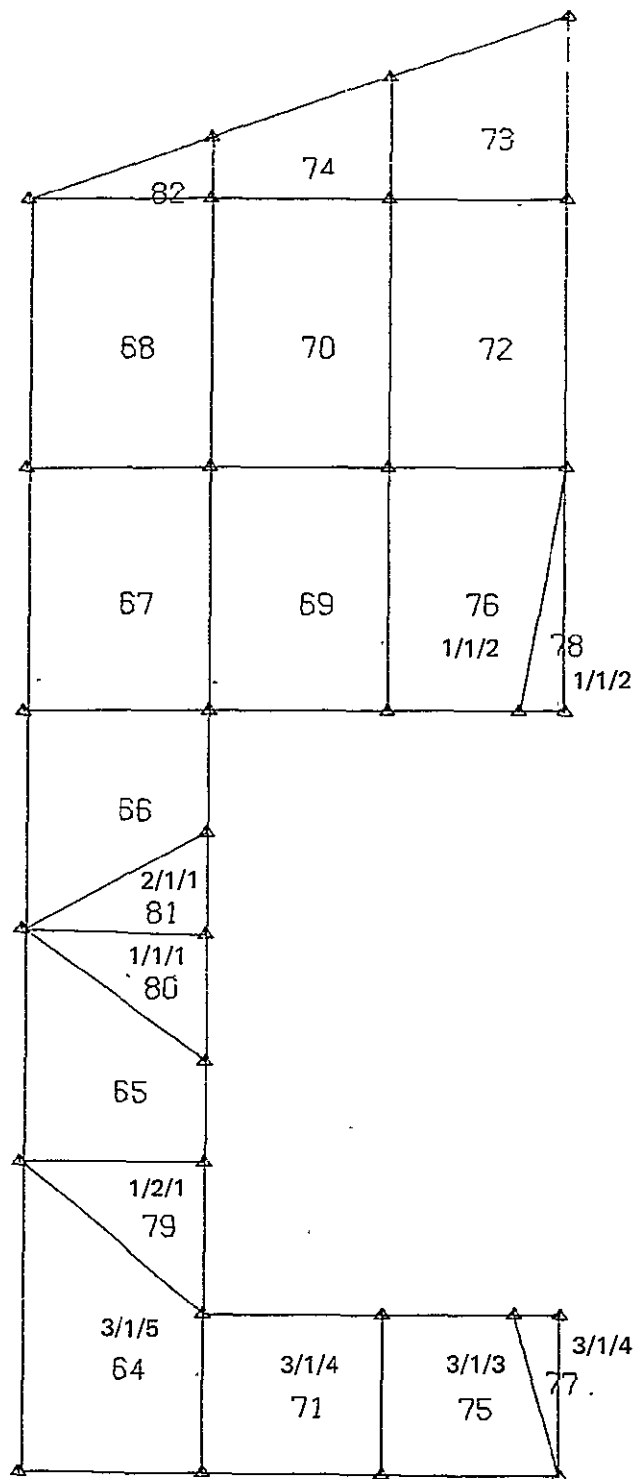


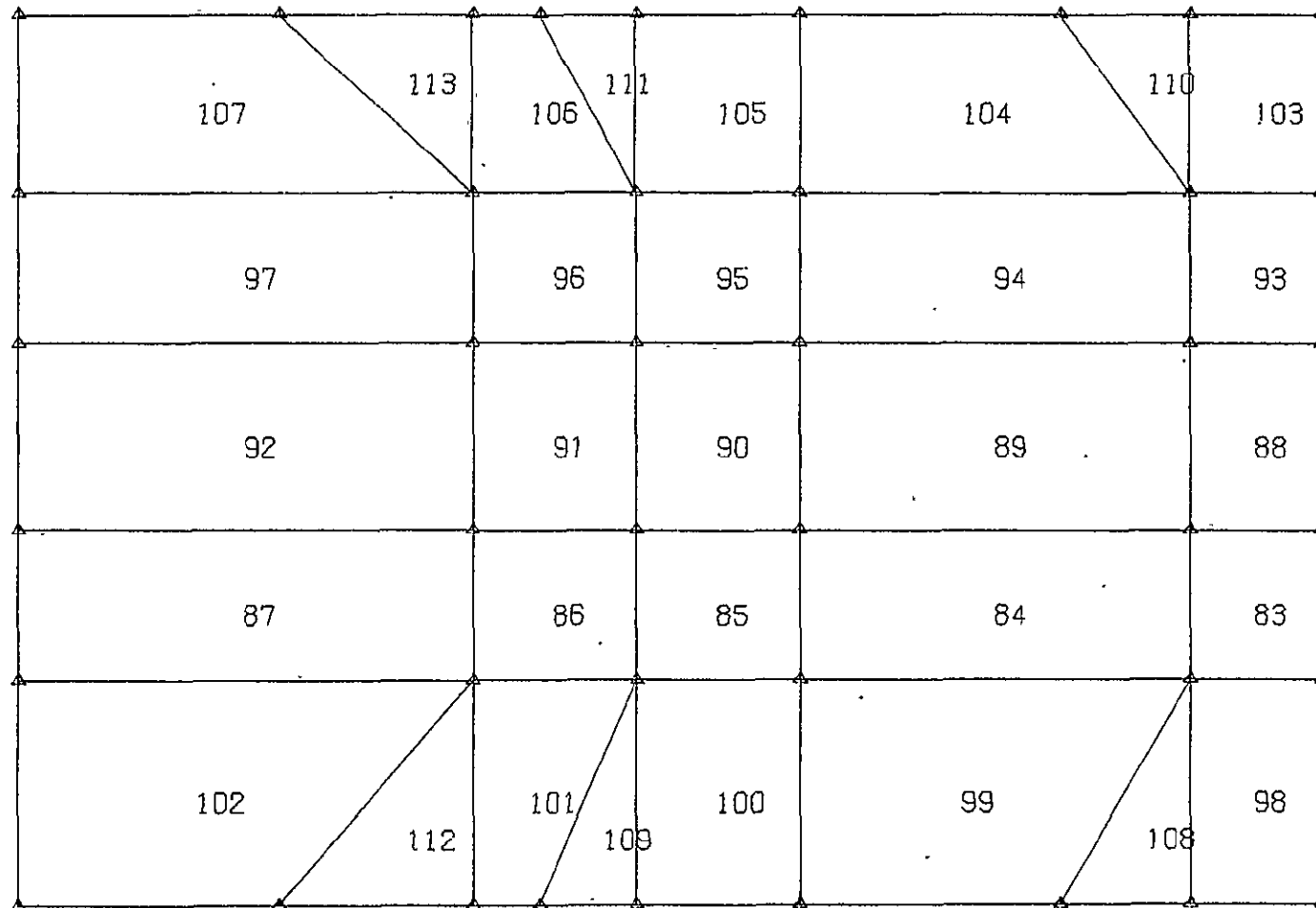
Figure 7-4.—Sizing of Elements, First Strength Resize



Zone 1b

Figure 7-4.—(Continued)

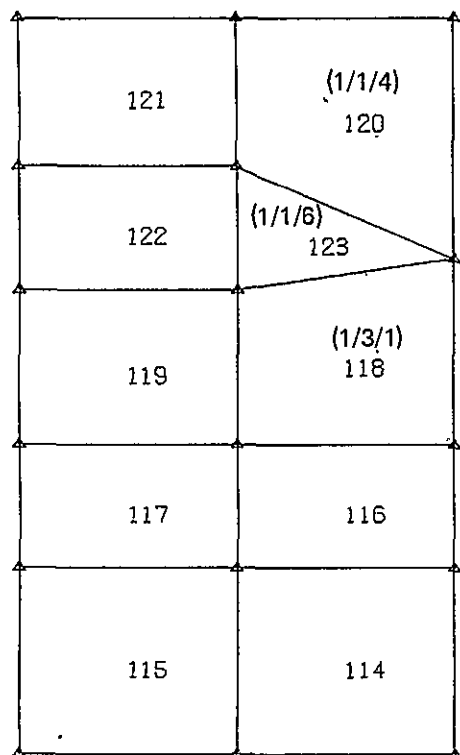
Note: No lower surface (wheel well cutout).



Zone 1c

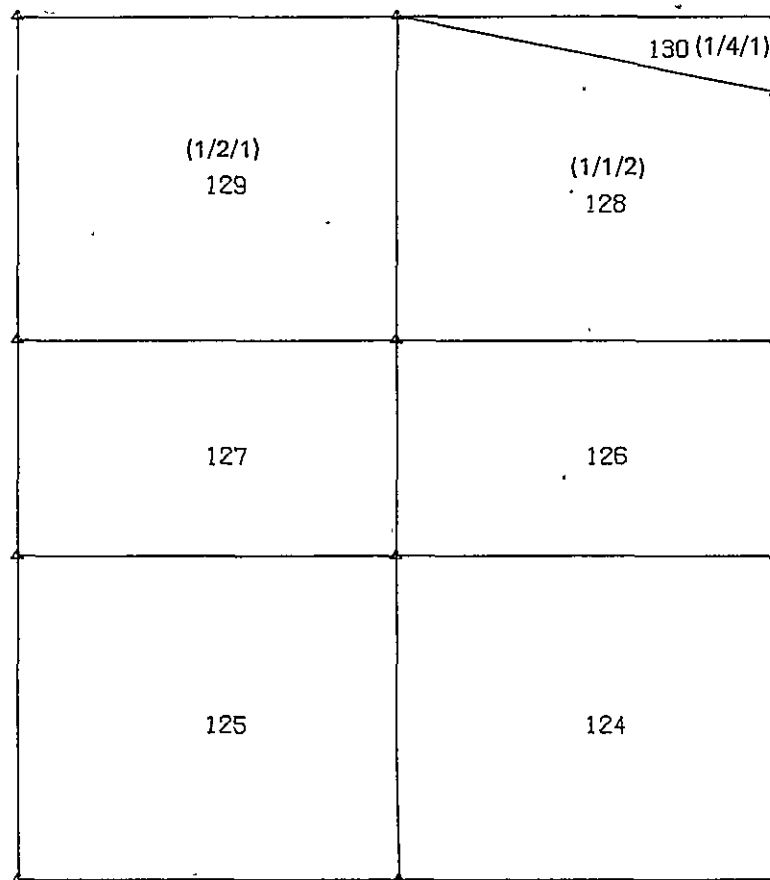
Figure 7-4.—(Continued)

Note: No lower surface (wheel well cutout).



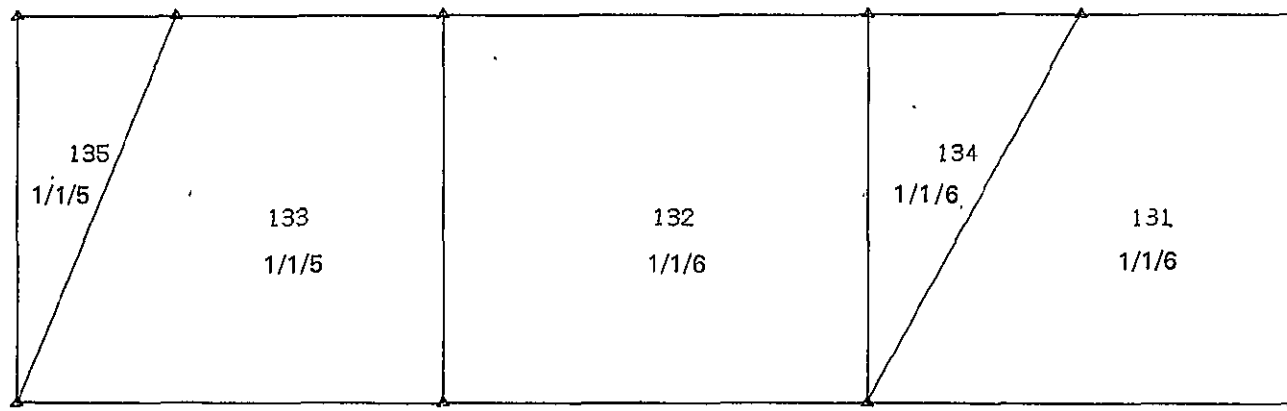
Zone 1d

Note: No lower surface (wheel well cutout).

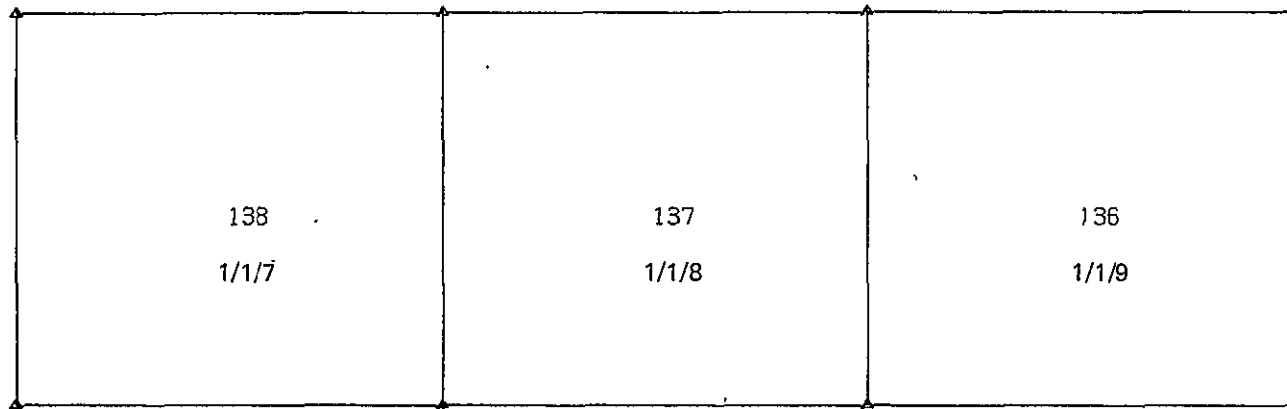


Zone 1e

Figure 7-4.—(Continued)



Zone 2



Zone 3

Figure 7-4.—(Continued)

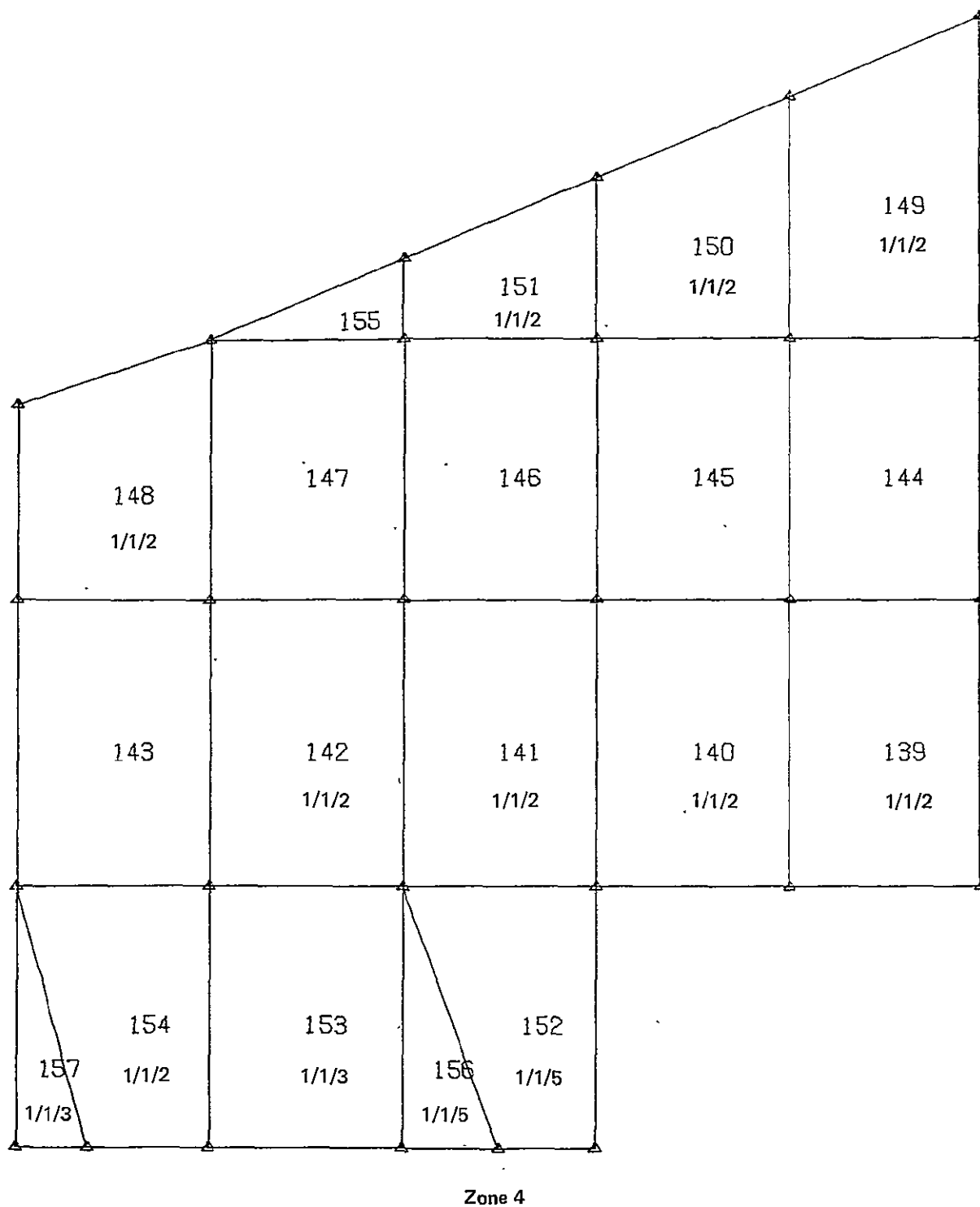


Figure 7-4.—(Continued)

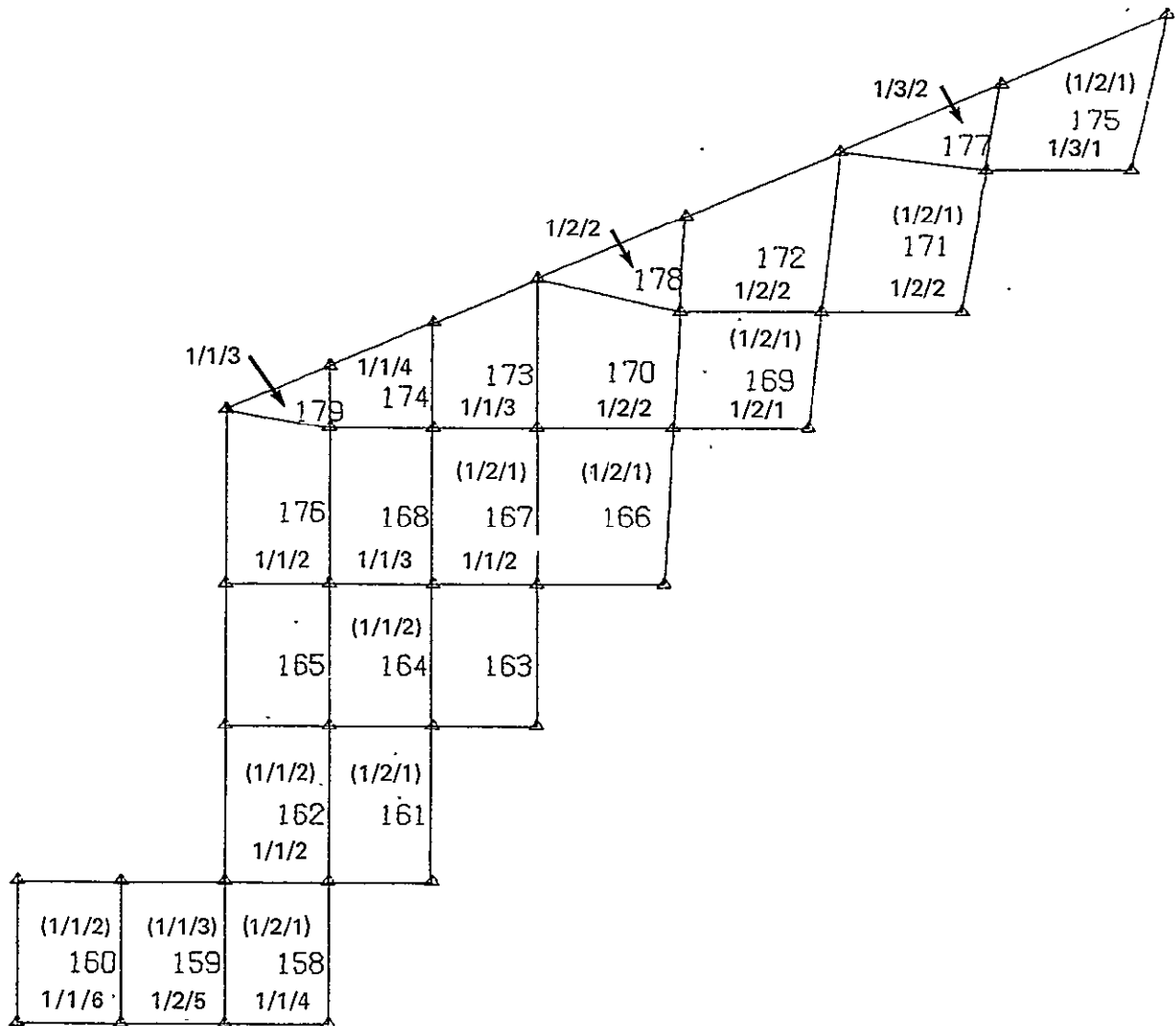


Figure 7-4.—(Continued)

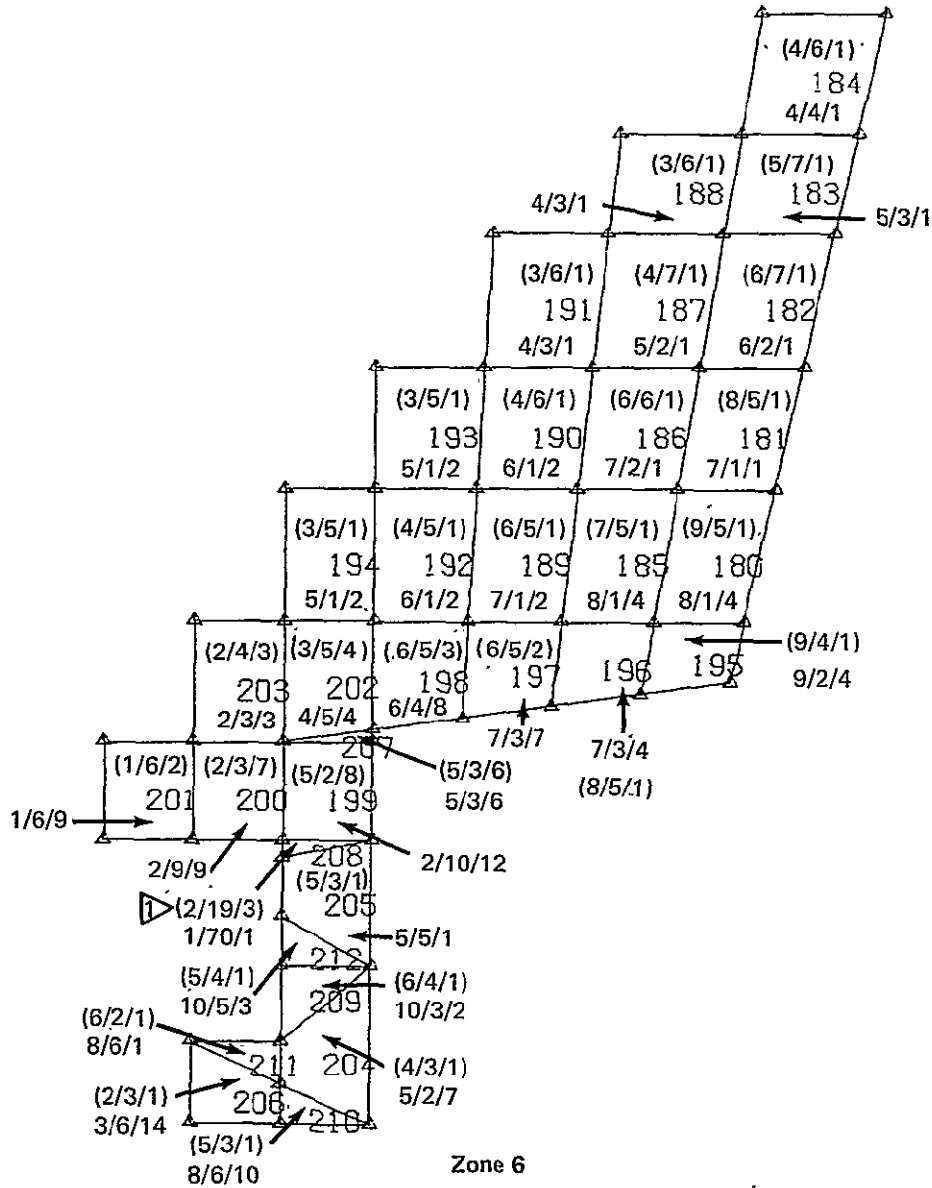
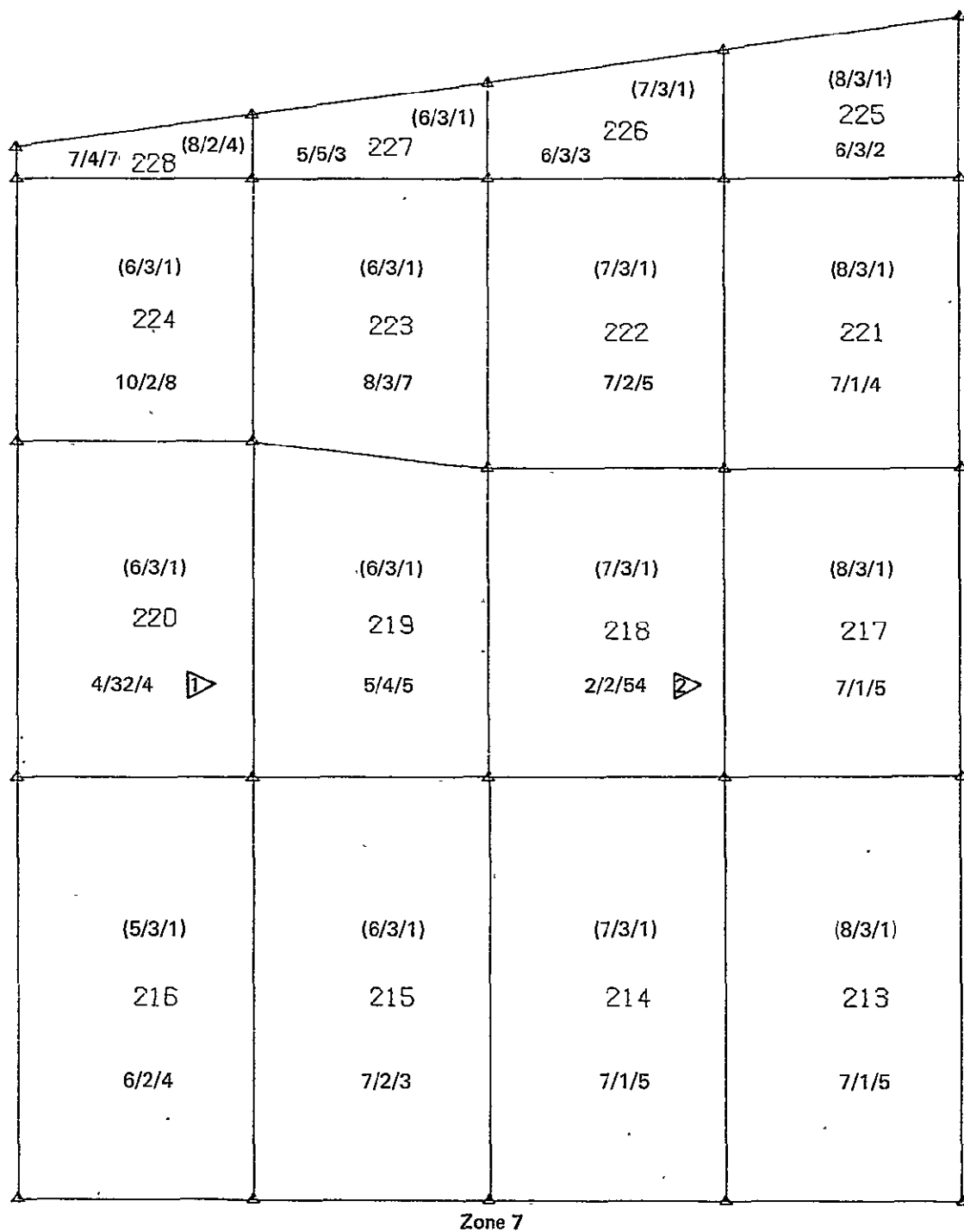


Figure 7-4.—(Continued)



- Element 220 lower surface sizing modified to 5/7/2 (based on COOPB analysis) prior to second cycle analysis.
- Element 218 lower surface sizing modified to 7/1/5 (based on COOPB analysis) prior to second cycle analysis.

Figure 7-4.—(Continued)

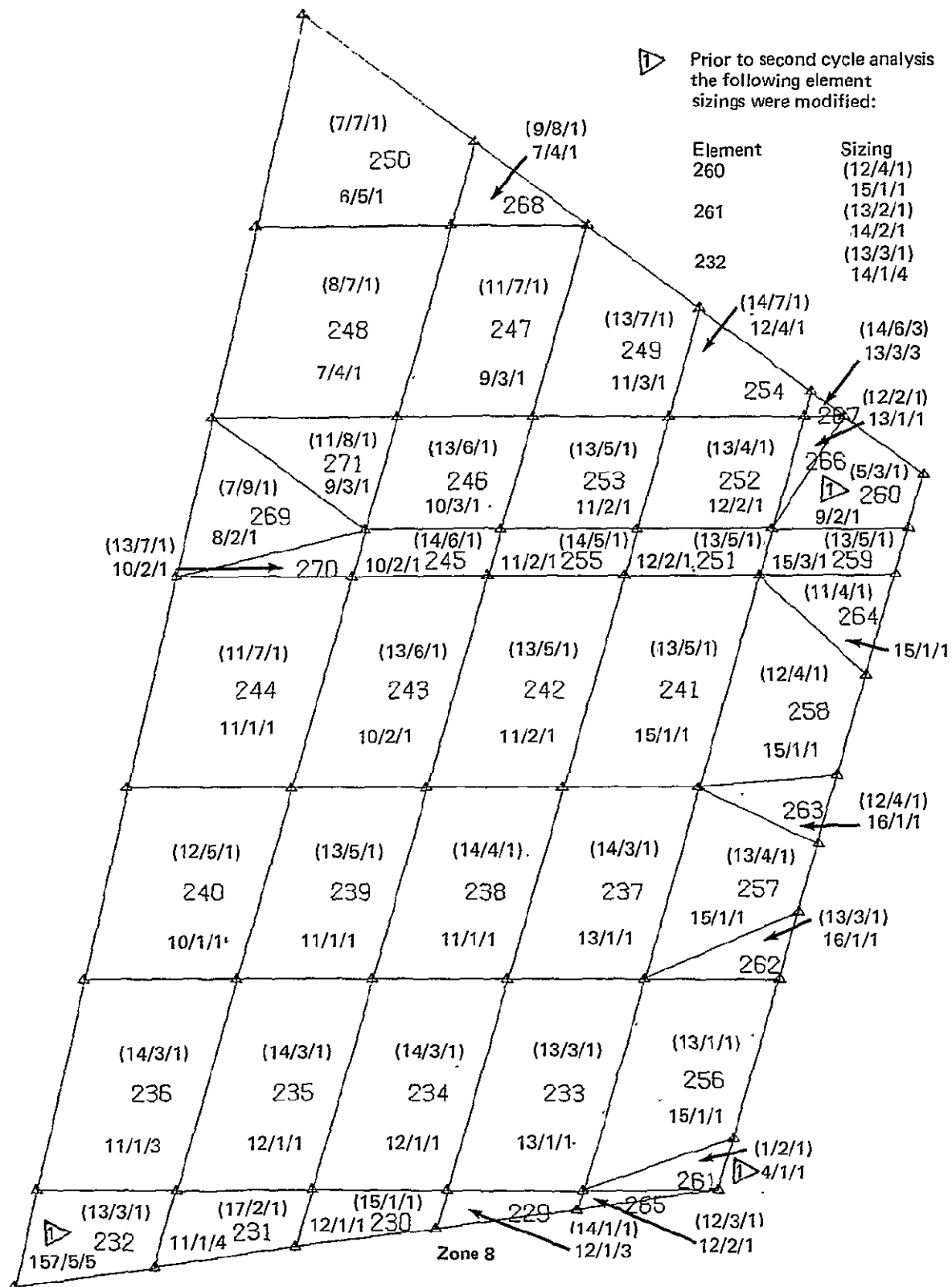
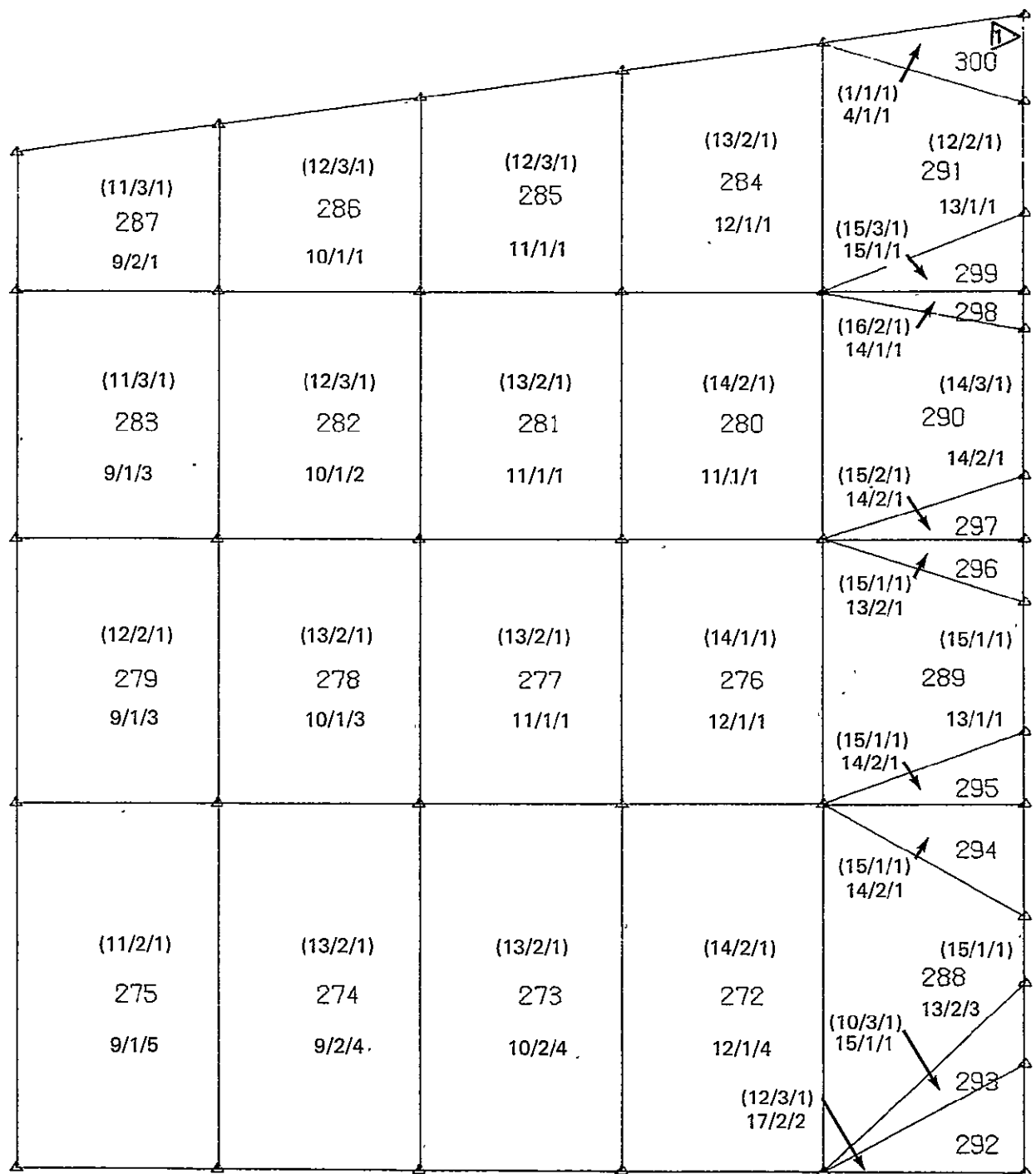


Figure 7-4.—(Continued)



Zone 9a

1 Prior to second cycle analysis element 300 sizing was modified to (12/2/1) 13/1/1

Figure 7-4.—(Continued)

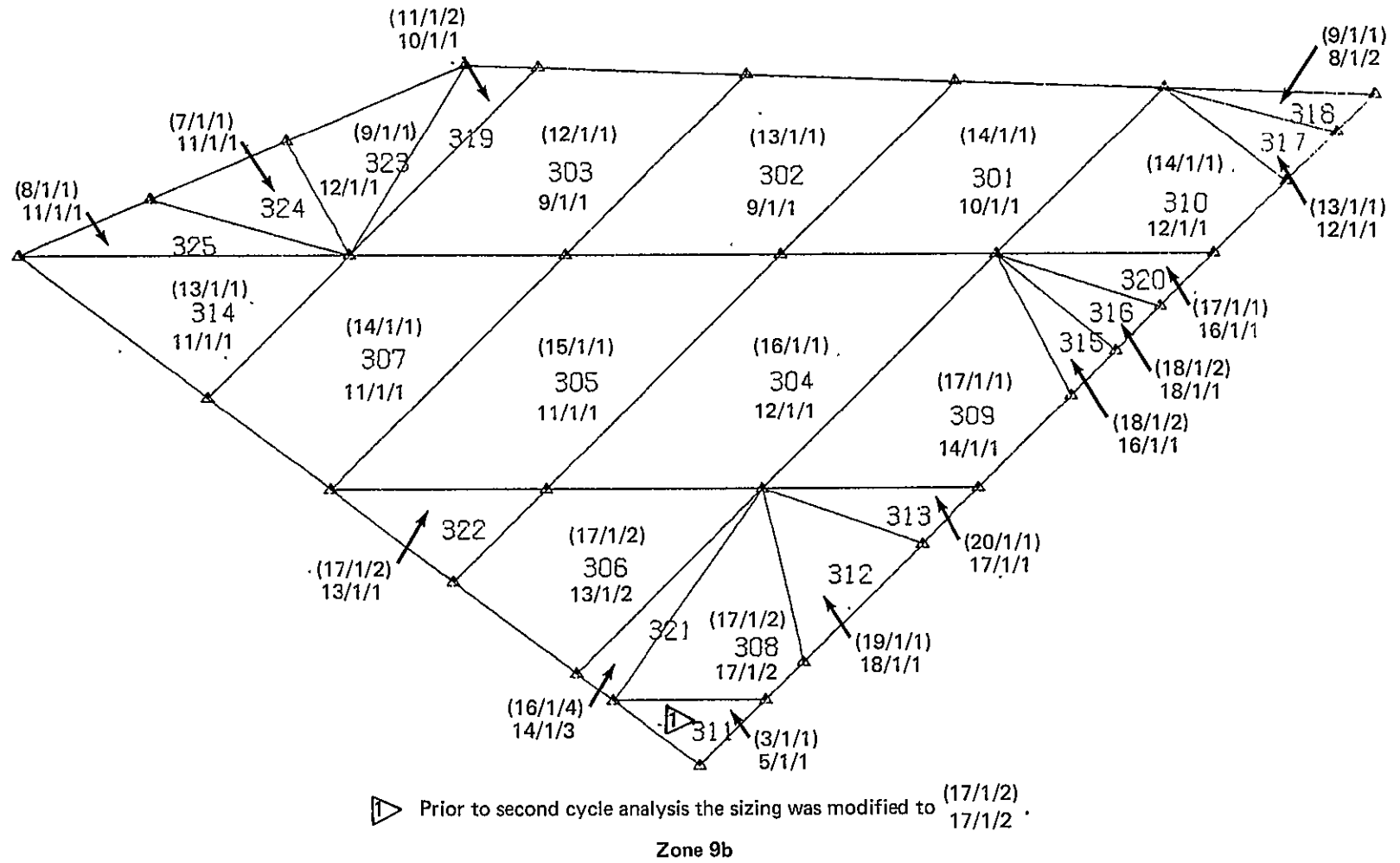


Figure 7-4.—(Continued)

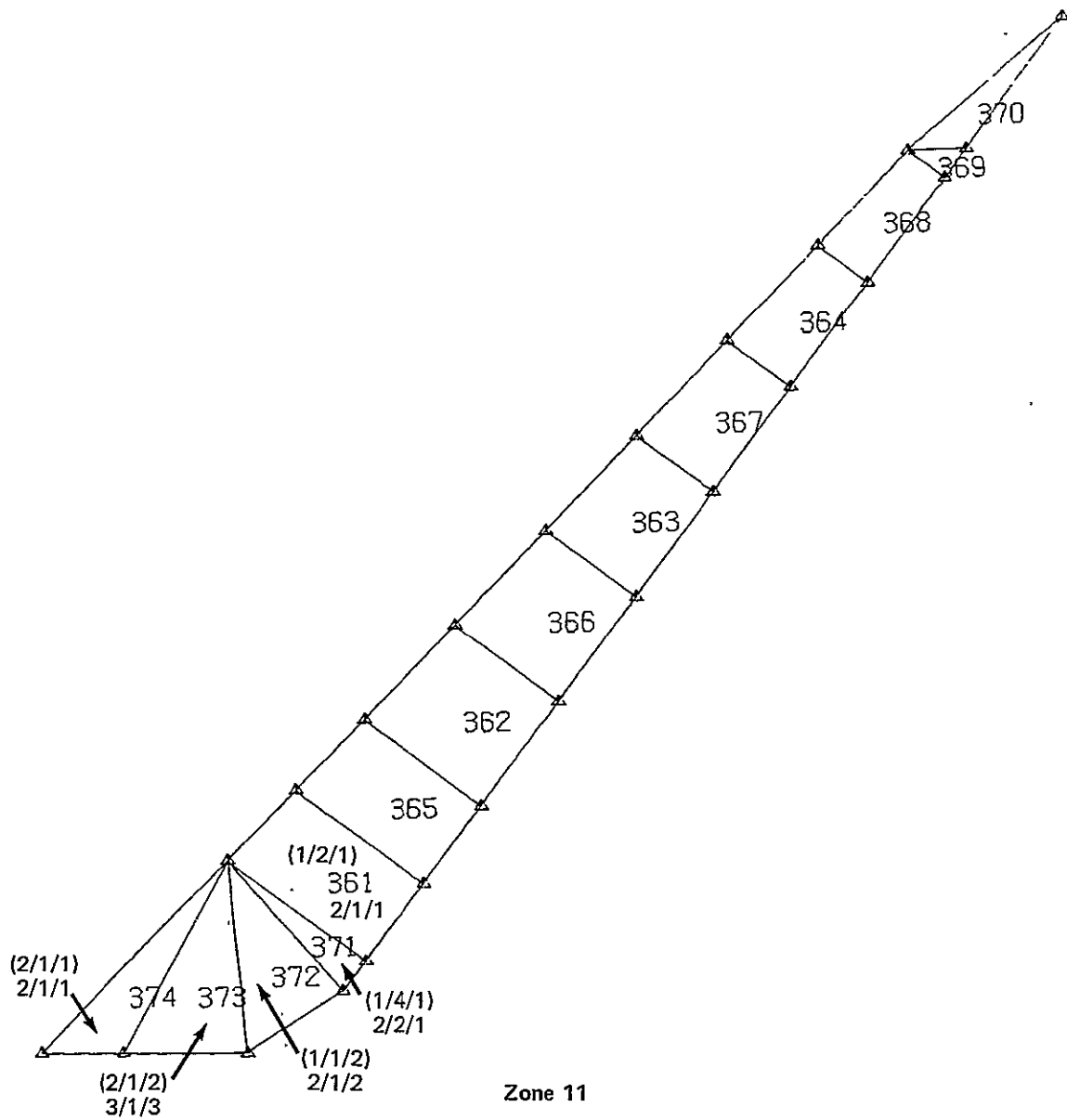


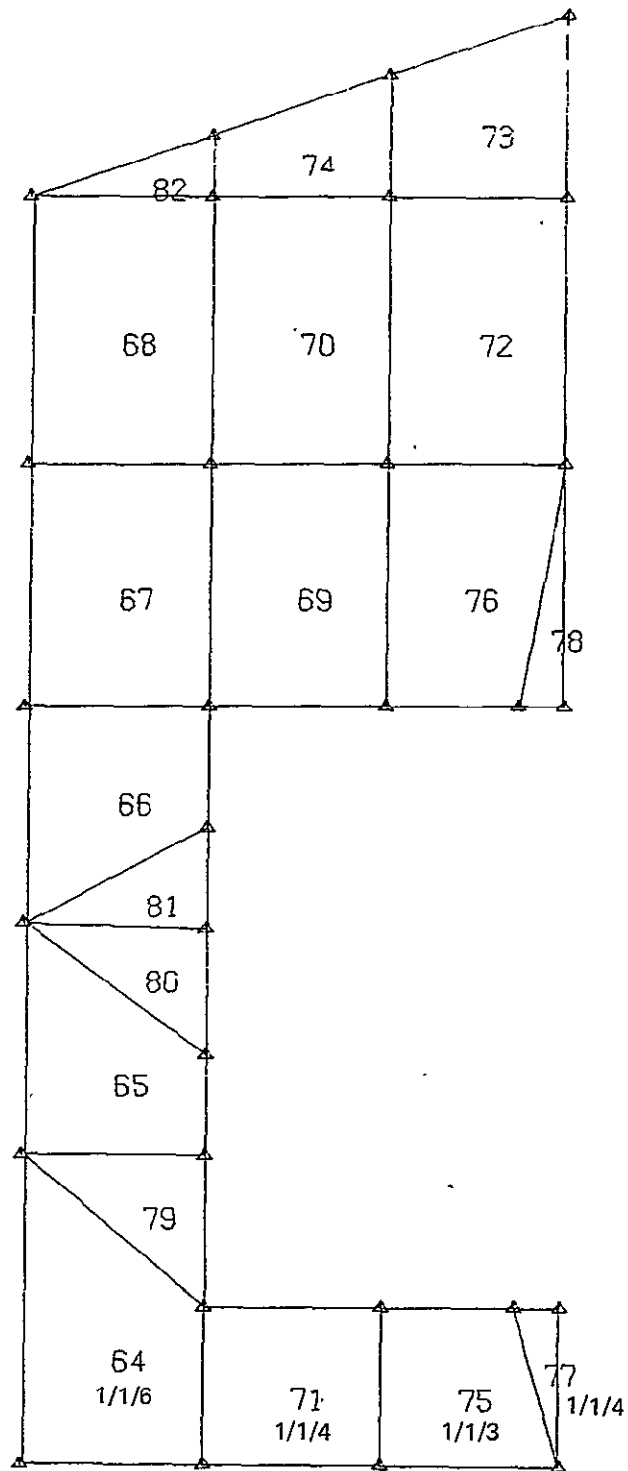
Figure 7-4.—(Concluded)

1. Sizing values $i/j/k$ define the subscripts in the standard laminate code for a $[0_i/45_j/90_k]_T$ laminate composed of 0.002 in.-thick plies. The lower (upper) panel sizing is shown without (within) parentheses. If a single set of sizing values is shown for either an upper or lower panel, it applies equally to the sandwich inner and outer face sheets. Otherwise, the two sets of values are shown within a brace with the thinner laminate being the inner face sheet.

- [illegible]

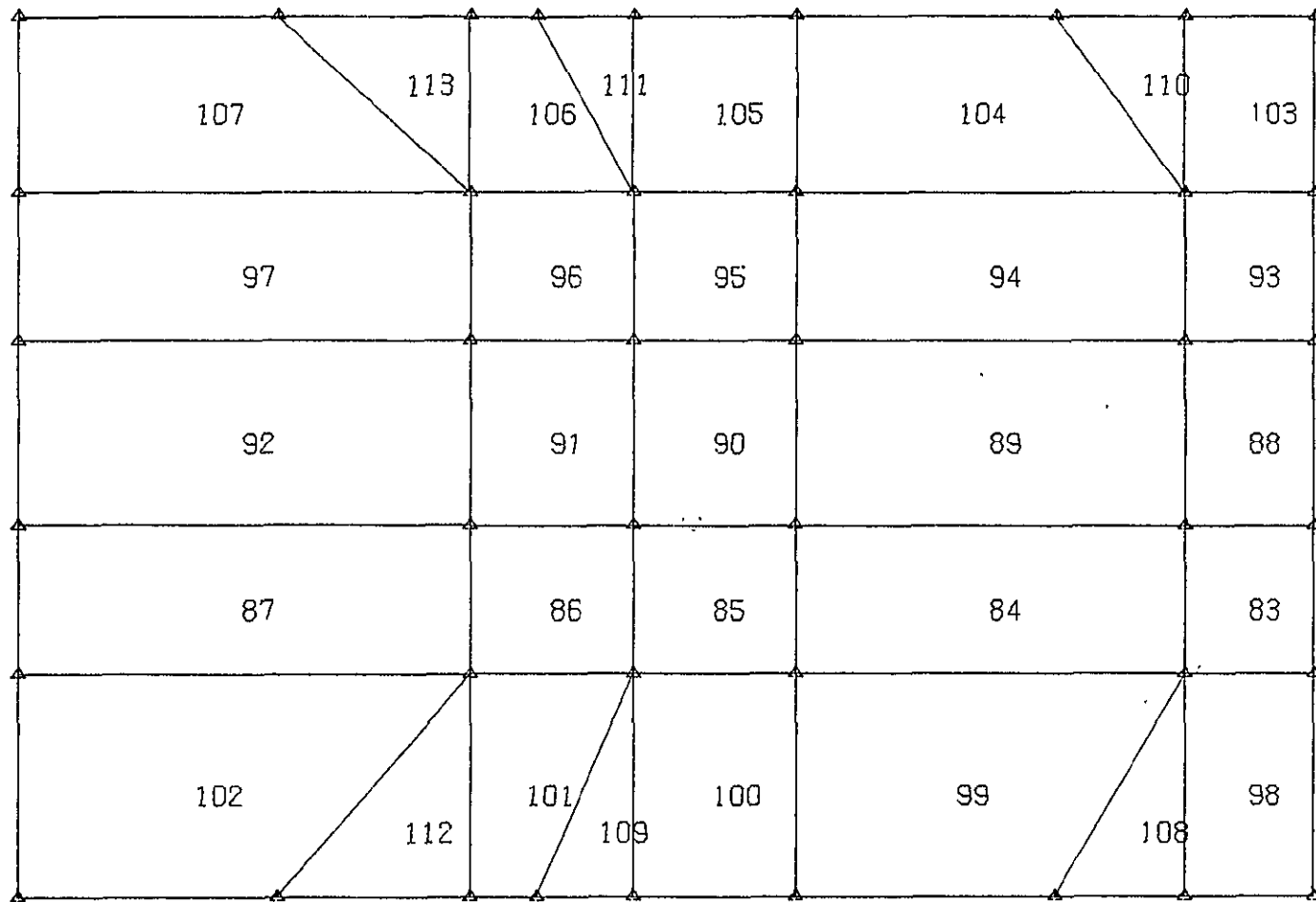
Zone 1a

Figure 7-5.—Sizing of Elements, Second Strength Resize



Zone 1b

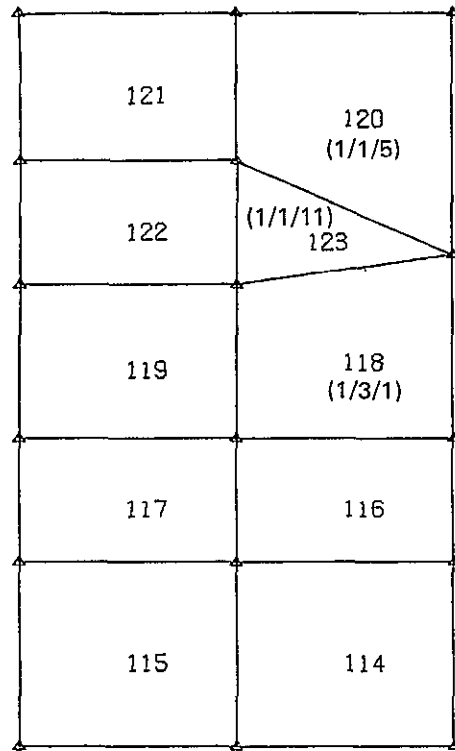
Figure 7-5.—(Continued)



Note: No lower surface (wheel well cutout).

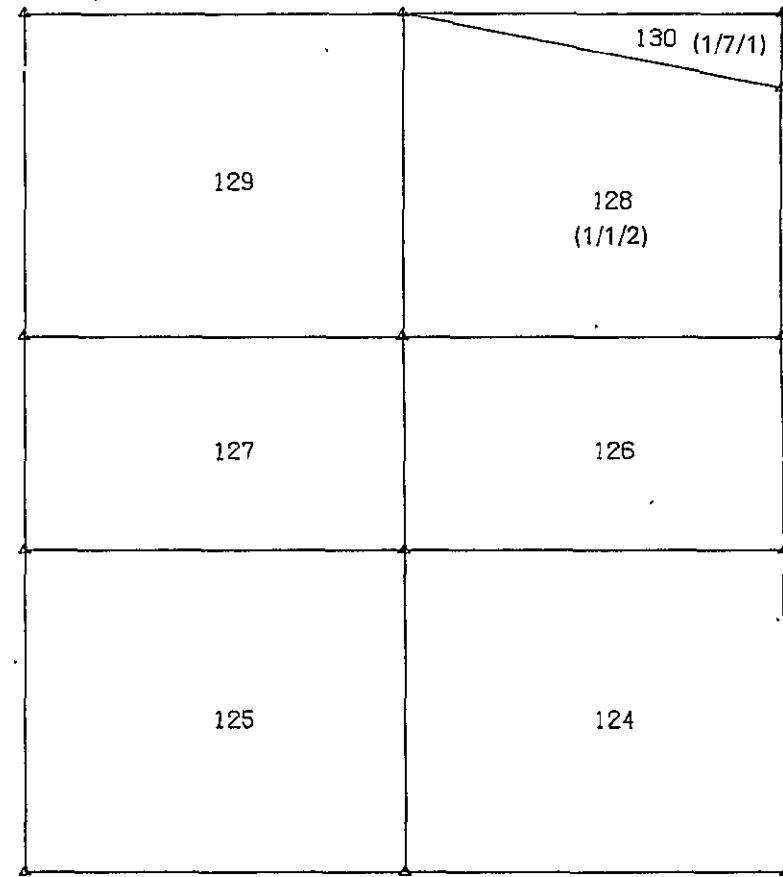
Zone 1c

Figure 7-5.—(Continued)



Note: No lower surface (wheel well cutout).

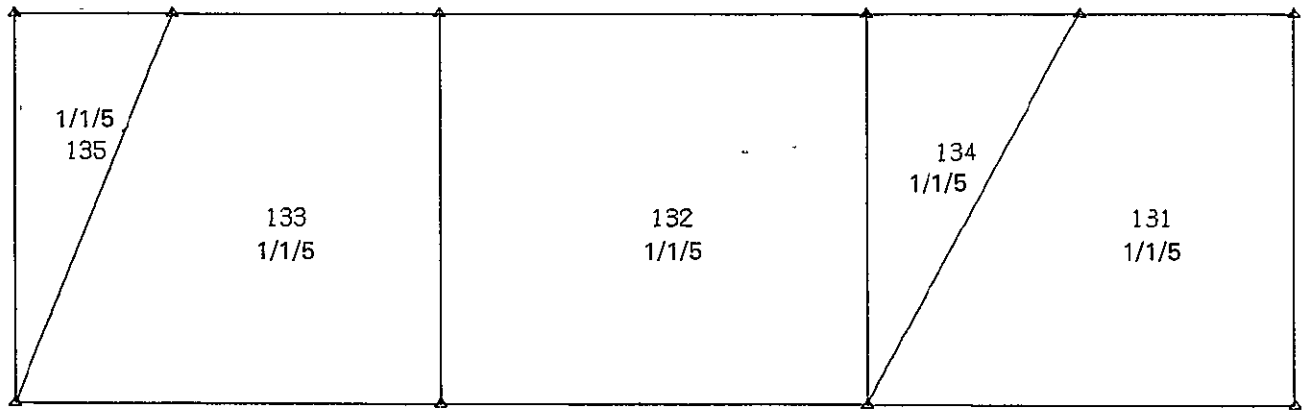
Zone 1d



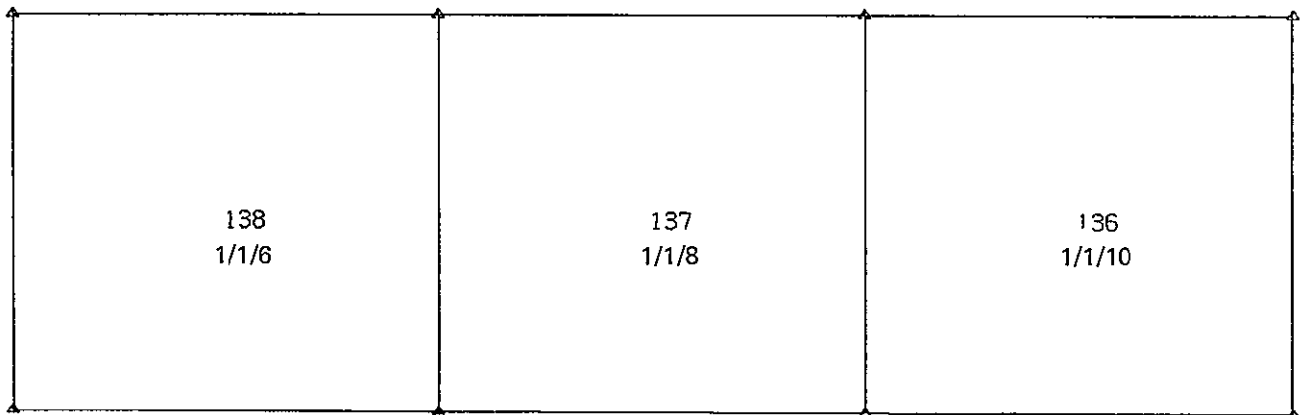
Note: No lower surface (wheel well cutout).

Zone 1e

Figure 7-5.—(Continued)



Zone 2



Zone 3

Figure 7-5.—(Continued)



230

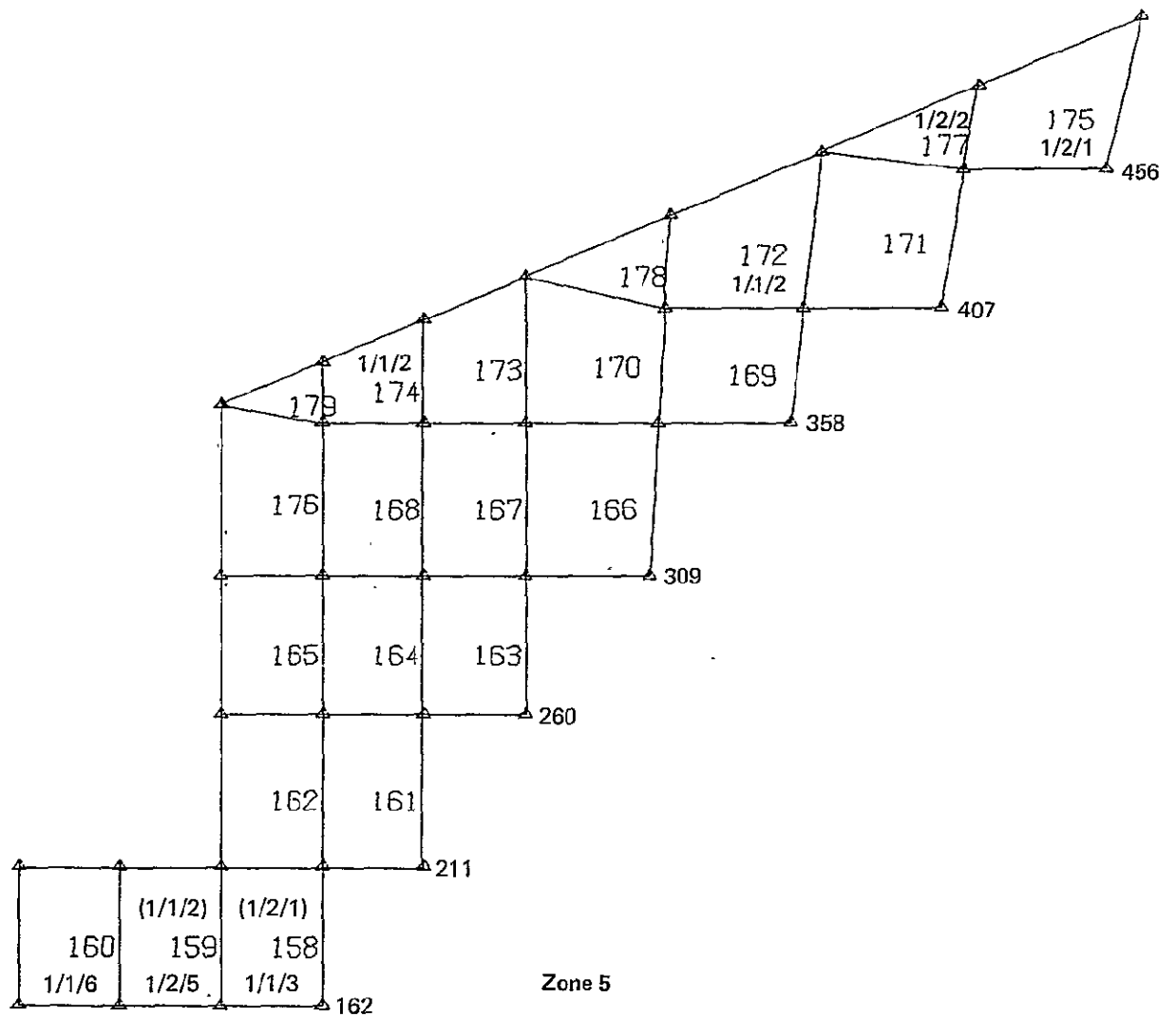
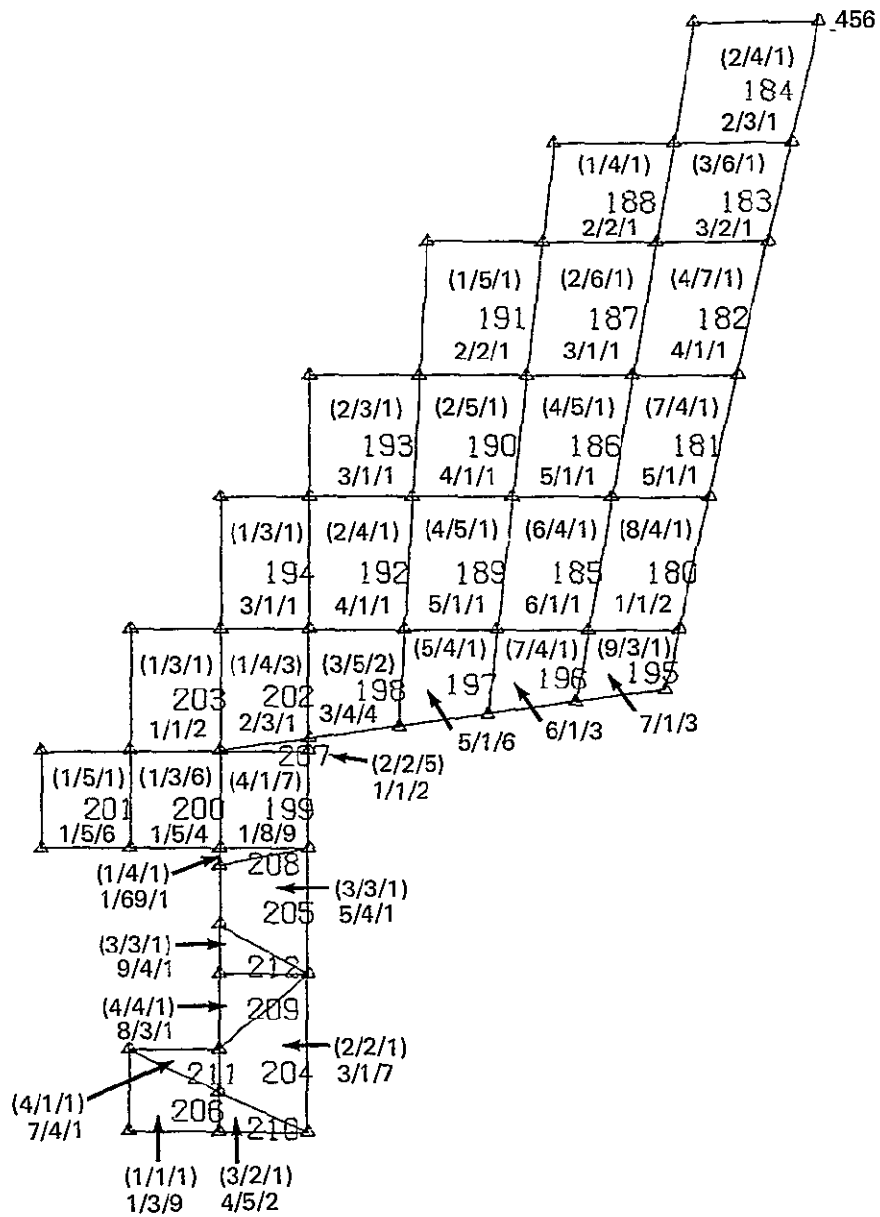
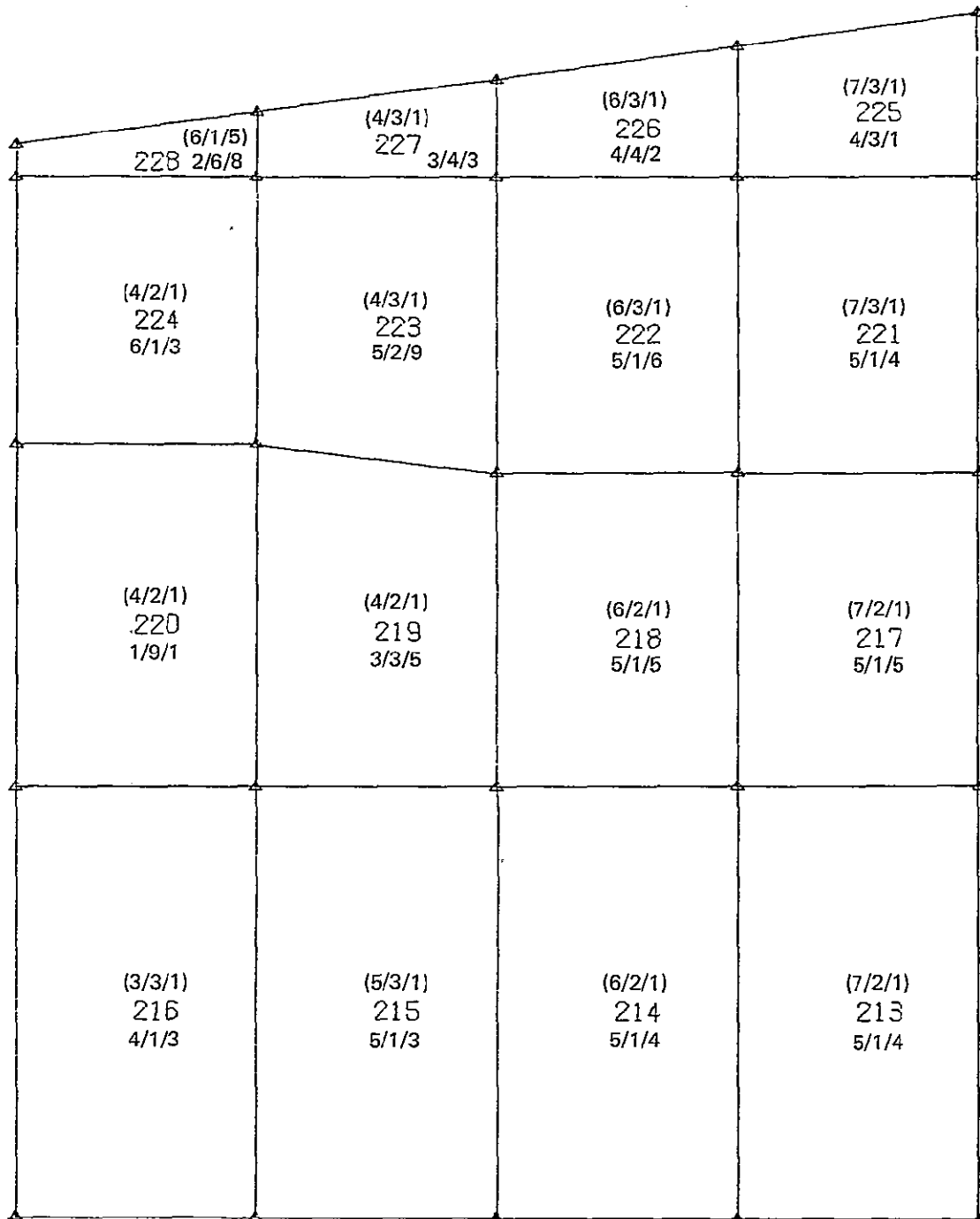


Figure 7-5.—(Continued)



Zone 6

Figure 7-5.—(Continued)



Zone 7

Figure 7-5.—(Continued)

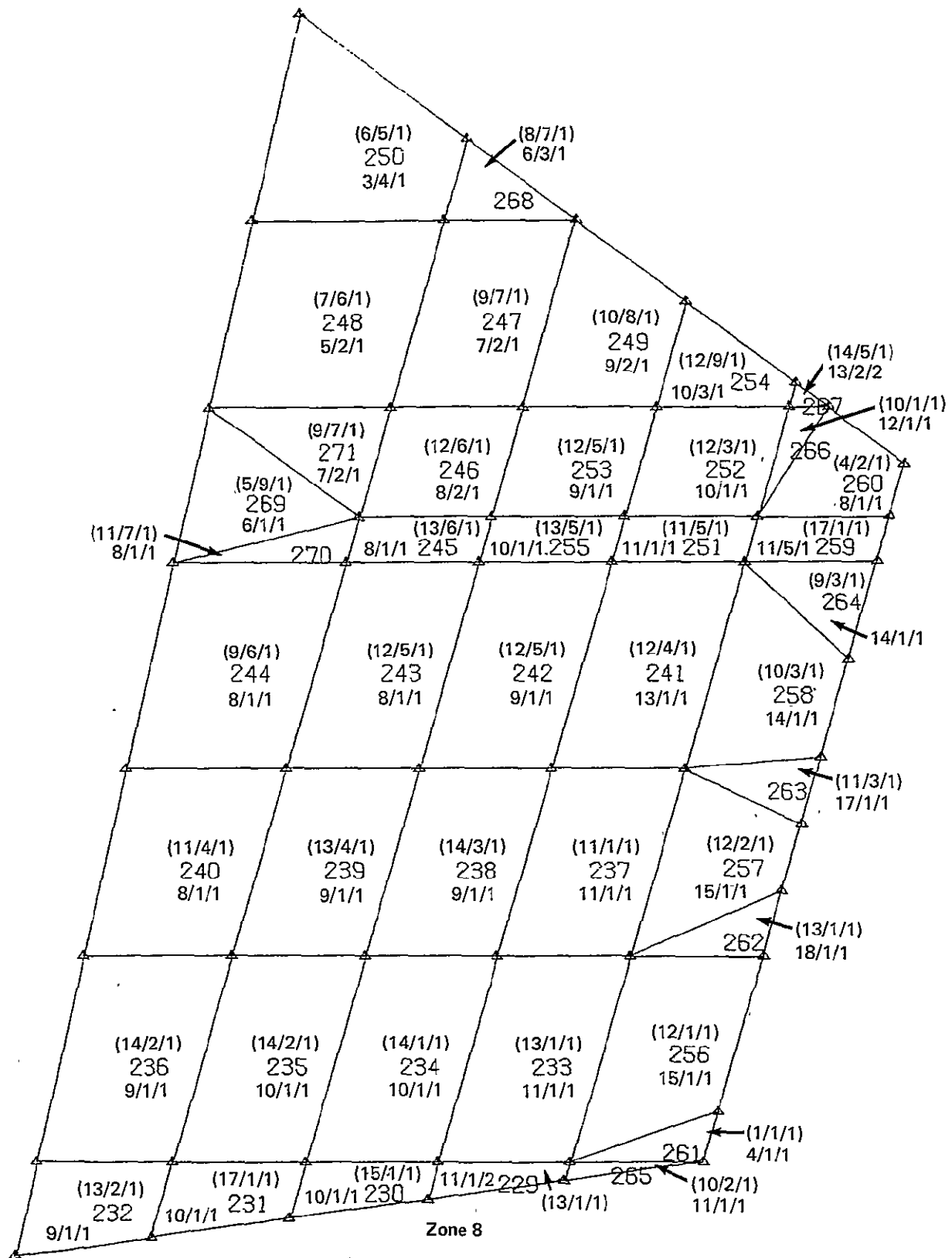
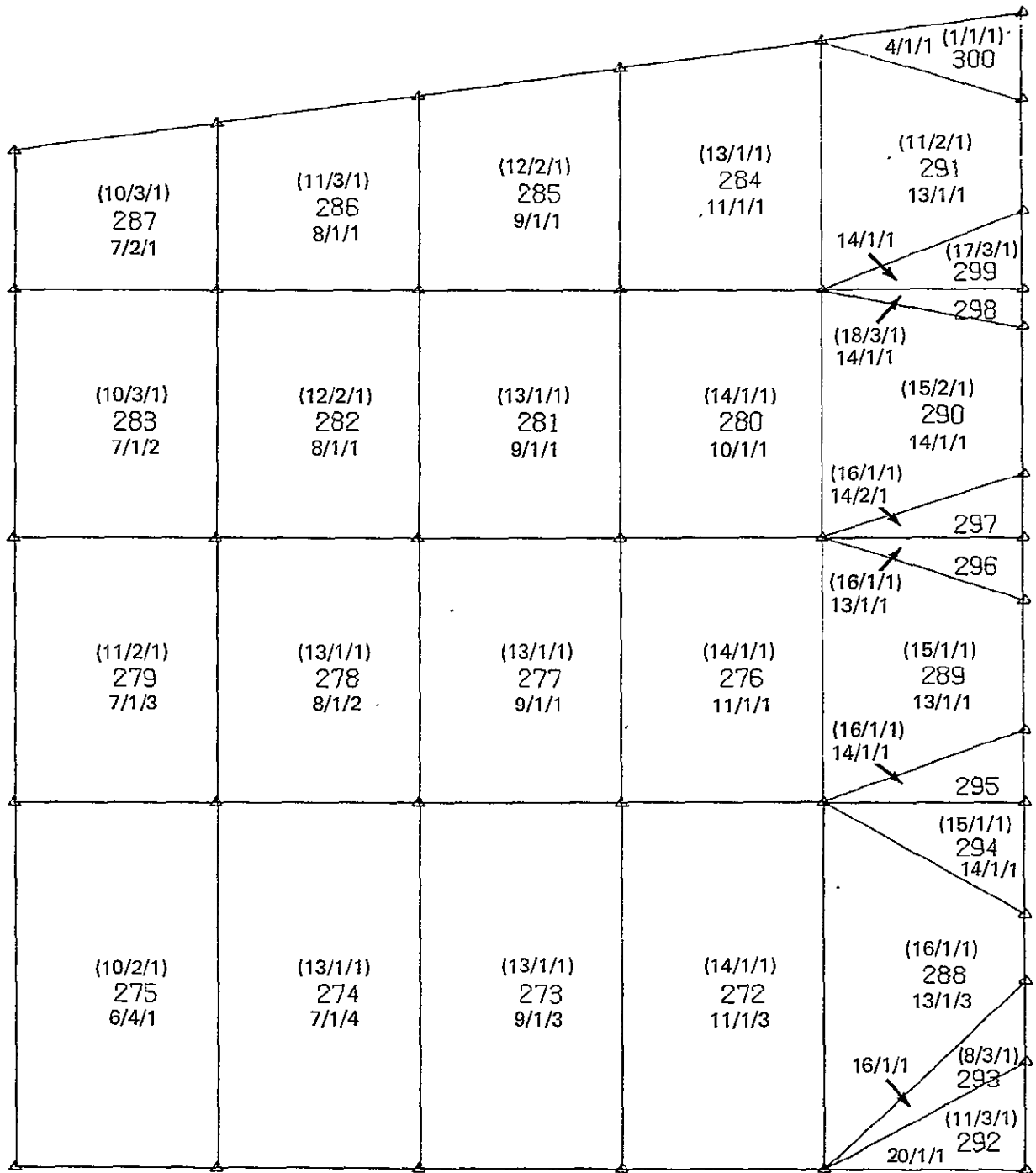


Figure 7-5.-(Continued)



Zone 9a

Figure 7-5.—(Continued)

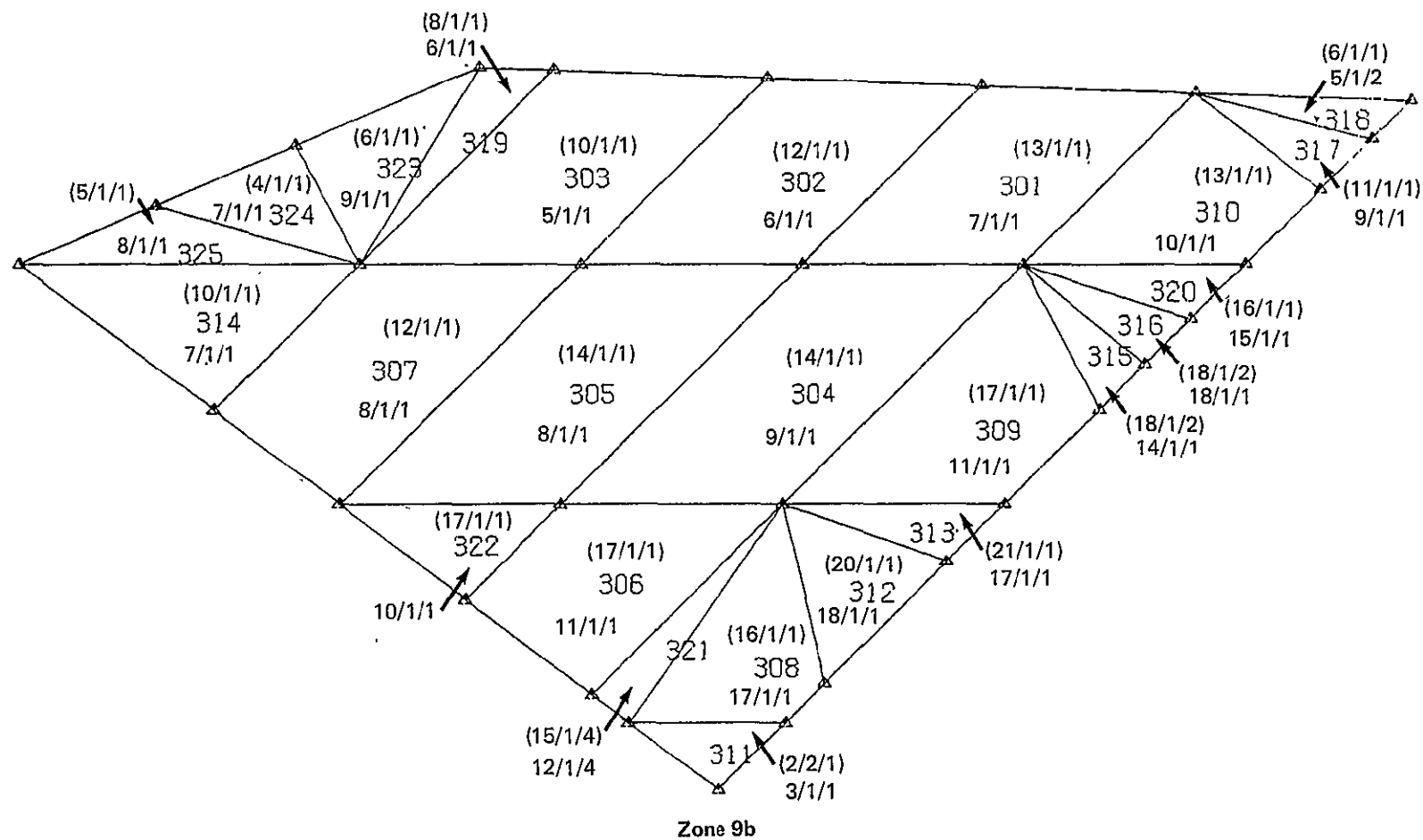
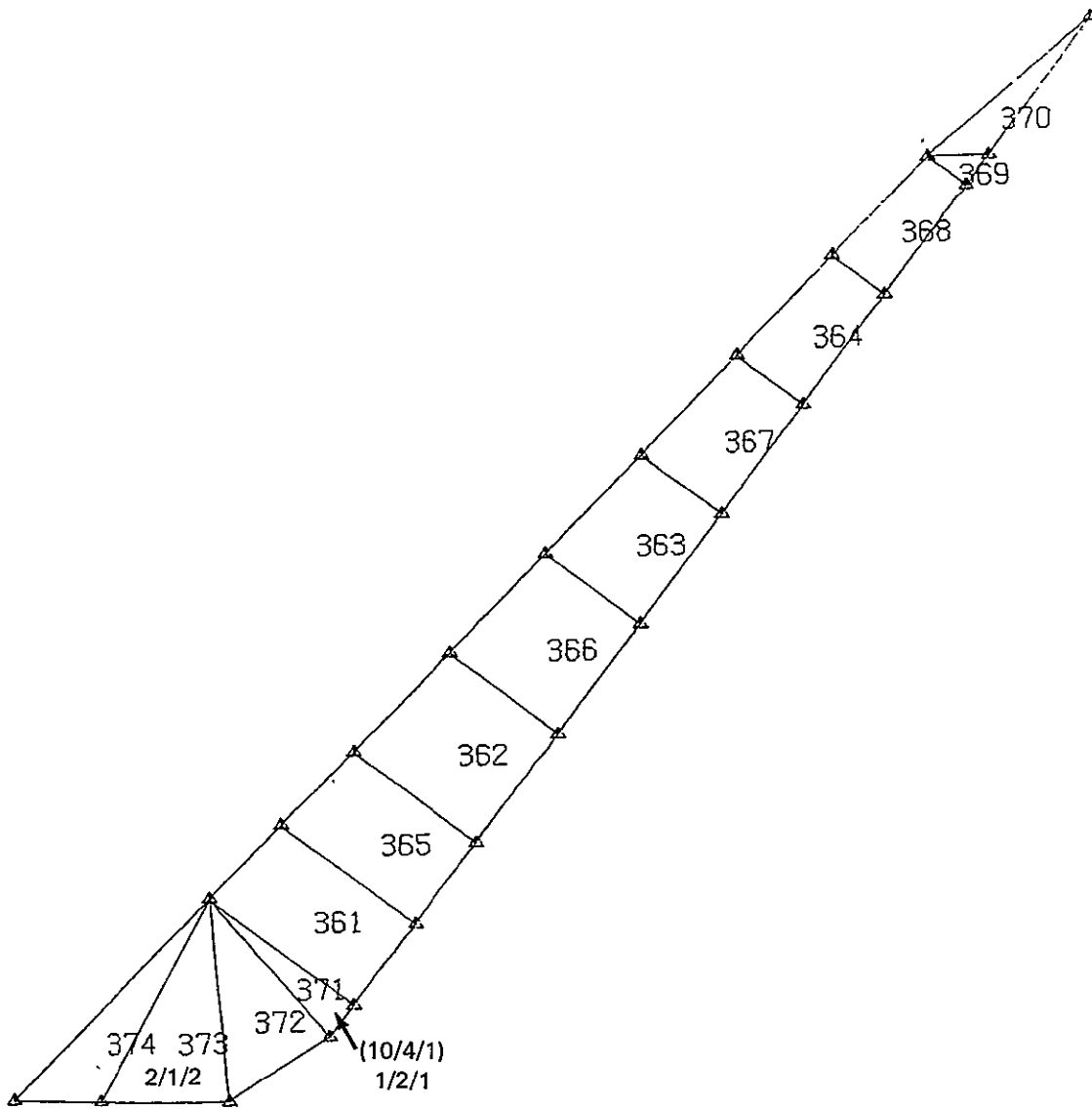


Figure 7-5.—(Continued) .



Zone 11

Figure 7-5.—(Concluded)

Note:

1. Sizing values $i/j/k$ define the subscripts in the standard laminate code for a $[0_i/45_j/90_k]_T$ laminate composed of 0.002 inch-thick plies. The lower (upper) panel sizing is shown without (within) parentheses. If a single set of sizing values is shown for either an upper or lower panel, it applies equally to the sandwich inner and outer face sheets. Otherwise, the two sets of values are shown within a brace with the thinner laminate being the inner face sheet.
2. Except as noted on the figures all face sheet sizing is:

Face Sheet	Sizing
Upper surface outer	3/3/3
Upper surface inner	2/2/2
Lower surface inner	2/2/2
Lower surface outer	4/4/4

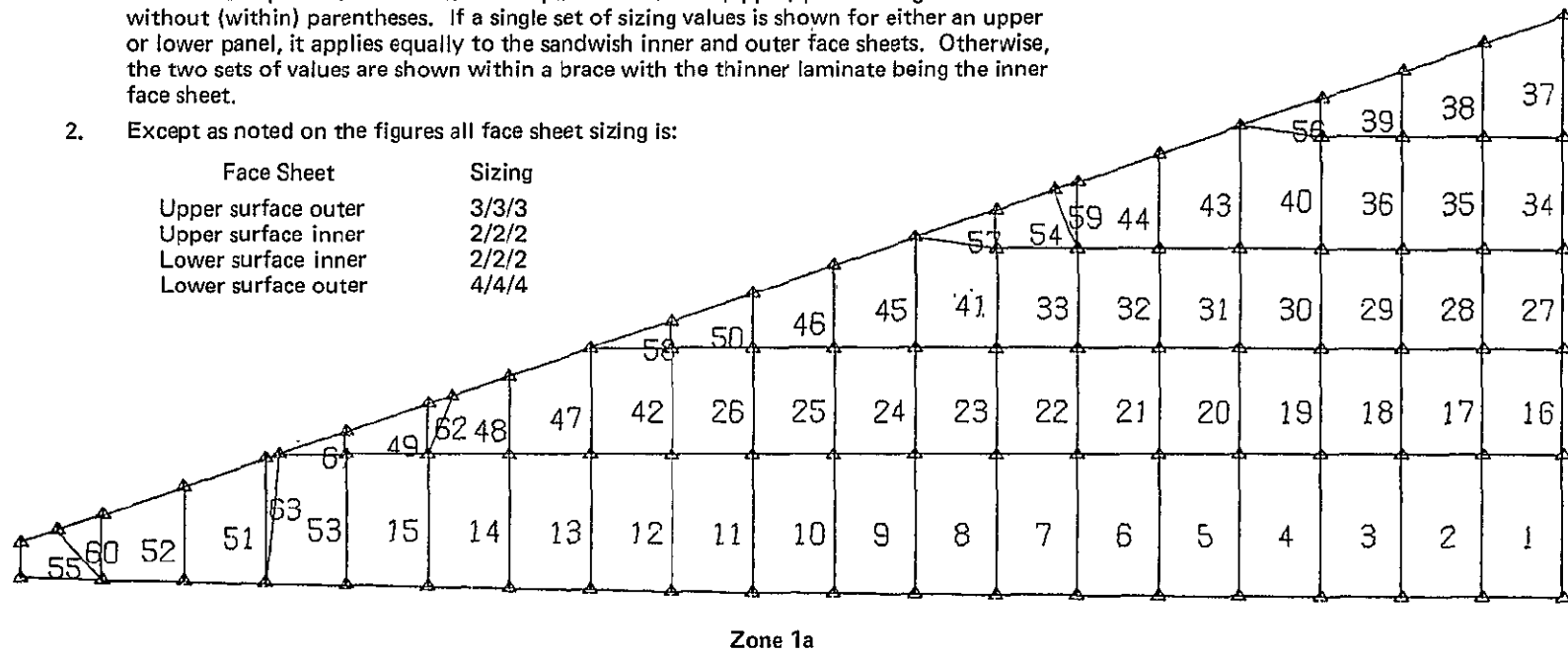


Figure 7-6.—Sizing of Elements, Third Strength Resize

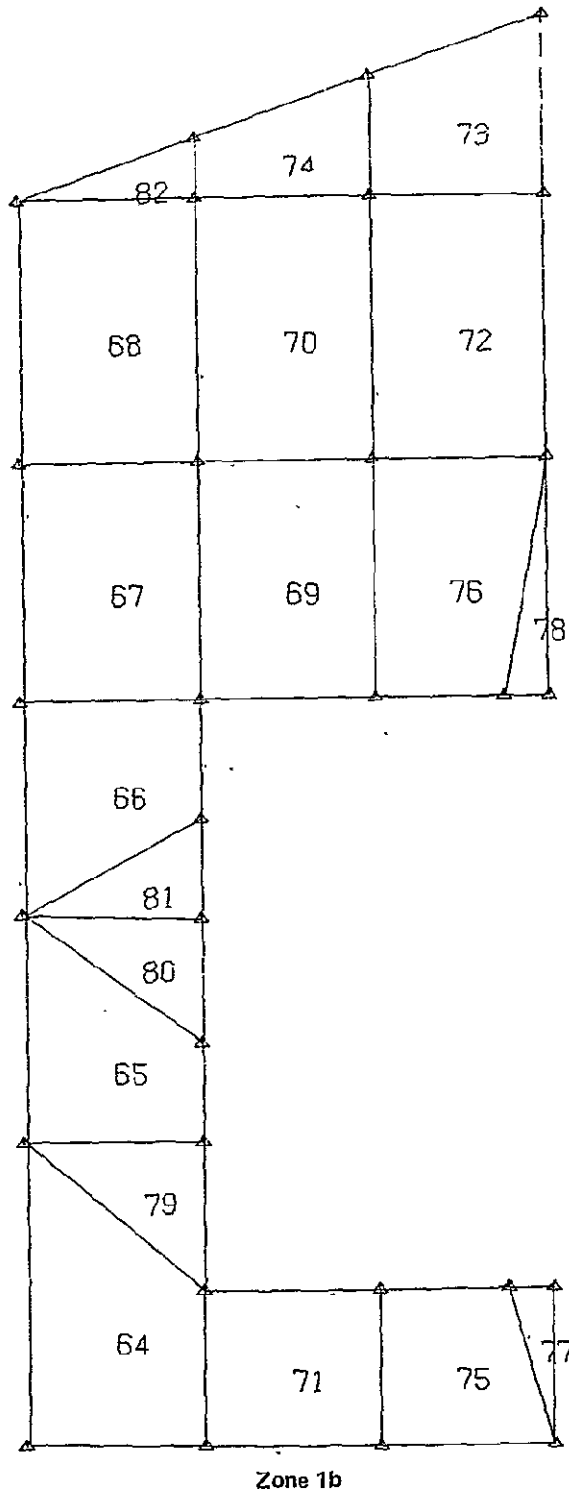
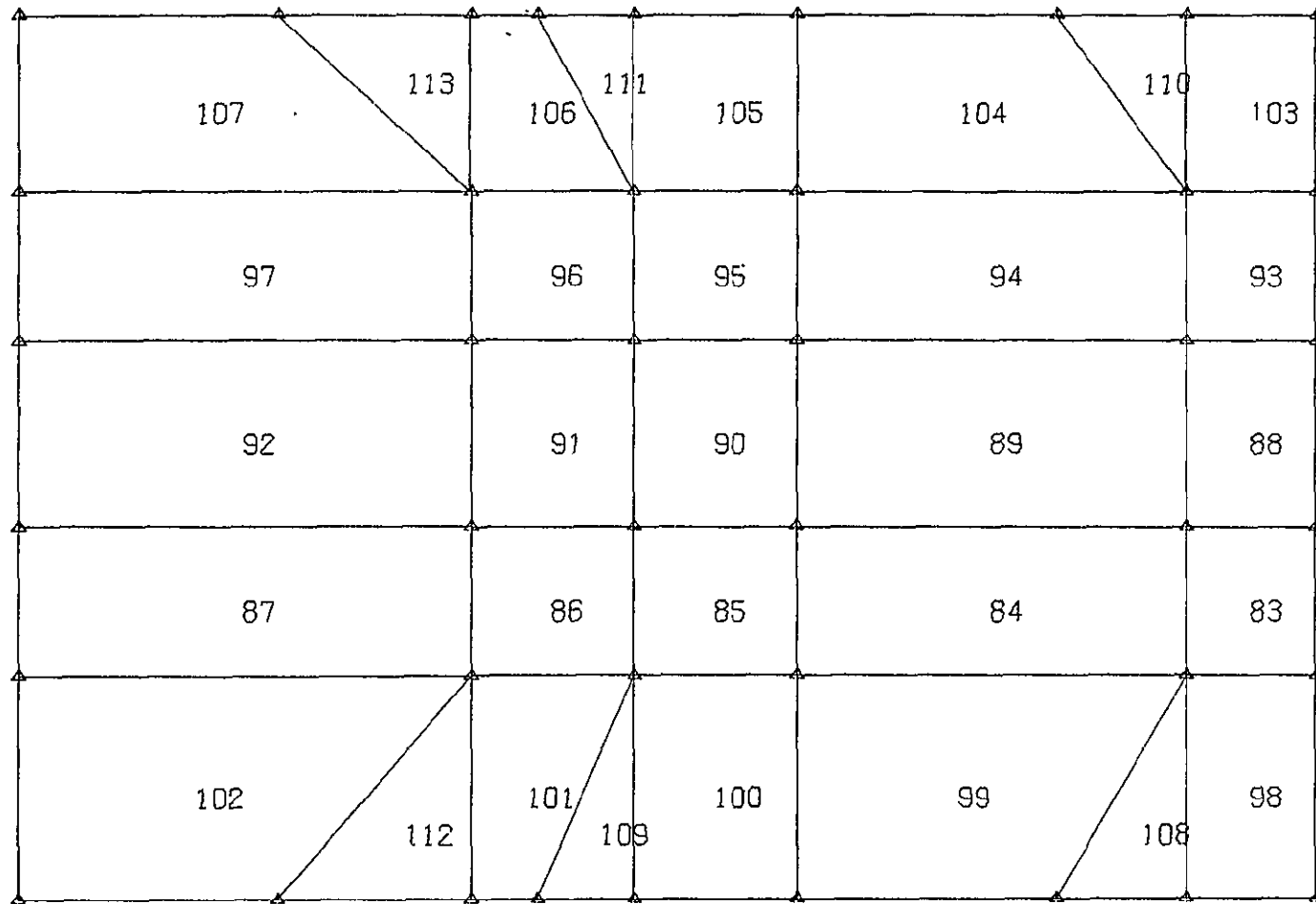


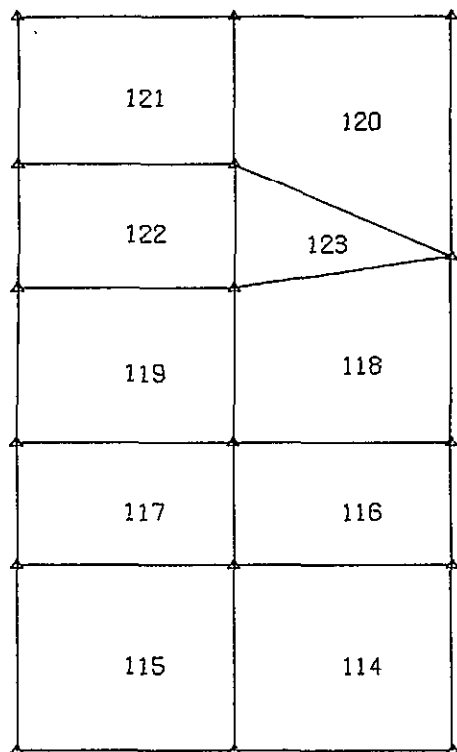
Figure 7-6.—(Continued)



Note: No lower surfaces (wheel well cutout).

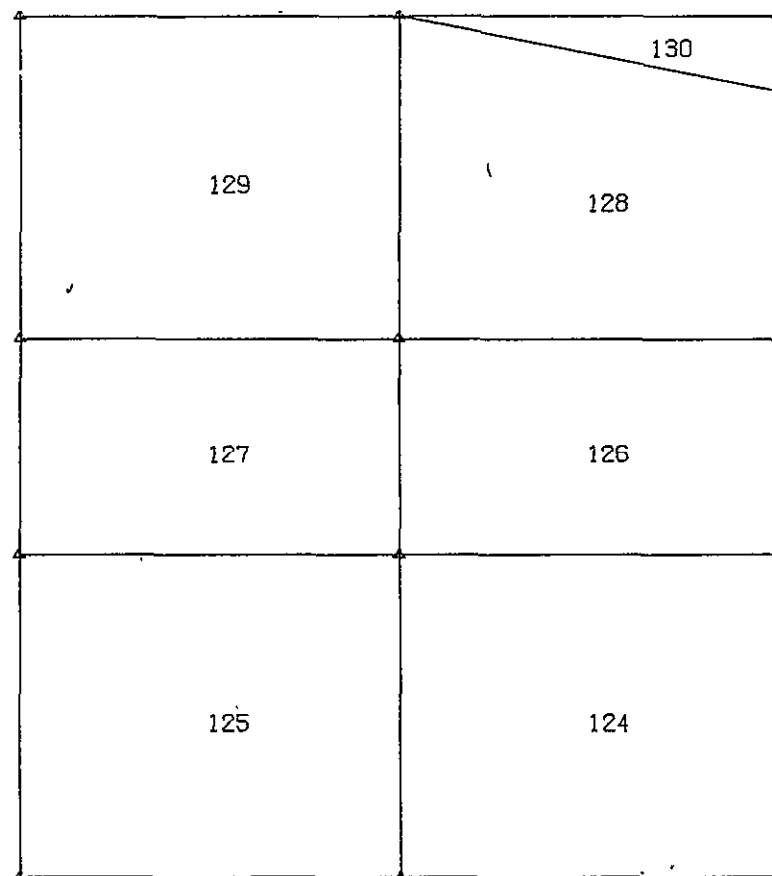
Zone 1c

Figure 7-6.—(Continued)



Note: No lower surface (wheel well cutout).

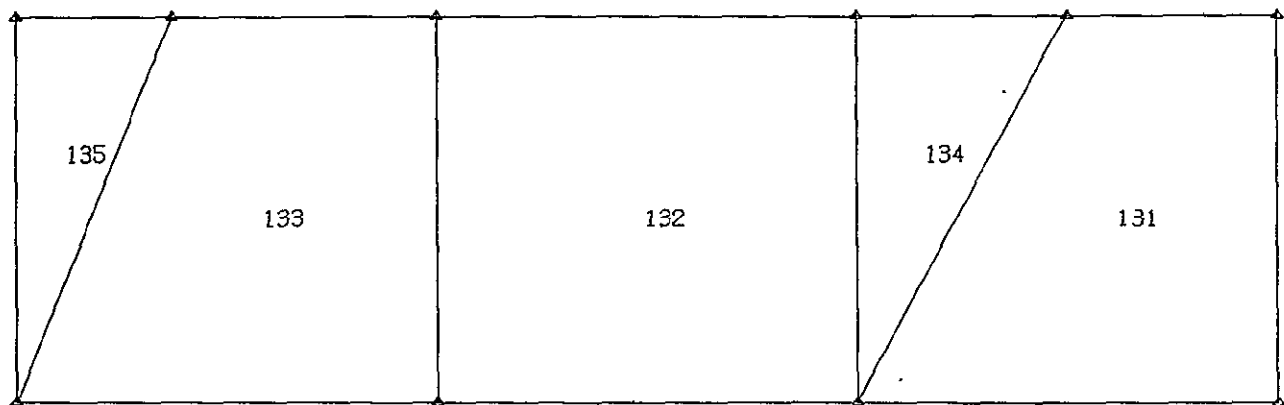
Zone 1d



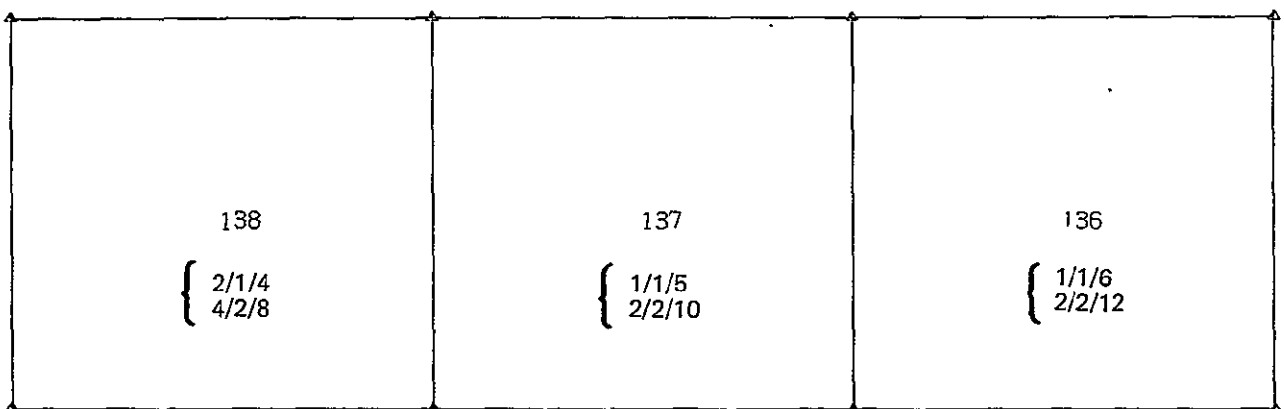
Note: No lower surface (wheel well cutout).

Zone 1e

Figure 7-6.—(Continued)

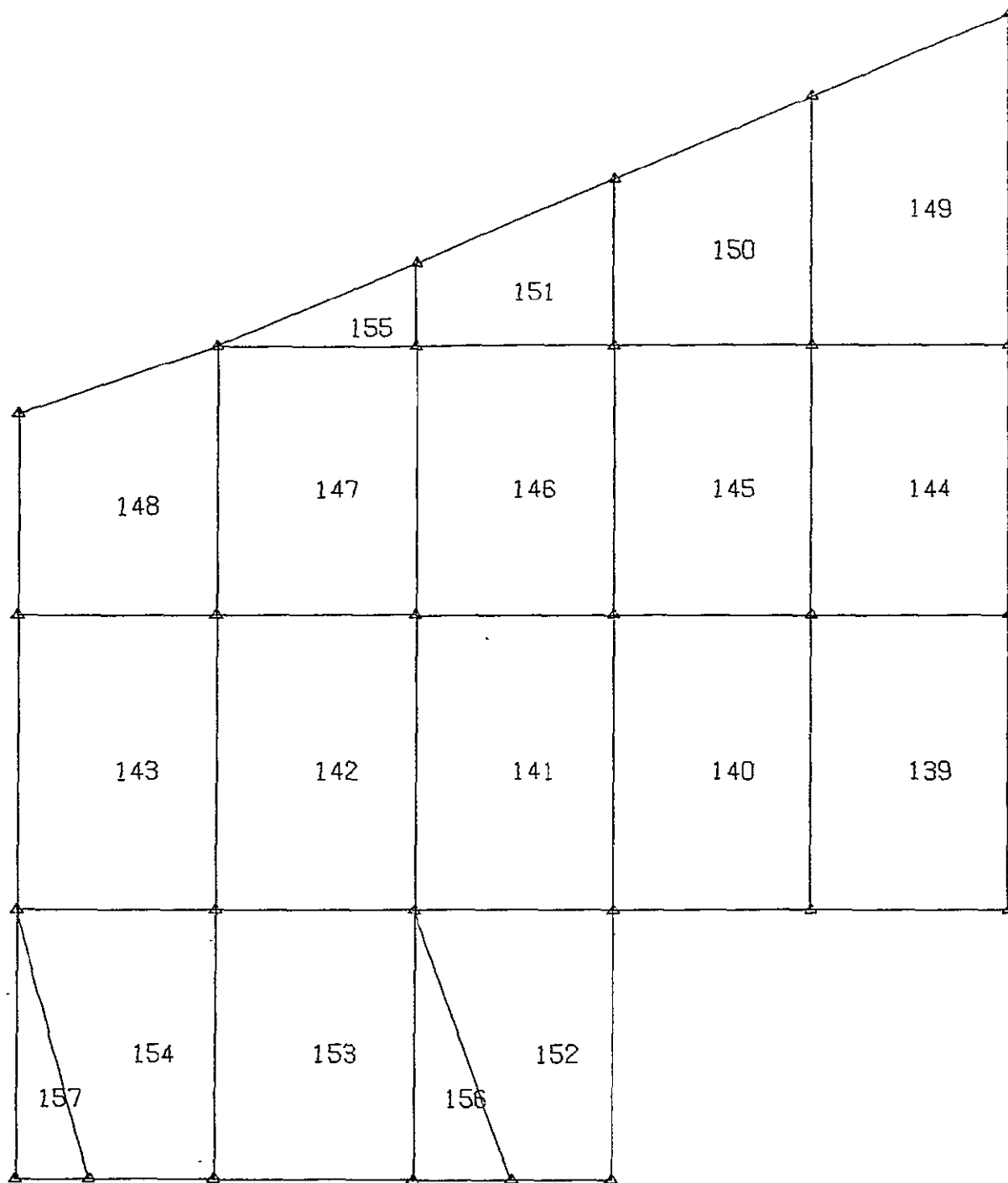


Zone 2



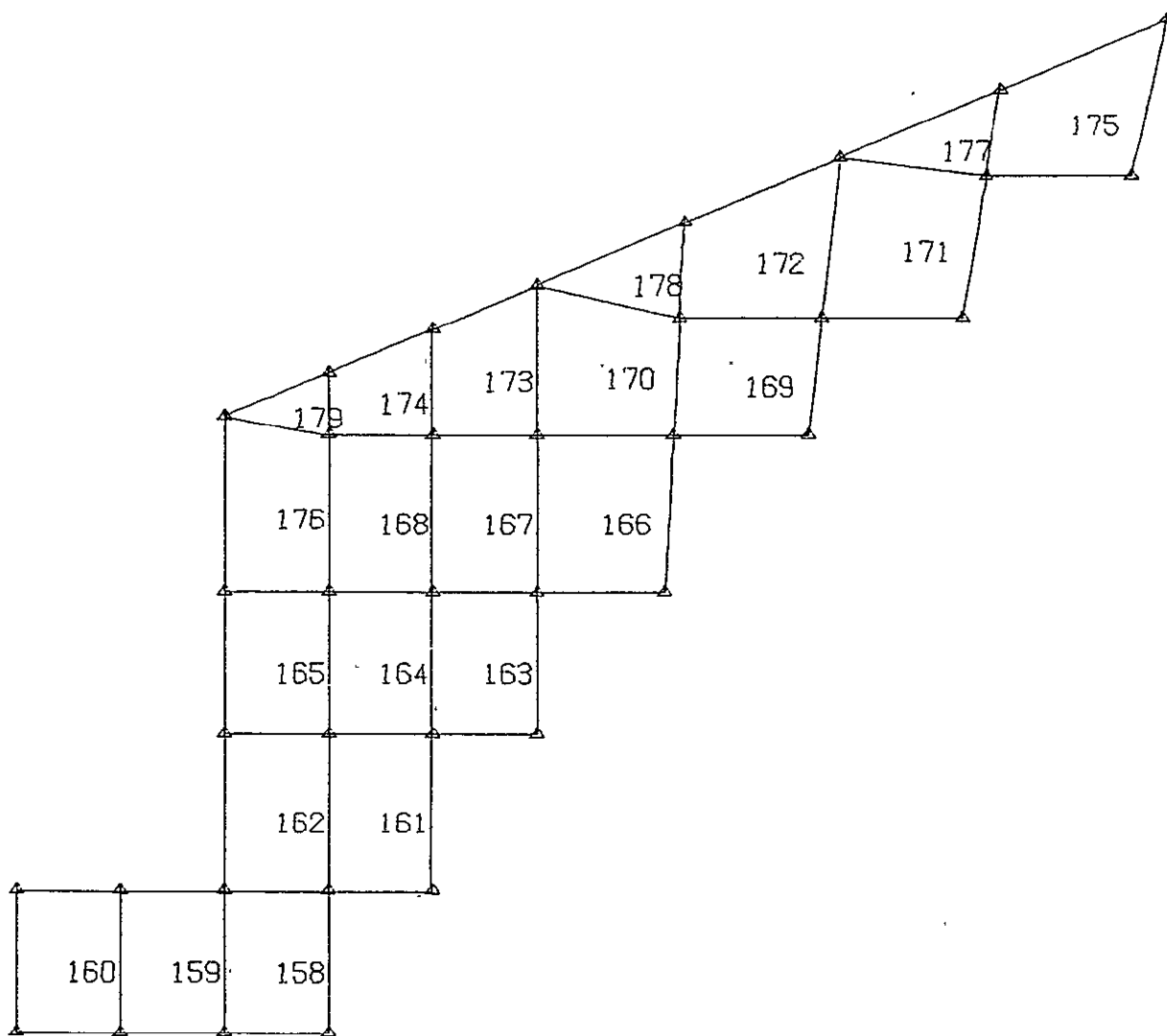
Zone 3

Figure 7-6.—(Continued)



Zone 4

Figure 7-6.—(Continued)



Zone 5

Figure 7-6.—(Continued)

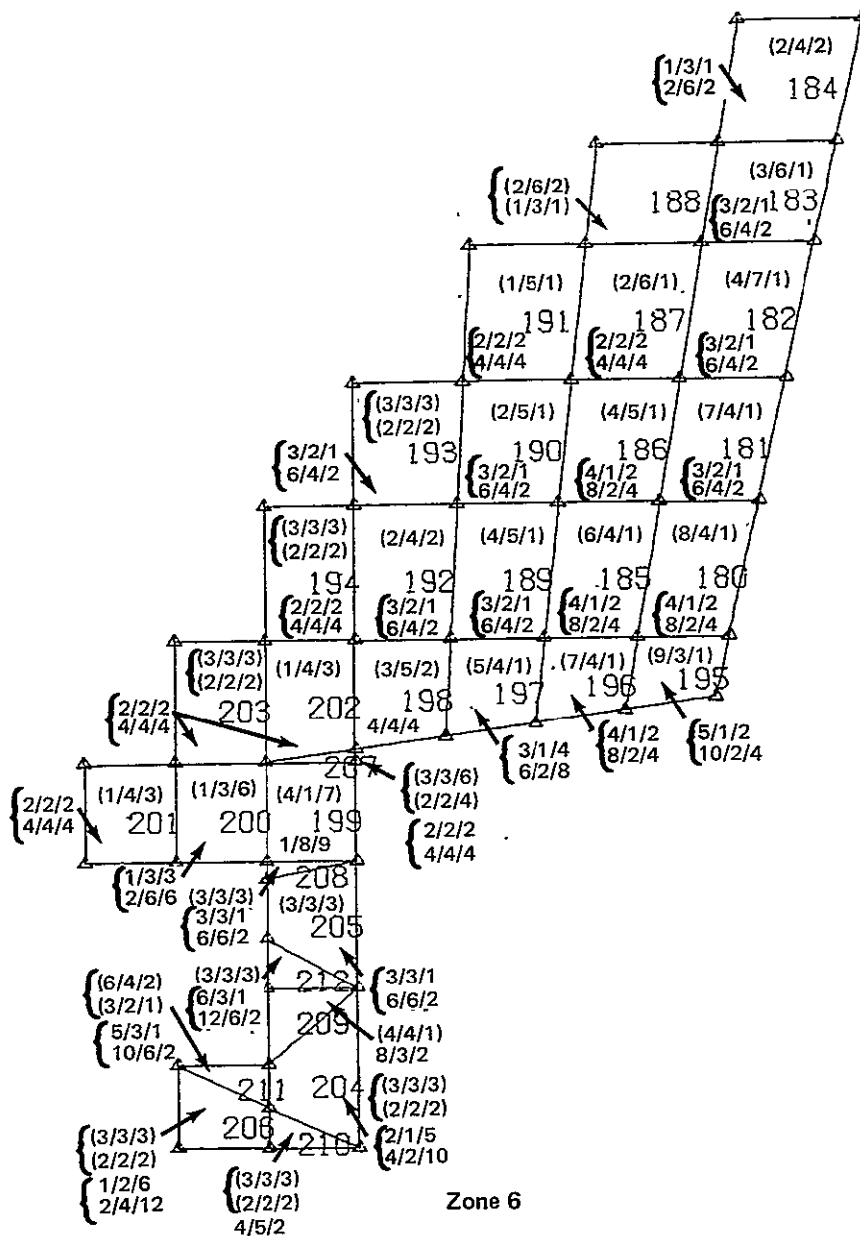
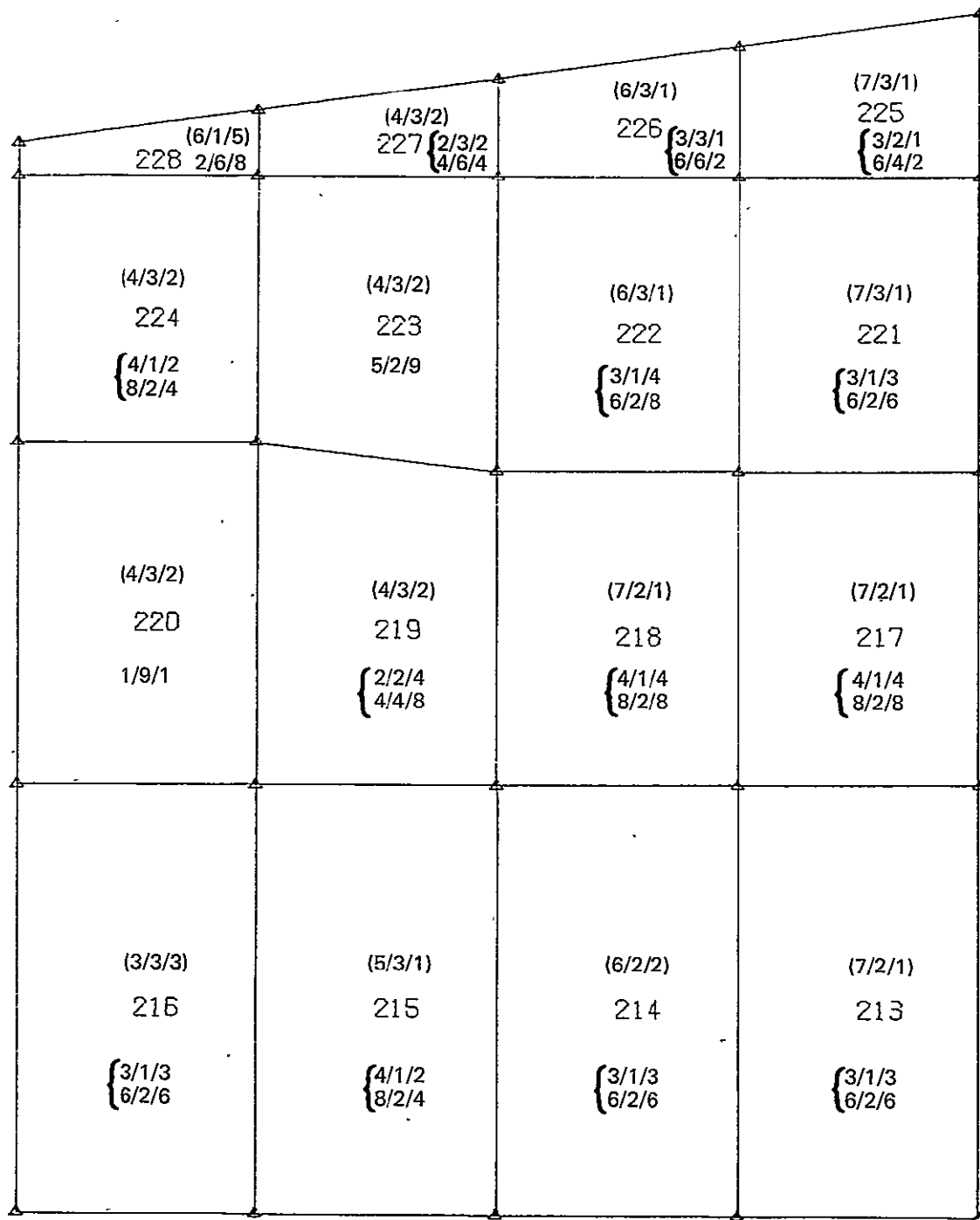


Figure 7-6.—(Continued)



Zone 7

Figure 7-6.—(Continued)

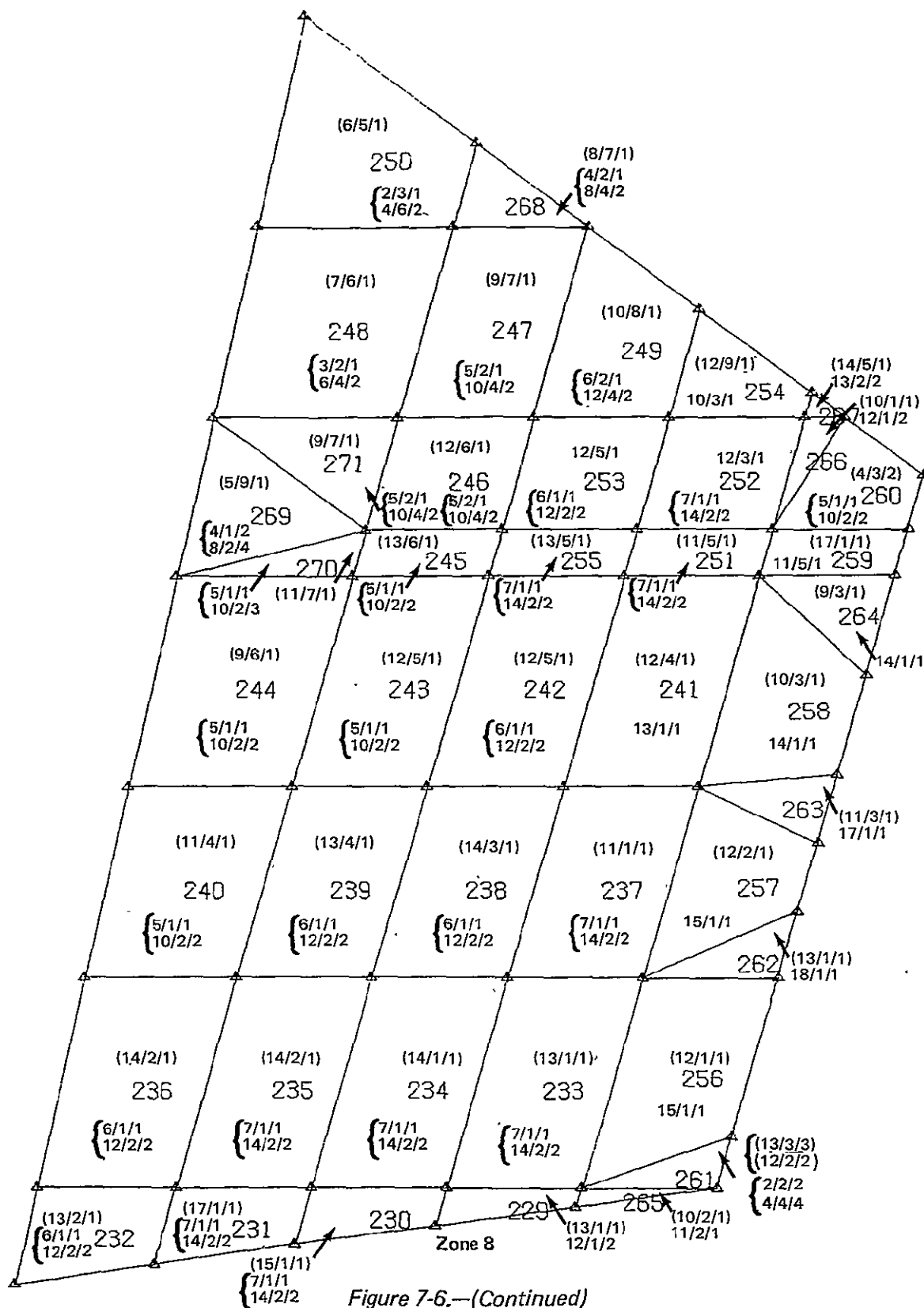


Figure 7-6.—(Continued)

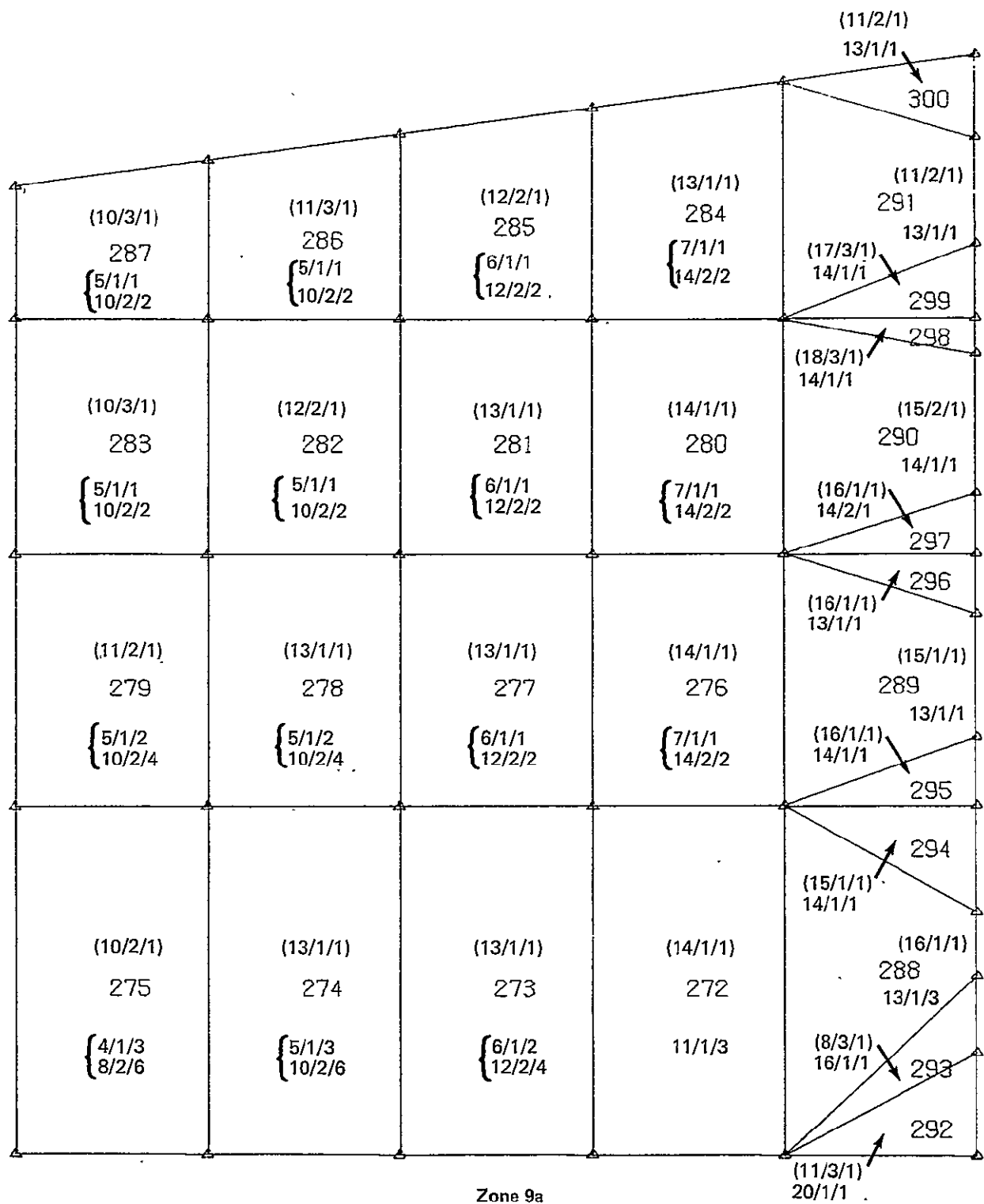
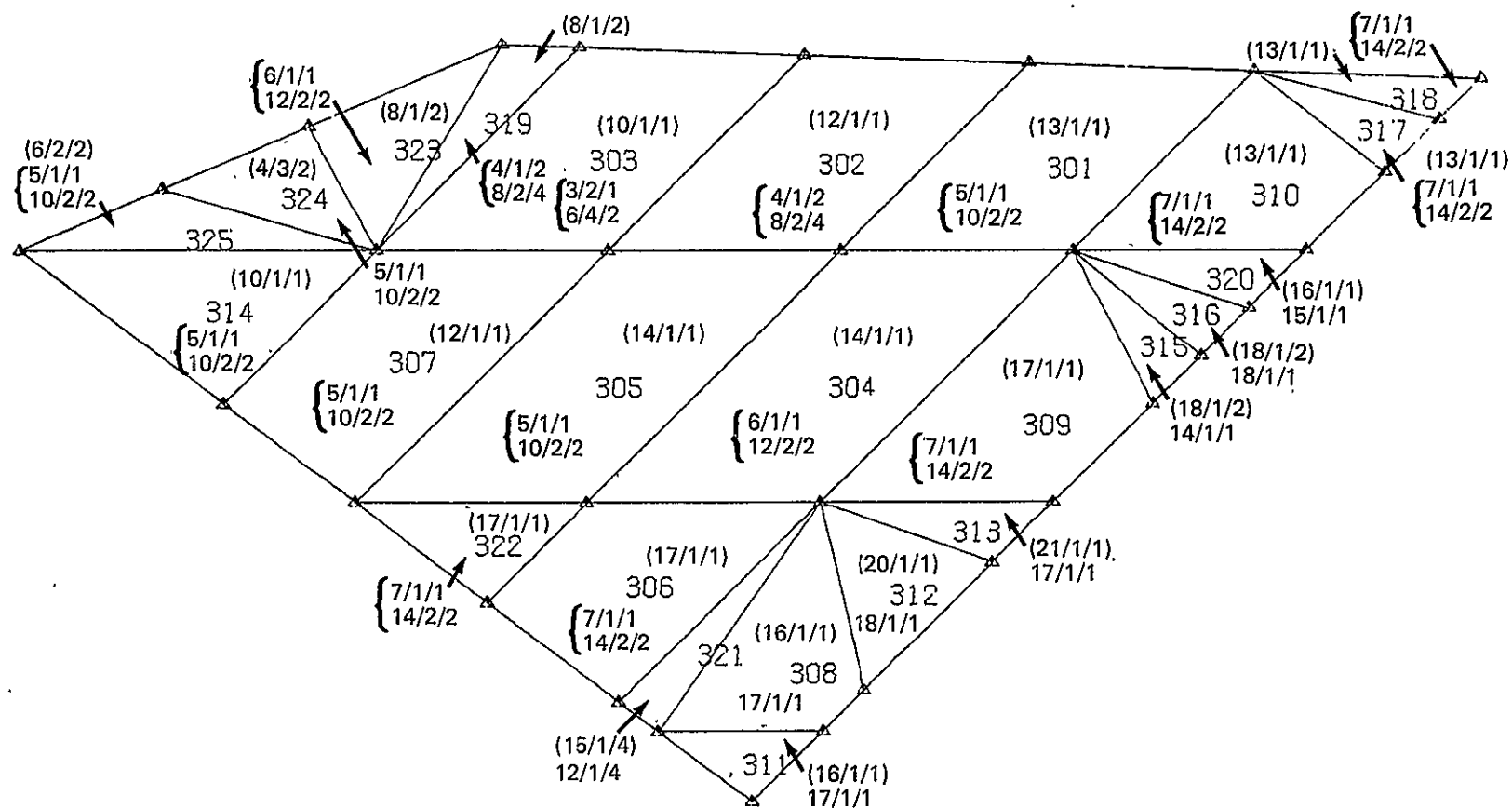


Figure 7-6.—(Continued)



Zone 9b

Figure 7-6.—(Continued)

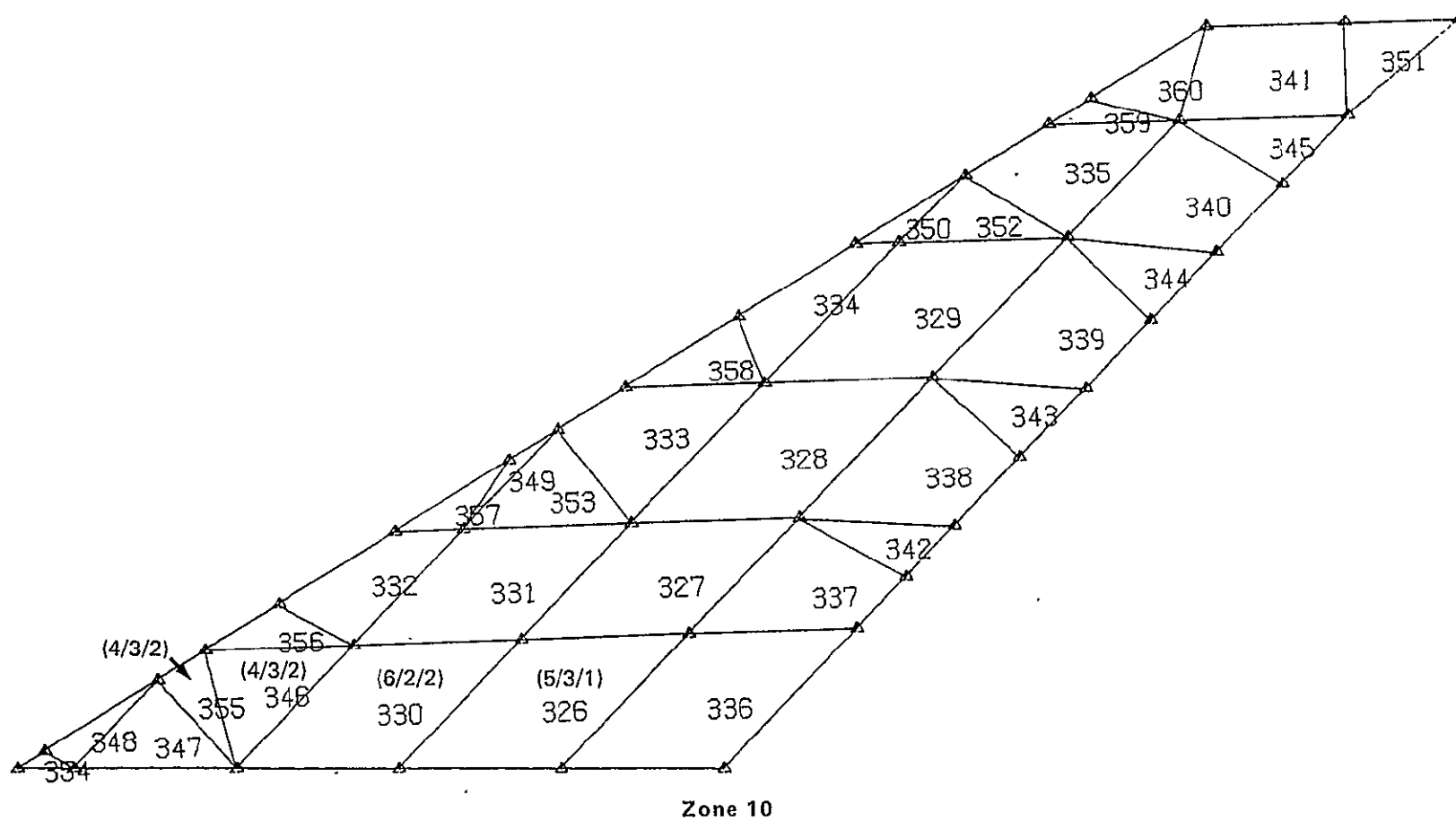
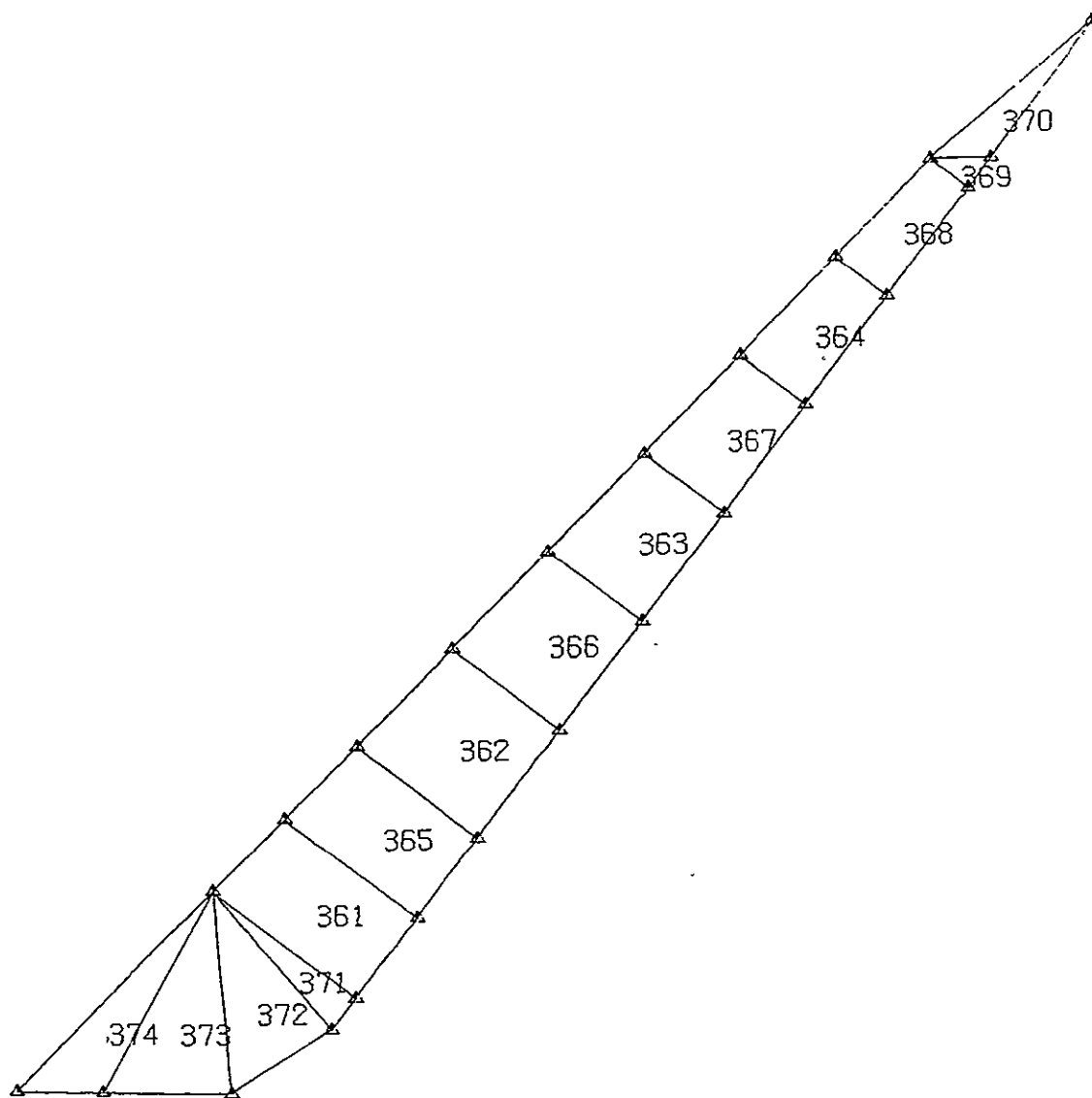


Figure 7-6.—(Continued)



Zone 11

Figure 7-6.—(Concluded)

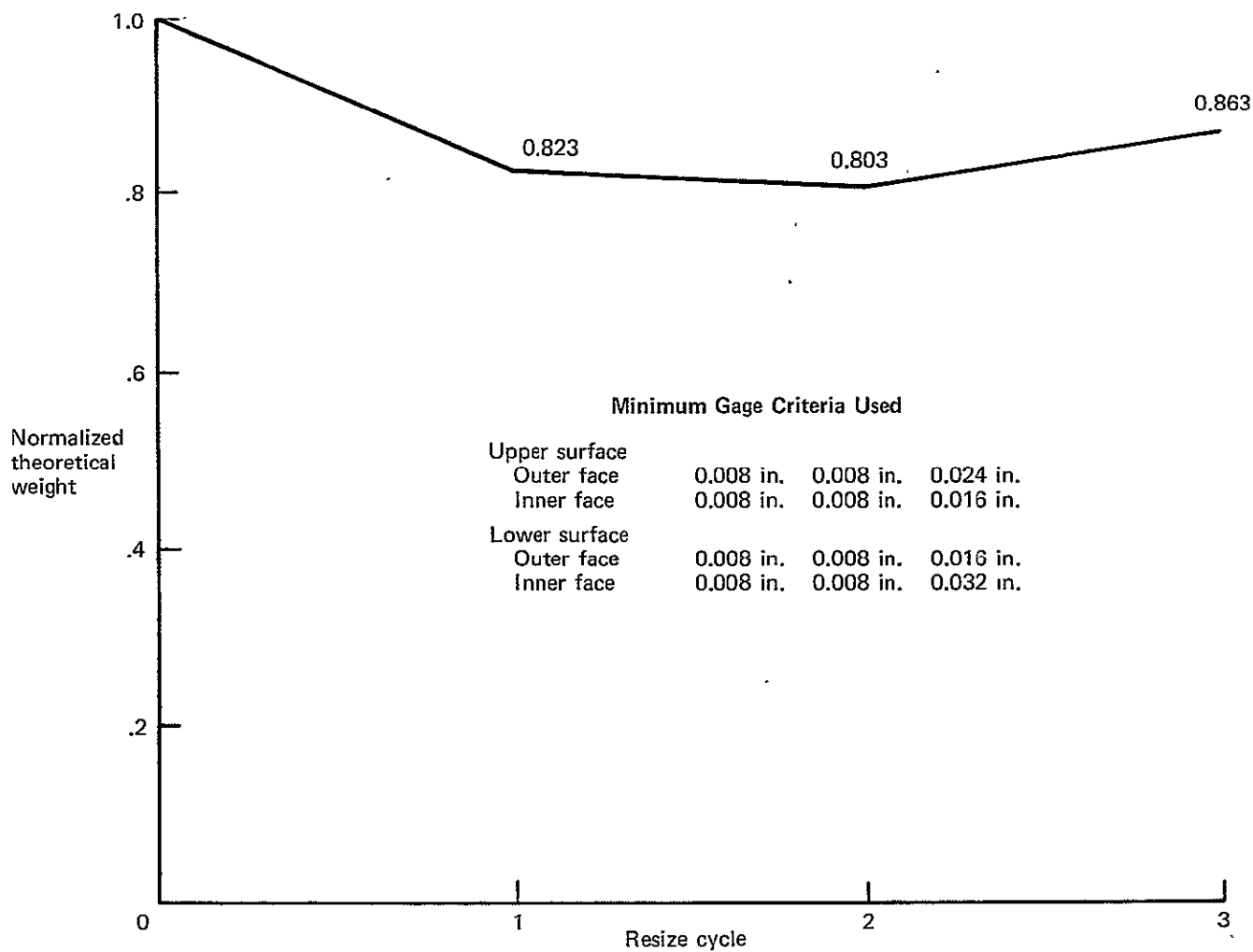
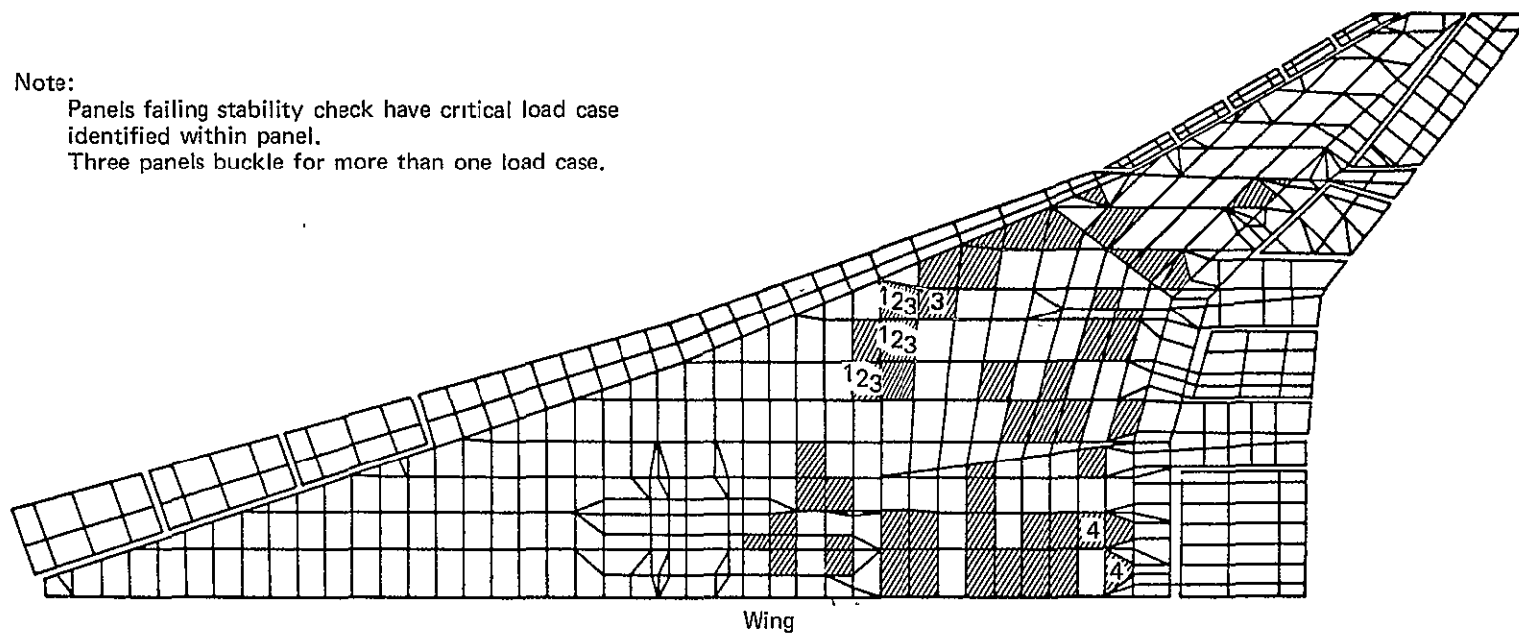


Figure 7-7.—Theoretical Wing Weight, Wing Box Primary Structure, ATLAS Resizing

Note:

Panels failing stability check have critical load case identified within panel.

Three panels buckle for more than one load case.



Load cases

- | | |
|---|--|
| 1 | positive maneuver at V_A , gross weight = 732 kips |
| 2 | positive maneuver at V_A , gross weight = 717 kips |
| 3 | positive maneuver at V_A , gross weight = 704 kips |
| 4 | flaps down maneuver at V_F , gross weight = 743 kips |

*Figure 7-8.—Upper Surface Panels Checked for Stability
After Resize Cycle 1*

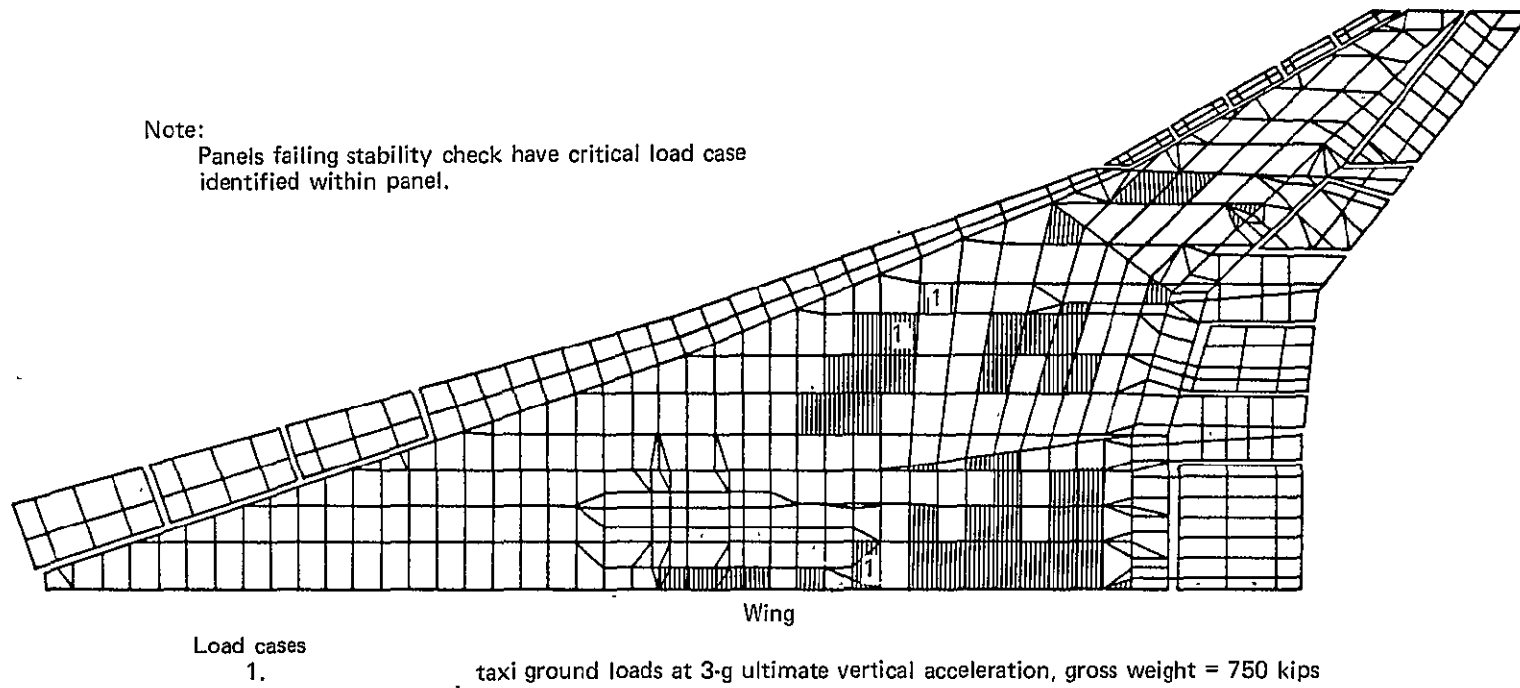
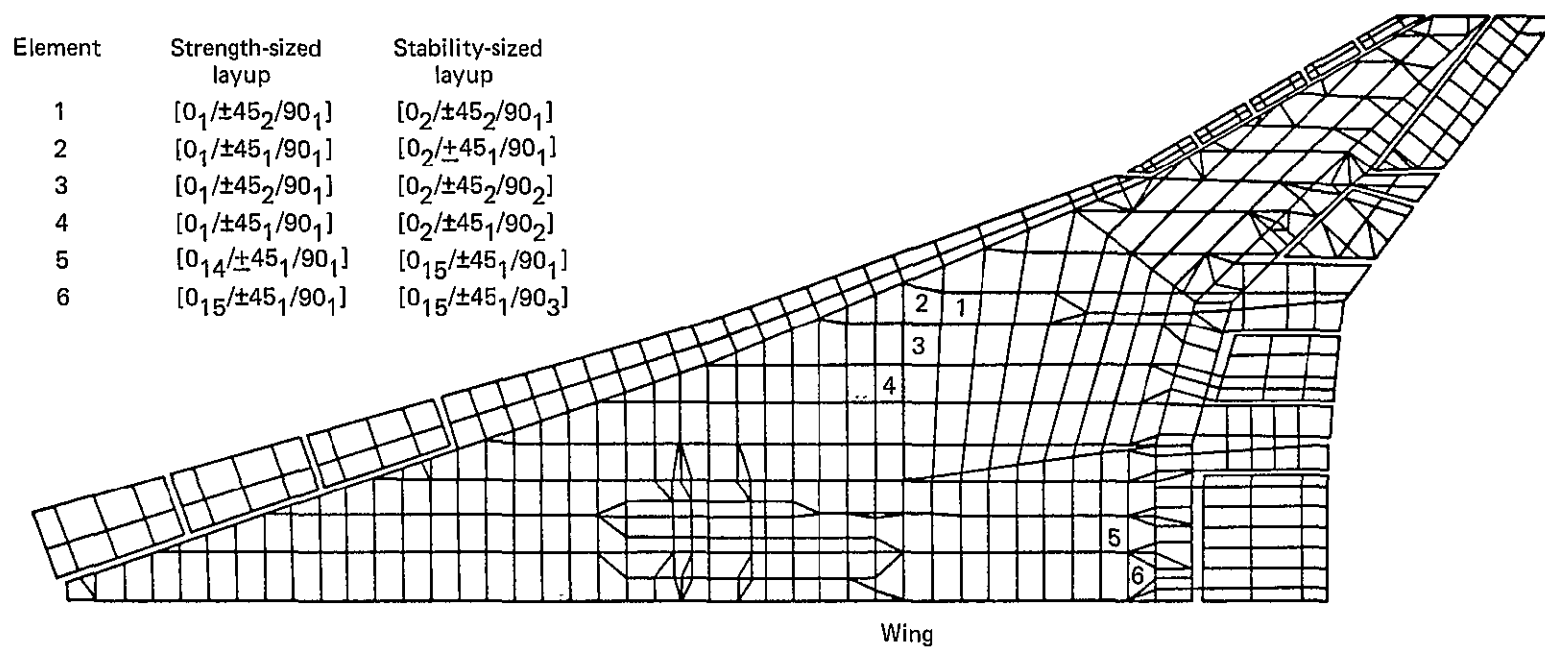
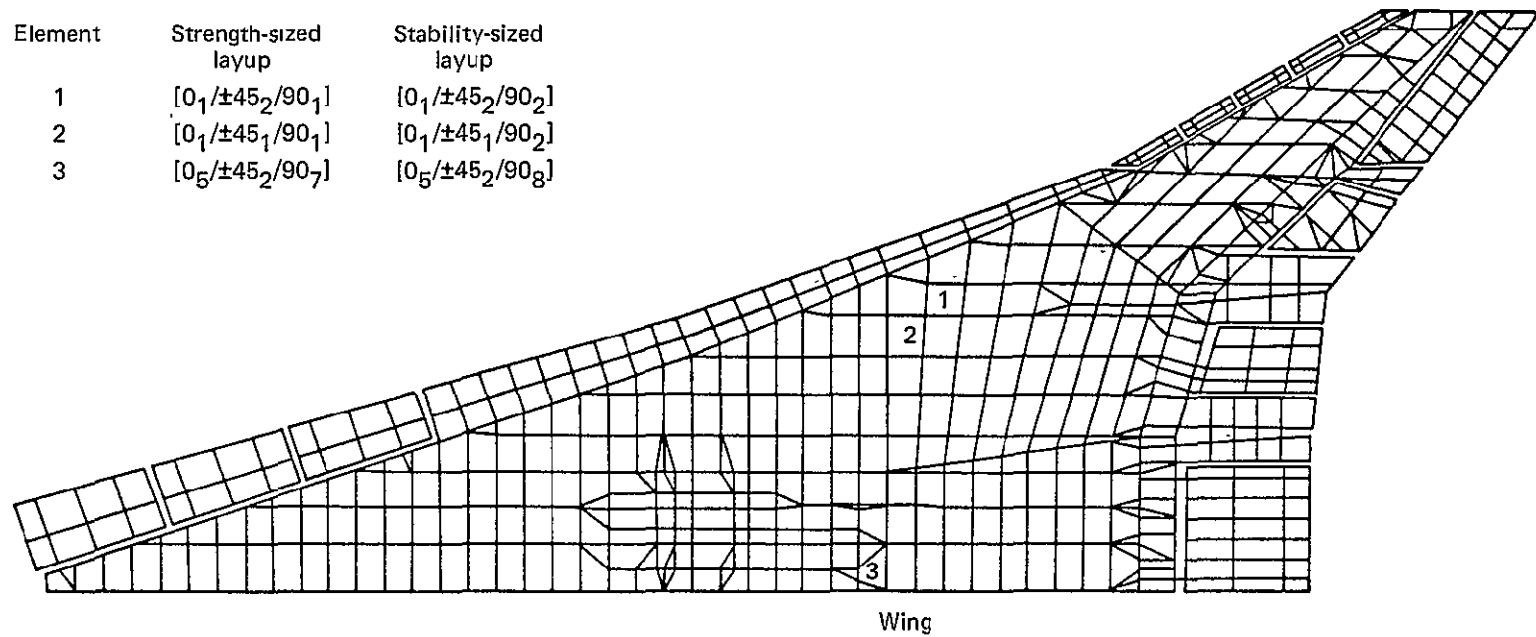


Figure 7-9.—Lower Surface Panels Checked for Stability After Resize Cycle 1



*Figure 7-10.—Layup Changes Required for Stability
After Resize Cycle 1 (Upper Surface)*

Element	Strength-sized layup	Stability-sized layup
1	$[0_1/\pm 45_2/90_1]$	$[0_1/\pm 45_2/90_2]$
2	$[0_1/\pm 45_1/90_1]$	$[0_1/\pm 45_1/90_2]$
3	$[0_5/\pm 45_2/90_7]$	$[0_5/\pm 45_2/90_8]$



*Figure 7-11.—Layup Changes Required for Stability
After Resize Cycle 1 (Lower Surface)*

Note:

Panel 1 failed stability check for flaps down maneuver at V_F , gross weight = 743 kips
(see fig. 6-1).

Layup change from $[0_{16}/\pm 45_1/90_1]$ to $[0_{17}/\pm 45_1/90_2]$

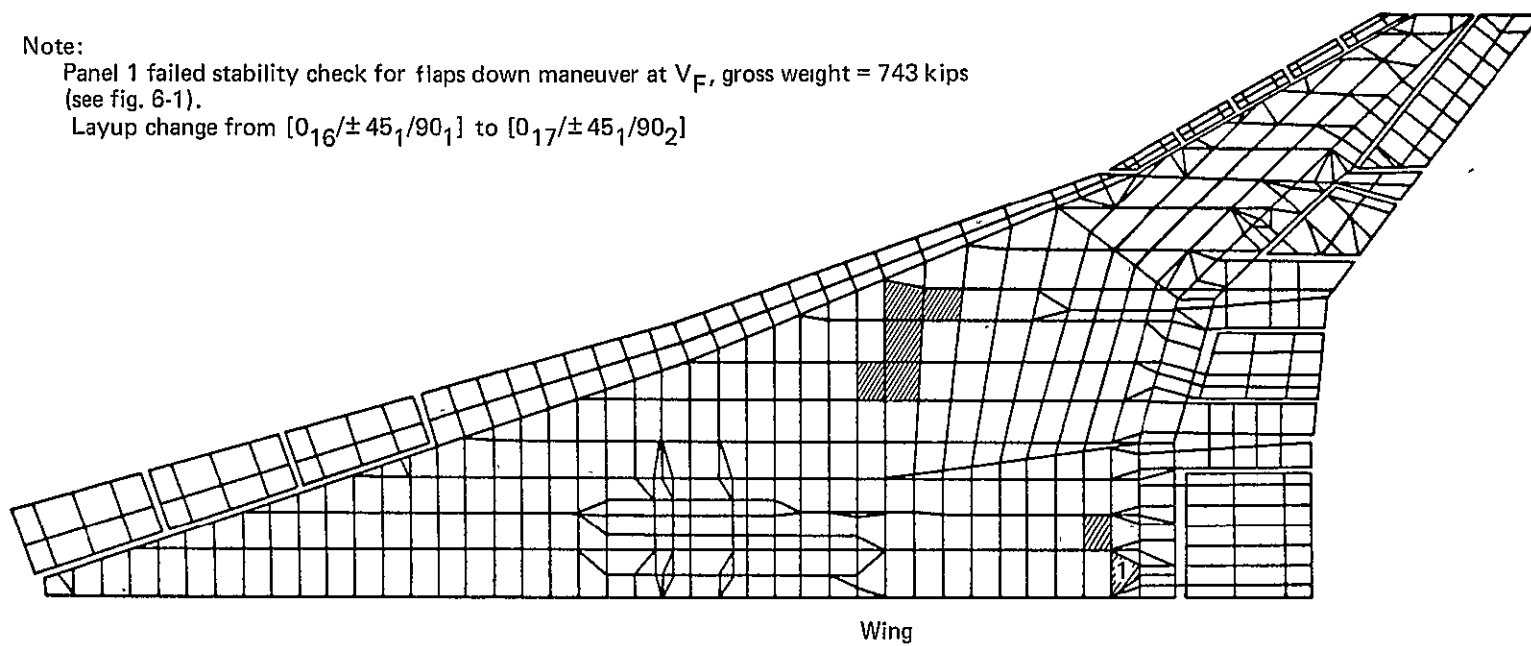
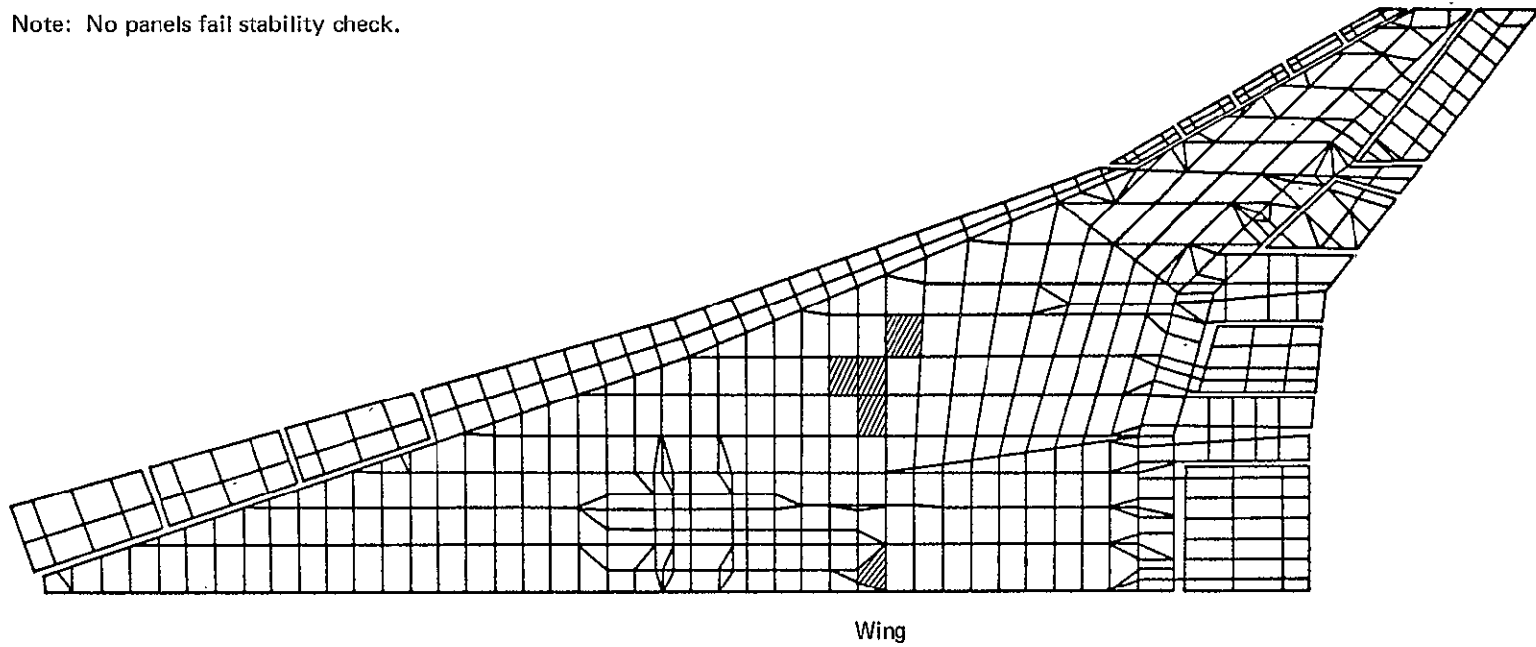


Figure 7-12.—Upper Surface Panel Stability Check
After Resize Cycle 2

Note: No panels fail stability check.



*Figure 7-13.—Lower Surface Panel Stability Check
After Resize Cycle 2*

SECTION 8

FLUTTER ANALYSIS

by

C. R. PRATT-BARLOW
J. G. LELONG

~~RECORDING PAGE BLANK NOT FILMED~~

CONTENTS

	Page
FLUTTER APPRAISAL AND REDESIGN PROCEDURE	266
FLUTTER ANALYSIS OF STRENGTH DESIGNED HYBRID STRUCTURE	266
STIFFNESS REDESIGN OF ADVANCED COMPOSITE COVER PANELS	267
STIFFNESS DESIGN OF HYBRID STRUCTURE	268
REFERENCES	269

TABLES

No.		Page
8-1	Stiffness Redesign, Typical Advanced Composite Honeycomb Wing Cover Panels . . .	270
8-2	Comparison of Flutter Energy Balance for Strength Designed Hybrid Structure . . .	271
8-3	Advanced Composite Material Properties, (1986)	271
8-4	Comparison of Flutter Energy Balance for Stiffness Designs	272
8-5	Airplane Vibration Mode Shapes, Hybrid Structure Stiffness Design	273

FIGURES

No.		Page
8-1	Stiffness Constraints on Hybrid Structure “Strength Design” from Use of Titanium Design Internal Structure	298
8-2	Effect of Stiffness Design Changes on Flutter Speed for $M = 0.9$, Symmetric, High Gross Weight Condition	299
8-3	Comparison of Wing Mode Shapes 1 through 6, Hybrid Structure, Strength Design . .	300
8-4	Anisotropic Coupling Trends, High Strength Graphite/Polyimide	301
8-5	Stiffness Designed Composite Cover Panels, Medium Modulus Graphite/Polyimide . .	302
8-6	Tailoring of Fiber Properties for Medium Modulus Graphite/Polyimide	303
8-7	Airplane Vibration Mode 1, Hybrid Structure Stiffness Design	304
8-8	Airplane Vibration Mode 2, Hybrid Structure Stiffness Design	305
8-9	Airplane Vibration Mode 3, Hybrid Structure Stiffness Design	306
8-10	Airplane Vibration Mode 4, Hybrid Structure Stiffness Design	307
8-11	Airplane Vibration Mode 5, Hybrid Structure Stiffness Design	308
8-12	Airplane Vibration Mode 6, Hybrid Structure Stiffness Design	309
8-13	Airplane Vibration Mode 7, Hybrid Structure Stiffness Design	310
8-14	Airplane Vibration Mode 8, Hybrid Structure Stiffness Design	311
8-15	Airplane Vibration Mode 9, Hybrid Structure Stiffness Design	312
8-16	Airplane Vibration Mode 10, Hybrid Structure Stiffness Design	313
8-17	Airplane Vibration Mode 11, Hybrid Structure Stiffness Design	314
8-18	Airplane Vibration Mode 12, Hybrid Structure Stiffness Design	315
8-19	Airplane Vibration Mode 13, Hybrid Structure Stiffness Design	316
8-20	Airplane Vibration Mode 14, Hybrid Structure Stiffness Design	317
8-21	Airplane Vibration Mode 15, Hybrid Structure Stiffness Design	318
8-22	Airplane Vibration Mode 16, Hybrid Structure Stiffness Design	319
8-23	Airplane Vibration Mode 17, Hybrid Structure Stiffness Design	320
8-24	Airplane Vibration Mode 18, Hybrid Structure Stiffness Design	321

SYMBOLS

E_1	Young's modulus in spanwise direction
E_2	Young's modulus in transverse direction
G_{12}	Shear modulus
μ_{12}	Poisson's ratio for strain in the 2-direction due to normal stress in the 1-direction
μ_{21}	Poisson's ratio for strain in the 1-direction due to normal stress in the 2-direction
F_1^{tu}	Ultimate tensile strength in direction of fibers
t	Thickness of layup for a cover panel
E'_1	$= E_1/(1-\mu_{12} \mu_{21})$
E'_2	$= E_2/(1-\mu_{12} \mu_{21})$
V_D	Dive speed
DOF	Degree of freedom
(N/M/P)	: Code for panel face layup
	N plies at 0°
	M plies at $+45^\circ$
	M plies at -45°
	P plies at 90°

FLUTTER APPRAISAL AND REDESIGN PROCEDURE

The same flutter appraisal technique used for the titanium airplane study (fig. 11-4 of ref. 8-1) was used for the hybrid structure airplane with advanced composite cover panels. Budget constraints limited analysis to only the $M = 0.9$ symmetric, high gross weight condition which was critical for the titanium airplane of Task II (ref. 8-1).

All variations of the hybrid structural model, including the strength design, had the stiffened wing fin, thickened wing tip with stiffened spars, stiff engine beams with diffusion ribs and spar and rib structure developed for the final titanium stiffness design but without its added wing tip ribs, figure 8-1. The body was modified to be the equivalent strength design in high strength graphite/polyimide as discussed in Section 7, with roughly seventy percent of the stiffness of the titanium strength design.

The effect of the stowed landing gear on the airplane vibration modes, inadvertently omitted during the final flutter analysis of the titanium airplane study, was included here. The landing gear resonance couples into the 5.0 Hz airplane mode, but has practically no effect on flutter.

The revised flutter clearance placard of Section 11 (ref. 8-1) was used to evolve a valid weight comparison with the titanium stiffness design. Airplane performance changes for both thickened wing tip and placard change apply to all hybrid structure designs.

FLUTTER ANALYSIS OF STRENGTH DESIGNED HYBRID STRUCTURE

Flutter analysis of the strength designed hybrid structure yielded a relatively low frequency critical flutter mode, 287 KEAS, 1.52 Hz, well below the requirement of 444 KEAS at $M = 0.9$ (figures 8-2 and 8-3). A comparison of front and rear spar deflections at the wing fin station and the wing tip showed that the hybrid strength design structure had excessive flexibility in torsion and in wing tip bending. This was confirmed by comparing stiffness levels of typical cover panels in the heavily loaded aft wing box and the wing tip with those for the stiffness designed titanium airplane as shown in table 8-1. A comparison of modal frequencies and relative contributions to the energy balance at flutter for the hybrid strength designed structure are shown in table 8-2. The substantial amount of wing tip torsion in mode 6 (see fig. 8-3) is believed to be a major factor in the large positive contribution of that mode to the energy balance at neutral stability.

STIFFNESS REDESIGN OF ADVANCED COMPOSITE COVER PANELS

Four stiffness redesign cycles, with modifications to the advanced composite cover panels, were conducted before achieving a hybrid structure stiffness design which meets the $M = 0.9$ flutter requirement. The typical composite panel layups and stiffness levels in the lower half of table 8-1 summarize the stiffness design development.

In Stiffness Redesign 1, the balanced, symmetric (orthotropic) composite panel layup philosophy used in the strength design was maintained but $\pm 45^\circ$ plies were restored to increase wing torsional stiffness in the heavily loaded aft wing box such that the effective shear stiffness of a typical composite panel layup was roughly half that of the titanium strength design. This resulted in a 13/9/1 layup for the typical panel (using the same coding scheme adopted in Section 6). The effective spanwise bending stiffness in the aft wing box of the hybrid structure strength design was already roughly half that of the titanium strength design. The strength design distribution of 0° and 90° plies in the aft wing box was preserved when adding a uniform number of $\pm 45^\circ$ plies. In addition, five 90° plies near the engine beam diffusion ribs were used to obtain effective load diffusion into the cover panels. Finally, both bending and torsional stiffnesses of the wing tip were increased to roughly half those of the titanium stiffness design by using a uniform 12/8/8 layup. Figure 8-2 shows the improvement in flutter characteristics for the stiffness redesign cycles. Stiffness Redesign 1 raised the critical flutter mode to 337 KEAS, 1.62 Hz and the second flutter mode to roughly the $1.2V_D$ requirement.

Stiffness Redesign 2 crudely exploited the potential anisotropic behavior of the composite layup in the wing tip. The findings of Austin and others (ref. 8-3), were confirmed for an isolated composite cover panel (fig. 8-4) in that unbalancing the $\pm 45^\circ$ plies lowers the effective shear modulus unduly whereas limited reorienting of the spanwise plies of an otherwise balanced layup provides favorable anisotropic behavior in terms of both increased effective shear modulus and changed twist coupling parameter. However, favorable twist coupling parameter trends for static aeroelastic tailoring of a sweptback wing appear to be more readily obtained than for increased flutter speed. Nevertheless, compared with the 12/8/8 wing tip layup of Stiffness Redesign 1, limited experiment yielded a 15/10/1 layup with spanwise fibers reoriented 15° aft, with the same overall thickness but 35% greater shear stiffness from a 22% more effective shear modulus together with a 15% decrease in the twist coupling parameter. This Stiffness Redesign 2 strategy was effective in raising the speed of the third flutter mode by 7% without any weight increase over Stiffness Redesign 1, but the critical flutter mode was raised by only 4 KEAS to 341 KEAS, 1.62 Hz, while the second flutter mode was similarly unaffected, as shown in figure 8-2. No further anisotropic effects were studied.

Table 8-1 shows that compared with the second stiffness modification, Stiffness Redesign 3 had twice the $\pm 45^\circ$ plies in the aft wing box typical 13/18/1 layup and twice the 0° and $\pm 45^\circ$ plies in the wing tip 30/20/1 layup, without sparwise fibers reoriented aft. Additionally, the 90° plies near the engine beam diffusion ribs were doubled to 10 plies. This raised wing stiffness levels to roughly the values for the titanium stiffness design. However, the critical flutter mode was raised to only 382 KEAS, 1.64 Hz. This is probably a direct consequence of a lower wing bending/torsion stiffness ratio from the reduced body stiffness and relatively lower bending stiffness in the aft wing box.

STIFFNESS DESIGN OF HYBRID STRUCTURE

For the hybrid structure final stiffness design, medium modulus graphite/polyimide cover panels were used, replacing the high strength material. With minimum weight increment this increased the stiffness level over stiffness redesign 3 by roughly 50% in shear and 80% in spanwise bending because 20% more spanwise plies were required to maintain adequate strength. The stiffness designed composite cover panels are shown in figure 8-5. Material suppliers have indicated that for the 1986 time period fibers with strength and moduli intermediate to values for T600 and T90 fibers could be provided, as indicated by the dashed line in figure 8-6. The medium modulus material selected had a moderate decrease in tensile strength, corresponding to the fiber properties at the intersection of the radial and dashed lines. This was regarded as a favorable choice for the hybrid structure from considerations of strain compatibility between the titanium and composite materials. Table 8-3 compares material properties considered.

Figure 8-2 shows $M = 0.9$ flutter clearance with the 450 KEAS, 1.75 Hz critical flutter mode of the hybrid structure stiffness design, for the symmetric, high gross weight condition. Table 8-4 compares the titanium and hybrid structure stiffness design vibration mode frequencies and energy balance at flutter. Higher frequency modes have less effect for the hybrid structure stiffness design flutter. Table 8-5 details the hybrid structure stiffness design mode shapes, which are shown in figures 8-7 through 8-24.

The stiffness redesign mass increment to the hybrid structure "strength design" to satisfy flutter criteria is 8702 lb as detailed in Section 9. Despite limitations imposed on the optimization of the stiffness design by budget limitation and technical approach, Section 9 weights analysis shows the hybrid structure stiffness design wing primary structure outboard of the center section to be 6730 lb lighter than the titanium stiffness design which has about the same $M = 0.9$ flutter speed, 453 KEAS, 1.91 Hz, for the symmetric, high gross weight condition. The hybrid structure stiffness design has a higher bending/torsion stiffness ratio than the titanium stiffness design, particularly in the wing tips. In fact, the wing tips are so stiff that moderate weight saving would result from changing cover panels to equivalent stiffness T90 high modulus graphite/polyimide layups outboard of the wing mounted fins. Conversely, table 8-1 shows that typical cover panels of the equivalent hybrid structure stiffness design in T600 high strength graphite/polyimide would be theoretically 47% heavier than with the selected medium modulus material.

REFERENCES

- 8-1 Boeing Staff: *Study of Structural Design Concepts for an Arrow Wing Supersonic Transport Configuration*. NASA CR 132576-2, 1976.
- 8-2 Gordon, C. K.; and Visor, O.E.: *SCAR Arrow-Wing Active Flutter Suppression System*. NASA CR 145147, 1977.
- 8-3 Austin, F.; et al.: *Aeroelastic Tailoring of Advanced Composite Lifting Surfaces in Preliminary Design*, AIAA/ASME/SAE 17th Structures, Structural Dynamics and Material Conference, King of Prussia, Pennsylvania, 1976.

Table 8-1.—Stiffness Redesign, Typical Advanced Composite Honeycomb Wing Cover Panels

		Typical wing honeycomb panel												
		Aft wing box							Wing tip					
		Structure	Panel plies	Face layup, in.	Theo. weight, lb/ft ²	Stiffness ratios			Panel plies	Face layup, in.	Theo. weight, lb/ft ²	Stiffness ratios ²		
						Sparwise	Transverse	Shear				Sparwise	Transverse	Shear
Ti		Stiffness design	—	0.065	3.0	1.0	1.0	1.0	—	0.08 in.	3.68	1.0	1.0	1.0
Hybrid structure composite covers	High strength (T600) graphite polyimide	Strength design	32	13/1/1	0.52	0.48	0.08	0.10	8	1/1/1	0.13	0.05	0.05	0.05
		Stiffness mod 1	64	13/9/1	1.03	0.66	0.26	0.51	72	12/8/8	1.16	0.51	0.40	0.39
		Stiffness mod 2	64	13/9/1	1.03	0.66	0.26	0.51	72	15 ^a /10/1	1.16	0.60	0.24	0.53
		Stiffness mod 3	100	13/18/1	1.61	0.85	0.45	0.98	142	30/20/1	2.29	1.25	0.44	0.93
		b	Stiffness design	106	16/18/1	1.74	1.41	0.65	1.45	154	36/20/1	2.53	2.11	0.64
	T600 equivalent stiffness design		158	24/27/1	2.55	1.38	0.65	1.42	230	54/30/1	3.71	2.14	0.66	1.41
					$E'_{11}t$	$E'_{22}t$	$G_{12}t$				$E'_{11}t$	$E'_{22}t$	$G_{12}t$	
Unit panel stiffness for stiffness ratio = 1.0 →					2.28	10 ⁶ lb/in. 2.28	0.80	2Unit Panel Stiffnesses →			2.73	10 ⁶ lb/in. 2.73	0.98	

Table 8-2.—Comparison of Flutter Energy Balance for Strength Designed Hybrid Structure

Mode	Airplane natural frequency, Hz	Energy contribution at neutral stability (source positive)
Plunge	0.0	-0.075
Pitch	0.0	-0.138
1	0.80	-1.0
2	0.97	-0.415
3	1.82	0.637
4	2.00	-0.551
5	2.69	-0.152
6	2.89	0.606
7	2.99	0.438
8	3.30	0.016
9	3.55	0.142
10	3.86	0.061
11	4.63	-0.041
12	5.04	0.267
13	5.43	-0.006
14	5.66	0.066
15	5.78	0.170
16	6.51	-0.008
17	7.36	-0.009
18	7.40	-0.010

Table 8-3.—Advanced Composite Material Properties, 1986

Graphite polyimide (unidirectional) 60% fiber volume					
Composite type			T600 high strength	T90 high modulus	Medium modulus
Density	ρ	lb/in ³	0.056	0.058	0.057
Elastic properties (relative to material axes, RT)	E_{11}	10 ⁶ psi	20.0	40.0	30.0
	E_{22}	10 ⁶ psi	1.13	1.8	1.4
	G_{12}	10 ⁶ psi	0.717	0.98	0.8
	ν_{12}	—	0.31	0.29	0.3
	ν_{21}	—	0.018	0.013	0.014
Longitudinal tensile ultimate	F_1^{tu}	ksi	295.0	148.0	234.0

Table 8-4.—Comparison of Flutter Energy Balance for Stiffness Designs

Mode	Airplane vibration mode frequency, Hz		Energy contribution at neutral stability (source positive)	
	Titanium	Hybrid structure	Titanium	Hybrid structure
Plunge	0.0	0.0	-0.097	-0.069
Pitch	0.0	0.0	-0.111	-0.046
1	0.97	0.87	-0.744	-0.104
2	1.18	1.14	-1.0	-1.0
3	2.18	1.92	0.524	0.511
4	2.43	2.49	0.467	0.027
5	2.79	2.93	0.035	0.012
6	3.00	3.39	0.040	0.137
7	3.37	3.53	0.377	0.225
8	3.63	3.56	0.003	0.137
9	3.81	4.23	0.110	0.067
10	4.00	4.36	-0.051	-0.001
11	4.41	5.09	0.200	0.050
12	4.68	5.78	-0.002	-0.006
13	6.22	5.97	0.112	0.037
14	6.35	6.06	0.036	-0.008
15	6.75	6.91	0.005	0.000
16	7.21	7.50	0.105	0.031
17	8.03	7.84	0.015	-0.000
18	8.62	8.15	-0.024	0.000

Table 8-5.—Airplane Vibration Mode Shapes*, Hybrid Structure Stiffness Design

Row	Node	DOF	Mode 1	Mode 2	Mode 3	Mode 4
1	1020	1	0.00000000	-.01763017	.01414464	-.00246597
2	1020	2	0.00000000	0.00000000	.00681722	.01617304
3	1020	3	1.00000000	-.27853248	.09156377	-.02265588
4	1020	4	0.00000000	0.00000000	.00017145	.00043833
5	1020	5	0.00000000	.00048709	-.00044882	.00002246
6	1020	6	0.00000000	0.00000000	.00000057	.00000030
7	1070	1	0.00000000	-.00906330	.01481598	.01781366
8	1070	2	0.00000000	0.00000000	.01205193	.02888156
9	1070	3	1.00000000	-.28654505	.17294126	.15549984
10	1070	4	0.00000000	0.00000000	.00034178	.00087914
11	1070	5	0.00000000	.00048709	-.00067659	-.00047996
12	1070	6	0.00000000	0.00000000	.00000284	.00000009
13	670	3	1.00000000	.44827772	-.00840345	.02174310
14	663	3	1.00000000	.31732466	-.11544393	.03254357
15	652	3	1.00000000	.14392235	-.16982519	.02042128
16	644	3	1.00000000	.00656381	-.14243762	.00694331
17	637	3	1.00000000	-.14085763	-.00150285	.08144992
18	792	3	1.00000000	-.22080793	.13286036	.22625777
19	784	3	1.00000000	-.28787966	.28116864	.43380687
20	779	3	1.00000000	-.33807874	.40358779	.61701612
21	775	3	1.00000000	-.37191661	.48857390	.74656916
22	620	3	1.00000000	.44135136	-.01413543	.02233175
23	618	3	1.00000000	.39468852	-.05716620	.02753816
24	615	3	1.00000000	.35823988	-.08717904	.03061794
25	613	3	1.00000000	.31158191	-.11756858	.03231718
26	610	3	1.00000000	.27720826	-.13606580	.03227871
27	608	3	1.00000000	.23055029	-.15362895	.02988652
28	605	3	1.00000000	.19099891	-.16301013	.02605792
29	603	3	1.00000000	.15661064	-.16685256	.02182523
30	600	3	1.00000000	.10502824	-.16792587	.01517961
31	597	3	1.00000000	.05423491	-.15993703	.00936259
32	692	3	1.00000000	.43414736	-.02016384	.02296141
33	693	3	1.00000000	.38784983	-.06215528	.02793042
34	694	3	1.00000000	.35168857	-.09023115	.03051827
35	562	3	1.00000000	.30539105	-.11980759	.03205908
36	560	3	1.00000000	.27129503	-.13680295	.03171800
37	695	3	1.00000000	.22499751	-.15359512	.02925151
38	555	3	1.00000000	.18605499	-.16189523	.02542289
39	553	3	1.00000000	.15195897	-.16536889	.02110606
40	550	3	1.00000000	.10081494	-.16563283	.01409369
41	547	3	1.00000000	.04967092	-.15706856	.00800838
42	544	3	1.00000000	-.00147311	-.13566238	.00436159
43	541	3	1.00000000	-.05261714	-.10116570	.00875037
44	539	3	1.00000000	-.09389768	-.06203774	.02683914
45	537	3	1.00000000	-.14552879	.00251767	.07633097
46	536	3	1.00000000	-.17280560	.04361189	.11587648

*Elastic modes start at Mode 3.

ORIGINAL PAGE IS
OF POOR QUALITY

ORIGINAL PAGE
OF POOR QUALITY

Table 8-5.—(Continued)

Row	Node	DOF	Mode 1	Mode 2	Mode 3	Mode 4
47	534	3	1.00000000	-.20251785	.09263493	.16839137
48	476	3	1.00000000	-.22239583	.12834145	.20992259
49	716	3	1.00000000	-.24263425	.16976796	.26448513
50	713	3	1.00000000	-.26014986	.20721133	.31545239
51	712	3	1.00000000	-.27702252	.24472833	.36802795
52	709	3	1.00000000	-.29347628	.28249344	.42216696
53	708	3	1.00000000	-.31034894	.32210998	.47988662
54	705	3	1.00000000	-.32679783	.36200907	.53933873
55	704	3	1.00000000	-.34367649	.40410724	.60323592
56	701	3	1.00000000	-.35948617	.44431486	.66497891
57	700	3	1.00000000	-.37750835	.49030568	.73575986
58	533	3	1.00000000	-.39429334	.53276704	.80074112
59	85	3	1.00000000	.35653508	-.08644390	.03015331
60	82	3	1.00000000	.30539105	-.11886552	.03182604
61	79	3	1.00000000	.25424702	-.14155929	.03071707
62	129	3	1.00000000	.25424702	-.14262818	.03093491
63	76	3	1.00000000	.20310300	-.15437532	.02692139
64	176	3	1.00000000	.20310300	-.15747515	.02721362
65	73	3	1.00000000	.15195897	-.15862167	.02102621
66	173	3	1.00000000	.15195897	-.16203486	.02106533
67	50	3	1.00000000	.10081494	-.15217667	.01276558
68	120	3	1.00000000	.10081494	-.15574254	.01222094
69	220	3	1.00000000	.10081494	-.16190736	.01276377
70	67	3	1.00000000	.04967092	-.14913895	.00161046
71	167	3	1.00000000	.04967092	-.14886663	.00261785
72	267	3	1.00000000	.04967092	-.15497544	.00654386
73	44	3	1.00000000	-.00147311	-.11954793	-.00760874
74	114	3	1.00000000	-.00147311	-.12795300	-.00962070
75	214	3	1.00000000	-.00147311	-.12978656	-.00386481
76	314	3	1.00000000	-.00147311	-.13378844	.00167190
77	41	3	1.00000000	-.05261714	-.09498684	-.01942564
78	111	3	1.00000000	-.05261714	-.09616530	-.01746680
79	211	3	1.00000000	-.05261714	-.09803070	-.01202128
80	311	3	1.00000000	-.05261714	-.09990046	-.00206396
81	58	3	1.00000000	-.10376117	-.06502756	-.03099185
82	158	3	1.00000000	-.10376117	-.06335210	-.02333582
83	209	3	1.00000000	-.08776039	-.07402843	-.01652320
84	309	3	1.00000000	-.09050756	-.06991578	-.00078742
85	409	3	1.00000000	-.09332579	-.06428051	.01912062
86	207	3	1.00000000	-.12319590	-.04712868	-.01837505
87	307	3	1.00000000	-.13152507	-.03288993	.00619332
88	407	3	1.00000000	-.13917719	-.01508087	.04060548
89	55	3	1.00000000	-.15490519	-.02953383	-.04415418
90	155	3	1.00000000	-.15490519	-.02464686	-.03006415
91	205	3	1.00000000	-.15754525	-.01856452	-.01939564
92	305	3	1.00000000	-.17142228	.00715438	.01751608

*Elastic modes start at Mode 3.

Table 8-5.—(Continued)

Row	Node	DOF	Mode 1	Mode 2	Mode 3	Mode 4
93	405	3	1.00000000	-.18416445	.03711991	.06734237
94	385	3	1.00000000	-.19360417	.06562104	.11919767
95	454	3	1.00000000	-.20716465	.07970692	.12057412
96	464	3	1.00000000	-.23328223	.13369861	.19419653
97	474	3	1.00000000	-.25348652	.18618387	.26218465
98	484	3	1.00000000	-.27656863	.22208521	.32591017
99	493	3	1.00000000	-.31059735	.30825575	.44256795
100	502	3	1.00000000	-.35406491	.40960724	.58862689
101	512	3	1.00000000	-.37367012	.46518332	.68040726
102	522	3	1.00000000	-.39004595	.51202006	.75810024
103	52	3	1.00000000	-.20604922	.00918915	-.05878685
104	152	3	1.00000000	-.20604922	.01744830	-.03801308
105	202	3	1.00000000	-.20671166	.02529950	-.01995674
106	302	3	1.00000000	-.22064232	.06002544	.03509024
107	382	3	1.00000000	-.23426559	.10607651	.11854741
108	452	3	1.00000000	-.25489907	.15024359	.17937382
109	462	3	1.00000000	-.28101662	.21227457	.27147466
110	482	3	1.00000000	-.31830305	.31037126	.42668609
111	492	3	1.00000000	-.33446457	.35477660	.49873627
112	179	3	1.00000000	-.24566392	.03558677	-.07905532
113	146	3	1.00000000	-.24566392	.04003567	-.06884985
114	192	3	1.00000000	-.24566392	.04975813	-.04740084
115	200	3	1.00000000	-.24566392	.06089287	-.02175822
116	298	3	1.00000000	-.25596092	.09080256	.02770046
117	350	3	1.00000000	-.26525939	.12666953	.09297847
118	398	3	1.00000000	-.27070988	.15025342	.13828432
119	819	3	1.00000000	-.29975482	.21943764	.23986895
120	816	3	1.00000000	-.32357332	.28264755	.34090683
121	470	3	1.00000000	-.34366075	.33766622	.42909271
122	810	3	1.00000000	-.35590122	.36917828	.47797049
123	808	3	1.00000000	-.36817579	.40743441	.54438526
124	806	3	1.00000000	-.38464903	.45918681	.63458607
125	804	3	1.00000000	-.40112228	.51142307	.72603426
126	803	3	1.00000000	-.40935403	.53769204	.77215886
127	801	3	1.00000000	-.41987509	.57125610	.83108729
128	531	3	1.00000000	-.43023054	.60407802	.88855405
129	890	3	1.00000000	-.28142577	.06508683	-.08529287
130	887	3	1.00000000	-.28142577	.07522009	-.06373749
131	940	3	1.00000000	-.31308636	.08888791	-.09601778
132	937	3	1.00000000	-.31308636	.09985076	-.07309280
133	1023	3	1.00000000	-.29603835	.10611959	-.02766270
134	878	3	1.00000000	-.28860542	.12665725	.03817241
135	876	3	1.00000000	-.29250211	.14808058	.08003377
136	928	3	1.00000000	-.31468888	.15731534	.05056845
137	926	3	1.00000000	-.31714379	.17721897	.09209456
138	1063	3	1.00000000	-.30334464	.20024074	.18226105

*Elastic modes start at Mode 3.

ORIGINAL PAGE IS
OF POOR QUALITY

Table 8-5.—(Continued)

Row	Node	DOF	Mode 1	Mode 2	Mode 3	Mode 4
139	916	3	1.00000000	-.34137632	.29789735	.33142171
140	915	3	1.00000000	-.35958846	.35318609	.42597783
141	908	3	1.00000000	-.38530173	.42636102	.54707160
142	906	3	1.00000000	-.40146811	.47880039	.63974469
143	904	3	1.00000000	-.41762962	.53168416	.73362228
144	902	3	1.00000000	-.43379601	.58535470	.82948800
145	920	3	1.00000000	-.44575884	.62655644	.90412453
146	909	3	1.00000000	-.45580742	.66023373	.96451856
147	1021	3	1.00000000	-.32648123	.13501884	-.02688445
148	1061	3	1.00000000	-.33891653	.24930054	.21634887
149	965	3	1.00000000	-.37528237	.37862240	.44878533
150	957	3	1.00000000	-.40130250	.46144689	.59492032
151	954	3	1.00000000	-.42548145	.54130582	.73718513
152	951	3	1.00000000	-.44961169	.62336523	.88517397
153	950	3	1.00000000	-.46818428	.68689403	1.00000000
154	767	3	1.00000000	-.22277575	.13408407	.22414456
155	766	3	1.00000000	-.23901033	.16778363	.26907379
156	763	3	1.00000000	-.25652594	.20566383	.32116563
157	762	3	1.00000000	-.27339860	.24351429	.37462266
158	759	3	1.00000000	-.28984749	.28163212	.42970813
159	758	3	1.00000000	-.30672015	.32161382	.48837926
160	755	3	1.00000000	-.32317391	.36175586	.54845880
161	754	3	1.00000000	-.34004657	.40377237	.61217171
162	751	3	1.00000000	-.35586225	.44362022	.67303370
163	750	3	1.00000000	-.37388443	.48917950	.74275680
164	237	2	0.00000000	0.00000000	-.00466627	-.01316444
165	235	2	0.00000000	0.00000000	-.01585457	-.04371027
166	232	2	0.00000000	0.00000000	-.03497496	-.09590053
167	229	2	0.00000000	0.00000000	-.04865246	-.13541237
168	227	2	0.00000000	0.00000000	-.05996807	-.16867408
169	226	2	0.00000000	0.00000000	-.07172626	-.20361984
170	475	2	0.00000000	0.00000000	-.00050551	-.00216068
171	285	2	0.00000000	0.00000000	-.01099463	-.03094947
172	282	2	0.00000000	0.00000000	-.02935007	-.08126730
173	472	2	0.00000000	0.00000000	-.00106137	-.00584409
174	332	2	0.00000000	0.00000000	-.01781127	-.05123939
175	329	2	0.00000000	0.00000000	-.03960832	-.11193838
176	277	2	0.00000000	0.00000000	-.05529603	-.15652582
177	862	2	0.00000000	0.00000000	.00002570	-.00558441
178	379	2	0.00000000	0.00000000	-.02048162	-.06224712
179	377	2	0.00000000	0.00000000	-.04124489	-.11995438
180	376	2	0.00000000	0.00000000	-.05680166	-.16353199
181	375	2	0.00000000	0.00000000	-.07267725	-.21808399
182	428	2	0.00000000	0.00000000	-.00218234	-.01648920
183	427	2	0.00000000	0.00000000	-.01825490	-.06003274
184	426	2	0.00000000	0.00000000	-.04540845	-.13389517

*Elastic modes start at Mode 3.

ORIGINAL PAGE IS
OF POOR QUALITY

ORIGINAL PAGE IS
OF POOR QUALITY

Table 8-5.—(Continued)

Row	Node	DOF	Mode 1	Mode 2	Mode 3	Mode 4
185	424	2	0.00000000	0.00000000	-.05749812	-.16678365
186	417	2	0.00000000	0.00000000	-.00281138	-.01969827
187	416	2	0.00000000	0.00000000	-.02999804	-.09373515
188	415	2	0.00000000	0.00000000	-.05844820	-.17122436
189	414	2	0.00000000	0.00000000	-.07372627	-.21301914
190	374	3	1.00000000	-.37530185	.40363978	.51397447
191	374	1	0.00000000	.03895704	-.05263124	-.02914391
192	471	5	0.00000000	.00048709	-.00088279	-.00098070
193	3191	3	1.00000000	1.00000000	1.00000000	-.18464158
194	3189	3	1.00000000	.91437029	.81293660	-.14320017
195	3187	3	1.00000000	.84252511	.66036566	-.10982347
196	3185	3	1.00000000	.77277439	.51908748	-.07956954
197	3181	3	1.00000000	.65310711	.29882154	-.03446162
198	2038	3	1.00000000	.61225521	.22436865	-.01943523
199	2098	3	1.00000000	.56111119	.14469570	-.00450610
200	2158	3	1.00000000	.50996716	.07138792	.00854683
201	2218	3	1.00000000	.45882313	.00688704	.01903789
202	2278	3	1.00000000	.40767910	-.04486726	.02597470
203	2338	3	1.00000000	.35653508	-.08581149	.02993111
204	2398	3	1.00000000	.30539105	-.11763927	.03138474
205	2458	3	1.00000000	.25424702	-.13995638	.03025327
206	2518	3	1.00000000	.20310300	-.15271289	.02663158
207	2578	3	1.00000000	.15195897	-.15639994	.02076657
208	2638	3	1.00000000	.10081494	-.15125473	.01295248
209	2698	3	1.00000000	.04967092	-.13812576	.00352092
210	2758	3	1.00000000	-.00147311	-.11885687	-.00742094
211	2818	3	1.00000000	-.05261714	-.09451730	-.01973499
212	2878	3	1.00000000	-.10376117	-.06522286	-.03356966
213	2938	3	1.00000000	-.15490519	-.03108865	-.04905609
214	2998	3	1.00000000	-.20604922	.00592100	-.06639837
215	3058	3	1.00000000	-.25719325	.04313547	-.08864692
216	3201	3	1.00000000	-.31581404	.08964431	-.12344657
217	3205	3	1.00000000	-.45512321	.20879040	-.21826520
218	3208	3	1.00000000	-.52633260	.27443774	-.27478171
219	3212	3	1.00000000	-.60412023	.34702324	-.33806562
220	3250	5	0.00000000	.00048709	-.00045682	.00040005
221	3250	3	1.00000000	-.55848027	.30511942	-.30210315
222	3225	3	1.00000000	-.52813482	.27602973	-.27609506
223	3225	5	0.00000000	.00048709	-.00045120	.00039066
224	3183	3	1.00000000	.70248789	.38602359	-.05195556
225	3203	3	1.00000000	-.38722085	.14875027	-.16859982
226	410	4	0.00000000	0.00000000	-.00000578	.00000437
227	410	5	0.00000000	.00048709	-.00025747	.00009521
228	410	3	1.00000000	.01596457	-.13286260	-.00550557

*Elastic modes start at Mode 3.

Table 8-5.—(Continued)

Row	Node	DOF	Mode 5	Mode 6	Mode 7	Mode 8
1	1020	1	-.00313472	-.04093259	.01294485	.01446483
2	1020	2	.00180415	-.00012027	-.00327211	-.00007031
3	1020	3	.12822397	-.21356674	.00108648	-.01173859
4	1020	4	.00022367	-.00029479	-.00004739	-.00000115
5	1020	5	.00018325	.00095228	-.00003854	-.00008433
6	1020	6	-.00000527	.00001547	-.00000265	-.00000172
7	1070	1	-.01127640	-.04024554	.01685384	.03411850
8	1070	2	-.02721228	.05774231	-.00816101	-.00737947
9	1070	3	.08743667	-.22275891	-.00863547	.03569257
10	1070	4	-.00029031	.00083772	-.00015742	-.00016836
11	1070	5	.00055216	.00104633	-.00009238	-.00052805
12	1070	6	-.00000930	.00001676	-.00000369	-.00000096
13	670	3	-.39058935	-.11976175	-.00799195	-.03849764
14	663	3	-.32363369	-.06955588	.00016683	.00439703
15	652	3	-.02901628	.06677184	.00620518	.04249152
16	644	3	.23258980	.13906362	-.00433066	-.00086252
17	637	3	.25876717	.04206434	-.03710098	-.07889191
18	792	3	.13276215	.05094774	-.05946078	-.07964125
19	784	3	-.09323872	.24002073	-.08538935	-.07147441
20	779	3	-.31565104	.47682908	-.12038140	-.07863470
21	775	3	-.47885041	.66016623	-.14934868	-.08481591
22	620	3	-.38731007	-.11736323	-.00767022	-.03674525
23	618	3	-.37357697	-.10269125	-.00479103	-.02228817
24	615	3	-.35535889	-.08884264	-.00249245	-.01019640
25	613	3	-.31588803	-.06659694	.00032143	.00513203
26	610	3	-.27381658	-.04537131	.00231570	.01645221
27	608	3	-.20007074	-.01187266	.00444577	.02874180
28	605	3	-.12700035	.02100493	.00572244	.03673826
29	603	3	-.06010510	.04962773	.00611119	.04004922
30	600	3	.04768459	.09431555	.00516144	.03843651
31	597	3	.15059493	.12743284	.00185105	.02448729
32	692	3	-.38398417	-.11487460	-.00733419	-.03490249
33	693	3	-.36873355	-.09987655	-.00445211	-.02053596
34	694	3	-.34726700	-.08543966	-.00225489	-.00901586
35	562	3	-.30741850	-.06338585	.00048357	.00589689
36	560	3	-.26408445	-.04264229	.00231833	.01617700
37	695	3	-.19118985	-.01014130	.00435233	.02781788
38	555	3	-.12082365	.02030557	.00552452	.03494490
39	553	3	-.05536004	.04806389	.00598412	.03850504
40	550	3	.04936078	.09083808	.00509565	.03687736
41	547	3	.15090219	.12339450	.00183807	.02294021
42	544	3	.22412726	.12686276	-.00390469	-.00241575
43	541	3	.26437630	.17419069	-.01223243	-.03189824
44	539	3	.27215994	.07259732	-.02087368	-.05344825
45	537	3	.24870577	.03203280	-.03405633	-.07236540
46	536	3	.22001708	.01862944	-.04181125	-.07748768

Table 8-5.—(Continued)

Row	Node	DOF	Mode 5	Mode 6	Mode 7	Mode 8
47	534	3	.17436518	.01916430	-.04913767	-.07567356
48	476	3	.13411029	.03035843	-.05373524	-.07178100
49	716	3	.07943424	.06369086	-.05888108	-.06681405
50	713	3	.02601696	.10214232	-.06410146	-.06258991
51	712	3	-.03128649	.14901733	-.07013656	-.05895072
52	709	3	-.09237744	.20377208	-.07701166	-.05593082
53	708	3	-.15936601	.26791600	-.08533877	-.05363384
54	705	3	-.23103378	.34255451	-.09569701	-.05377498
55	704	3	-.31054323	.43036013	-.10839777	-.05645885
56	701	3	-.38910298	.52011116	-.12182901	-.06078240
57	700	3	-.47976707	.62448123	-.13831690	-.06581913
58	533	3	-.56266952	.71845843	-.15329906	-.06888044
59	85	3	-.34965819	-.08726377	-.00258676	-.01074655
60	82	3	-.30609070	-.06367297	.00029376	.00489325
61	79	3	-.23794093	-.03354955	.00276166	.01833996
62	129	3	-.24020853	-.03302991	.00297052	.01977499
63	76	3	-.15363134	-.00209187	.00430758	.02578674
64	176	3	-.15390350	.00335844	.00483367	.03027552
65	73	3	-.06896423	.02615908	.00525895	.02961105
66	173	3	-.06370183	.03712446	.00580145	.03527969
67	50	3	.01028224	.04079064	.00482212	.02241834
68	120	3	.02007999	.05504665	.00505395	.02720637
69	220	3	.03589972	.07754463	.00535819	.03509758
70	67	3	.10726556	.08691337	.00601921	.02834354
71	167	3	.10881157	.08752399	.00367175	.02112496
72	267	3	.13997994	.11618298	.00265261	.02451759
73	44	3	.11652435	.04638120	.00282516	.00445934
74	114	3	.15506654	.08135406	.00289718	.00732101
75	214	3	.17736404	.09564330	.00029723	.00353785
76	314	3	.20958364	.11774904	-.00255409	-.00034078
77	41	3	.14968976	.04187521	.00140896	-.00548750
78	111	3	.16378831	.05069469	.00028857	-.00773657
79	211	3	.19236471	.06638828	-.00238897	-.01353015
80	311	3	.23044622	.08658423	-.00716740	-.02260436
81	58	3	.16647919	.02865820	-.00046343	-.01672420
82	158	3	.18295672	.03077142	-.00303452	-.02199620
83	209	3	.19652543	.04428122	-.00433467	-.02325246
84	309	3	.23060365	.05507606	-.01040189	-.03473756
85	409	3	.26134812	.06788945	-.01786857	-.04786127
86	207	3	.19269383	.01804181	-.00582720	-.02894976
87	307	3	.21851364	.01263520	-.01293554	-.04100510
88	407	3	.23691014	.01743534	-.02256297	-.05473445
89	55	3	.15504209	.00534766	-.00148139	-.02314141
90	155	3	.17159605	-.00404274	-.00414427	-.02738286
91	205	3	.17993671	-.01217756	-.00616141	-.02993357
92	305	3	.19699756	-.03515672	-.01361702	-.03933690

Table 8-5.—(Continued)

Row	Node	DOF	Mode 5	Mode 6	Mode 7	Mode 8
93	405	3	.20228337	-.03259607	-.02544869	-.05489522
94	385	3	.19074067	-.01166673	-.03652148	-.06358798
95	454	3	.17224684	-.03539336	-.03180382	-.05131670
96	464	3	.11838500	-.00690070	-.04115304	-.04999850
97	474	3	.05993481	.04078851	-.04983109	-.04950776
98	484	3	.00034044	.09880448	-.05935592	-.05015042
99	493	3	-.14104863	.20859613	-.06635499	-.03534986
100	502	3	-.32579366	.38802838	-.09044728	-.02886658
101	512	3	-.43577697	.52379534	-.11567286	-.04127897
102	522	3	-.52097043	.64174707	-.13654729	-.05278766
103	52	3	.12295049	-.02545657	-.00123317	-.02306924
104	152	3	.14475752	-.05715456	-.00262762	-.02428836
105	202	3	.15546277	-.07608782	-.00427856	-.02375976
106	302	3	.16394277	-.11377954	-.01016657	-.02186430
107	382	3	.14225172	-.09994565	-.02091621	-.02190434
108	452	3	.09718014	-.08272050	-.02494908	-.01439175
109	462	3	.01431883	-.01375936	-.03167956	-.00975585
110	482	3	-.14656854	.16498914	-.05298070	-.01293955
111	492	3	-.22514144	.26080486	-.06826911	-.01869872
112	179	3	.08081687	-.02706589	-.00031644	-.02095635
113	146	3	.09698744	-.05743325	-.00011673	-.02047954
114	192	3	.12272834	-.11106249	-.00003986	-.01917167
115	200	3	.13938092	-.14651678	-.00147142	-.01716601
116	298	3	.14252315	-.18929570	-.00370314	-.00402712
117	350	3	.12752515	-.20817234	-.00775896	.01351436
118	398	3	.10567774	-.18846723	-.01143350	.01803091
119	819	3	.01916293	-.13368553	-.01072009	.03461071
120	816	3	-.08567470	-.01939532	-.01351347	.03774978
121	470	3	-.18310195	.09694802	-.02403534	.03178080
122	810	3	-.24016595	.16016656	-.03269836	.03240011
123	808	3	-.31297865	.26215230	-.05191613	.01963978
124	806	3	-.41308340	.40395475	-.07914276	.00267863
125	804	3	-.51588234	.55124785	-.10808604	-.01403368
126	803	3	-.56815207	.62668648	-.12310378	-.02238474
127	801	3	-.63494379	.72310762	-.14229184	-.03309219
128	531	3	-.69945788	.81571725	-.16057153	-.04347791
129	890	3	.06647859	-.06943019	.00081617	-.02077644
130	887	3	.09696126	-.13671101	.00169122	-.01866231
131	940	3	.04676375	-.09407740	.00186727	-.02060386
132	937	3	.07978449	-.16964116	.00310960	-.01783643
133	1023	3	.11977439	-.24369707	.00275606	-.00883271
134	878	3	.12325971	-.26755176	.00092107	.01716985
135	876	3	.11618993	-.28613605	-.00134977	.03149569
136	928	3	.10841751	-.33839458	.00457522	.03742861
137	926	3	.10200721	-.35371622	.00210855	.05113095
138	1063	3	.06281516	-.24483260	-.00657578	.05145109

Table 8-5.—(Continued)

Row	Node	DOF	Mode 5	Mode 6	Mode 7	Mode 8
139	916	3	-.10193090	-.08969149	.00668209	.07622631
140	915	3	-.20025829	.03638873	.00049043	.07376715
141	908	3	-.33897999	.21667162	-.03296145	.05762985
142	906	3	-.44376350	.36858186	-.06301117	.03837971
143	904	3	-.55155386	.52702504	-.09466156	.01854007
144	902	3	-.66423419	.69493479	-.12881140	-.00162337
145	920	3	-.75639277	.83552074	-.15857995	-.01627290
146	900	3	-.82839031	.94350614	-.18694921	-.02808423
147	1021	3	.11017945	-.30741459	.00495806	-.00410710
148	1061	3	.02398718	-.32591695	.00024749	.09133642
149	965	3	-.24060447	.02704272	.01343978	.10434416
150	957	3	-.40389308	.27234617	-.03943374	.06526718
151	954	3	-.56843959	.51525068	-.08818790	.03413280
152	951	3	-.74762443	.78673263	-.14454223	.00248272
153	950	3	-.88789402	1.00000000	-.18947211	-.02009252
154	767	3	.12968641	.04563503	-.05778187	-.07652399
155	766	3	.08424590	.07545535	-.06243691	-.07318545
156	763	3	.02900351	.11771565	-.06815704	-.06984456
157	762	3	-.02991632	.16817112	-.07470178	-.06729694
158	759	3	-.09292738	.22725923	-.08244264	-.06600472
159	758	3	-.16184140	.29564818	-.09176173	-.06572307
160	755	3	-.23470405	.37304556	-.10310421	-.06761422
161	754	3	-.31385922	.46049732	-.11617852	-.07084586
162	751	3	-.39062913	.54710167	-.12948892	-.07443965
163	750	3	-.47915212	.64758286	-.14547411	-.07811410
164	237	2	-.00947229	.01119128	.00041267	.00045976
165	235	2	.00210893	-.02820491	.00953926	.01186027
166	232	2	.04157675	-.14024194	.04562217	.06858440
167	229	2	.07150849	-.26043647	.12256842	.26911378
168	227	2	.09765875	-.37345432	.19887739	.48649467
169	226	2	.12567585	-.49987912	.28713881	.74693119
170	475	2	-.01278621	.02397795	-.00289760	-.00353654
171	285	2	-.00448652	-.00852026	.00387691	.00235223
172	282	2	.02900562	-.10935117	.03866563	.05940477
173	472	2	-.02399786	.03651723	-.00189127	-.00022426
174	332	2	.00323209	-.04587446	.02424550	.04003922
175	329	2	.05064145	-.20901105	.11077718	.25219500
176	277	2	.08684587	-.34661599	.19258284	.47748842
177	862	2	-.03962725	.03599082	.00046657	.00511215
178	379	2	.00637713	-.09926202	.08504134	.21401585
179	377	2	.05424130	-.26513353	.17295643	.44797207
180	376	2	.09093922	-.39728183	.24628118	.65082235
181	375	2	.12872189	-.53451176	.32309109	.86537698
182	428	2	-.03661491	-.01464773	.08841286	.26724018
183	427	2	.00069940	-.12993470	.13903741	.39315282
184	426	2	.06451354	-.33156816	.23082853	.62869699

Table 8-5.—(Continued)

Row	Node	DOF	Mode 5	Mode 6	Mode 7	Mode 8
185	424	2	.09296291	-.42145093	.27167987	.73344944
186	417	2	-.03540412	-.03736658	.11432299	.34938437
187	416	2	.02858985	-.24105461	.20844307	.59340855
188	415	2	.09577176	-.45474572	.30663663	.84749177
189	414	2	.13240091	-.57416081	.36361531	1.00000000
190	374	3	-.30532829	.17651172	.71082004	-.00708493
191	374	1	.05443909	.03777696	1.00000000	-.10325103
192	471	5	.00143078	-.00050502	-.00012601	-.00045318
193	3191	3	1.00000000	.29020919	.02519929	.14083102
194	3189	3	.65052179	.16908037	.01311640	.06664468
195	3187	3	.38933317	.07763930	.00419717	.01347851
196	3185	3	.16097816	.00352012	-.00275057	-.02561978
197	3181	3	-.13977472	-.08284764	-.01006937	-.06057392
198	2038	3	-.23043973	-.10502234	-.01142375	-.06426834
199	2098	3	-.30488271	-.11908631	-.01180223	-.06244678
200	2158	3	-.35732176	-.12469571	-.01079049	-.05497704
201	2218	3	-.38224691	-.12022842	-.00871219	-.04223899
202	2278	3	-.37610773	-.10643549	-.00574587	-.02679124
203	2338	3	-.34630503	-.08617381	-.00265628	-.01094132
204	2398	3	-.29764405	-.06122644	.00013768	.00390070
205	2458	3	-.23069807	-.03276347	.00242982	.01587758
206	2518	3	-.15167554	-.00419938	.00398814	.02312886
207	2578	3	-.06978930	.02053452	.00475139	.02516001
208	2638	3	.00595514	.03699733	.00462679	.02122616
209	2698	3	.06692933	.04370552	.00389202	.01357164
210	2758	3	.11479524	.04422220	.00279832	.00420146
211	2818	3	.14620491	.03936700	.00158881	-.00521305
212	2878	3	.15609578	.02694934	.00049784	-.01359554
213	2938	3	.14264268	.00927541	-.00030285	-.01905104
214	2998	3	.10883527	-.00817617	-.00058600	-.02083991
215	3058	3	.05483149	-.01119123	-.00052763	-.02072496
216	3201	3	-.05464648	.00866919	-.00033660	-.01702054
217	3205	3	-.40654178	.08718458	.00082816	.00738025
218	3208	3	-.64181039	.14954234	.00181372	.02866661
219	3212	3	-.91136014	.22297646	.00299207	.05448411
220	3253	5	.00172140	-.00047442	-.00000767	-.00016961
221	3250	3	-.76166924	.18334956	.00236339	.04081416
222	3225	3	-.64688998	.15075243	.00183174	.02903428
223	3225	5	.00164417	-.00044141	-.00000703	-.00015285
224	3183	3	-.03000169	-.05340933	-.00775164	-.05078462
225	3203	3	-.21215143	.03982257	.00010614	-.00782300
226	410	4	.00005080	.00004510	-.00000422	-.00000399
227	410	5	-.00021769	.00021441	.00002327	.00016544
228	410	3	.13004857	.07828306	.00422565	.01673362

ORIGINAL PAGE IS
OF POOR QUALITY

ORIGINAL PAGE IS
OF POOR QUALITY

Table 8-5.—(Continued)

Row	Node	DOR	Mode 9	Mode 10	Mode 11	Mode 12
1	1020	1	.02696501	-.01455468	-.00899450	.12440528
2	1020	2	-.02736661	.00479122	.01666985	-.03229600
3	1020	3	.09242949	-.02160619	.06643277	.31707276
4	1020	4	-.00057012	.00005091	.00039127	.00030372
5	1020	5	-.00049777	.00017127	-.00004410	-.00224764
6	1020	6	-.00001375	.00000533	.00000568	-.00006958
7	1070	1	.00244060	-.01376413	-.11145402	-.04502133
8	1070	2	-.01494618	.01007554	.05614457	-.04381302
9	1070	3	-.11025247	.00164039	-.06443409	-.13615634
10	1070	4	-.00066252	.00018465	.00131962	-.00016108
11	1070	5	.00002690	.00014413	.00206900	.00145710
12	1070	6	-.00000110	.00000338	.00000104	-.00001722
13	670	3	.00671467	.01470718	-.03279601	-.00075034
14	663	3	.00291601	-.00635653	.14163868	-.03805343
15	652	3	-.03693978	-.01376479	-.02244829	.21982228
16	644	3	-.12223243	.01869808	-.16067947	.51225267
17	637	3	-.20478976	.04556601	.35192205	.19775155
18	792	3	-.23318605	.04269220	.47267363	.13307459
19	784	3	-.11929708	.03115366	.40441419	.15334882
20	779	3	.04404779	.00738559	.29410943	.22406282
21	775	3	.18061468	-.01170636	.19752585	.29049534
22	620	3	.00655110	.01388460	-.02696401	-.00205676
23	618	3	.00538422	.00663149	.03669976	-.01647993
24	615	3	.00439625	.00065124	.08756589	-.02810829
25	613	3	.00283687	-.00656380	.13937501	-.03778223
26	610	3	.00065140	-.01130494	.15591466	-.03234327
27	608	3	-.00425901	-.01527504	.13514580	-.00015473
28	605	3	-.01341069	-.01631638	.08111834	.06668086
29	603	3	-.02499809	-.01491043	.01813640	.14492139
30	600	3	-.05319783	-.00829767	-.09743813	.31058197
31	597	3	-.08759067	.00369434	-.17830815	.45714756
32	692	3	.00637733	.01301786	-.02075582	-.00344716
33	693	3	.00521586	.00583859	.04126899	-.01742606
34	694	3	.00425295	.00023074	.08669108	-.02786017
35	562	3	.00275346	-.00676964	.13667849	-.03744789
36	560	3	.00090634	-.01100503	.14930342	-.03352345
37	695	3	-.00357028	-.01475463	.12931465	-.00452059
38	555	3	-.01117307	-.01571109	.08138613	.05095006
39	553	3	-.02144122	-.01462561	.02161530	.12217988
40	550	3	-.04684414	-.00832944	-.09225101	.27587742
41	547	3	-.08049403	.00358703	-.17411305	.42145761
42	544	3	-.10376602	.01709526	-.14416937	.42680389
43	541	3	-.12295135	.02930180	-.01668520	.33801080
44	539	3	-.14558253	.03668895	.12994060	.25399132
45	537	3	-.18619663	.04192859	.31907387	.17411162
46	536	3	-.20846098	.04267549	.39903879	.14803571

Table 8-5.—(Continued)

Row	Node	DOF	Mode 9	Mode 10	Mode 11	Mode 12
47	534	3	-.21902757	.04107010	.42953353	.12975055
48	476	3	-.21577742	.03904373	.42880963	.11718670
49	716	3	-.19828210	.03727683	.41382140	.11054212
50	713	3	-.17547302	.03539605	.39600807	.10878411
51	712	3	-.14566373	.03326360	.37576969	.11243709
52	709	3	-.10867904	.03068061	.35226287	.12169133
53	708	3	-.06349743	.02728022	.32454784	.13750635
54	705	3	-.01014999	.02172457	.29164733	.16089356
55	704	3	.05362855	.01299250	.24758091	.19026151
56	701	3	.11976785	.00232120	.19693930	.22057527
57	700	3	.19791470	-.01030635	.13617190	.25729984
58	533	3	.27043953	-.02078783	.07978659	.29105164
59	85	3	.00437701	.00110936	.07866446	-.02601742
60	82	3	.00304906	-.00624932	.13239245	-.03859827
61	79	3	.00149985	-.01172197	.14555783	-.03996853
62	129	3	.00065352	-.01240728	.15134142	-.03526710
63	76	3	.00045380	-.01363323	.11137271	-.03018316
64	176	3	-.00438272	-.01512867	.11114765	.00227867
65	73	3	.00041319	-.01391052	.06752972	-.02120351
66	173	3	-.00986436	-.01500108	.04988113	.04649575
67	50	3	.00876467	-.01008758	.01698961	-.05582103
68	120	3	-.00283124	-.01014935	-.01737207	.01854715
69	220	3	-.02708041	-.01007245	-.06699442	.17084925
70	67	3	.01661006	-.00918296	-.18509636	-.11443594
71	167	3	-.01881439	-.00318594	-.11169061	.11100441
72	267	3	-.06581600	.00131725	-.17542406	.36797614
73	44	3	.02573460	-.00269912	-.02014048	-.11799415
74	114	3	.00935510	.00062902	-.12311111	-.04986498
75	214	3	-.03543699	.00689729	-.12436100	.15448267
76	314	3	-.08357573	.01404074	-.14169150	.35221852
77	41	3	.03217162	.00119518	-.02754927	-.13246747
78	111	3	.01714023	.00419424	-.03785411	-.08688710
79	211	3	-.01621015	.01078970	-.04692760	.01716052
80	311	3	-.07130781	.02050900	-.03927392	.19118136
81	58	3	.03806902	.00501665	-.00982939	-.15117978
82	158	3	.01329010	.00966607	.00826153	-.10239502
83	209	3	-.00771793	.01239615	.00415933	-.04612752
84	309	3	-.06401003	.02281555	.04268930	.09179039
85	409	3	-.12352878	.03294159	.10174588	.21538448
86	297	3	-.00358607	.01330423	.04306851	-.07663177
87	307	3	-.06002708	.02211410	.11467777	.02953437
88	407	3	-.12402603	.03201351	.20493255	.11508850
89	55	3	.04823218	.00563887	.01084842	-.15825340
90	155	3	.02077801	.00935009	.03846418	-.11748627
91	205	3	.00126880	.01157757	.06069115	-.08165597
92	305	3	-.05640786	.01837247	.14735361	.02150233

Table 8-5.—(Continued)

Row	Node	DOF	Mode 9	Mode 10	Mode 11	Mode 12
93	405	3	-.12657988	.02874848	.27408033	.09076134
94	385	3	-.17733557	.03560153	.34677459	.10813858
95	454	3	-.15568492	.03040753	.29400964	.07945727
96	464	3	-.17094460	.03151022	.31858350	.07410538
97	474	3	-.16455684	.03146190	.32692972	.07427432
98	484	3	-.14618370	.03162312	.33476322	.08571573
99	493	3	-.04703197	.02250231	.23135728	.08765189
100	502	3	.10228789	.00601232	.10537018	.13141801
101	512	3	.17896805	-.00478590	.08195461	.19241585
102	522	3	.24750961	-.01568674	.05425427	.24467469
103	52	3	.06543899	.00182537	.01859785	-.11339063
104	152	3	.04504679	.00162850	.04277308	-.03875166
105	202	3	.02295312	.00259867	.05962422	.00152925
106	302	3	-.04343298	.00803081	.10550591	.03937296
107	382	3	-.11899720	.01900464	.16668078	.01360572
108	452	3	-.12941125	.02027538	.15715214	-.01260519
109	462	3	-.10868504	.02097422	.14565336	-.01739655
110	482	3	-.01801318	.01814573	.12768293	.03672135
111	492	3	.03283204	.01409308	.12041918	.07591431
112	179	3	.07546870	-.00035744	.01107056	-.10456939
113	146	3	.07918811	-.00339987	.02099687	-.04123835
114	192	3	.07824640	-.00858654	.04167278	.08314627
115	200	3	.05741556	-.00957435	.06033482	.15253116
116	298	3	-.00504305	-.00599520	.03985524	.09407735
117	350	3	-.07859775	.00048920	.00087778	-.03375289
118	398	3	-.10713749	.00613493	.00389312	-.08481360
119	819	3	-.09531618	.01251569	-.02978048	-.13637586
120	816	3	-.02920609	.01569387	-.04702350	-.10823985
121	470	3	.03511709	.01041831	-.06881574	-.07005518
122	810	3	.07974678	.00811931	-.09179981	-.04734281
123	808	3	.12844585	-.00010420	-.09815288	-.00192640
124	806	3	.19974235	-.01050674	-.10521304	.06762213
125	804	3	.27762910	-.02016873	-.11076790	.14645712
126	803	3	.31864272	-.02486069	-.11334779	.18868574
127	801	3	.37103284	-.03086727	-.11649512	.24275628
128	531	3	.41994116	-.03650103	-.11764064	.29371677
129	893	3	.09947427	-.00664297	.02052353	-.02646425
130	887	3	.11113164	-.01469562	.04094899	.12855713
131	940	3	.12086471	-.01115452	.02349475	.01624670
132	937	3	.13712593	-.02072496	.04441873	.19111867
133	1023	3	.11304273	-.02765453	.06437489	.38649900
134	878	3	.00705985	-.01707074	-.03099424	.11345759
135	876	3	-.04488840	-.01344141	-.07193588	.01431858
136	928	3	.01099755	-.02656170	-.10063630	.12013385
137	926	3	-.04190705	-.02245682	-.13998452	.01789472
138	1063	3	-.11333246	-.00113364	-.12015112	-.18279352

Table 8-5.—(Continued)

Row	Node	DOF	Mode 9	Mode 10	Mode 11	Mode 12
139	916	3	.00314998	.01308042	-.19078216	-.19534844
140	915	3	.07166144	.01693226	-.18968464	-.14477641
141	908	3	.17406231	.00339476	-.21766632	-.06102653
142	906	3	.25269348	-.00939596	-.23224429	.01382218
143	904	3	.33880933	-.02235159	-.24748533	.09900016
144	902	3	.43735311	-.03611048	-.27095315	.19617423
145	920	3	.53267233	-.04719990	-.30418346	.28789778
146	900	3	.60001449	-.05521423	-.32116280	.35455274
147	1021	3	.14574489	-.03905943	.07367052	.55093888
148	1061	3	-.11731177	-.01223312	-.27788509	-.29470940
149	965	3	.11863067	.01949052	-.30209776	-.20205999
150	957	3	.23481128	-.00192784	-.28233301	-.05191205
151	954	3	.36785050	-.02338929	-.31303252	.07595329
152	951	3	.53982519	-.04686374	-.36894664	.24184054
153	950	3	.68122754	-.06332557	-.41414297	.37962126
154	767	3	-.22612504	.04131022	.45643131	.12691914
155	766	3	-.21107069	.03979333	.44631593	.12277899
156	763	3	-.18629464	.03762366	.42995196	.12361675
157	762	3	-.15460580	.03490930	.41044488	.13009976
158	759	3	-.11557810	.03099526	.38611753	.14222199
159	758	3	-.06886167	.02581251	.35646988	.15973268
160	755	3	-.01514894	.01855995	.32144812	.18339692
161	754	3	.04740722	.00935329	.27778733	.21219628
162	751	3	.11098383	-.00630182	.23131512	.24208725
163	750	3	.18668241	-.01117630	.17611030	.27889646
164	237	2	.01489073	-.00029051	-.00908614	-.02685010
165	235	2	.02565942	-.00405485	-.07010550	-.06775234
166	232	2	.03700557	.02946368	-.11707622	-.13423611
167	229	2	.23133024	.22986457	.08194793	.06346337
168	227	2	.45024954	.45293238	.32704234	.31071878
169	226	2	.71687699	.72325150	.63640242	.62520749
170	475	2	.00676098	.00154200	.01347207	-.01867002
171	285	2	.01592305	-.00785646	-.05451899	-.06454984
172	282	2	.04077959	.02693187	-.09966505	-.11531673
173	472	2	.02691846	.00245961	-.00535647	-.02926399
174	332	2	.04784444	.02116424	-.06460291	-.07723823
175	329	2	.23608077	.22376051	.10831631	.09193227
176	277	2	.45264179	.44961502	.34106567	.32592999
177	862	2	.05419573	.00574172	-.02503574	-.03465691
178	379	2	.24380024	.20840687	.16169411	.14969746
179	377	2	.45722921	.43701390	.37991876	.36821145
180	376	2	.64750611	.63866429	.58503695	.57506318
181	375	2	.84969376	.85272845	.80582590	.79955444
182	428	2	.35626012	.29301582	.34356645	.33793208
183	427	2	.45755795	.40922391	.43378430	.42723344
184	426	2	.65341025	.63051968	.61971017	.61329793

Table 8-5.—(Continued)

Row	Node	DOF	Mode 9	Mode 10	Mode 11	Mode 12
185	424	2	.74029030	.72885456	.70202506	.69566066
186	417	2	.44981738	.38280696	.45906791	.45545241
187	416	2	.65559889	.61365989	.65891162	.65615088
188	415	2	.86836609	.85341670	.86411508	.86206817
189	414	2	1.00000000	1.00000000	1.00000000	1.00000000
190	374	3	.08065251	-.00127883	-.16354826	-.10769690
191	374	1	-.10238079	-.00656725	.17068535	.09241676
192	471	5	-.00128350	.00010492	.00228163	.00067993
193	3191	3	-.01900631	-.06499356	.56661164	-.11998229
194	3189	3	-.00861470	-.02948636	.21591984	-.04470191
195	3187	3	-.00121672	-.00430622	-.02209605	.00584873
196	3185	3	.00415884	.01383030	-.17846312	.03822247
197	3181	3	.00884774	.02899830	-.26937783	.05440681
198	2038	3	.00924768	.02986204	-.24489165	.04777968
199	2098	3	.00906239	.02811975	-.20026334	.03662142
200	2158	3	.00835186	.02365018	-.13623532	.02207322
201	2218	3	.00705135	.01681082	-.05829278	.00479477
202	2278	3	.00566767	.00898470	.01393052	-.01110965
203	2338	3	.00431943	.00133715	.07331068	-.02474227
204	2398	3	.00308618	-.00541251	.11462563	-.03528011
205	2458	3	.00228381	-.01027455	.12552568	-.04041949
206	2518	3	.00257610	-.01253864	.10547454	-.04232463
207	2578	3	.00486437	-.01239153	.06801686	-.04815480
208	2638	3	.01028524	-.00996035	.02773622	-.06657062
209	2698	3	.01823565	-.00659117	.06179322	-.09516946
210	2758	3	.02673168	-.00282338	-.01536575	-.12130298
211	2818	3	.03500539	.00061464	-.02307595	-.14005183
212	2878	3	.04521454	.00282388	-.01526939	-.15499373
213	2938	3	.05610543	.00329848	-.00279593	-.15433453
214	2998	3	.06593695	.00201650	.00581415	-.13520975
215	3058	3	.06880566	.00119011	.00867062	-.12406181
216	3201	3	.05713976	.00120865	.00878628	-.11838874
217	3205	3	-.01724455	.00030958	-.00148781	-.02243154
218	3208	3	-.08349637	-.00027695	-.01389458	.06823029
219	3212	3	-.16429262	-.00097151	-.02970378	.18236615
220	3250	5	.00053239	.00000454	.00010634	-.00076685
221	3250	3	-.12166944	-.00058912	-.02166935	.12306370
222	3225	3	-.08461175	-.00028866	-.01405230	.06952302
223	3225	5	.00047697	.00000417	.00009109	-.00066245
224	3183	3	.00754794	.02501746	-.25588565	.05300599
225	3203	3	.02948282	.00078267	.00612253	-.08292093
226	410	4	-.00006826	.00001164	-.00006226	.00027214
227	410	5	-.00007177	-.00005166	-.00075428	.00017857
228	410	3	.01778722	-.00463054	-.14618089	-.10036550

ORIGINAL PAGE IS
OF POOR QUALITY

Table 8-5.—(Continued)

Row	Node	DOF	Mode 13	Mode 14	Mode 15	Mode 16
1	1020	1	.01590217	.24937640	-.46133774	-.14191312
2	1020	2	.02138088	-.02613737	.01940364	.01085639
3	1020	3	.14656150	-.00080717	.08210176	.07628983
4	1020	4	.00068161	.00027250	.00061561	.00083097
5	1020	5	-.00129631	-.00004402	.00020445	.00022593
6	1020	6	-.00002025	-.00005827	.00005252	-.00000212
7	1070	1	-.13545088	.29164768	-.44031146	-.12912678
8	1070	2	.07349995	-.11941160	-.20584382	-.17436383
9	1070	3	-.01892490	-.03586309	.03102852	-.00233484
10	1070	4	.00178691	-.00151359	-.00322023	-.00228516
11	1070	5	.00165859	-.00034079	-.00012440	.00047648
12	1070	6	.00001173	-.00003659	-.00005798	-.000006199
13	670	3	-.04002423	.12618319	.19130598	-.30676141
14	663	3	-.08590493	.14008655	.12427102	-.25157295
15	652	3	-.13526117	-.40553773	-.16561629	.16320659
16	644	3	-.46721819	.10212800	.19213940	-.45037489
17	637	3	.20179725	.17977472	-.23581538	-.11064149
18	792	3	.54747084	-.07527248	-.72354611	-.24850149
19	784	3	.51407914	-.07117452	-.84277127	-.30286805
20	779	3	.34779247	.07780150	-.74517924	-.21002160
21	775	3	.17683988	.24445289	-.59565517	-.08646439
22	620	3	-.04056678	.12424398	.18715957	-.29961645
23	618	3	-.05970498	.15048175	.17955872	-.31845378
24	615	3	-.07326724	.15921394	.16459418	-.30977148
25	613	3	-.08247062	.13415259	.11794653	-.23739241
26	610	3	-.07781155	.05668363	.04251221	-.10071198
27	608	3	-.06277360	-.09701215	-.07288973	.10766350
28	605	3	-.06665335	-.25142775	-.15310193	.22344207
29	603	3	-.09057172	-.34467146	-.17262414	.21969993
30	600	3	-.19176602	-.38731793	-.09549213	.01267956
31	597	3	-.35022878	-.20862468	.06918661	-.30031573
32	692	3	-.04115950	.12220073	.18279267	-.29204506
33	693	3	-.05938535	.14660417	.17244818	-.30692410
34	694	3	-.07001086	.15103799	.15523137	-.29108228
35	562	3	-.07860459	.12761568	.11105529	-.22181126
36	560	3	-.07103643	.05721436	.04047580	-.09046415
37	695	3	-.05526430	-.08577062	-.06838114	.10832697
38	555	3	-.05481334	-.22160572	-.14353922	.22313198
39	553	3	-.07179528	-.32143191	-.17367126	.24287631
40	550	3	-.15636774	-.36640166	-.09738997	.03635647
41	547	3	-.31529864	-.18420713	.07214710	-.28954383
42	544	3	-.39509414	.12765631	.17387803	-.38211582
43	541	3	-.32824177	.33833283	.15978566	-.28087348
44	539	3	-.15374335	.34725006	.05099666	-.16163367
45	537	3	.17220438	.17581318	-.20368463	-.08766376
46	536	3	.34814282	.04715524	-.37319296	-.10628303

ORIGINAL PAGE IS
OF POOR QUALITY

Table 8-5.—(Continued)

Row	Node	DOF	Mode 13	Mode 14	Mode 15	Mode 16
47	534	3	.45351536	-.03003056	-.53955923	-.16665479
48	476	3	.49255122	-.06899454	-.62833176	-.20843460
49	716	3	.49951474	-.08854240	-.67604945	-.23802164
50	713	3	.49491811	-.09678976	-.70888569	-.25886481
51	712	3	.48182002	-.09555870	-.73397087	-.27322642
52	709	3	.45835704	-.08310008	-.74563799	-.27751375
53	708	3	.42341730	-.05628446	-.74329640	-.26967658
54	705	3	.37391915	-.01100207	-.72062342	-.24469573
55	704	3	.29982844	.05565585	-.65764693	-.19470748
56	701	3	.21022069	.13380464	-.56253147	-.12736535
57	700	3	.10010053	.23401815	-.44530636	-.04260499
58	533	3	-.03376632	.32978208	-.33350399	.03802170
59	85	3	-.06727459	.14875648	.15682294	-.29032892
60	82	3	-.07550909	.13437795	.11911242	-.22974907
61	79	3	-.03489527	.04483823	.01825432	-.02971859
62	129	3	-.06297997	.03349290	.01228654	-.02858302
63	76	3	-.01502730	-.05911728	-.07566207	.16586773
64	176	3	-.03965519	-.12918744	-.10390806	.18656464
65	73	3	.02266798	-.14747534	-.15476144	.33324234
66	173	3	-.01925343	-.26018521	-.19153054	.34337661
67	50	3	.07955878	-.06739500	-.10876276	.27037708
68	120	3	.05954064	-.15500380	-.10741895	.21419517
69	220	3	-.04606966	-.33655287	-.12334307	.14017219
70	67	3	1.00000000	.04185944	.17403363	-.59704214
71	167	3	.03052927	-.09396762	.00625011	-.03985387
72	267	3	-.24422394	-.20647630	.06532924	-.27775025
73	44	3	.05747551	.03794805	-.06811307	.22751493
74	114	3	.17636866	.16156019	.03468027	-.00110758
75	214	3	-.12739260	.12500037	.09696120	-.14918555
76	314	3	-.32772856	.12915306	.15711750	-.32602360
77	41	3	.01097219	.07218352	-.04808084	.17997186
78	111	3	-.01668114	.11698941	-.01275735	.12388525
79	211	3	-.11541184	.22193036	.05135786	.02952920
80	311	3	-.24977832	.30437015	.12522090	-.14104262
81	58	3	-.07530111	.08737990	-.04230864	.17404176
82	158	3	-.09995559	.14356424	-.00083667	.15965547
83	209	3	-.12676720	.21489515	.02793445	.12895752
84	309	3	-.17214662	.30147007	.07699261	.00145111
85	409	3	-.16894956	.34148485	.06706813	-.12314558
86	277	3	-.10471216	.14560180	.02851899	.15154543
87	307	3	-.05876197	.19020970	.03761805	.09255052
88	407	3	.03102485	.20439990	-.04866465	.00192991
89	55	3	-.12445708	.01000306	-.02686704	.09233859
90	155	3	-.11191875	.04863353	.03565025	.13194427
91	205	3	-.08775564	.06301508	.06176705	.13894744
92	305	3	.03081047	.06816129	.05089101	.12057282

Table 8-5.—(Continued)

Row	Node	DOF	Mode 13	Mode 14	Mode 15	Mode 16
93	405	3	.21459385	-.00495265	-.06835633	.04959947
94	385	3	.32545458	-.01907759	-.28029439	-.05812641
95	454	3	.28241535	-.04244356	-.20134326	-.02962700
96	464	3	.35895702	-.07350559	-.38104470	-.11746271
97	474	3	.39667515	-.09120624	-.50249176	-.17957908
98	484	3	.42351320	-.09891570	-.59983679	-.22495233
99	493	3	.29724785	-.06435976	-.47246962	-.17858428
100	502	3	.10695336	.05487701	-.27208438	-.06402368
101	512	3	.04739162	.16562031	-.27776006	-.01779187
102	522	3	-.01991505	.27172347	-.25068556	.03851281
103	52	3	-.12363494	-.08215957	-.01964793	-.04204001
104	152	3	-.07839731	-.02710076	.05842242	.05484296
105	202	3	-.03513900	.00086980	.09887273	.10649304
106	302	3	.05689519	.00267531	.11200045	.12595644
107	382	3	.16940798	-.06601805	-.03970414	.01867570
108	452	3	.19002411	-.09586202	-.11781134	-.04231786
109	462	3	.19657458	-.11903529	-.17428709	-.09079667
110	482	3	.16653629	-.07862111	-.21308030	-.09871429
111	492	3	.14673245	-.03081337	-.24320495	-.09020804
112	179	3	-.12959133	-.13249571	-.05451726	-.15806327
113	146	3	-.09149046	-.10489276	-.01200118	-.09220692
114	192	3	-.01276552	-.04881904	.05534805	.01505602
115	200	3	.05041689	-.00761593	.09728799	.08768022
116	298	3	.04854809	.00053945	.17047962	.13847148
117	350	3	.02204827	-.01357051	.12591652	.09233183
118	398	3	.03575207	-.04810566	.03476092	.01738383
119	819	3	.01923804	-.13466213	.05144788	-.04667652
120	816	3	-.01784782	-.15997055	.16658244	-.01782858
121	470	3	-.06385698	-.12879706	.22720319	.01602978
122	810	3	-.10788879	-.09104178	.27201068	.04673463
123	808	3	-.13756644	-.02187758	.26089465	.07354700
124	806	3	-.18103623	.09146276	.23548655	.11603053
125	804	3	-.22879852	.22678926	.20049343	.16617925
126	803	3	-.25456781	.30159612	.18143167	.19432890
127	801	3	-.28718616	.39730912	.15605924	.23002607
128	531	3	-.31337517	.48317270	.12344674	.25833757
129	893	3	-.11402739	-.19064620	-.04512319	-.23269072
130	887	3	-.01742587	-.13557228	.03060034	-.10913487
131	940	3	-.11524450	-.25389473	-.05421977	-.32435326
132	937	3	-.00569103	-.19566600	.02436412	-.19199917
133	1023	3	.18238121	-.00516321	.07556574	.06243006
134	878	3	.03545081	-.00568157	.25627113	.16473184
135	876	3	.00098898	-.01017987	.27528148	.16374581
136	928	3	.01811060	-.01125684	.36998394	.21009401
137	926	3	-.01742388	-.01554512	.38655739	.20809610
138	1063	3	-.05850051	-.04247857	.02479944	-.03039929

Table 8-5.—(Continued)

Row	Node	DOF	Mode 13	Mode 14	Mode 15	Mode 16
139	916	3	-.17887104	-.20571588	.47480266	.05706309
140	915	3	-.20634975	-.19919865	.54775514	.08515249
141	908	3	-.28236461	-.04946303	.53424341	.14646718
142	906	3	-.34510433	.08321714	.53945961	.20905212
143	904	3	-.41751699	.24589952	.54308477	.28643447
144	902	3	-.51885955	.45572660	.58350851	.40075095
145	920	3	-.64732918	.69062410	.68867465	.55213062
146	900	3	-.72260330	.84361874	.72894279	.64003448
147	1021	3	.28142753	.00493308	.05489410	.05133770
148	1061	3	-.18699030	-.00828048	.02866859	-.06481671
149	965	3	-.35642956	-.27232991	.91674528	.16762169
150	957	3	-.38400692	.00333081	.67183665	.21397285
151	954	3	-.50814259	.25446598	.70890739	.34433771
152	951	3	-.72326362	.65567504	.86248982	.59224598
153	950	3	-.90567692	1.00000000	1.00000000	.80812993
154	767	3	.52907024	-.07472940	-.69363328	-.23657218
155	766	3	.53742385	-.09075351	-.74083624	-.26337096
156	763	3	.53389666	-.09720975	-.77712148	-.28358805
157	762	3	.52065405	-.09290322	-.80201006	-.29517465
158	759	3	.49456965	-.07540071	-.80880154	-.29403306
159	758	3	.45595777	-.04430052	-.79998096	-.28091487
160	755	3	.40329189	.00395059	-.77269988	-.25258975
161	754	3	.33101874	.07001927	-.71467945	-.20473236
162	751	3	.24990084	.14474835	-.63856902	-.14605776
163	750	3	.15013182	.24080625	-.54355128	-.07129998
164	237	2	-.01266667	-.02903524	-.02391732	-.03291976
165	235	2	-.09035194	-.04201457	.11575796	.00278865
166	232	2	-.15010279	-.13179288	.27435798	-.00377340
167	229	2	-.04455445	-.07087593	.19617423	.02142699
168	227	2	.10088888	.02711546	.04706272	.05063994
169	226	2	.29230981	.16375895	-.16656816	.08872054
170	475	2	.01662461	-.03299733	-.07738317	-.05578317
171	285	2	-.06689710	-.04775793	.06440616	-.02117931
172	282	2	-.13411399	-.11426405	.23083528	-.00996888
173	472	2	-.01925615	-.03852163	-.03523697	-.05496888
174	332	2	-.10158005	-.07860914	.14178428	-.02279363
175	329	2	-.01929041	-.04269644	.11979549	.00779115
176	277	2	.11462121	.04269220	.00481663	.04317102
177	862	2	-.06373098	-.03825548	.02584057	-.04632840
178	379	2	.03310995	.01657949	-.04328920	-.02227680
179	377	2	.15374334	.08788343	-.12020989	.01991603
180	376	2	.27420415	.16629174	-.21604898	.05962368
181	375	2	.40590024	.25363202	-.32369979	.10360425
182	428	2	.16734592	.13865149	-.32909622	-.05138320
183	427	2	.21086419	.15619952	-.31622485	-.01996535
184	426	2	.30836023	.20522620	-.32188333	.04088308

Figure 8-5.—(Continued)

Row	Node	DOF	Mode 13	Mode 14	Mode 15	Mode 16
185	424	2	.35144341	.22660058	-.32281773	.06846787
186	417	2	.24142314	.19528592	-.43609072	-.04792090
187	416	2	.34920973	.25367700	-.45922296	.61379764
188	415	2	.45901382	.31099548	-.47205682	.08110165
189	414	2	.53859339	.35967775	-.50542148	.12455367
190	374	3	-.17828794	-.26317410	.68518598	.13731578
191	374	1	.17244498	.13174555	-.42322331	-.08101973
192	471	5	.00290381	.00005904	-.00498126	-.00149332
193	3191	3	-.17955264	.24651244	.58932502	-.66928167
194	3189	3	-.05128146	.05109845	.11887436	-.12346889
195	3187	3	.03081711	-.06813932	-.16162028	.20130496
196	3185	3	.07793900	-.12874811	-.29328659	.35396242
197	3181	3	.08777368	-.12127411	-.23909920	.29667197
198	2038	3	.06369512	-.06668724	-.10679330	.13224041
199	2098	3	.03675480	-.01502127	.01139453	-.01239671
200	2158	3	.00426401	.04719317	.10584405	-.15458765
201	2218	3	-.02762078	.10044140	.17027385	-.25956192
202	2278	3	-.05082759	.13382366	.17754949	-.29784319
203	2338	3	-.05250881	.13863004	.14962921	-.27098374
204	2398	3	-.06028537	.10986807	.09790052	-.17957963
205	2458	3	-.03877159	.04543321	.01970580	-.02205019
206	2518	3	-.00287003	-.02569569	-.05709826	.14239036
207	2578	3	.03720848	-.06872212	-.10578645	.25670623
208	2638	3	.06944901	-.05120092	-.10530603	.27689290
209	2698	3	.07284887	-.01763532	-.09130435	.26882891
210	2758	3	.04931028	.03489721	-.07333478	.24139917
211	2818	3	.00830457	.06027264	-.05676146	.19384123
212	2878	3	-.05337189	.04547464	-.05381825	.14317697
213	2938	3	-.10110914	-.01302872	-.05322039	.04683089
214	2998	3	-.12458760	-.08671029	-.05696500	-.08076802
215	3058	3	-.15060331	-.15397638	-.08160342	-.22983502
216	3201	3	-.18416561	-.24209501	-.13437624	-.45716645
217	3205	3	-.05333384	-.11370757	-.06903447	-.25425789
218	3208	3	.12816852	.14375191	.06569917	.26217085
219	3212	3	.36939602	.50323490	.25603937	1.00000000
220	3250	5	-.00166304	-.00254184	-.00135529	-.00527733
221	3250	3	.24930868	.32966533	.16449935	.64867219
222	3225	3	.12970510	.14436201	.06580711	.26174327
223	3225	5	-.00135705	-.00196264	-.00103146	-.00397007
224	3183	3	.09274320	-.13785742	-.29324192	.35697196
225	3203	3	-.15466787	-.23596574	-.13135565	-.47909433
226	410	4	-.00030266	.00006484	.00010380	-.00015613
227	410	5	.00423859	-.00035936	.00095892	-.00336652
228	410	3	.62447487	.05687475	.10929934	-.32130819

ORIGINAL PAGE IS
OF POOR QUALITY

Table 8-5.—(Continued)

Row	Node	DQF	Mode 17	Mode 18	Mode 19	Mode 20
1	1020	1	-.02314168	.04478124	-.03951053	-.04928244
2	1020	2	.01575665	.01438086	.00120003	-.02248158
3	1020	3	-.02276216	-.00370230	.01073736	.01544605
4	1020	4	.00046649	.00045998	.00000512	-.00049870
5	1020	5	.00045798	.00001492	-.00041502	-.00035788
6	1020	6	.00001332	.00000054	-.00000298	-.00001028
7	1070	1	.01258850	.00809172	-.04396339	-.03846238
8	1070	2	-.13712158	-.03123729	-.00099305	.08143452
9	1070	3	.02015366	-.03405190	.01849936	.02956109
10	1070	4	-.00192479	-.00013747	-.00008309	.00092424
11	1070	5	-.00000350	.00080869	-.00040358	-.00076047
12	1070	6	-.00004246	-.00002376	.00000781	.00004538
13	670	3	-.01957339	-.18369989	-.05196679	-.05718703
14	663	3	-.00392009	.02504426	.00505913	.02039269
15	652	3	.03423388	-.04503851	-.08954375	-.05963992
16	644	3	-.00072927	.10585896	-.02197266	.05695571
17	637	3	.06671431	.17524311	-.02468738	-.04650415
18	792	3	.03100699	-.17204478	.03475469	-.01549524
19	784	3	.00996895	-.29862127	.06492232	.00000205
20	779	3	.11758510	-.40304965	.10277053	.06280362
21	775	3	.25908314	-.48905080	.14269749	.16530387
22	620	3	-.01892095	-.17590867	-.04954884	-.05439336
23	618	3	-.01657661	-.12869158	-.03724262	-.03703169
24	615	3	-.01264585	-.07103760	-.02107053	-.01497703
25	613	3	-.00388726	.02454393	.00567053	.01987076
26	610	3	.00735638	.09569898	.02098589	.03711995
27	608	3	.02120934	.11813924	.01209141	.02364172
28	605	3	.03053944	.07018697	-.02459979	-.01375762
29	603	3	.03238965	.00165837	-.06007179	-.04334397
30	600	3	.02339508	-.11526088	-.10575856	-.06191079
31	597	3	.00377929	-.09703767	-.07950427	-.00939242
32	692	3	-.01821320	-.16739078	-.04689937	-.05130991
33	693	3	-.01574500	-.11993951	-.03460255	-.03416121
34	694	3	-.01208652	-.06751432	-.01958341	-.01438150
35	562	3	-.00387915	.02354446	.00625817	.01915614
36	560	3	.00590624	.08738648	.02146453	.03508088
37	695	3	.01862881	.10961484	.01445828	.02342526
38	555	3	.02693711	.07229967	-.01500658	-.00794677
39	553	3	.02993570	.00883210	-.04920214	-.03920867
40	550	3	.02065950	-.11737024	-.09723691	-.06247849
41	547	3	-.00010957	-.10051682	-.06677618	-.00633977
42	544	3	-.00653826	.10141387	.00204731	.05831355
43	541	3	.01451502	.28200897	.01016914	.05597476
44	539	3	.04279940	.30947807	-.01321151	.01023262
45	537	3	.06316822	.16813690	-.02684190	-.04541400
46	536	3	.05803698	.04070987	-.01400850	-.05182945

Table 8-5.—(Concluded)

Row	Node	DOF	Mode 17	Mode 18	Mode 19	Mode 20
47	534	3	.04704685	-.07521295	.01053099	-.03729131
48	476	3	.03277506	-.14217048	.02633744	-.02417640
49	716	3	.01280241	-.17147276	.03260668	-.02481128
50	713	3	-.00218542	-.19529333	.03772610	-.02519672
51	712	3	-.01155143	-.22112582	.04368134	-.02283390
52	709	3	-.01213692	-.24850578	.05081452	-.01627044
53	708	3	.00066910	-.28055112	.06056607	-.00376078
54	705	3	.03211017	-.31767708	.07349002	.01675592
55	704	3	.08330629	-.34924467	.08725514	.04746624
56	701	3	.14595625	-.37603201	.09982766	.08548393
57	700	3	.23047380	-.40044947	.11824884	.14395401
58	533	3	.31363622	-.43078660	.13741391	.20955402
59	85	3	-.01272855	-.07709415	-.02213656	-.01817337
60	82	3	-.00586951	.01182673	.00515035	.01666129
61	79	3	.00613033	.10633447	.03464464	.04439944
62	129	3	.00881825	.11847674	.03366610	.04662740
63	76	3	.01105629	.09208550	.02861365	.02396634
64	176	3	.02017791	.10215992	.01271499	.01576865
65	73	3	-.01322219	.06302799	.02116973	.00088405
66	173	3	.02568540	.05132249	-.01221402	-.02345622
67	50	3	-.00418344	-.00618056	.02165570	.00196040
68	120	3	.00158361	-.04384866	-.00314621	-.01935008
69	220	3	.01609800	-.12471033	-.07780291	-.07115745
70	67	3	.06918307	.16786183	.00015161	-.08017127
71	167	3	-.01293836	-.08751595	.02267785	-.00989969
72	267	3	-.00598396	-.16505605	-.06685801	-.01640827
73	44	3	-.02259471	-.04850885	.02309531	.00812358
74	114	3	-.08729028	-.21881570	1.00000000	-.42066354
75	214	3	-.03468139	.00594604	.10323190	.05545586
76	314	3	-.01546465	.07793524	.02990067	.06202030
77	41	3	-.02734301	-.06142715	.01455117	.00877400
78	111	3	-.02606613	-.02795274	.03239479	.01085666
79	211	3	-.02407637	.06948519	.05166797	.03455093
80	311	3	-.00470186	.20357301	.03276654	.05320158
81	58	3	-.02525702	-.06863112	-.02345279	.00542483
82	158	3	-.00989067	.00014026	-.02514037	-.00229734
83	209	3	-.00895481	.06801361	-.00870325	.00732736
84	309	3	.01584940	.20836581	-.01036528	.01105452
85	409	3	.03567001	.29109192	-.01219235	.01224001
86	207	3	.01365425	.03965221	-.04966261	-.02402328
87	307	3	.04090211	.13989558	-.05113199	-.04263004
88	407	3	.05601383	.18532711	-.04246260	-.04684052
89	55	3	-.00520185	-.08025298	-.07015109	-.01459713
90	155	3	.02273709	-.02379395	-.07504920	-.03575273
91	205	3	.03652762	.01348661	-.06930129	-.04499690
92	305	3	.05477346	.08357541	-.06012707	-.07125362

Table 8-5.—(Continued)

Row	Node	DOF	Mode 17	Mode 18	Mode 19	Mode 20
93	405	3	.04943518	.08476835	-.04412089	-.08286793
94	385	3	.04153172	.02566135	-.01969190	-.05975964
95	454	3	.02995352	.03136798	-.02285730	-.06009654
96	464	3	.01384980	-.04556889	-.00103869	-.05235055
97	474	3	-.00690847	-.10108077	.01302373	-.04202014
98	484	3	-.02050913	-.15123268	.02491092	-.03552650
99	493	3	-.03093804	-.12624831	.01815375	-.04316890
100	502	3	.03358324	-.12005919	.02174872	-.02819984
101	512	3	.14065381	-.23651802	.06533929	.06124298
102	522	3	.24482552	-.32897421	.10336367	.15229917
103	52	3	-.00311401	-.06575598	-.05248584	-.00068108
104	152	3	.02258459	-.03038686	-.05767907	-.02171911
105	202	3	.03683993	-.00081990	-.04660094	-.03271543
106	302	3	.06422342	.04595413	-.03657516	-.06428578
107	382	3	.01369901	.04039434	-.02146026	-.04422853
108	452	3	-.02491742	.03421439	-.01975497	-.04853637
109	462	3	-.07523351	.05206244	-.02900422	-.07750271
110	482	3	-.07915311	.03234099	-.02808410	-.10300105
111	492	3	-.04333754	-.02214106	-.01166108	-.08441470
112	179	3	-.00634560	-.04503022	-.02280625	.01039762
113	146	3	-.00719866	-.04403810	-.02598870	.01083724
114	192	3	-.00388385	-.02995496	-.02464586	.00768187
115	200	3	.01035961	-.00411435	-.01740841	-.00863843
116	298	3	.06609987	.01134395	-.00427153	-.03258396
117	350	3	.07522431	-.00871447	.01111487	-.01363498
118	398	3	.02051598	-.00576535	.00523963	.00306903
119	819	3	-.11990128	.12423265	-.04223689	-.05869107
120	816	3	-.19333078	.27004640	-.09406688	-.16263000
121	470	3	-.18800469	.29470218	-.10148274	-.18035041
122	810	3	-.16826261	.30131451	-.10270909	-.17872523
123	808	3	-.10720557	.24373051	-.08248784	-.14010893
124	806	3	.00347833	.12873141	-.04057580	-.05561924
125	804	3	.14450076	-.02413450	.01631698	.06294697
126	803	3	.22499736	-.11191456	.04948324	.13386657
127	801	3	.32825228	-.22538786	.09228491	.22497116
128	531	3	.41948375	-.33152368	.13109089	.30277751
129	890	3	-.01601958	-.06841026	-.02598131	.03792002
130	887	3	-.02420429	-.07034362	-.02614968	.04726245
131	940	3	-.02627670	-.09176550	-.02713632	.06435632
132	937	3	-.03912744	-.09808932	-.02589195	.07839694
133	1023	3	-.03927682	-.00800315	.02449093	.03012404
134	878	3	.09482280	-.03979848	.05364738	.02065009
135	876	3	.13559093	-.07855344	.09217504	.05350108
136	928	3	.14870891	-.10926209	.13483130	.09054382
137	926	3	.19033249	-.14905768	.17406809	.12451577
138	1063	3	-.00050147	-.04580522	.02571578	.04931008

Table 8-5.—(Continued)

Row	Node	DOF	Mode 17	Mode 18	Mode 19	Mode 20
139	916	3	-.28997833	.48966425	-.16162675	-.25997984
140	915	3	-.32427618	.57214724	-.19078599	-.31663536
141	908	3	-.18096525	.42134510	-.13540188	-.20555098
142	906	3	-.05297249	.31231688	-.09329804	-.11621031
143	904	3	.11947787	.15335381	-.02959407	.03944295
144	902	3	.35863325	-.05005848	.05950055	.27723069
145	921	3	.64430356	-.25884476	.16281610	.59646445
146	900	3	.82523386	-.40670733	.23052487	.78876679
147	1021	3	-.07341456	-.00522457	.05225559	.05298655
148	1061	3	.00844017	-.11487935	.05848050	.11017304
149	965	3	-.51436128	1.00000000	-.34002141	-.57673698
150	957	3	-.15437790	.45878255	-.14226646	-.19364556
151	954	3	.10650512	.24096967	-.05241367	.02724216
152	951	3	.58143513	-.11975140	.11927801	.53377257
153	950	3	1.00000000	-.43568701	.27285945	1.00000000
154	767	3	.03022781	-.16364940	.03224973	-.01856559
155	766	3	.01424025	-.19424312	.03890163	-.01541849
156	763	3	.00182663	-.22314886	.04527527	-.01401032
157	762	3	-.00337600	-.25217150	.05215317	-.01163349
158	759	3	.00217718	-.28109007	.05998169	-.00572375
159	758	3	.01978824	-.31291784	.06984774	.00593477
160	755	3	.05436470	-.34977285	.08285326	.02653347
161	754	3	.10556555	-.38435257	.09737472	.05744167
162	751	3	.16660254	-.41563534	.11265814	.09735559
163	750	3	.24914758	-.45854643	.13429090	.15799354
164	237	2	-.01715902	-.01888406	.00316538	.01390542
165	235	2	-.04224314	.05591195	-.01812872	-.00394735
166	232	2	-.17529098	.24106145	-.07941677	-.08042674
167	229	2	-.13021148	.22335079	-.07463164	-.09342177
168	227	2	-.03107078	.12989157	-.04340557	-.07764824
169	226	2	.11859368	-.02446824	.00923195	-.04295008
170	475	2	-.01887811	-.03688283	.00809554	.01892260
171	285	2	-.04718319	.03651357	-.01353785	.00298563
172	282	2	-.15308297	.20390972	-.06798144	-.06392910
173	472	2	-.03831178	-.00852605	-.00216047	.01573454
174	332	2	-.10775177	.12783700	-.04455292	-.03017210
175	329	2	-.09258789	.15226310	-.05238826	-.05895068
176	277	2	-.00960469	.08873154	-.03036948	-.05726320
177	862	2	-.05813044	.63520250	-.01641618	.00742109
178	379	2	-.01227308	-.00230515	-.00388851	.01705786
179	377	2	.05320152	-.03416659	.00851736	.00445081
180	376	2	.13436385	-.09091242	.02961188	.00152029
181	375	2	.22706152	-.15708067	.05431685	-.00139981
182	428	2	.13976213	-.25997368	.07819058	.13476393
183	427	2	.14891646	-.22827528	.06965653	.10420034
184	426	2	.18860847	-.19567175	.06292083	.05383063

Table 8-5.—(Continued)

Row	Node	DOF	Mode 17	Mode 18	Mode 19	Mode 20
185	424	2	.20556002	-.17890608	.05919977	.02977350
186	417	2	.20429656	-.34719018	.10675035	.16707108
187	416	2	.25697771	-.33347562	.10650407	.12468651
188	415	2	.30603545	-.30326870	.10116178	.06973196
189	414	2	.35859961	-.31342328	.10838376	.04373202
190	374	3	-.20836632	.33744639	-.08449058	-.14094884
191	374	1	.17457126	-.29051306	.08203183	.13218361
192	471	5	.00109917	-.00307096	.00091851	.00121918
193	3191	3	-.03327703	-.30191872	-.07222179	-.08077719
194	3189	3	-.00334647	-.01244852	-.00013820	.00227586
195	3187	3	.01323388	.13981335	.03679507	.04357733
196	3185	3	.01929994	.18404839	.04625371	.05232131
197	3181	3	.01183681	.08891571	.02117467	.02035800
198	2038	3	.00039706	-.03502521	-.01225201	-.01960256
199	2098	3	-.00831449	-.11955722	-.03359763	-.04390803
200	2158	3	-.01508515	-.17327063	-.04854976	-.05886367
201	2218	3	-.01811740	-.17950024	-.04987517	-.05662801
202	2278	3	-.01676957	-.14092109	-.03977982	-.04164325
203	2338	3	-.01225640	-.07613953	-.02114297	-.01835892
204	2398	3	-.00547834	.00021385	.00296217	.00846713
205	2458	3	.00198519	.06137398	.02373287	.02578962
206	2518	3	.00564854	.07264844	.03039212	.02278849
207	2578	3	.00369114	.04759358	.02916722	.01220391
208	2638	3	-.00491938	.00527993	.02610828	.00722699
209	2698	3	-.01444759	-.02498635	.02441217	.00791194
210	2758	3	-.02288657	-.05066208	.01935289	.00891518
211	2818	3	-.02706717	-.06705036	.00795715	.00891809
212	2878	3	-.02547601	-.07792089	-.01560027	.00709764
213	2938	3	-.01810417	-.07549984	-.03316472	.00429311
214	2998	3	-.00995906	-.05575194	-.02837054	.00596996
215	3058	3	.00211946	-.02272800	-.01286192	.00490785
216	3201	3	.02769350	.04951242	.02376450	-.00235026
217	3205	3	.02452364	.06347590	.03363735	-.00526710
218	3208	3	-.01273365	-.01942437	-.00591734	.00067507
219	3212	3	-.07015243	-.15544539	-.07309517	.01123896
220	3250	5	.00042652	.00104136	.30052310	-.00008385
221	3250	3	-.04389225	-.09511351	-.04363739	.00671732
222	3225	3	-.01224493	-.01730905	-.00459675	.00040977
223	3225	5	.00029355	.00066409	.00031907	-.00004836
224	3183	3	.01674699	.14398768	.03514700	.03738089
225	3203	3	.03615621	.08084515	.04013058	-.00572378
226	410	4	-.00002151	.00000421	.00010996	-.00000761
227	410	5	.00038482	.00069612	-.00047823	-.00003572
228	410	3	.02277987	.04342973	-.03894199	.00989365

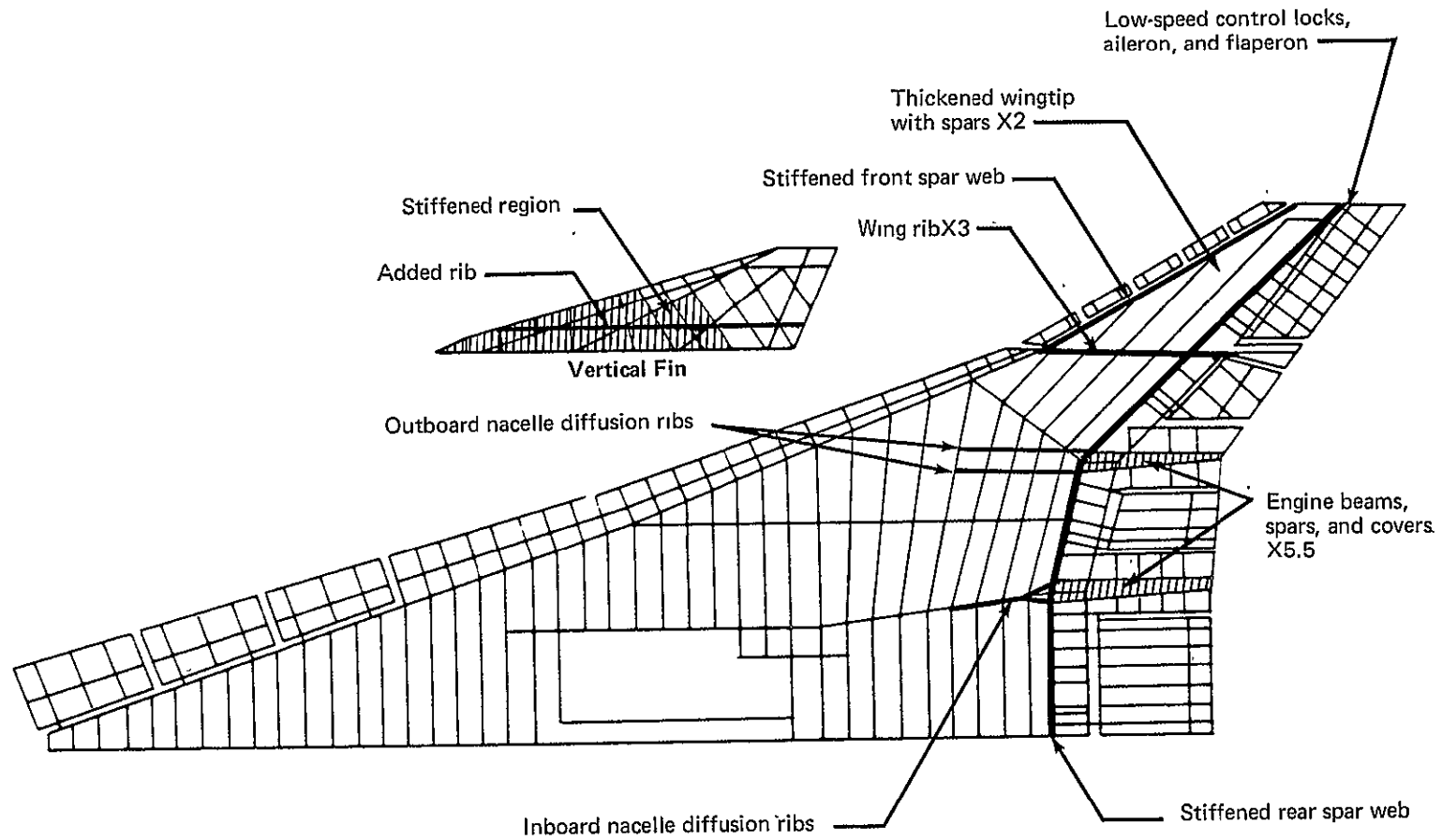


Figure 8-1.—Stiffness Constraints on Hybrid Structure “Strength-Design” from Use of Titanium Design Internal Structure

6-5

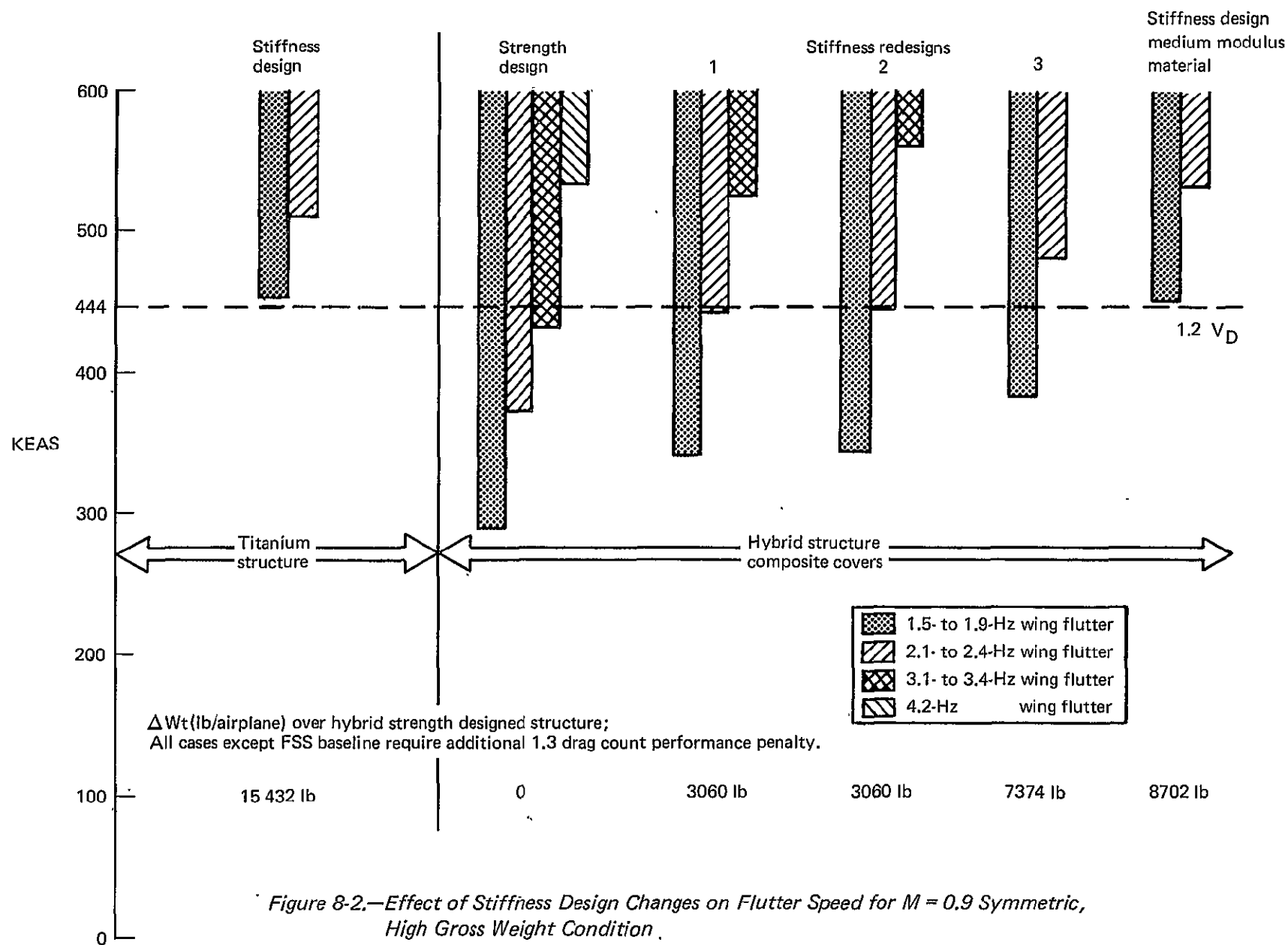


Figure 8-2.—Effect of Stiffness Design Changes on Flutter Speed for $M = 0.9$ Symmetric, High Gross Weight Condition.

Titanium "strength design"

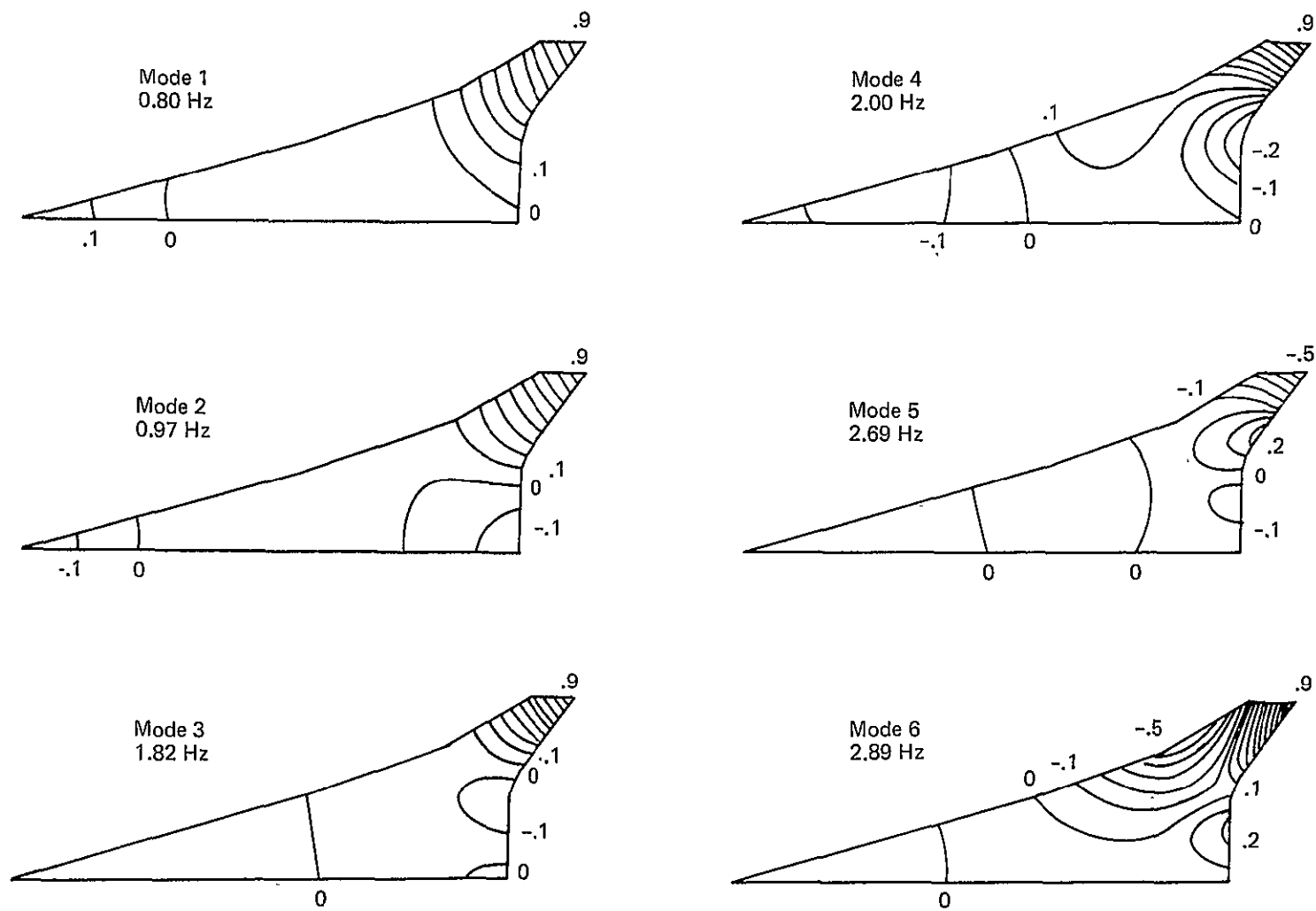


Figure 8-3.—Comparison of Wing Mode Shapes 1 Through 6, Hybrid Structure, Strength Design

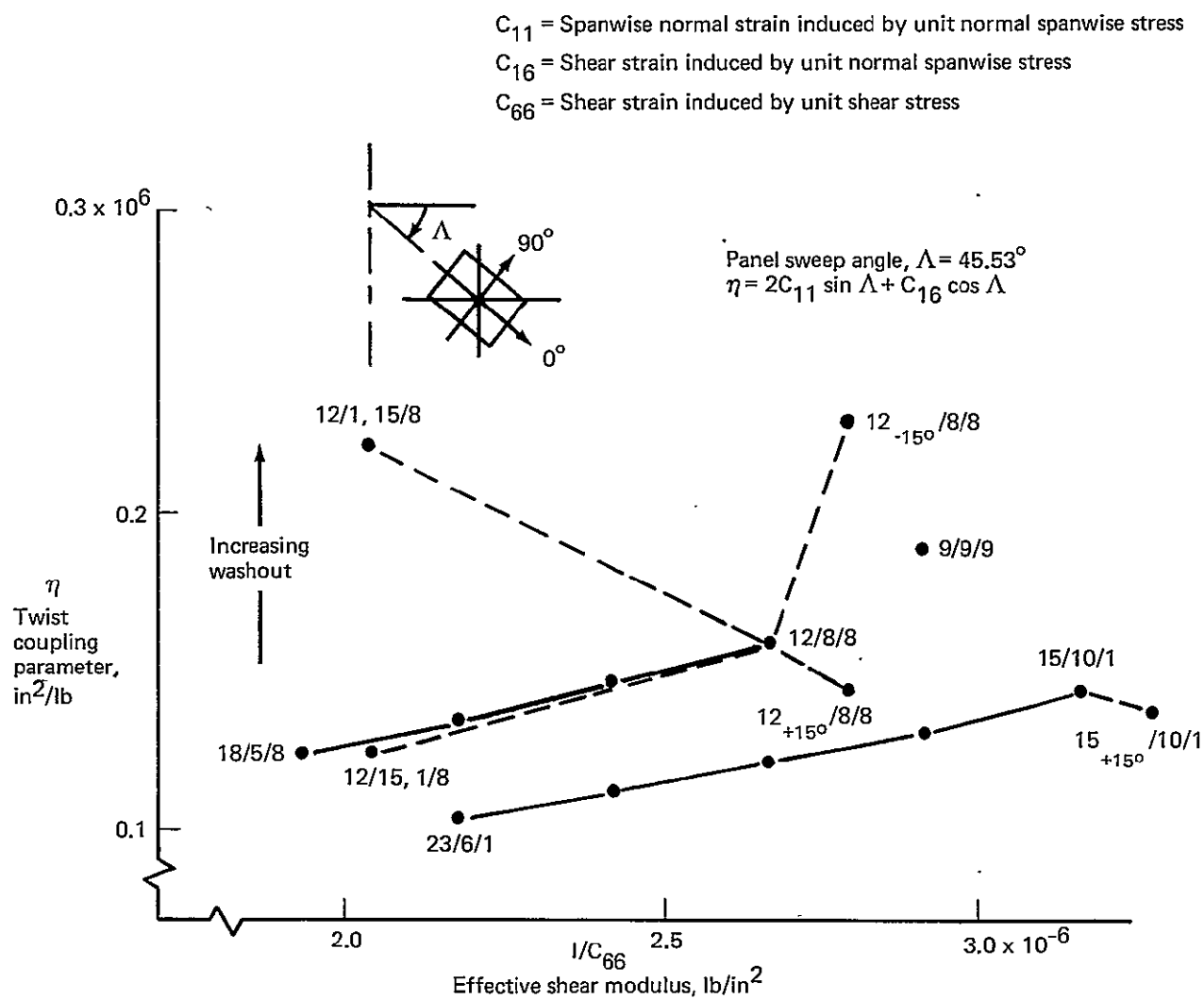


Figure 8-4.—Anisotropic Coupling Trends, High-Strength Graphite/Polyimide

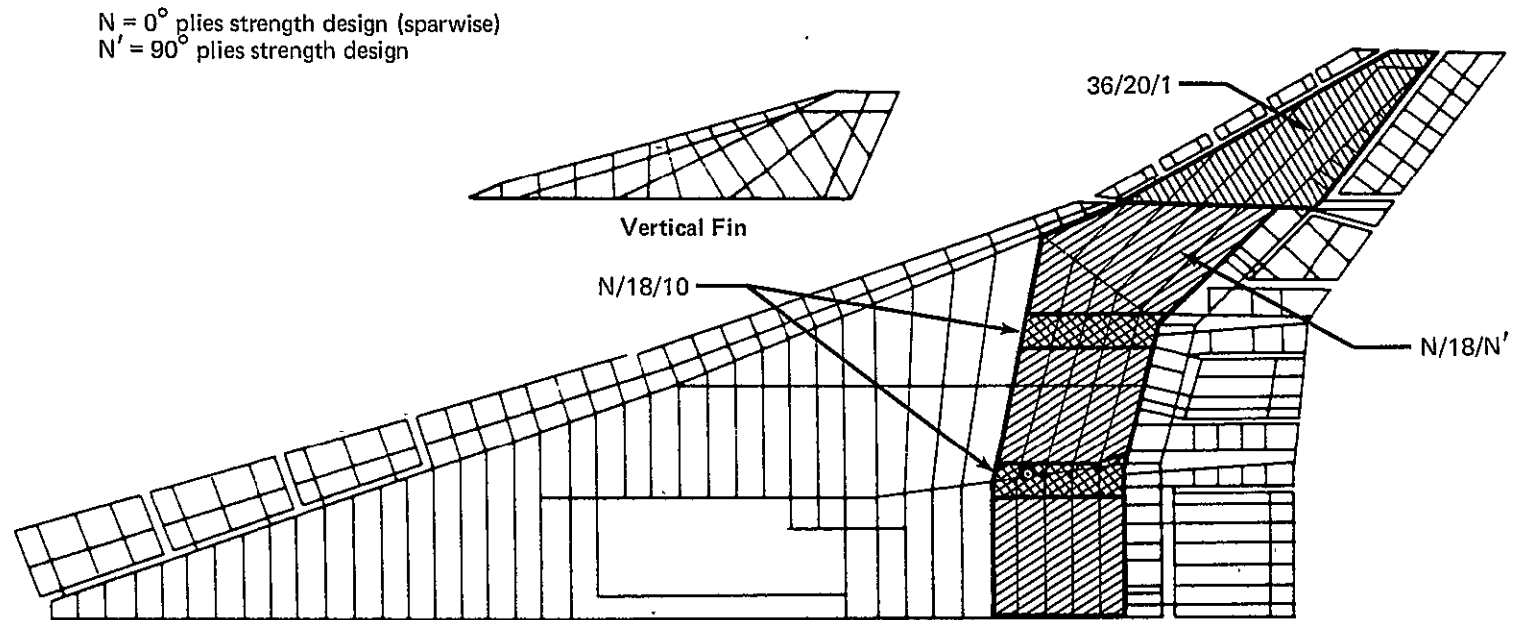


Figure 8-5.—Stiffness Designed Composite Cover Panels, Medium Modulus Graphite/Polyimide

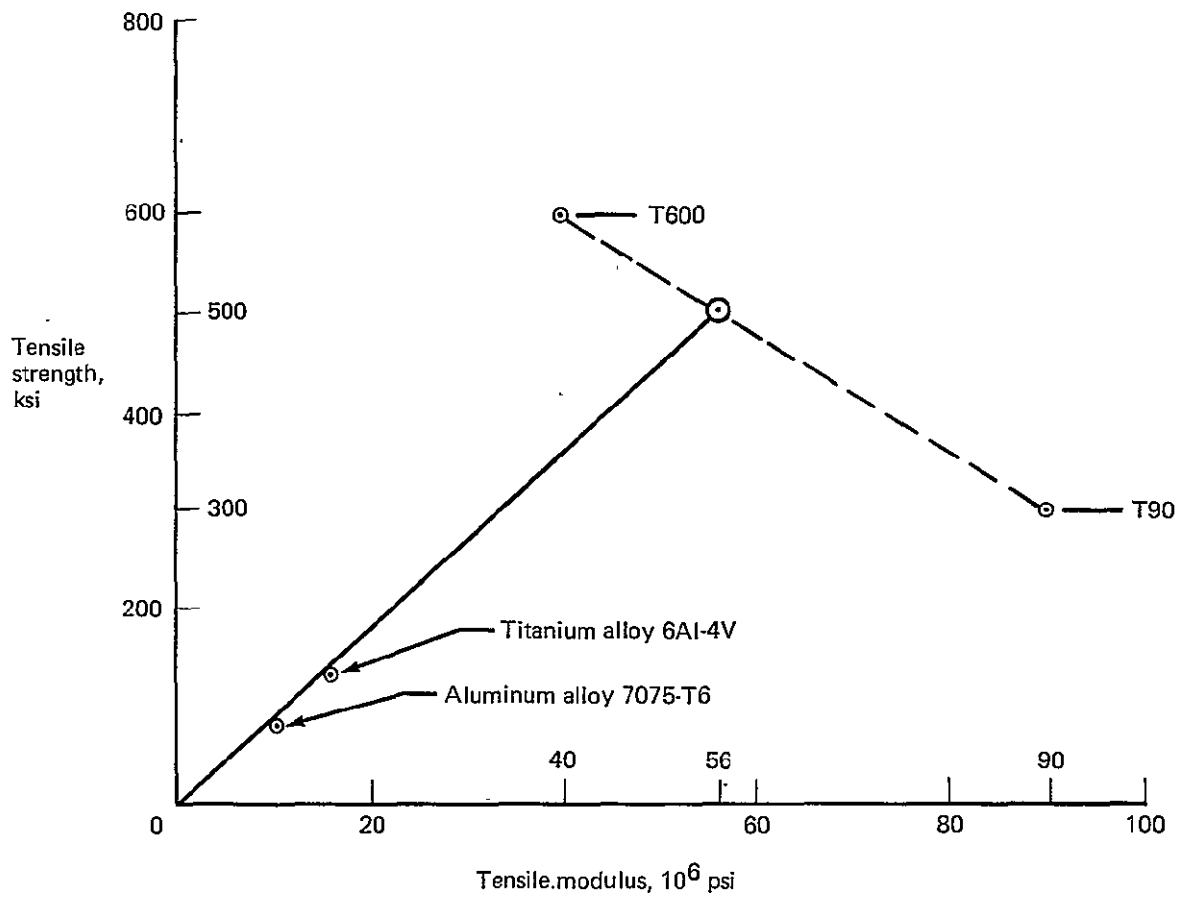


Figure 8-6.—Tailoring of Fiber Properties for Medium Modulus Graphite/Polyimide

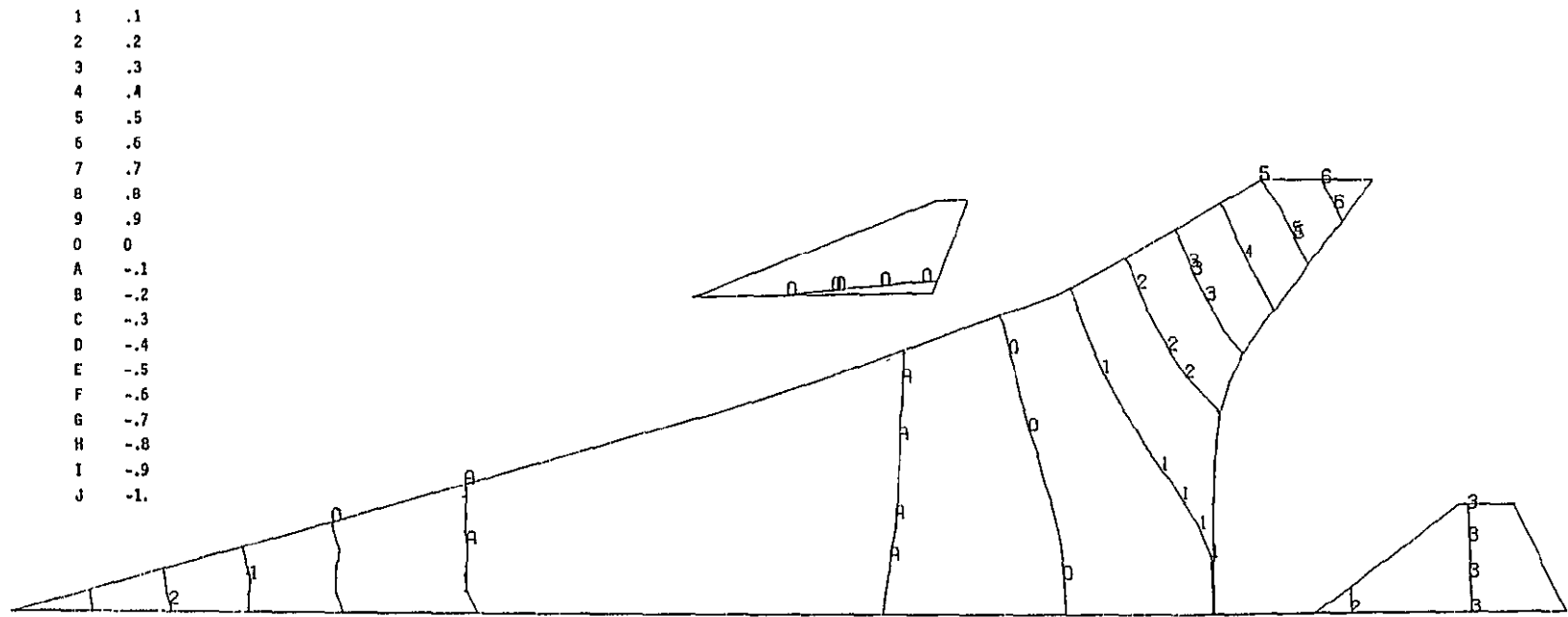


Figure 8-7.—Airplane Vibration Mode 1, Hybrid Structure Stiffness Design; Symmetric, High Gross Weight Condition, 0.867 Hz

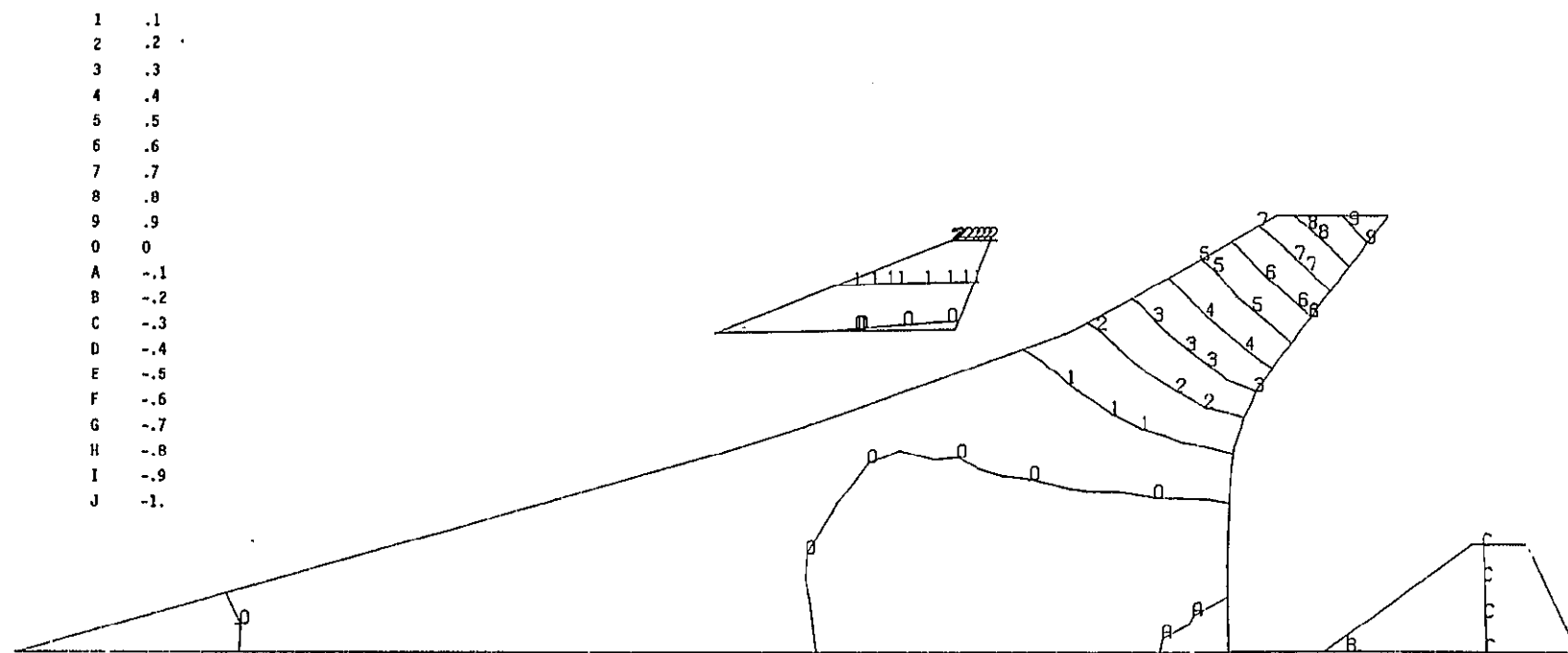


Figure 8-8.—Airplane Vibration Mode 2, Hybrid Structure Stiffness Design; Symmetric, High Gross Weight Condition, 1.141 Hz

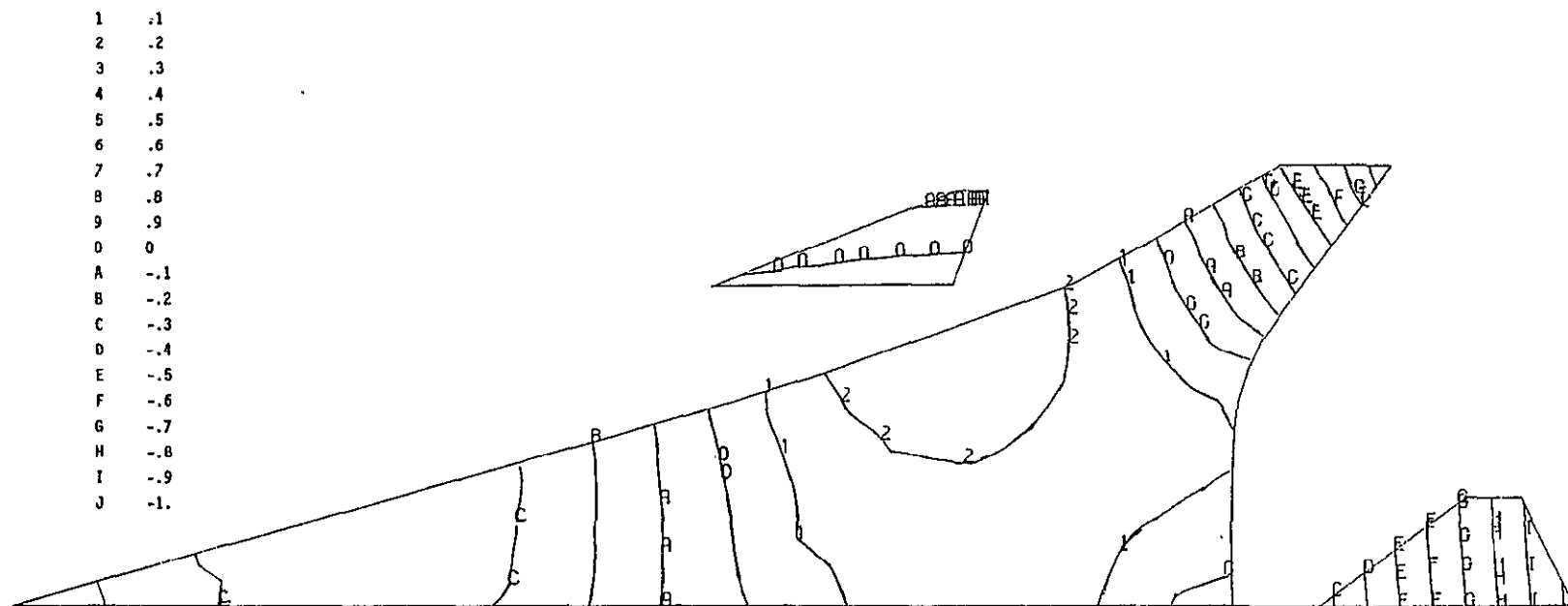


Figure 8-9.—Airplane Vibration Mode 3, Hybrid Structure Stiffness Design; Symmetric, High Gross Weight Condition, 1.915 Hz

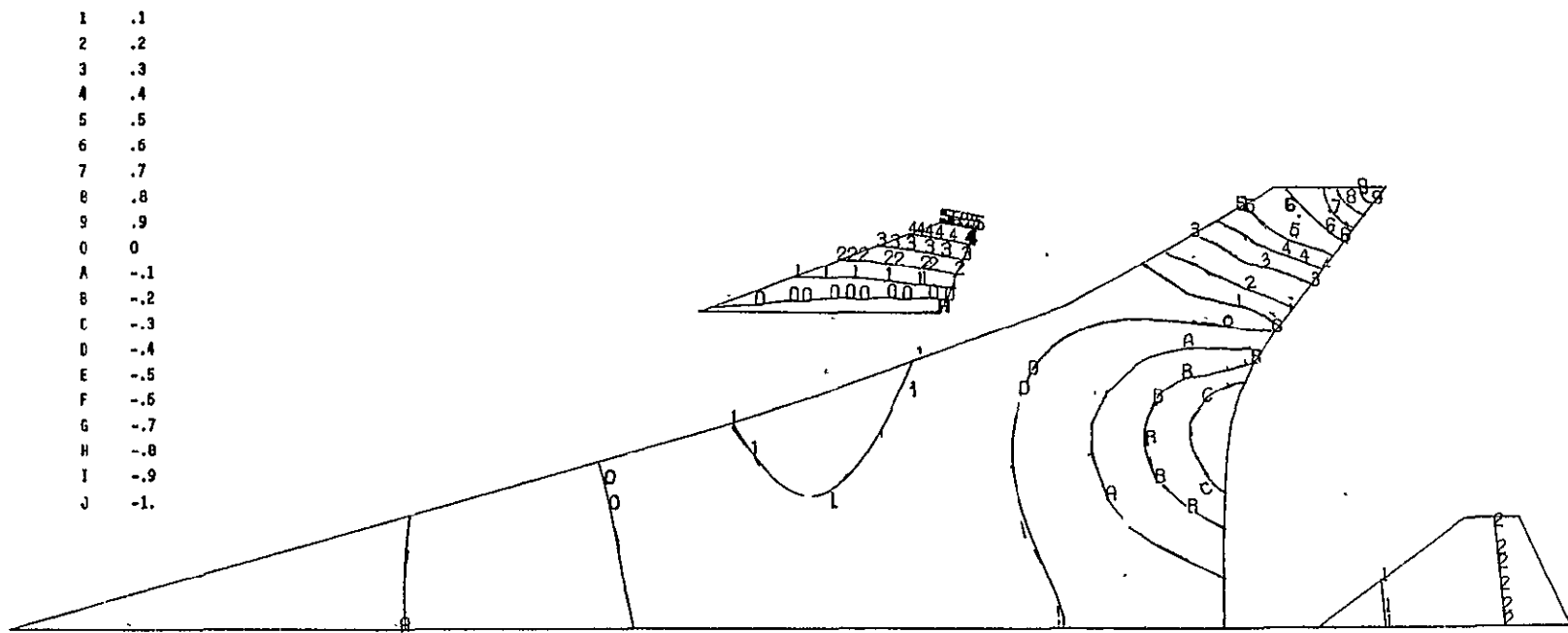


Figure 8-10.—Airplane Vibration Mode 4, Hybrid Structure Stiffness Design; Symmetric, High Gross Weight Condition, 2.487 Hz

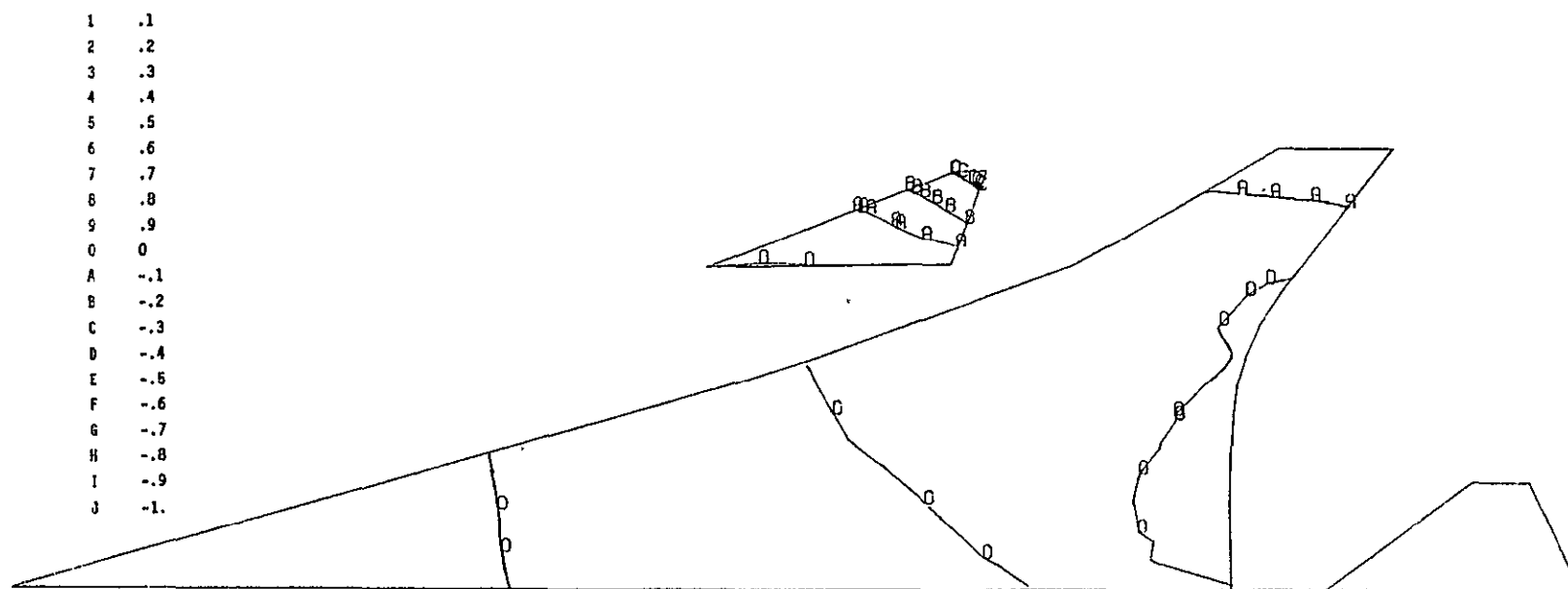


Figure 8-11.—Airplane Vibration Mode 5, Hybrid Structure Stiffness Design; Symmetric, High Gross Weight Condition, 2.929 Hz

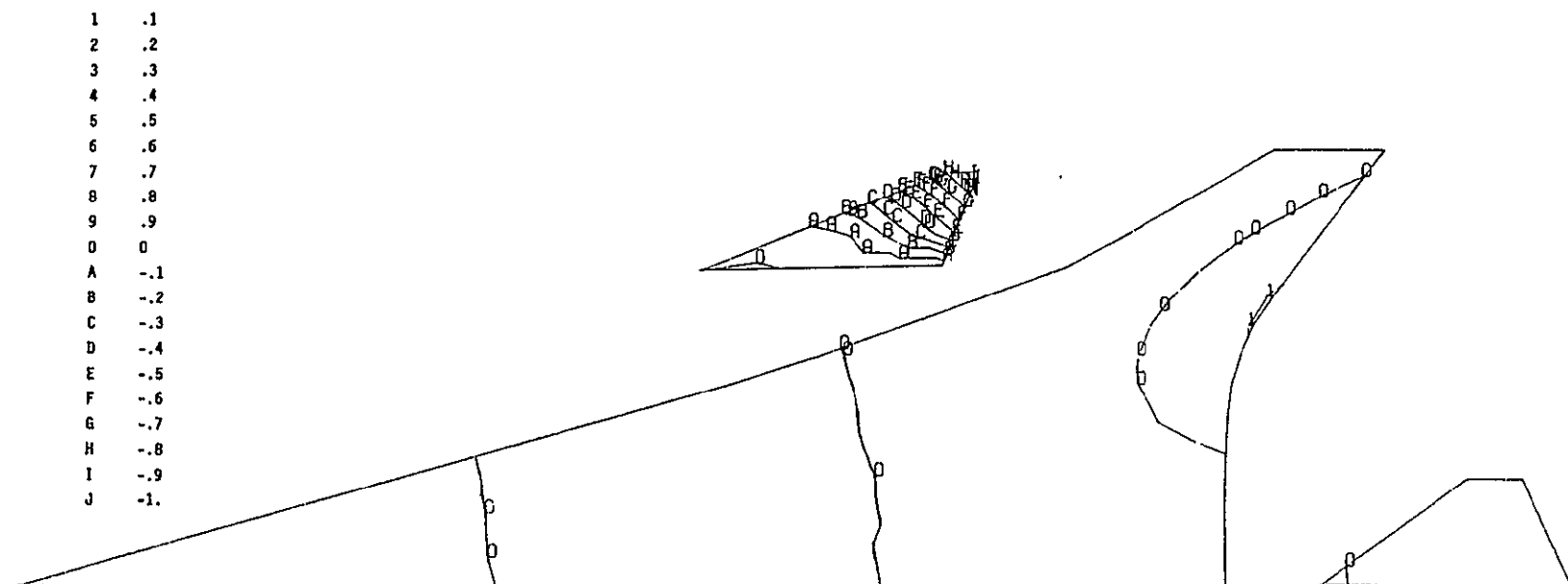


Figure 8-12.—Airplane Vibration Mode 6, Hybrid Structure Stiffness Design; Symmetric,
High Gross Weight Condition, 3.391 Hz

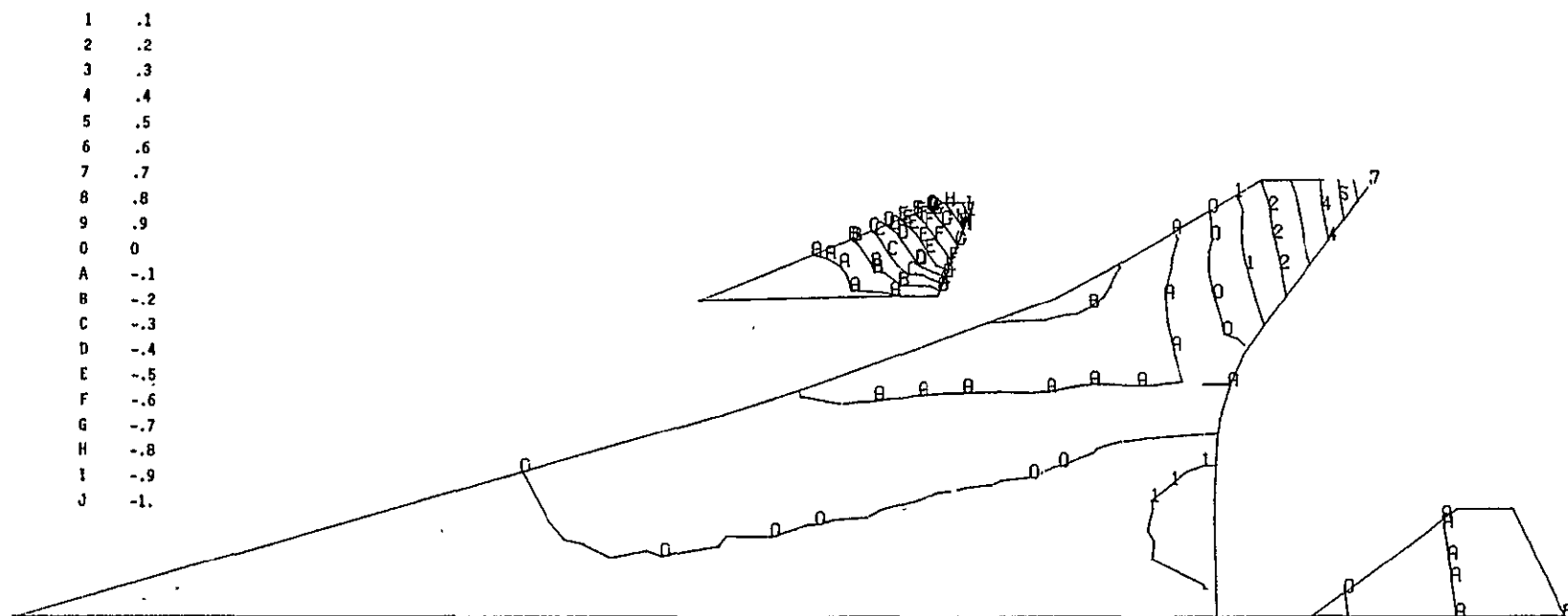


Figure 8-13.—Airplane, Vibration Mode 7, Hybrid Structure Stiffness Design; Symmetric,
High Gross Weight Condition, 3.525 Hz

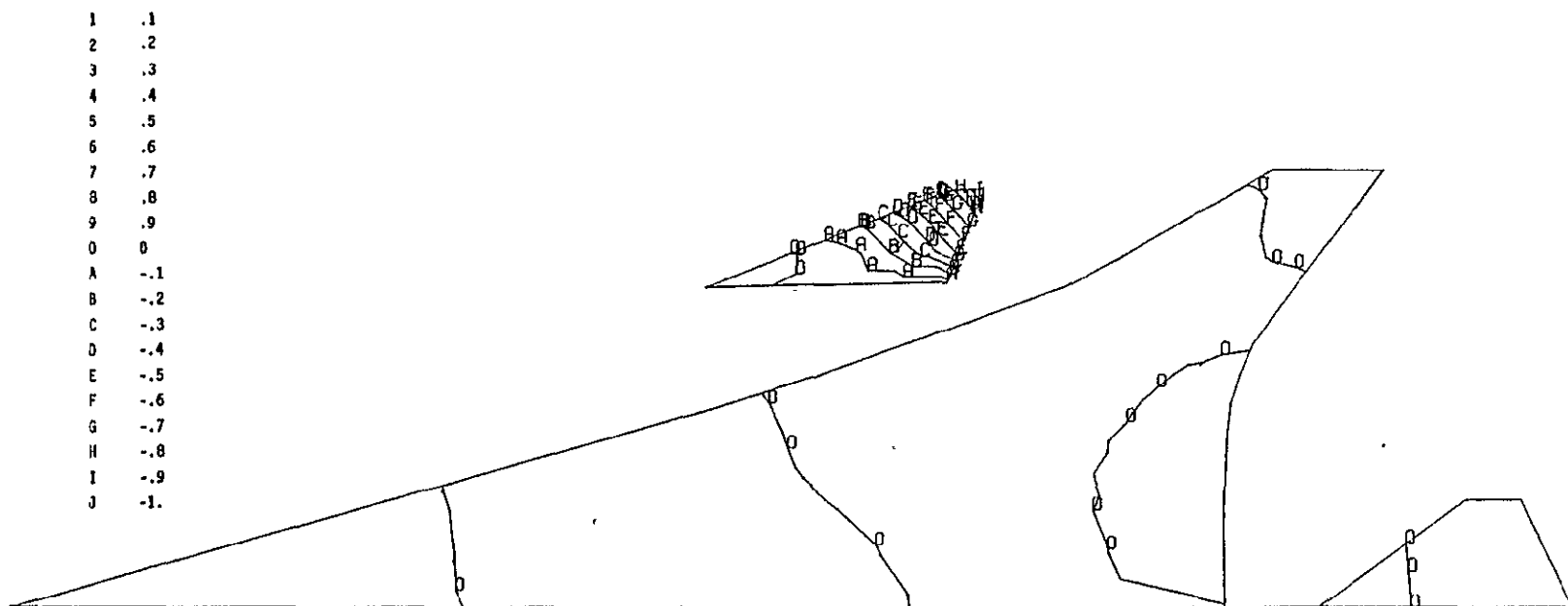


Figure 8-14.—Airplane Vibration Mode 8, Hybrid Structure Stiffness Design; Symmetric,
High Gross Weight Condition, 3.561 Hz

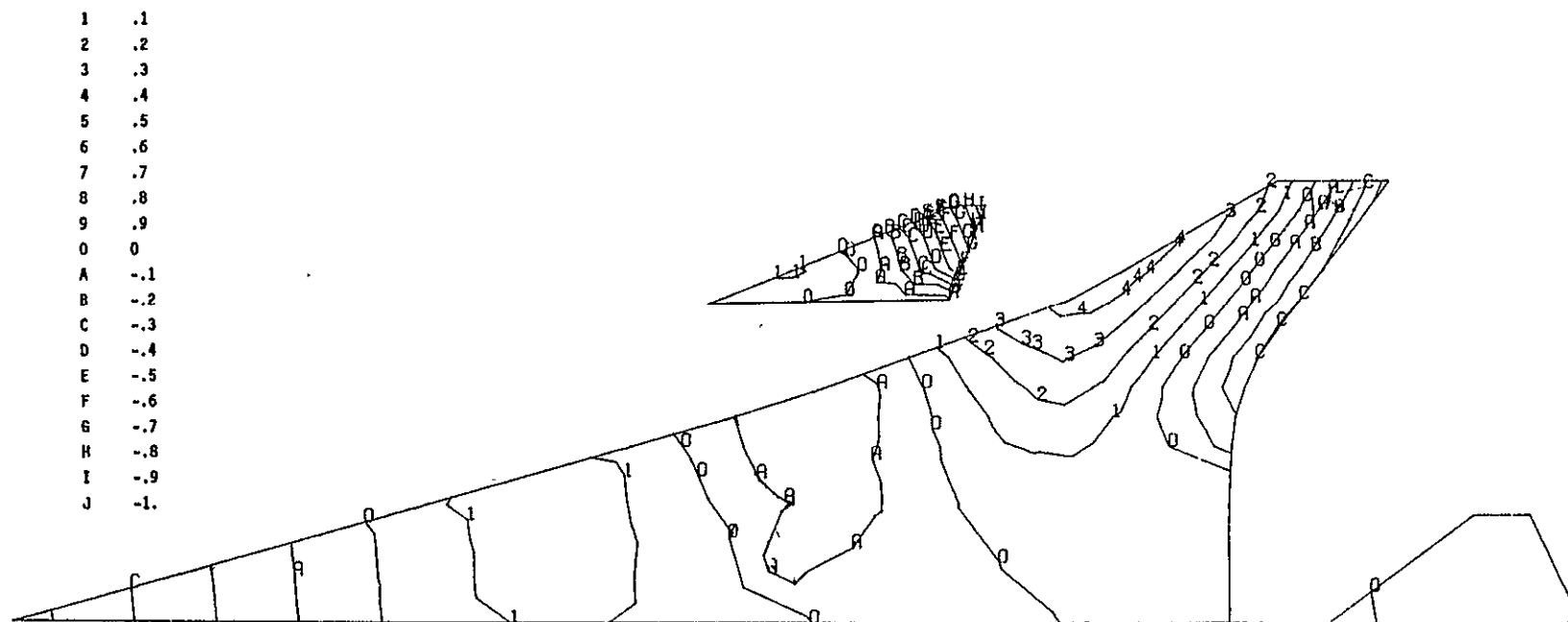


Figure 8-15.—Airplane Vibration Mode 9, Hybrid Structure Stiffness Design; Symmetric High Gross Weight Condition, 4.229 Hz

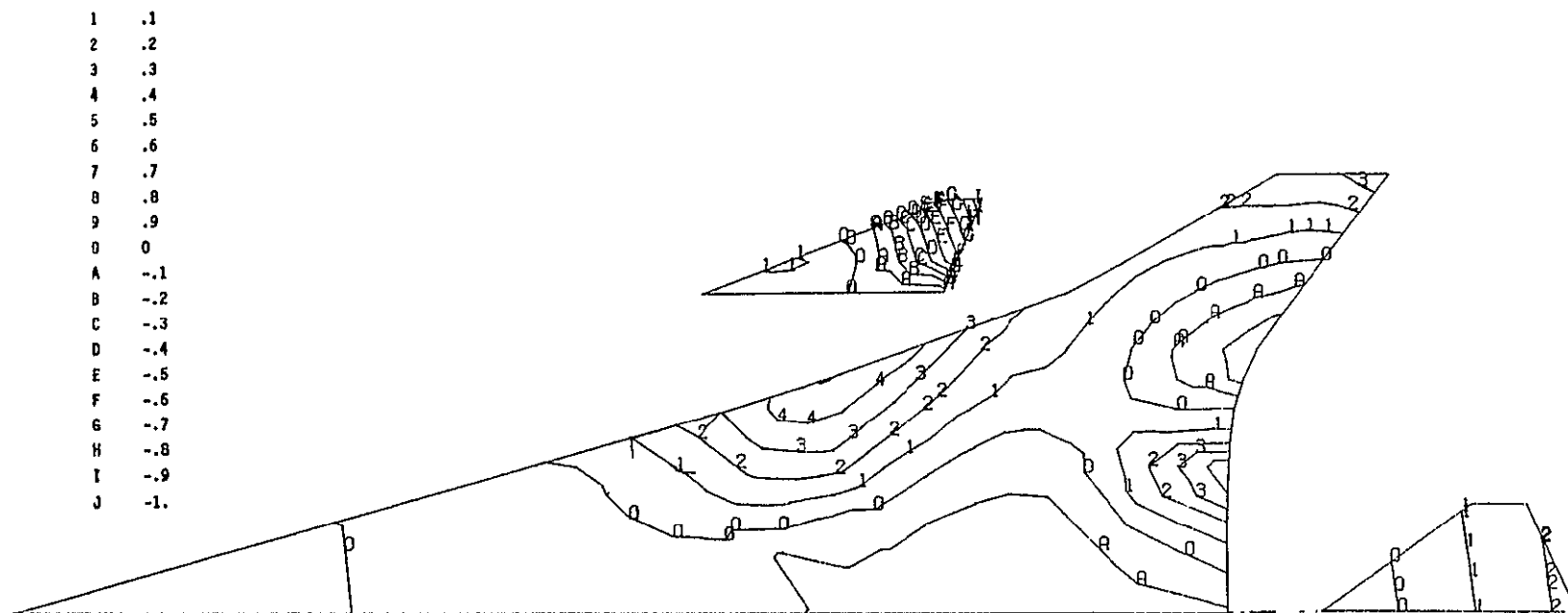


Figure 8-16.—Airplane Vibration Mode 10, Hybrid Structure Stiffness Design; Symmetric,
High Gross Weight Condition, 4.355 Hz

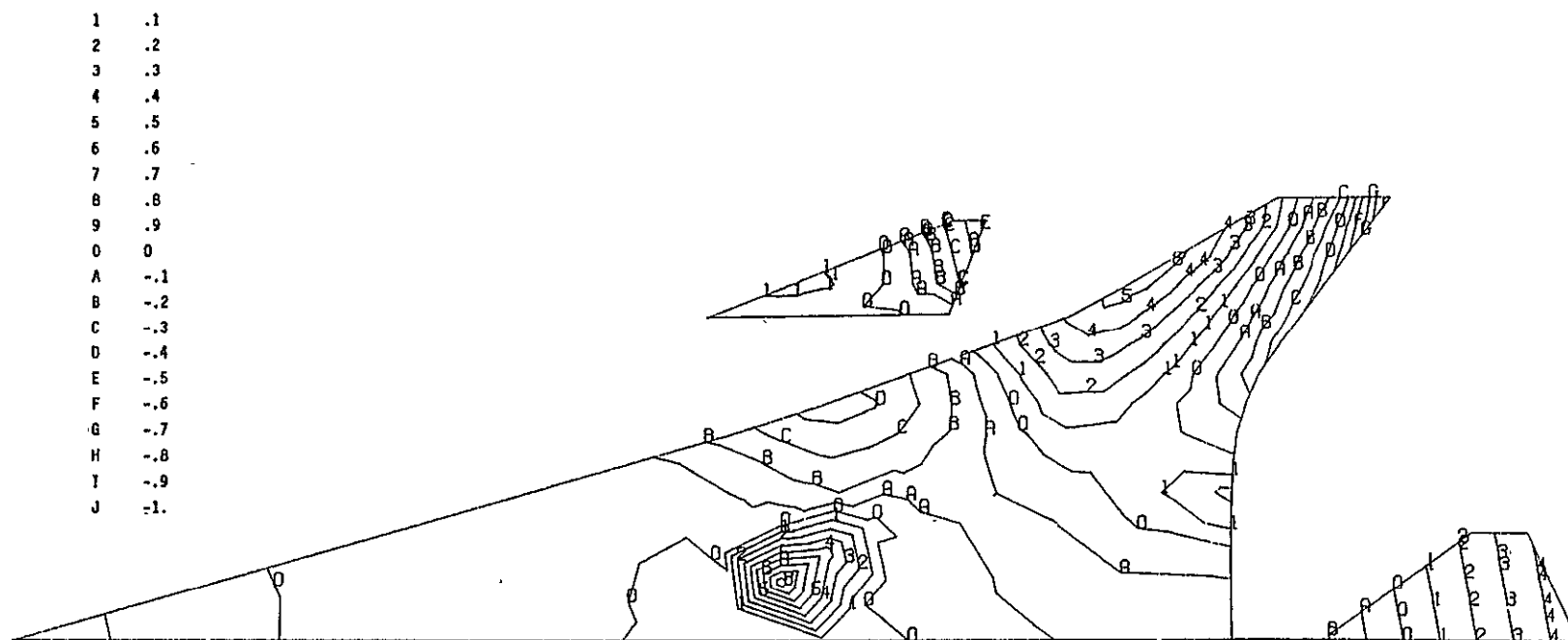


Figure 8-17.—Airplane Vibration Mode 11, Hybrid Structure Stiffness Design; Symmetric, High Gross Weight Condition, 5.090 Hz

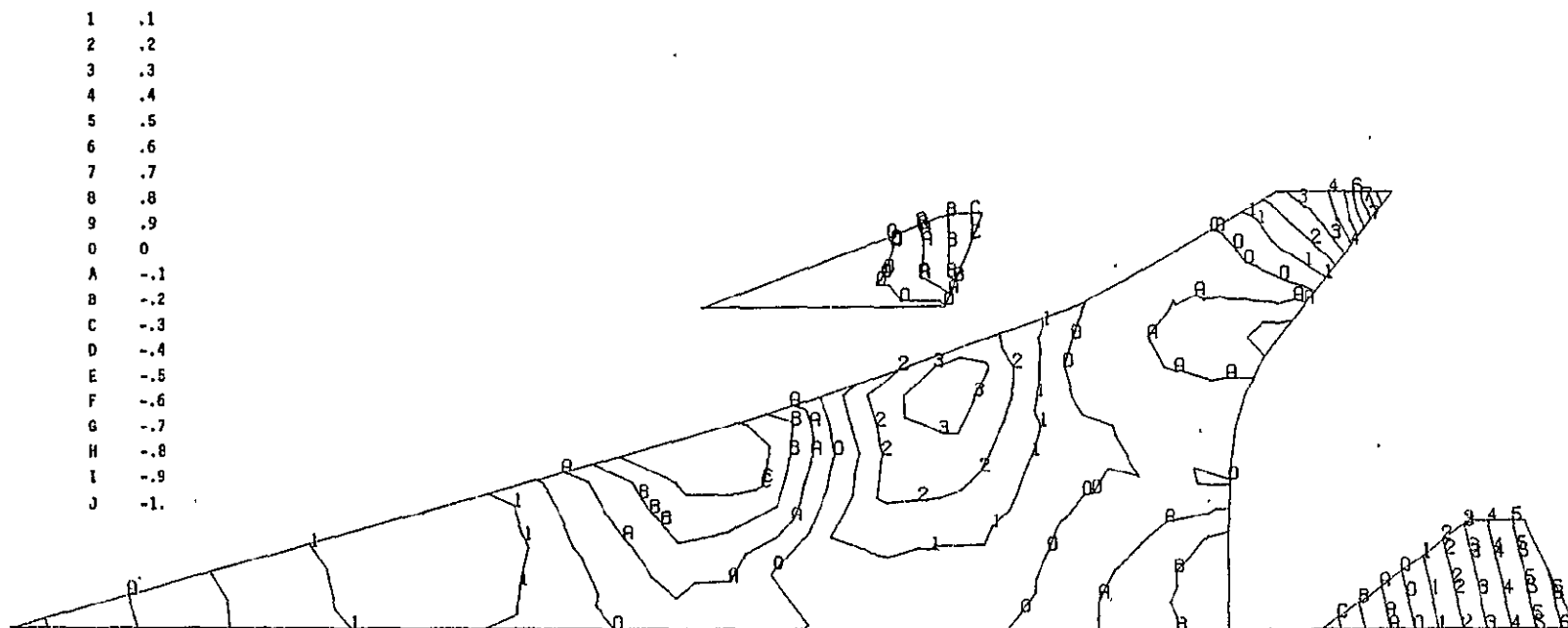


Figure 8-18.—Airplane Vibration Mode 12, Hybrid Structure Stiffness Design; Symmetric, High Gross Weight Condition, 5.777 Hz

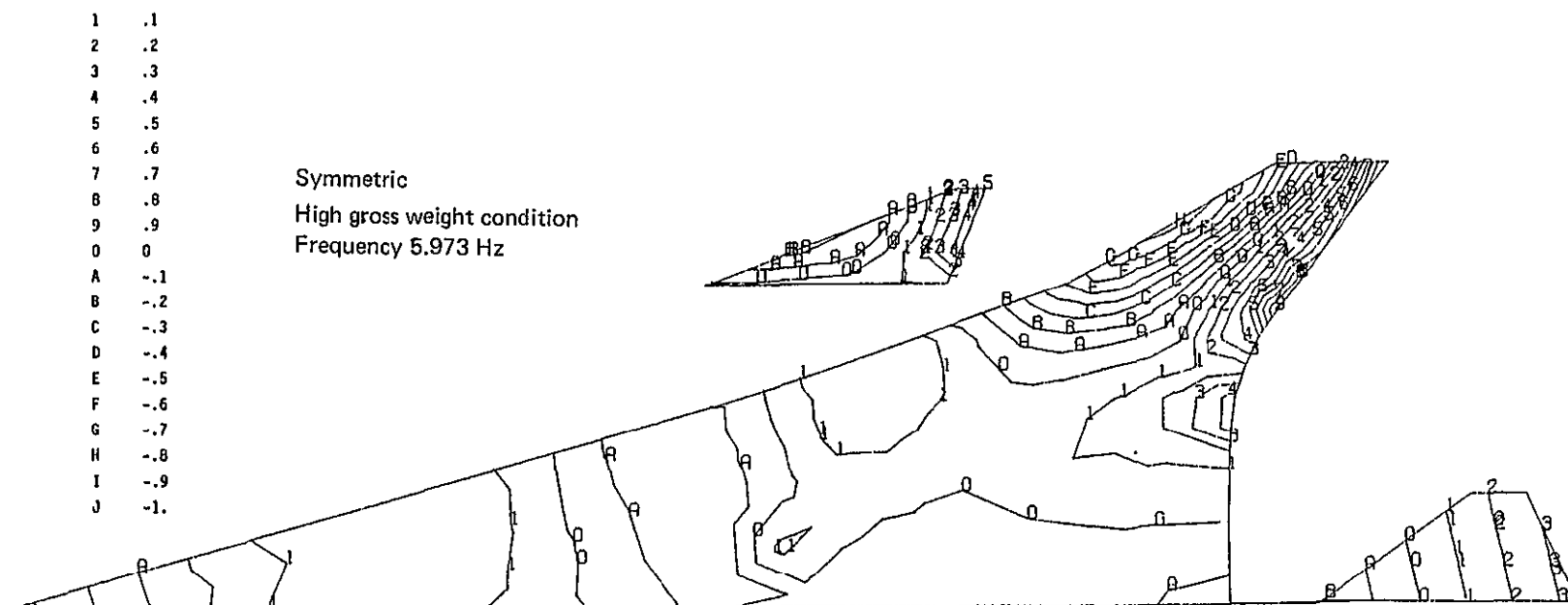


Figure 8-19.—Airplane Vibration Mode 13, Hybrid Structure Stiffness Design; Symmetric, High Gross Weight Condition, 5.973 Hz

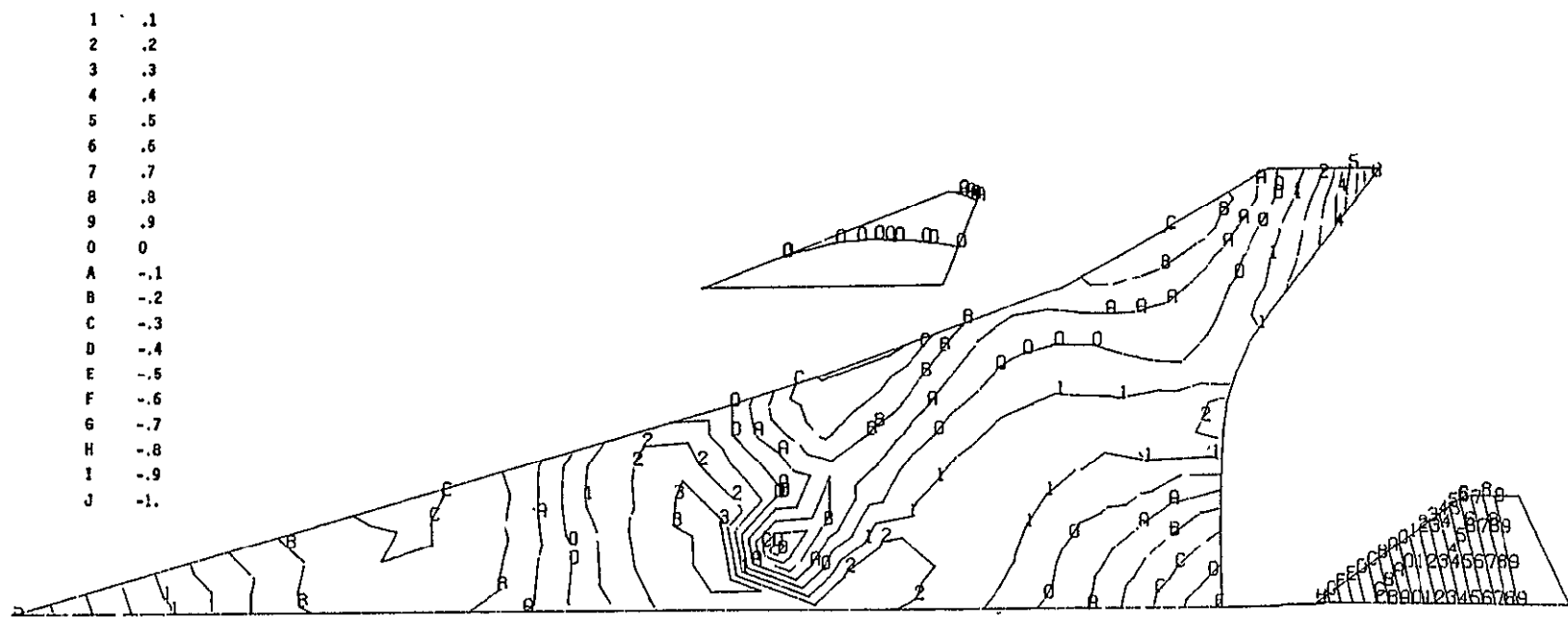


Figure 8-20.—Airplane Vibration Mode 14, Hybrid Structure Stiffness Design; Symmetric, High Gross Weight Condition, 6.058 Hz

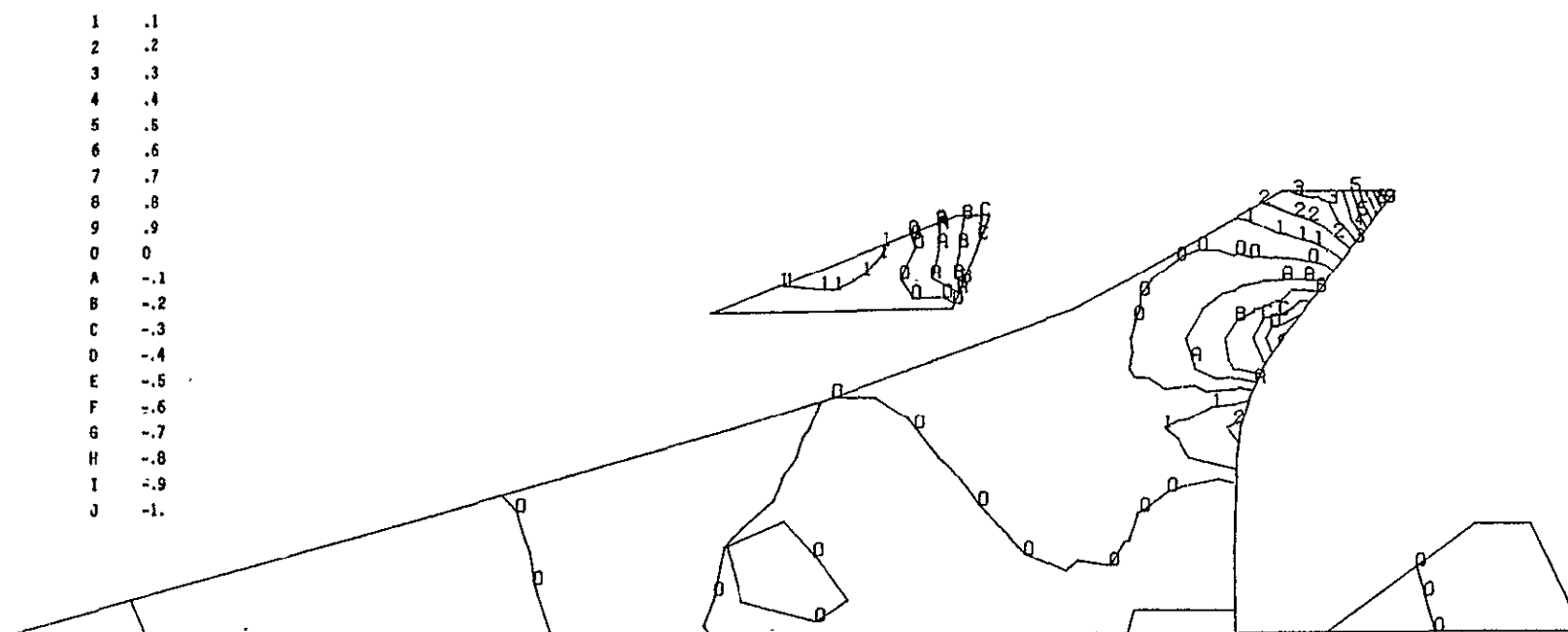


Figure 8-21.—Airplane Vibration Mode 15, Hybrid Structure Stiffness Design; Symmetric, High Gross Weight Condition, 6.911 Hz

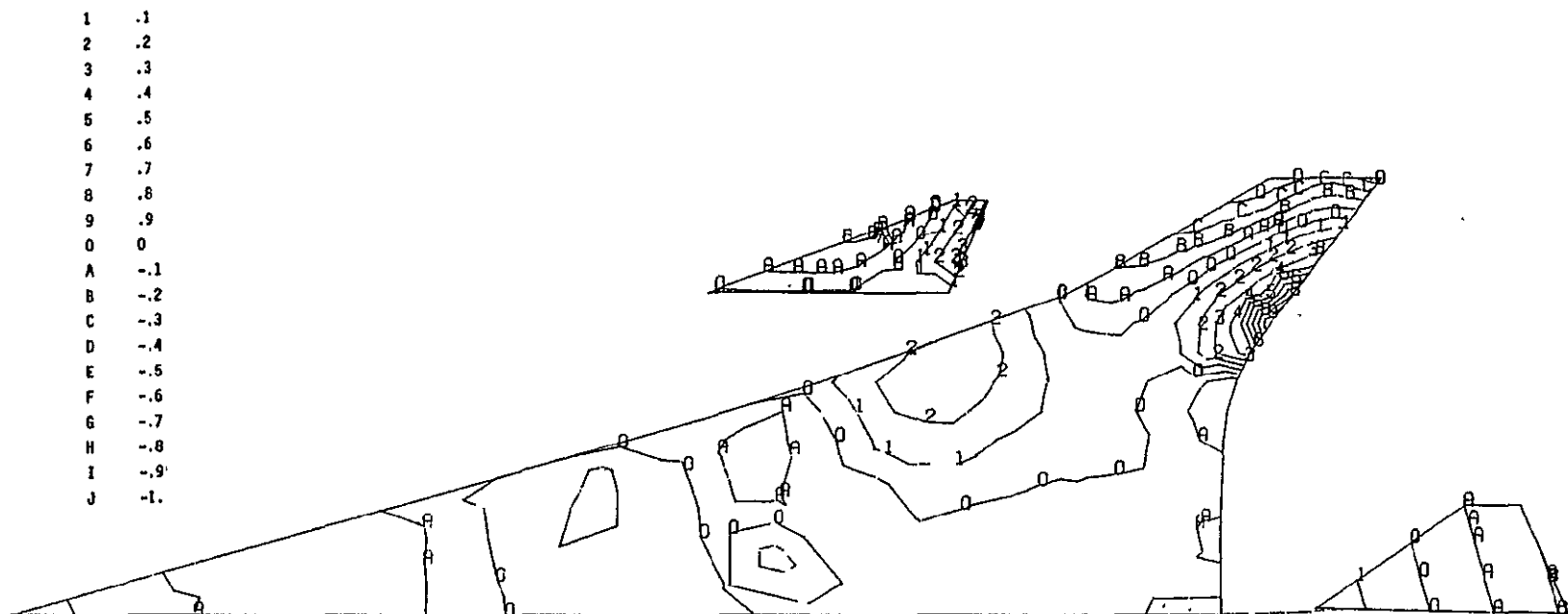


Figure 8-22.—Airplane Vibration Mode 16, Hybrid Structure Stiffness Design; Symmetric, High Gross Weight Condition, 7.504 Hz

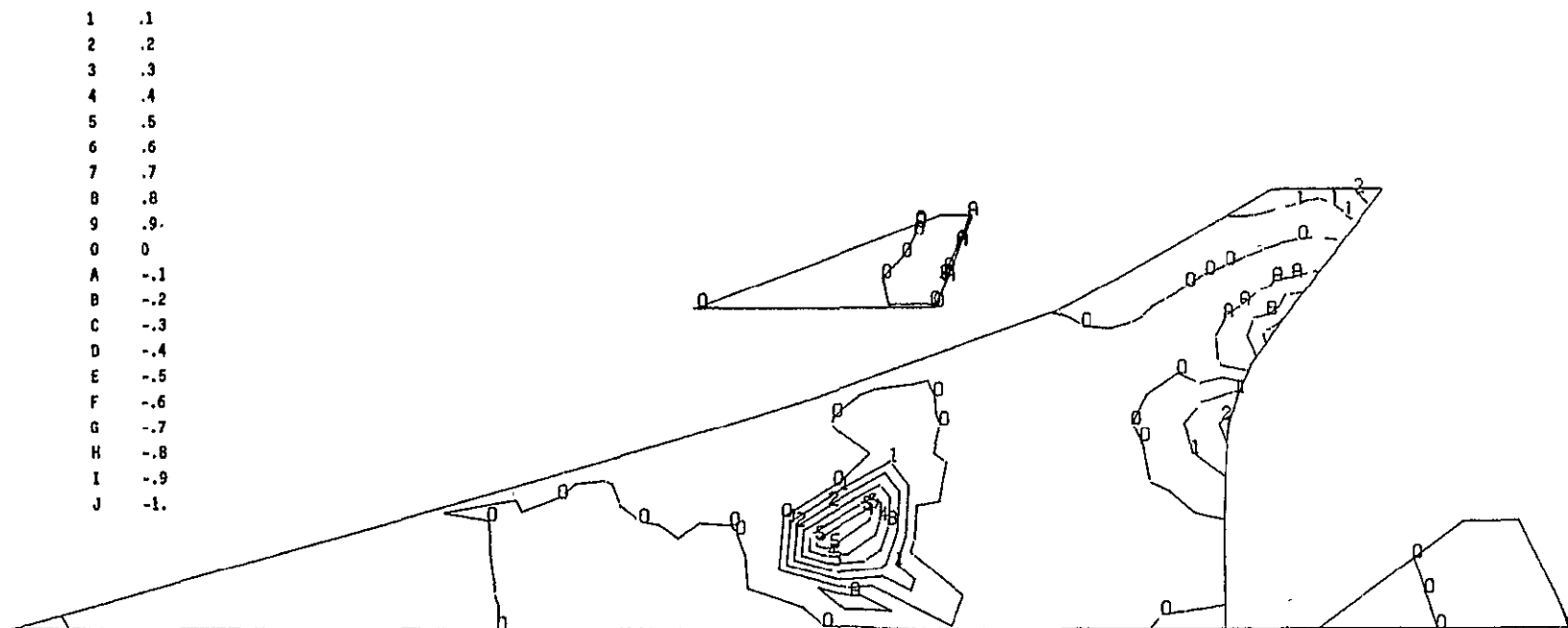


Figure 8-23.—Airplane Vibration Mode 17, Hybrid Structure Stiffness Design; Symmetric, High Gross Weight Condition, 7.840 Hz

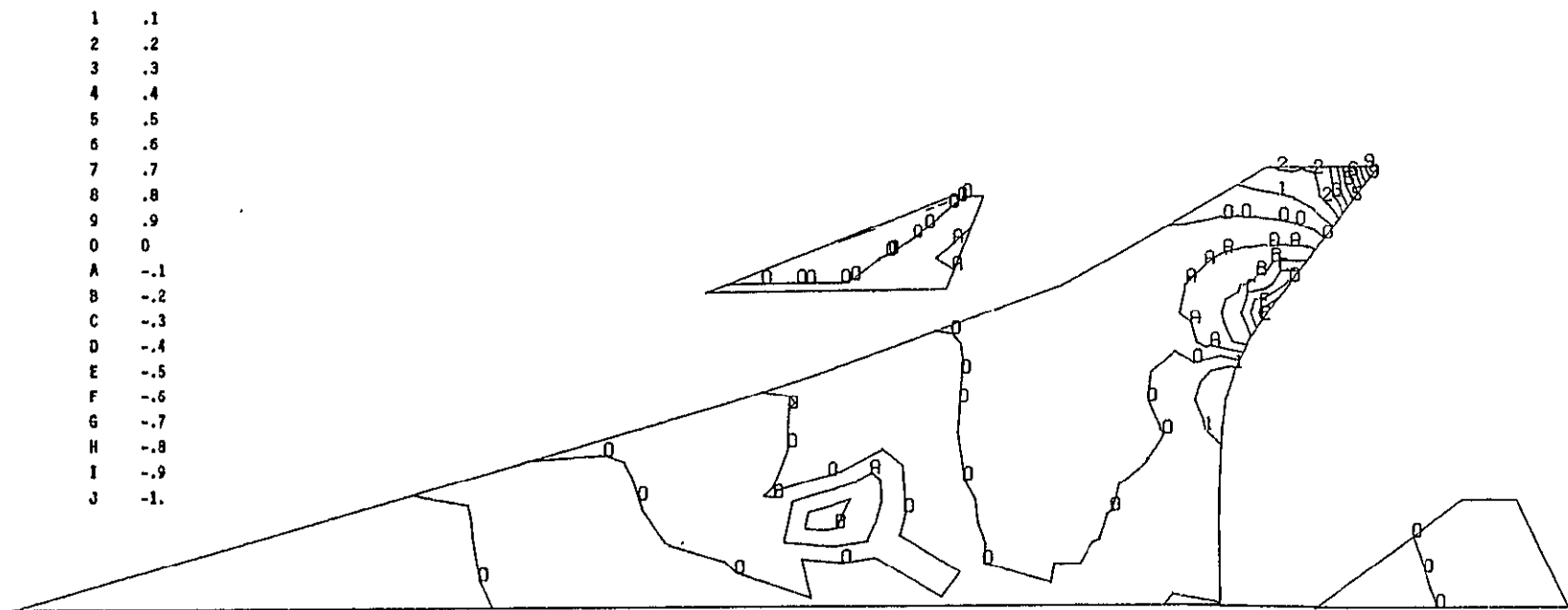


Figure 8-24.—Airplane Vibration Mode 18, Hybrid Structure Stiffness Design; Symmetric, High Gross Weight Condition, 8.154 Hz

SECTION 9

~~RECORDING PAGE BLANK NOT FILMED~~

FINAL WEIGHT ANALYSIS

by

K. J. DEBORD
M. D. HALVORSEN

CONTENTS

	Page
INTRODUCTION	328
REVISED TASK II TITANIUM WING WEIGHT	328
WEIGHT ANALYSIS OF ADVANCED COMPOSITE COVERED WING	328
WING WEIGHT COMPARISON SUMMARY	328
WING SECTION WEIGHT COMPARISON	329
GROUP WEIGHT AND BALANCE STATEMENT	329
REFERENCES	330

TABLES

No.		Page
9-1	Revised Task II Titanium Wing Weight, Model 969-512B	331
9-2	Wing Weight Comparison Summary, Model 969-512B	332
9-3	Group Weight and Balance Statement, Model 969-512B	333

FIGURES

No.		Page
9-1	Wing Section Weight Comparison, Upper Surface Cover, Stiffness Design, Model 969-512B	334
9-2	Wing Section Weight Comparison, Lower Surface Cover, Stiffness Design, Model 569-512B	335
9-3	Total Wing Section Weight Comparison, Total Wing, Stiffness Design, Model 969-512B	336

SYMBOLS

Δ Increment

GR/PI Graphite/Polyimide

lb Pounds

TI Titanium

INTRODUCTION

This section provides the operational empty weight of the configuration developed in reference 1 utilizing advanced composite structural material. The weight of the structural wing box outboard of the side of body was derived from the ATLAS finite structural analysis. This analysis showed that there was a 6730 lb or 10.4% weight reduction of the wing box outboard of the center section utilizing advanced composite cover panels but retaining titanium substructure compared to an all titanium wing box. The remainder of structural component weight changes from titanium to advanced composite were based on a previous NASA study as described in a later paragraph.

REVISED TASK II TITANIUM WING WEIGHT

It was necessary to make a number of revisions to the Task II titanium wing weight in order to have a valid base from which to assess the advantages of composite construction. Table 9-1 lists the weight changes to the final stiffness titanium wing presented in reference 9-1, table 12-6. These revisions increase the titanium wing weight from 95 760 lb to 97 812 lb. Most of these changes result from corrections to the weight of the structural model. All weights and weight savings are quoted per airplane.

Table 9-2 also tabulates the revised final stiffness all titanium wing.

ADVANCED COMPOSITE COVERED WING WEIGHT ANALYSIS

Combining the non-optimum weight factors outlined in Section 5 with the weight of the modeled structure from the ATLAS finite element analysis, produces the weight of the wing primary structural elements. To this must be added the weight of the honeycomb core and bond, landing gear doors, the wing center section, the leading and trailing edge secondary structure and miscellaneous items.

Table 9-2 presents the weight build-up of the Model 969-512B wing with five combinations of advanced composite covers: the strength design, three stiffness redesigns and the final stiffness design. All five wings have identical titanium internal structure. The final stiffness design wing weighs 88 572 lbs, which is 8702 lb more than the strength design. Section 8 describes the additional cover material added over strength design.

WING WEIGHT COMPARISON SUMMARY

The last two columns of table 9-2 show the weight increment between the final stiffness all titanium wing from Task II and the final stiffness advanced composite covered wing from the Task III analysis. As can be seen, the theoretical composite covers are 9504 lb or 48.6% lighter than the titanium. However, when this is combined with the higher non-optimum factors, and core and bond weight, the weight saving is reduced to 17.8%. The considerably higher core and bond weight with the composite wing cover compared to core and braze weight of the titanium cover is due in part to a difference in honeycomb area. The titanium covered wing has a portion of the lower surface which is integral skin stiffener construction where no honeycomb is used. Four outboard wing tip ribs which were added in

the titanium wing for stiffness have been eliminated in the composite cover wings. Otherwise, the substructure is identical in the two wings. A hand calculation was made of the weight reduction for composite landing gear door covers. This was small, compared to the total weight of the door hinges and mechanism and shows a 5% reduction of the total door weight. The wing center section weight reduction of 12 percent for the composite panel was derived from the adjacent outboard wing panel weight reduction.

In summary, the total weight reduction of the theoretical structural elements of the composite wing is 8284 lb or 15.7%; the weight reduction for the total outboard wing box is 6730 lb or 10.4%; and the reduction for the total wing including the center section, leading and trailing edge is 9240 lb or 9.4%.

WING SECTION WEIGHT COMPARISON

Figures 9-1 and 9-2 show a section weight comparison of the titanium wing upper and lower cover panels from Task II and the graphite/polyimide covers used in Task III for the stiffness designed wings. In figure 9-1, the forward strake upper panel T9 with minimum skin gage shows a 13.9% weight reduction when changing from titanium to advanced composite. As would be expected in the more highly loaded area, aft, the weight reduction increases to 35.3% in section T6. However, in sections T1, T2, T3 and T4, there is a significant reduction in the weight improvement in changing to a composite cover. This is due to the large increase in the thickness of the cover skins to satisfy the stiffness requirements shown in figure 8-24. The same pattern of weight reduction is shown on the lower surface in figure 9-2. However, sections T2, T3 and T4 show high percent weight reductions because the titanium design was integral skin, stringer construction. These sections would have been lighter if they had originally been designed as titanium honeycomb sandwich. With the lighter titanium sections; T2, T3 and T4, the weight reductions due to changing to composite structure would then be similar to the upper surface for these sections.

The total upper surface cover weight reduction for composite design was 13.9% while the lower surface showed 21.5% reduction. The combined upper and lower surface cover weight reduction was 17.8%.

Figure 9-3 provides a weight comparison of the Task II titanium wing with the Task III advanced composite wing by sections combining all structural elements. These are the weights shown in table 9-2 for the stiffness designed wing but they are shown as weight per side rather than weight per airplane.

While the cover weight reduction for changing from titanium to composite amounted to 17.8%, the total wing structural weight reduction was 9.4%.

GROUP WEIGHT AND BALANCE STATEMENT

Table 9-3 presents a group weight and balance comparison of the Task II titanium airplane with the Task III advanced composite structure. The wing weights are taken from table 9-2. The weight reduction shown for the remainder of the structure on Task III using advanced composite was based on the NASA study, reference 9-2.

The total structural weight reduction for advanced composite compared to titanium is 10.5%. This is reduced to 6.6% when related to the total operational empty weight.

REFERENCES

- 9-1 Boeing Staff: *Study of Structural Design Concepts for an Arrow Wing Supersonic Transport Configuration*. NASA CR-132576-1 and -2, 1976.

Table 9-1.—Revised Task II Titanium Wing Weight, Model 969-512B

	Wt, lb
Wing weight — final stiffness design (ref. 9-1, table 12-6)	95 760
Delete skin over lower surface wheel well	-590
Revised cover material non optimum factors	+2 137
Add spar web stiffeners	+1 035
Add rib web stiffeners	+1 028
Change element designation from spars to ribs (Spars) (Ribs)	-406 +414
Delete core and braze in lower surface integral stiffened cover area	-1 244
Correct landing gear door area	-864
Incorporate outboard fixed T.E. panel into wing structural box	+542
Revised wing weight—final stiffness design	97 812

Table 9-2.—Wing Weight Comparison Summary, Model 969-512B

Item	Task II Titanium	Task III Advanced composite covers					Wt change Titanium to composite,	
	Final stiffness, lb	Strength design, lb	Stiffness redesigns			Final stiffness, lb		
			1, lb	2, lb	3, lb			
			lb	%				
Theoretical cover material	19 566	4 650	6 686	6 686	9 344	10 062	-9 504	-48.6
Nonoptimum cover material	7 028	5 350	6 374	6 374	8 030	8 640	+1 612	+22.9
Theoretical spar material	14 094	14 094	14 094	14 094	14 094	14 094		
Nonoptimum spar material (incl. web stiffeners)	3 152	3 152	3 152	3 152	3 152	3 152		
Theoretical rib material	5 952	5 654	5 654	5 654	5 654	5 654	- 298	- 5.0
Nonoptimum rib material (incl. web stiffeners)	2 128	2 034	2 034	2 034	2 034	2 034	- 94	- 4.4
Theoretical beam material	654	654	654	654	654	654		
Nonoptimum beam material	98	98	98	98	98	98		
Total structural element weight	52 672	35 686	38 746	38 746	43 060	44 388	-8 284	-15.7
Core and braze/bond	8 050	9 766	9 766	9 766	9 766	9 766	+1 716	+21.3
Landing gear doors and mech.	3 236	3 074	3 074	3 074	3 074	3 074	- 162	- 5.0
Fairing, fence, and misc	960	960	960	960	960	960		
Total wing box (less center section)	64 918	49 486	52 546	52 546	56 860	58 188	-6 730	-10.4
Wing center section	8 560	7 530	7 530	7 530	7 530	7 530	-1 030	-12.0
Fixed leading edge	8 460	7 868	7 868	7 868	7 868	7 868	- 592	- 7.0
Moveable leading edge	5 770	5 482	5 482	5 482	5 482	5 482	- 288	- 5.0
Fixed trailing edge	4 864	4 474	4 474	4 474	4 474	4 474	- 390	- 8.0
Moveable trailing edge	5 240	5 030	5 030	5 030	5 030	5 030	- 210	- 4.0
Total wing structure	97 812	79 870	82 930	82 930	87 244	88 572	-9 240	- 9.4

Table 9-3.—Group Weight and Balance Statement, Model 969-512B

Group	Revised Task II		Weight change		Task III	
	Weight, lb	Arm, in.	lb	%	Weight, lb	Arm, in.
Wing	97 812	2604.0	- 9 240	- 9.4	88 572	2604.0
Horizontal tail	6 530	3623.0	- 914	-14.0	5 616	3623.0
Vertical tail (body and wing mounted)	5 850	3406.0	- 585	-10.0	5 265	3406.0
Body	56 140	2117.0	- 8 421	-15.0	47 719	2117.0
Main gear	37 320	2548.0	- 3 172	- 8.5	34 148	2548.0
Nose gear	3 760	1178.0	- 320	- 8.5	3 440	1178.0
Nacelle	19 080	2949.0	- 1 049	- 5.5	18 031	2949.0
Total structure	226 492	2529.5	-23 701	-10.5	202 791	2535.5
Engine (incl T/R, S/S and nozzle)	45 200	3076.0			45 200	3076.0
Engine accessories	1 350	2944.0			1 350	2944.0
Engine controls	780	2308.0			780	2308.0
Starting system	300	2919.0			300	2919.0
Fuel system	9 110	2495.0			9 110	2495.0
Total propulsion	56 740	2968.2			56 740	2968.2
Instruments	1 865	1710.0			1 865	1710.0
Flight controls	14 700	2679.0			14 700	2679.0
Hydraulics	5 795	2854.0			5 795	2854.0
Electrical	5 160	2092.0			5 160	2092.0
Electronics	2 885	1282.0			2 885	1282.0
Furnishings	19 010	1817.0			19 010	1817.0
ECS	8 430	2440.0			8 430	2440.0
Anti-icing	135	558.0			135	558.0
APU	250	2978.0			250	2978.0
Insulation	2 900	1913.0			2 900	1913.0
Total systems and equipment	61 130	2209.7			61 130	2209.7
Options	2 500	2491.0			2 500	2491.0
Manufacturer's empty weight	346 862	2544.6	-23 701	- 6.8	323 161	2549.5
Standard items	8 200	2193.0			8 200	2193.0
Operational items	5 260	1716.0			5 260	1716.0
Operational empty weight	360 322	2524.5	-23 701	- 6.6	336 621	2527.8
Payload	48 906	1882.0			48 906	1882.0
Zero fuel weight	409 228	2447.7	-23 701	- 5.8	385 527	2445.9

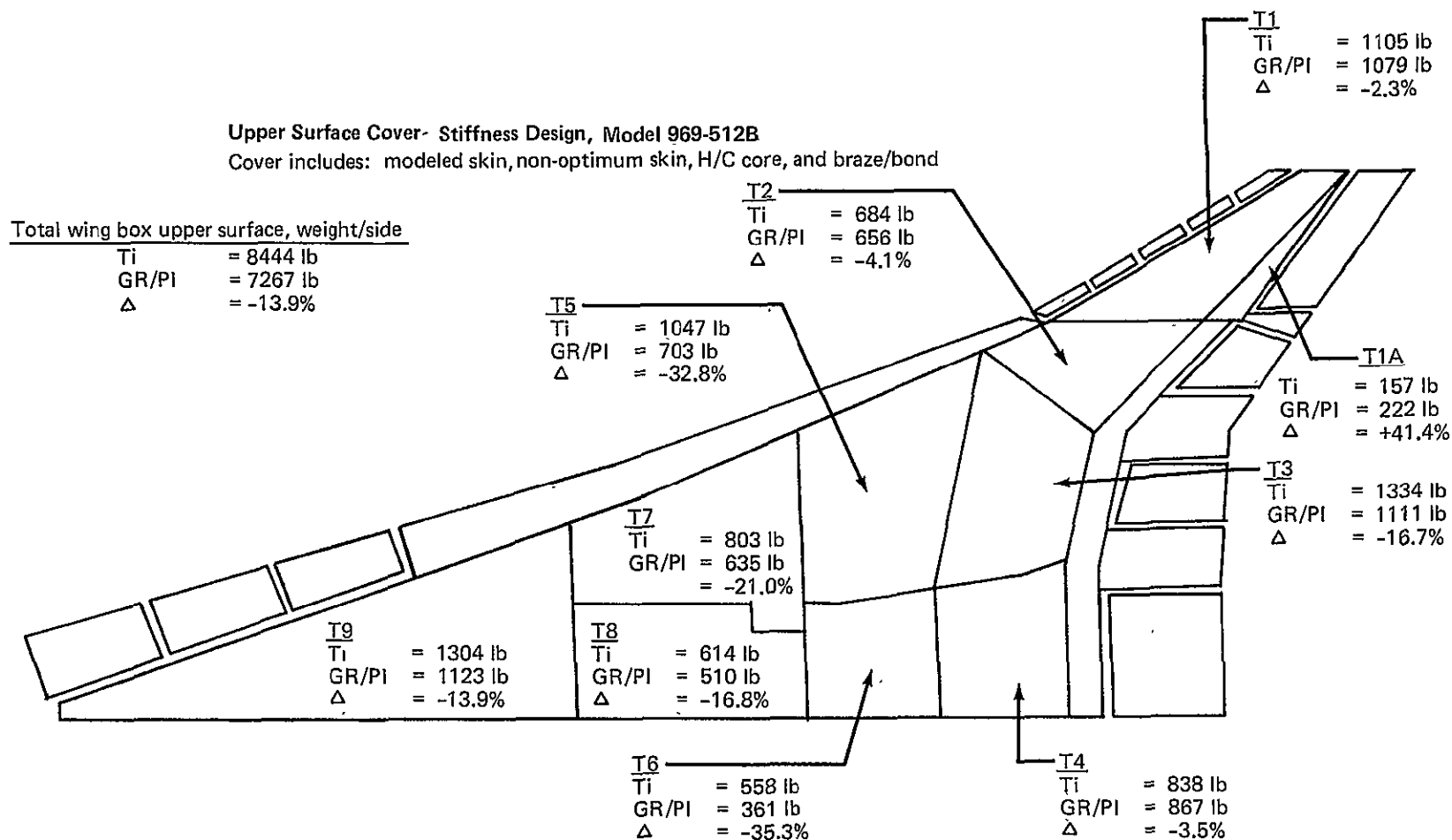


Figure 9-1.—Wing Upper Surface Section Weight Comparison, Upper Surface Cover^a,
 Stiffness Design, Model 969-512B

Lower Surface Cover Stiffness Design Model 969-512B

Cover includes: modeled skin, non-optimum skin, H/C core, and braze/bond

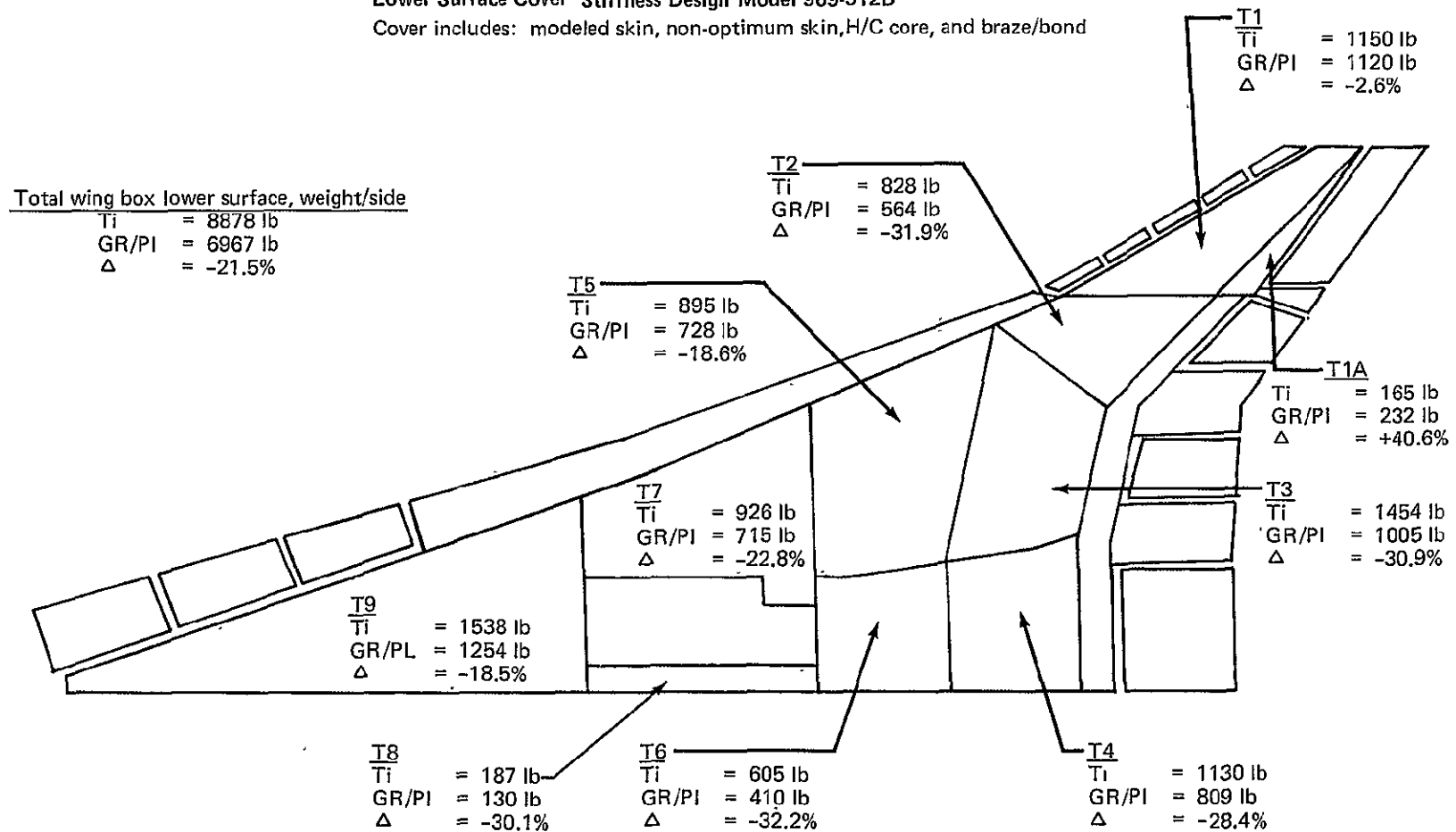


Figure 9-2.—Wing Lower Surface Section Weight Comparison, Lower Surface Cover^a, Stiffness Design, Model 969-512B

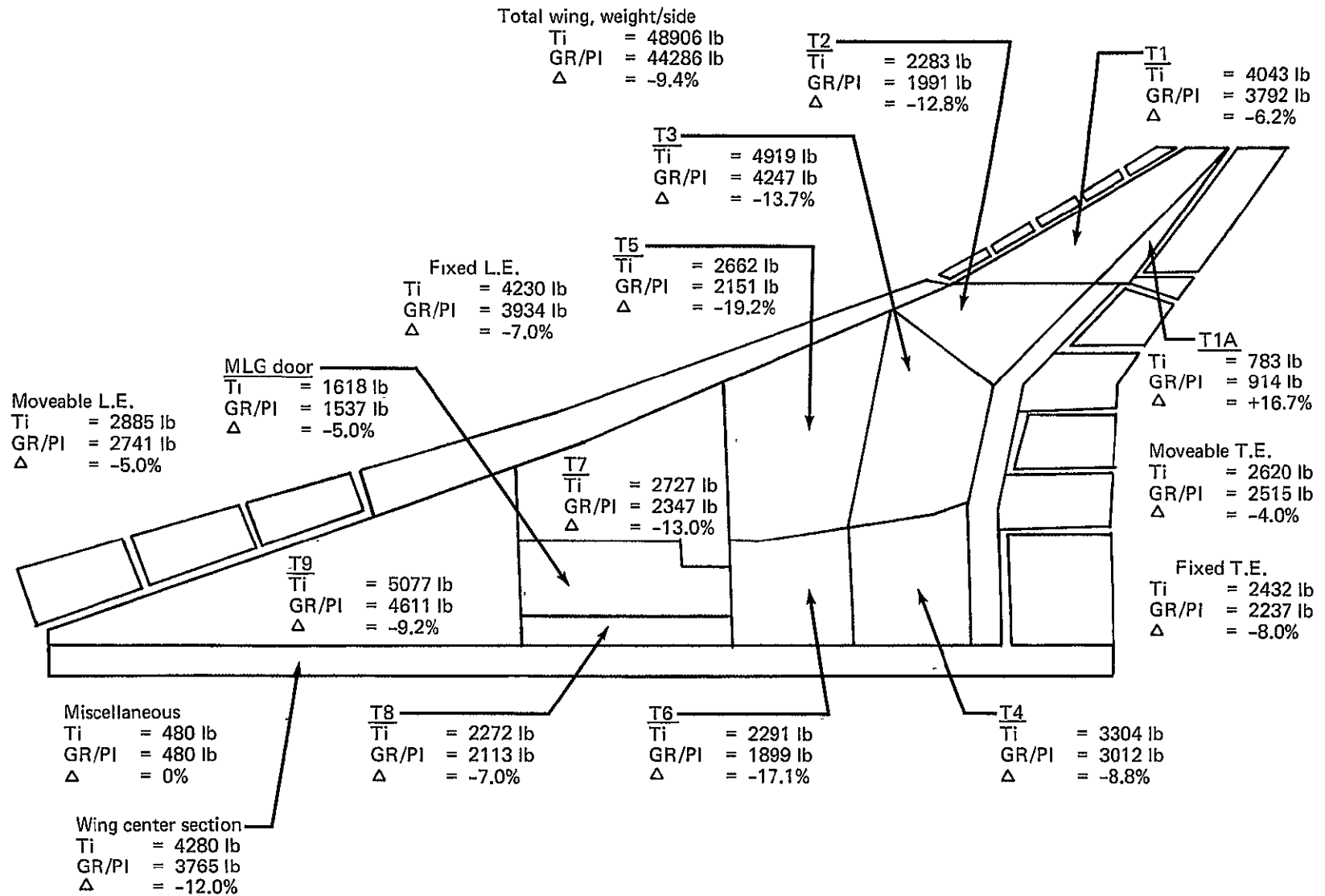


Figure 9-3.—Total Wing Section Weight Comparison, Total Wing, Stiffness Design, Model 969-512B

SECTION 10

AERODYNAMIC HEATING ANALYSIS

by

V. DERIUGIN

CONTENTS

Page

SUMMARY	341
INVESTIGATION OF TEMPERATURE DISTRIBUTIONS IN COMPOSITE LAMINATES . .	341
METHODOLOGY FOR DETERMINING AVERAGE CONDUCTIVITIES	342
METHODOLOGY FOR THERMAL ANALYSIS USING SIMPLIFIED MODEL	342
MODELING OF LIGHT GAGE AND HEAVY GAGE CROSS SECTIONS	343
DETERMINATION OF TEMPERATURE DISTRIBUTION FOR MISSION PROFILE	343
REFERENCES	344

TABLES

No.		Page
10-1	Node Plan for Advanced Composite Model	345
10-2	Conductors in Composite Model	345
10-3	Layups of Honeycomb Panels for Wing Structural Sections	346
10-4	Properties Used for Thermal Analysis	347

FIGURES

No.		Page
10-1	Layup Model Breakdown	348
10-2	Node Arrangement, Layup Direction [0]	349
10-3	Node Arrangement, Layup Direction [+45]	350
10-4	Node Arrangement, Layup Direction [-45]	351
10-5	Node Arrangement, Layup Direction [90]	352
10-6	Basic Material Conductivities and Sample Layup, Average Conductivity	353
10-7	Light Gage Structural Section	354
10-8	Heavy Gage Structural Section	355
10-9	Average Thermal Conductivities for Light and Heavy Gage Designs (Dimensions A, B, C, and D)	356
10-10	Fuel Tank Temperatures, Light Gage, Wet Upper Panel: T1, T2, T24, T25	357
10-11	Fuel Tank Temperatures, Light Gage, Wet Upper Panel: T5, T6, T20, T21	358
10-12	Fuel Tank Temperatures, Light Gage, Wet Upper Panel: T8, T10, T12	359
10-13	Fuel Tank Temperatures, Light Gage, Wet Upper Panel: T14, T16, T18	360
10-14	Fuel Temperature, Light Gage, Wet Upper Panel: T35	361
10-15	Fuel Tank Thermal Gradients, Light Gage, Wet Upper Panel: T1, T2, T5-7, T19-T21, T24-T25	362
10-16	Fuel Tank Thermal Gradients, Light Gage, Wet Upper Panel: T7, T8, T8-10, T8-T13	363
10-17	Fuel Tank Thermal Gradients, Light Gage, Dry Upper Panel: T1, T2, T24, T25	364
10-18	Fuel Tank Temperatures, Light Gage, Dry Upper Panel: T5, T6, T20, T21	365
10-19	Fuel Tank Temperatures, Light Gage, Dry Upper Panel: T8, T10, T12	366
10-20	Fuel Tank Temperatures, Light Gage, Dry Upper Panel: T14, T16, T18	367
10-21	Fuel Temperatures, Light Gage, Dry Upper Panel: T35	368
10-22	Fuel Tank Thermal Gradients, Light Gage, Dry Upper Panel: T1-T2, T5-T7, T19-T21, T24-T25	369
10-23	Fuel Tank Thermal Gradients, Light Gage, Dry Upper Panel: T7-T8, T8-T10, T8-T13	370
10-24	Fuel Tank Temperatures, Heavy Gage, Dry Upper Panel: T1, T2, T24, T25	371
10-25	Fuel Tank Temperatures, Heavy Gage, Dry Upper Panel: T5, T6, T20, T21	372
10-26	Fuel Tank Temperatures, Heavy Gage, Dry Upper Panel: T14, T16, T18	373
10-27	Fuel Temperature, Heavy Gage, Dry Upper Panel: T35	374
10-28	Fuel Tank Temperatures, Heavy Gage, Wet Upper Panel: T1, T2, T24, T25	375
10-29	Fuel Tank Temperatures, Heavy Gage, Wet Upper Panel: T5, T6, T20, T21	376
10-30	Fuel Tank Temperatures, Heavy Gage, Wet Upper Panel: T8, T10, T12	377
10-31	Fuel Temperature, Heavy Gage, Wet Upper Panel: T35	378

SUMMARY

The structural thermal analysis for Task III was performed using the same methods as those employed during the Task II study (ref. 10-1). The analysis consisted of determining the external thermal environment as well as the resulting structural temperature distributions. Whereas the external environments were identical to those of reference 10-1 due to the same vehicle mission profile, the temperatures and temperature distributions throughout the structure were different due to the introduction of graphite/polyimide material in the honeycomb sandwich skin panels instead of the titanium previously used. In order to be able to apply the same methodology as in Task II, a study was made of the effects of laminations and their thermal properties on structural temperature distributions. Because of very pronounced directionality of the thermal conductivity, particular attention was focused on local temperature gradients which might conceivably introduce differential thermal stresses and, thus, delaminations between laminae if appropriate stress levels were reached. None of these effects were observed, and it was therefore possible to avoid excessively detailed modeling and to work with averaged and lumped properties and geometric arrangements.

The results showed that the temperatures were predominantly lower than those obtained in the titanium airframe at the same time exhibiting similar time and spatial characteristics. The differences in magnitudes are largely due to the differences in surface emissivities and absorptivities as well as in the material conductivities. The gradients through the graphite/polyimide honeycomb sandwich panels were generally somewhat larger than for titanium of similar configuration.

INVESTIGATION OF TEMPERATURE DISTRIBUTIONS IN COMPOSITE LAMINATES

Representative arrays of material layups were examined with respect to possible analytical approaches that would yield a manageable model with acceptable accuracy. A 24 lamina layup of 0.1 mm (.004 in.) thick laminae was selected and grouped into 7 layers having different layup directions as shown in figure 10-1. A 3x3 basic node arrangement was selected for the 0° and 90° layup directions whereas for the ±45° layup directions the same basic node array was augmented by intermediate nodes for modeling convenience. The node plan is shown in table 10-1. The basic model covered an area of 76.2 cm x 76.2 cm (30x30 in.). The arrangement of the nodes is shown in figures 10-2 through 10-5. Each node, shown in figures 10-2 through 10-5 represents a capacitor and is also connected with adjacent nodes by appropriate conductors as listed in table 10-2. Aerodynamic heating representative of a typical supersonic cruise environment exhibiting a sharp temperature rise at approximately 30 minutes into the mission profile was also simulated by conductors. The resulting temperature rise of 194K (350°F) over a period of 14 minutes resulted in a maximum temperature difference of approximately .89K (1.6°F) between the upper (Layer 1) and lower (Layer 7) layers and is insignificant from the point of view of generating delaminating differential stresses. It was therefore decided to treat graphite/polyimide laminate layups as lumped nodes with appropriately averaged conductivities.

METHODOLOGY FOR DETERMINING AVERAGE CONDUCTIVITIES

The average conductivities in the streamwise direction were obtained by averaging the directional conductivities weighted by the associated layup layer thicknesses. Thus the average conductivity can be expressed as:

$$K_{avg} = \frac{\sum K_i \delta_i}{\sum \delta_i}$$

where

K_i = directional conductivity of basic material

δ_i = layer thickness.

The basic material conductivities and the average conductivity of the sample layup as functions of temperature are shown in figure 10-6. For comparison, the figure also shows the thermal conductivity of 6Al-4V titanium.

METHODOLOGY FOR THERMAL ANALYSIS USING SIMPLIFIED MODEL

The methodology of the thermal analysis was identical to that employed in reference 10-1 with regard to use of the Boeing Engineering Thermal Analyzer (BETA) program. However, averaged conductivities were used as inputs to this program utilizing the experience of the preliminary investigation. The average conductivities of layups intended for the actual design (see table 10-3) were determined as discussed above. The longitudinal conductivities are considerably larger and show more variation with temperature than transverse conductivities. Therefore, emphasis was placed on obtaining average longitudinal conductivity values whereas for transverse conductivity a single value of

$$1.44 \frac{W}{mK} (1.93 \times 10^{-5} \frac{Btu \text{ in.}}{\text{in.}^2 \text{ sec } ^\circ F)$$

was used for the selected high strength graphite/polyimide material. Furthermore, since the honeycomb core of this material consists of layers with fiber directions of $\pm 45^\circ$, appropriate conductivity values had to be used in determining analytically the conductances through the respective honeycomb panels. These conductances are shown in table 10-4. In addition, radiation between the honeycomb face sheets was accounted for using radiation exchange factors as described in reference 10-2. These radiation exchange factors were computed as:

- .178 for 56.1 Kg/m³ (3.5 lb/ft³) Graphite/Polyimide Honeycomb
- .178 for 112.1 Kg/m³ (7.0 lb/ft³) Graphite/Polyimide Honeycomb
- .148 for 224.2 Kg/m³ (14.0 lb/ft³) Graphite/Polyimide Honeycomb

Accounting for radiation interchange between the honeycomb face sheets improves the accuracy of predicting effective honeycomb conductance by having the program include the effects of changing face sheet temperatures on actual honeycomb conductance.

MODELING OF LIGHT GAGE AND HEAVY GAGE CROSS SECTIONS

The wing cross section selected for analysis was geometrically similar to that analyzed in reference 10-1. The same node arrangement was used. All layups were treated as one compound layer with averaged properties. The titanium spar was identical to that in reference 10-1. The analysis was performed on light gage and on heavy gage honeycomb sandwich panel designs each with wet and dry upper panels. The structural cross section model with the light gage is shown in figure 10-7. The heavy gage model is shown in figure 10-8. The layups for the respective dimensions shown in figures 10-7 and 10-8 are presented in table 10-3. The average thermal conductivities, shown in figure 10-9, were computed using the methodology discussed above using the basic material conductivities, the layup direction and the thicknesses of the respective layers.

DETERMINATION OF TEMPERATURE DISTRIBUTION FOR MISSION PROFILE

The aerodynamic heating rates were calculated using a 6190 km (3340nm) mission profile as in reference 10-1. Solar heating and radiation to space were also included. As shown in table 10-4, the painted graphite/polyimide solar absorptance was assumed to be 0.3 and the emittance to space 0.8. For the internal radiation exchange 0.2 was assumed for the titanium emittance and 0.8 for the graphite/polyimide. Honeycomb panel conductances were used as described in table 10-4. The fuel management scheme as well as the conductance between fuel and structure, were assumed identical to those of reference 10-1.

The initial temperature before flight was assumed as 289K (60°F). Temperature distributions, thermal gradients, and fuel temperatures for both light and heavy gage designs with wet and dry upper panels are shown in figures 10-10 through 10-31. The node designations are shown in figures 10-7 and 10-8, respectively.

Most of the temperatures obtained in the present analysis are lower than those obtained in reference 10-1 but exhibit the same general characteristics. The lower temperatures can be partially explained by the lower absorptance-emittance ratio of the surface of the graphite/polyimide material (see table 10-4). The largest temperature difference of 67K (120°F) occurs at Node 2 due to a combination of higher emittance during the internal radiation exchange with internal structure and fuel, and a lower conductance assumed for the upper panel (see table 10-4). The temperatures of the outer lower surface skin are nearly the same as in reference 10-1. However, over the lower spar they are approximately 44K (80°F) higher which is caused by the significantly lower panel conductance assumed for the lower panel as compared with Task II.

The thermal gradients are generally somewhat higher but show similar characteristics to those of the titanium airframe. They are generally consistent with the differences in conductances, emittances and lower density-specific heat product of the graphite/polyimide material. Very little difference in temperatures and thermal gradients is observed between light gage and heavy gage designs. The similarity of temperatures and thermal gradients with those of reference 10-1 can be explained by comparable conductivities of some of the graphite polyimide layups with the thermal conductivity of titanium, particularly in the heavy gage design (see fig. 10-9).

REFERENCES

- 10-1 Boeing Staff: *Study of Structural Design Concepts for an Arrow Wing Supersonic Transport Configuration*. NASA CR 132576-1 and -2, 1976.
- 10-2 Swan, R. T.; and Pittman, C. M.: *Analysis of Effective Conductivities of Honeycomb-Core and Corrugated-Core Sandwich Panels*. NASA TN D-714.

Table 10-1.—Node Plan for Advanced Composite Model

Sample Model Layup Order: Total 24 Layers
 $[0_5/\pm 45_3/90]_S$

Number of layers	Layup direction	Node numbers	Number of nodes
5	0	1-9	9
3	+45	11-35	25
3	-45	41-65	25
2	90	71-79	9
3	-45	81-105	25
3	+45	111-135	25
5	0	141-149	9
Total number of nodes			127

Table 10-2.—Conductors in Composite Model

	Number of conductors
Nodes 1-9	12
Nodes 11-35	36
Nodes 41-65	36
Nodes 71-79	12
Nodes 81-105	36
Nodes 111-135	36
Nodes 141-149	12
Layers 1, 2	45
Layers 2, 3	25
Layers 3, 4	45
Layers 4, 5	45
Layers 5, 6	25
Layers 6, 7	45
Aeroheating	9
Total conductors	419

Table 10-3.—Layups of Honeycomb Panels for Wing Structural Sections

Light gage				Heavy gage			
Dimension (fig. 10-7)	Gage		Layup	Dimension (fig. 10-7)	Gage		Layup
	Total	Titanium			Total	Titanium	
A	0.081 (0.032)		[0/+45/90/-45] _S	A	0.183 (0.072)		[0/+45/0/-45/90/ 0/±45/0] _S
B	0.041 (0.016)		Same as A	B	0.183 (0.072)		Same as A
C	0.234 (0.092)	0.081 (0.032)	[0/Ti/+45/90/ Ti/-45] _S	C	0.396 (0.156)	0.107 (0.042)	[0/Ti/+45/0/Ti/ -45/90/0/+45/ Ti/-45/0] _S
D	0.229 (0.090)	0.041 (0.016)	Same as C plus 0.076 (0.03) thick (±45) GR/PI shim	D	0.498 (0.196)	0.107 (0.042)	Same as C plus 0.102 (0.04) thick (±45) GR/PI shim
Center core $\rho_{CC} = 56.1$ (3.5) Edge core $\rho_{EC} = 112.1$ (7.0)				Center core $\rho_{CC} = 56.1$ (3.5) Edge core $\rho_{EC} = 224.2$ (14.0)			

GR/PI = Graphite polyimide

Dimensions: cm (in.)

ρ = density, kg/m³ (lbm/ft³)

Titanium interleaves are 0.02 (0.008) and 0.01 (0.004), respectively. They are bonded in place with 0.009 (0.0035) thick layer of polyimide adhesive.

Dimensions are given in figures 10-7 and 10-8.

Table 10-4.—Properties Used for Thermal Analysis

		Titanium	Graphite polyimide
Solar absorptance Upper panel Lower panel (Assuming 10% of solar energy reflected from ground)	α_{upper} α_{lower}	0.7 0.07	0.3 0.03
Emittance	ϵ	0.2	0.8
Ratio	$\alpha/\epsilon_{\text{upper}}$ $\alpha/\epsilon_{\text{lower}}$	3.5 0.35	0.375 0.0375
(Density)•(Specific heat) $\frac{\text{MJ}}{\text{m}^3\text{K}} \left(\frac{\text{Btu}}{\text{in.}^3\text{°F}} \right)$	ρC_p	2.41 (0.0208) at 283 K (50° F) 3.65 (0.0229) at 505 K (450° F)	1.42 (0.0123)
Thermal conductivity		See figures 10-6 and 10-9.	
Honeycomb panel conductance $\frac{\text{W}}{\text{m}^2\text{K}} \left(\frac{\text{Btu}}{\text{ft}^2 \text{ hr } \text{°F}} \right)$ Center core Edge core		Effective 34 (6.0) (Task II) 216 (38.0) (Task II)	Pure conductance with radiation component accounted for by program 14.98 (2.64) — light and heavy gage 29.96 (5.28) — light gage 59.92 (10.56) — heavy gage

Lamina		Layup direction	Layer direction
1		0	1
2			
3	⊙		
4	↑		
5	4 Laminae	+45	2
6	↓		
7	⊙		
8	3 Laminae		
9	↓	-45	3
10	⊙		
11	2.5 Laminae		
12	↓		
13	⊙	90	4
14	2.5 Laminae		
15	↓		
16	⊙		
17	3 Laminae	-45	5
18	↑		
19	⊙		
20	4 Laminae		
21	↓	+45	6
22	⊙		
23			
24			
		0	7

Material: High strength graphite/polyimide, 0.1 mm (0.004 in.) thick

Figure 10-1.—Layup Model Breakdown

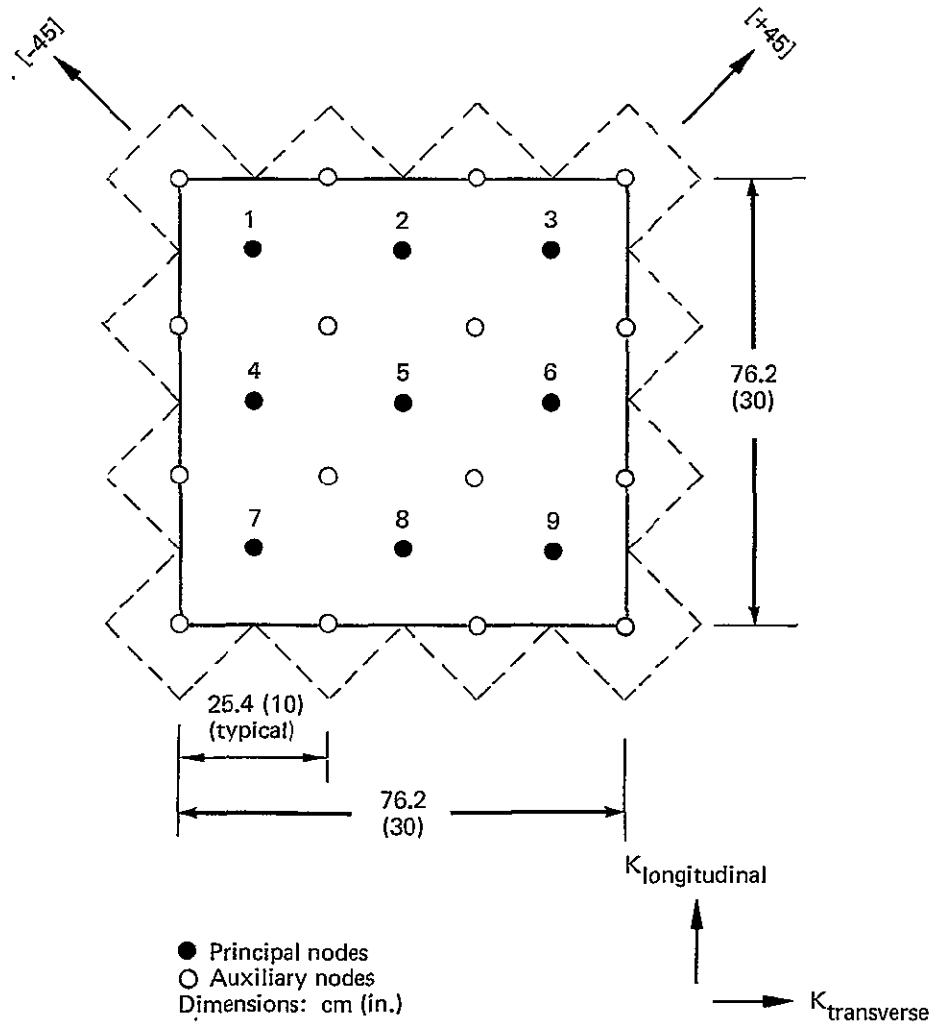


Figure 10-2.—Node Arrangement, Layup Direction [0]

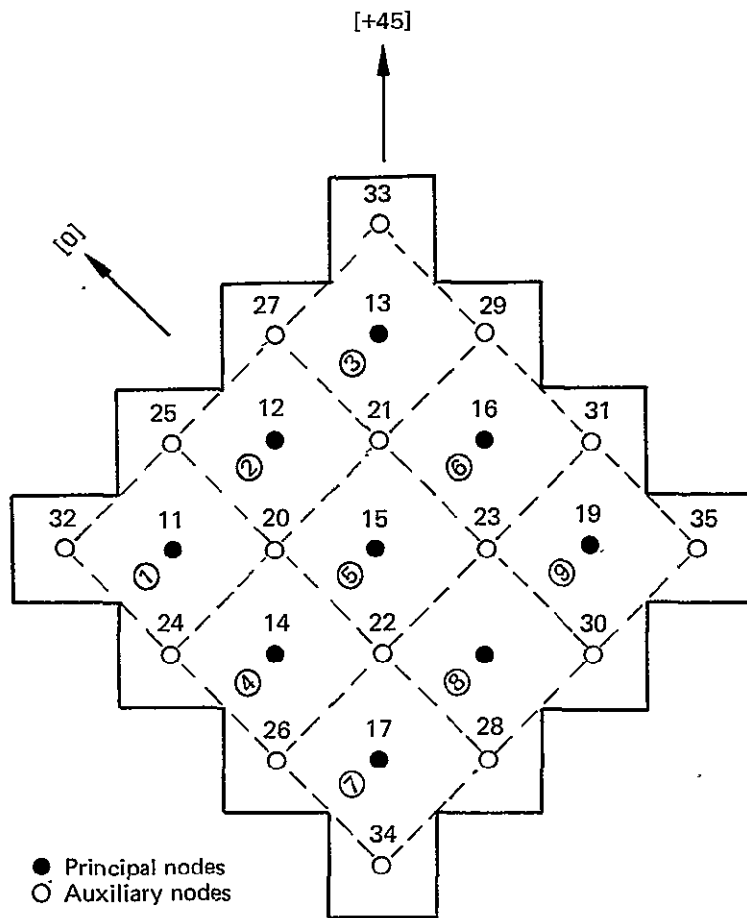


Figure 10-3.—Node Arrangement, Layup Direction $[+45]$

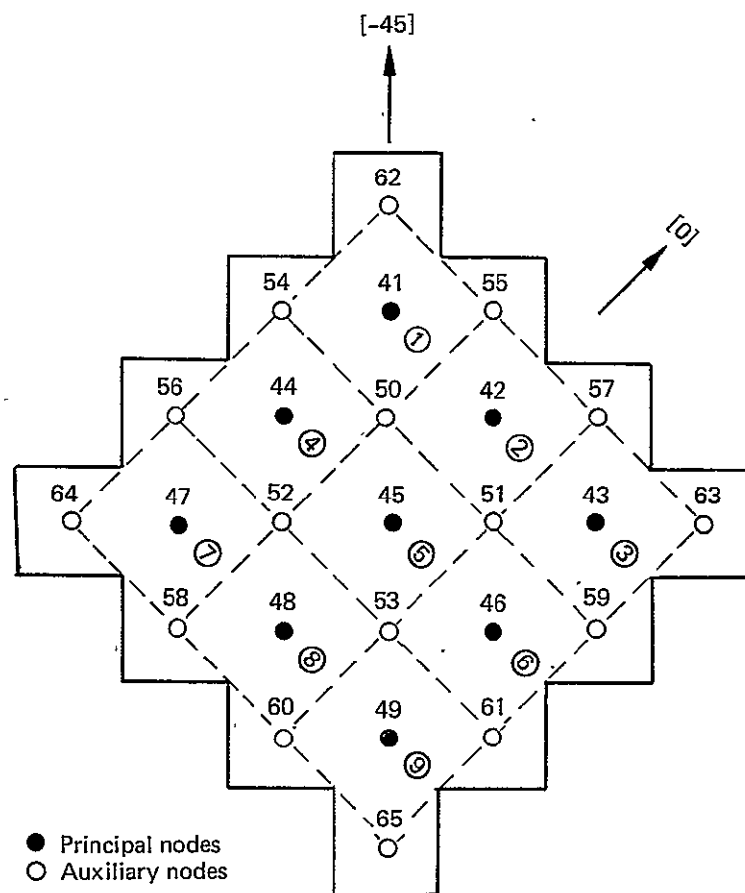


Figure 10-4.—Node Arrangement, Layup Direction $[-45]$

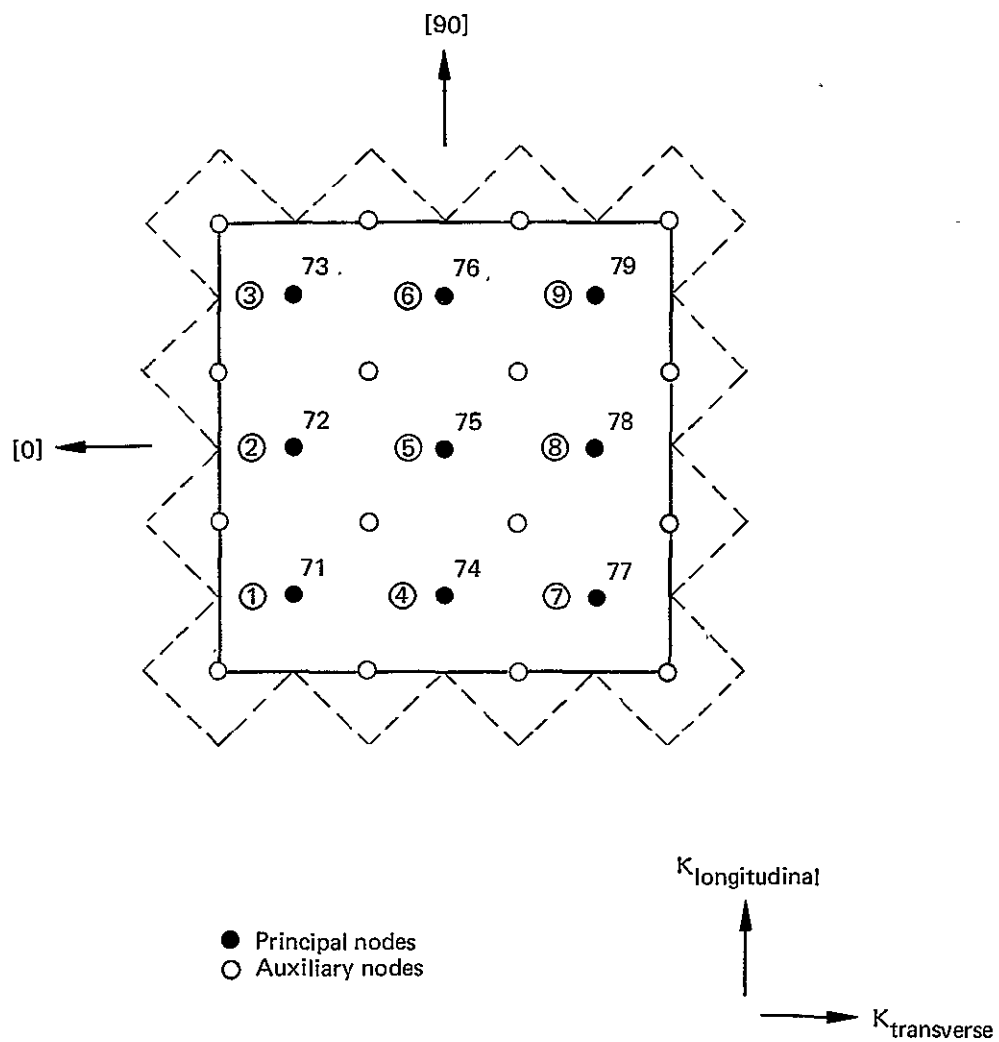


Figure 10-5.—Node Arrangement, Layup Direction $[90]$

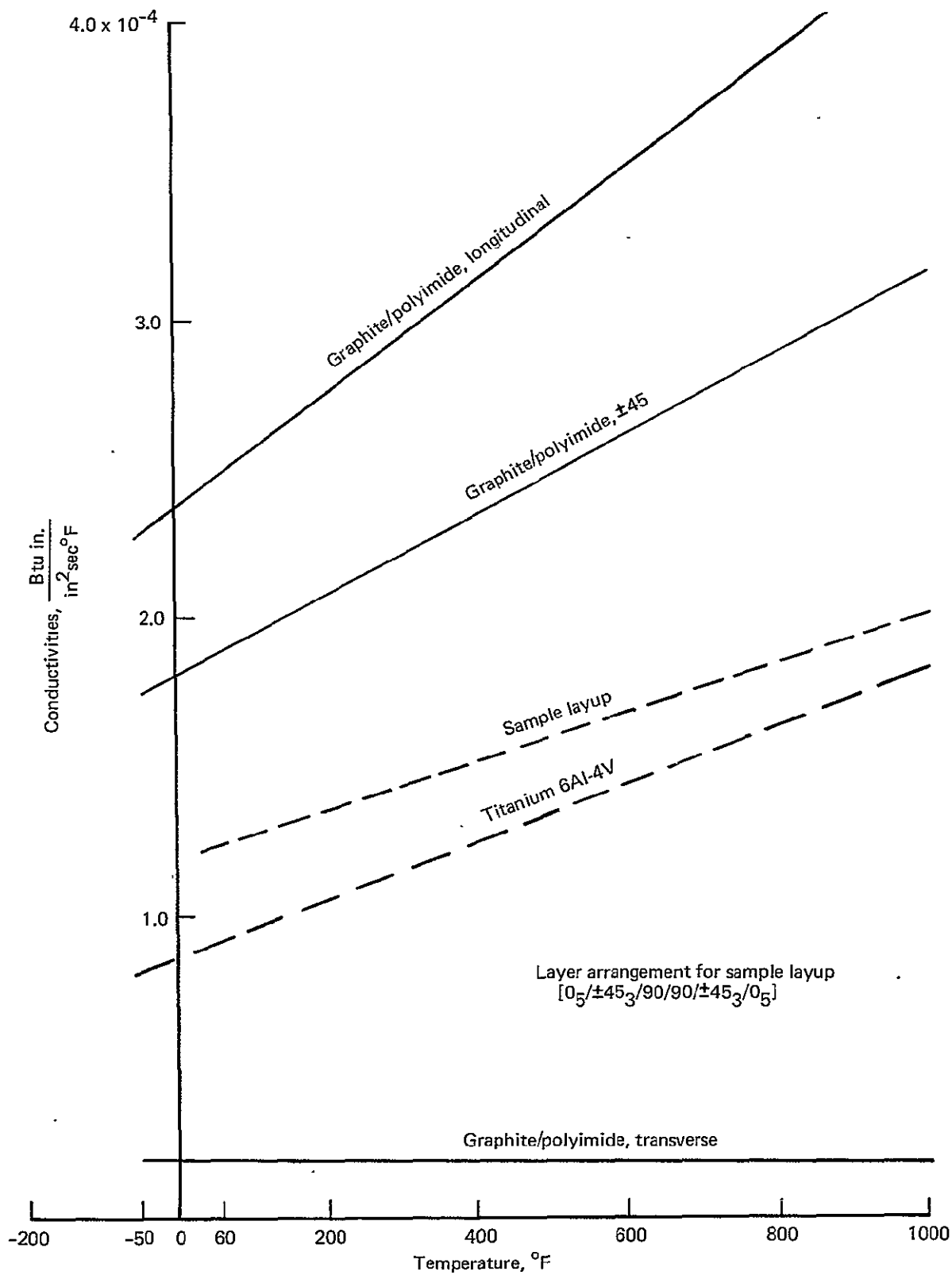


Figure 10-6.—Basic Material Conductivities and Sample Layup, Average Conductivity

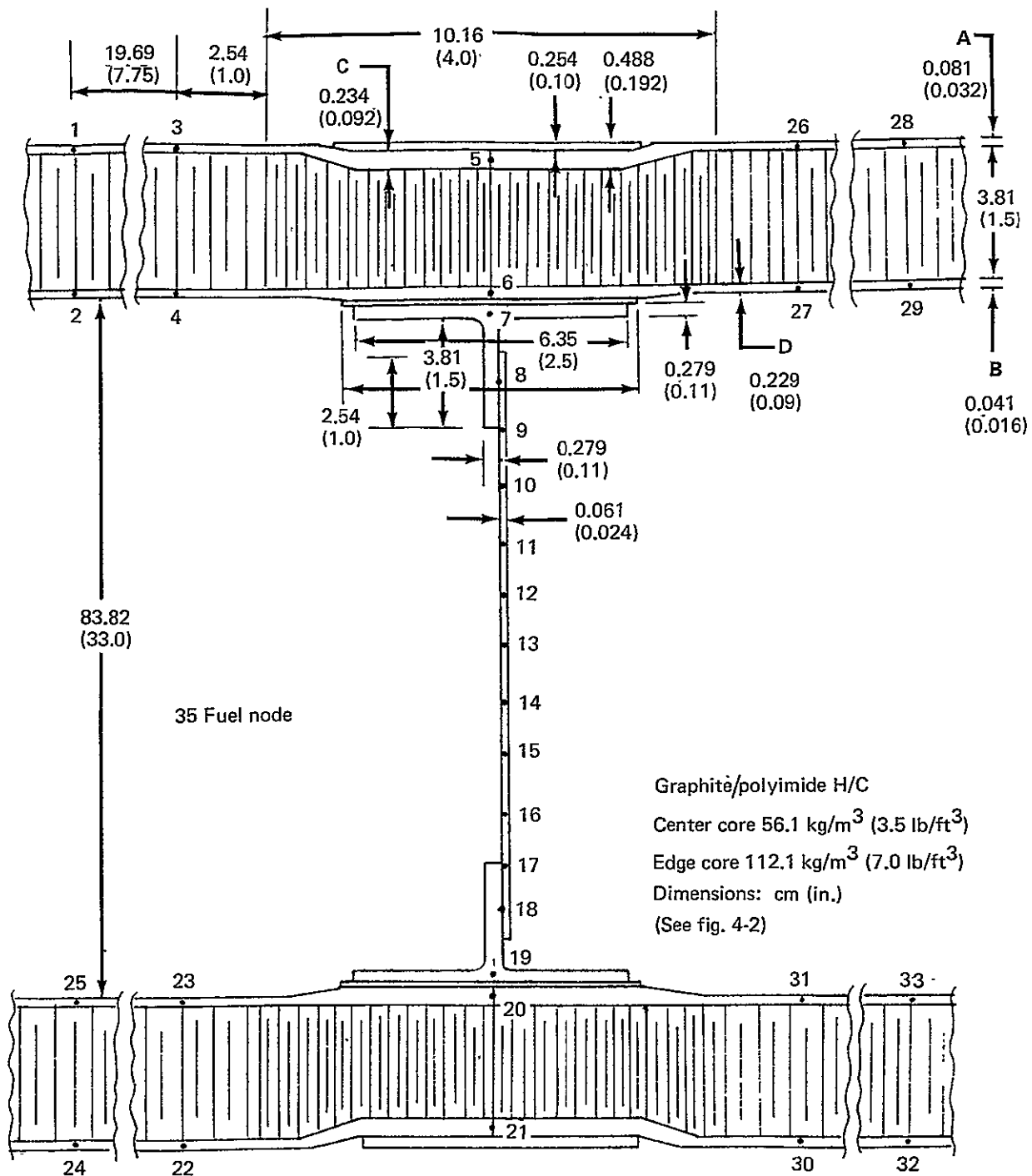


Figure 10-7.—Light Gage Structural Section

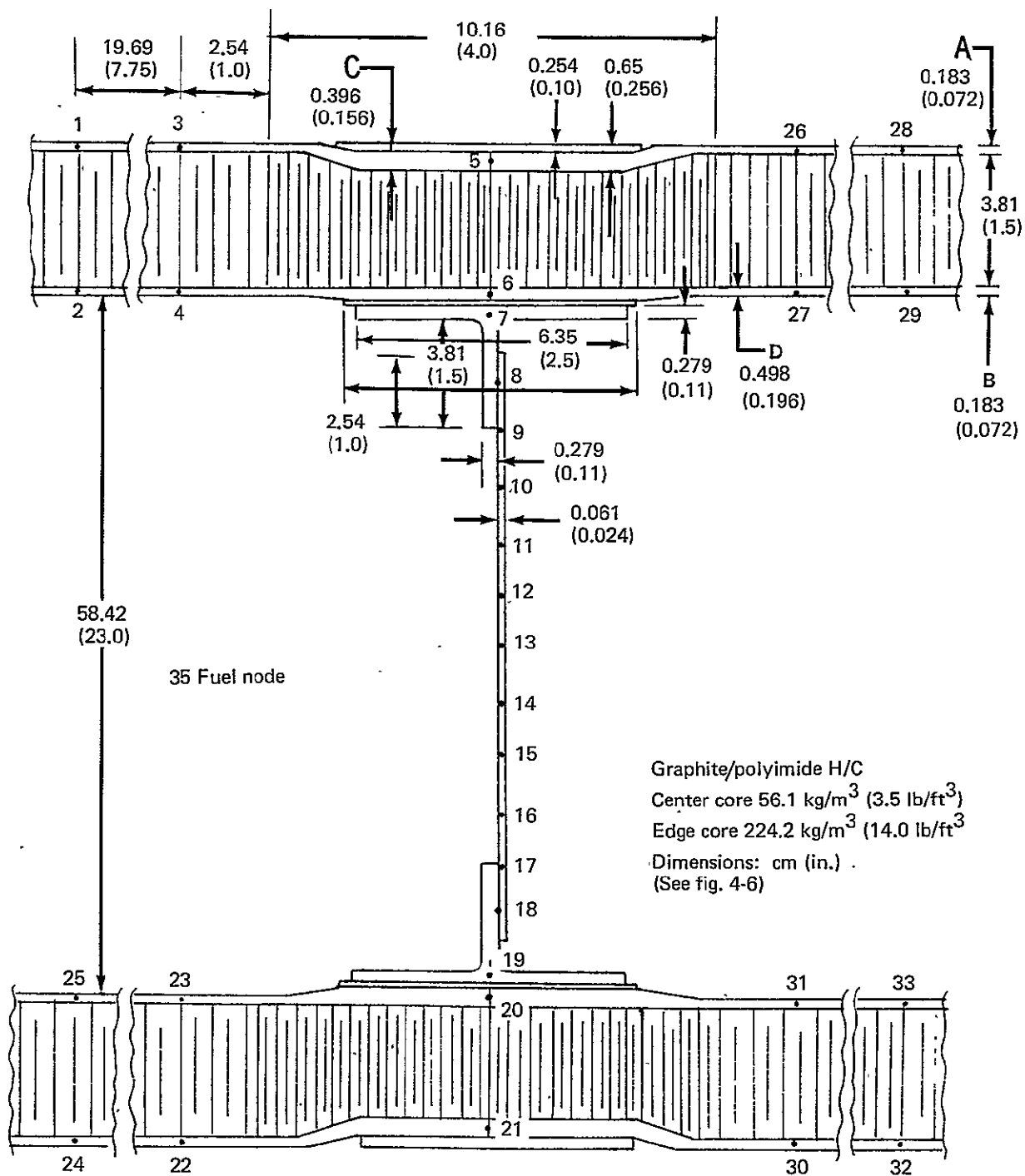


Figure 10-8.—Heavy Gage Structural Section

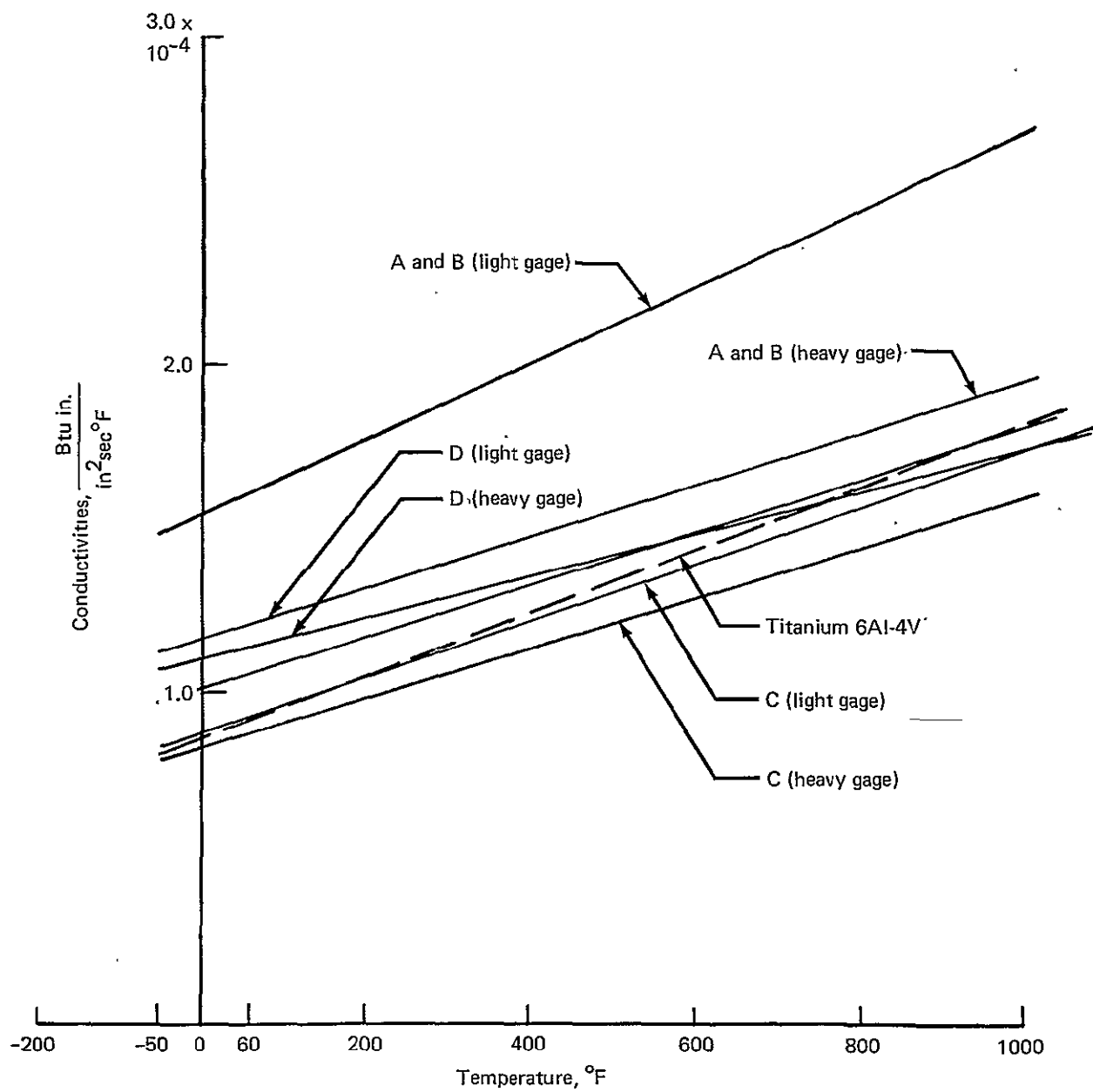


Figure 10-9.—Average Thermal Conductivities for Light and Heavy Gage Designs (Dimensions A, B, C, and D)

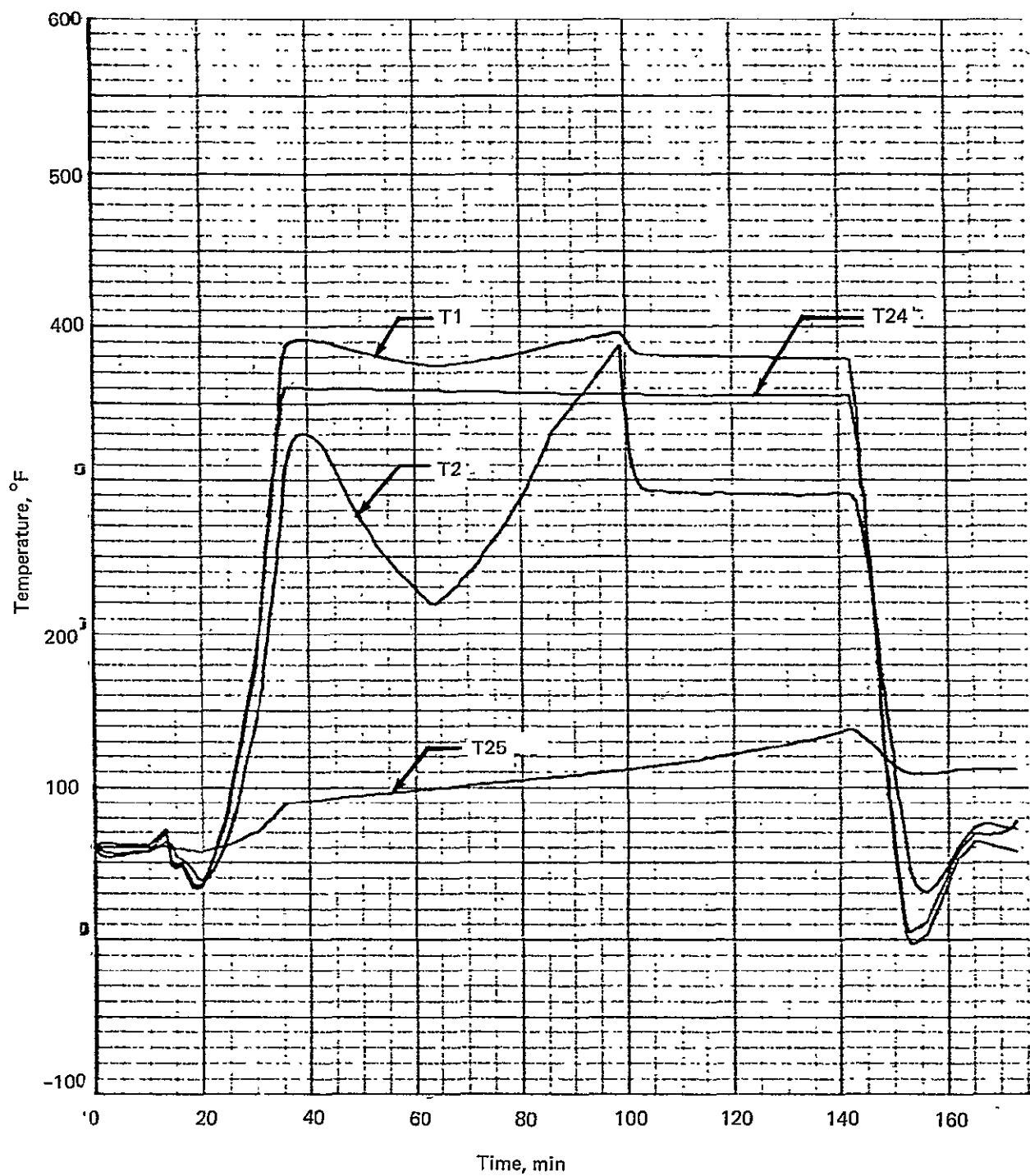


Figure 10-10.—Fuel Tank Temperatures, Light Gage, Wet Upper Panel: T1, T2, T24, T25

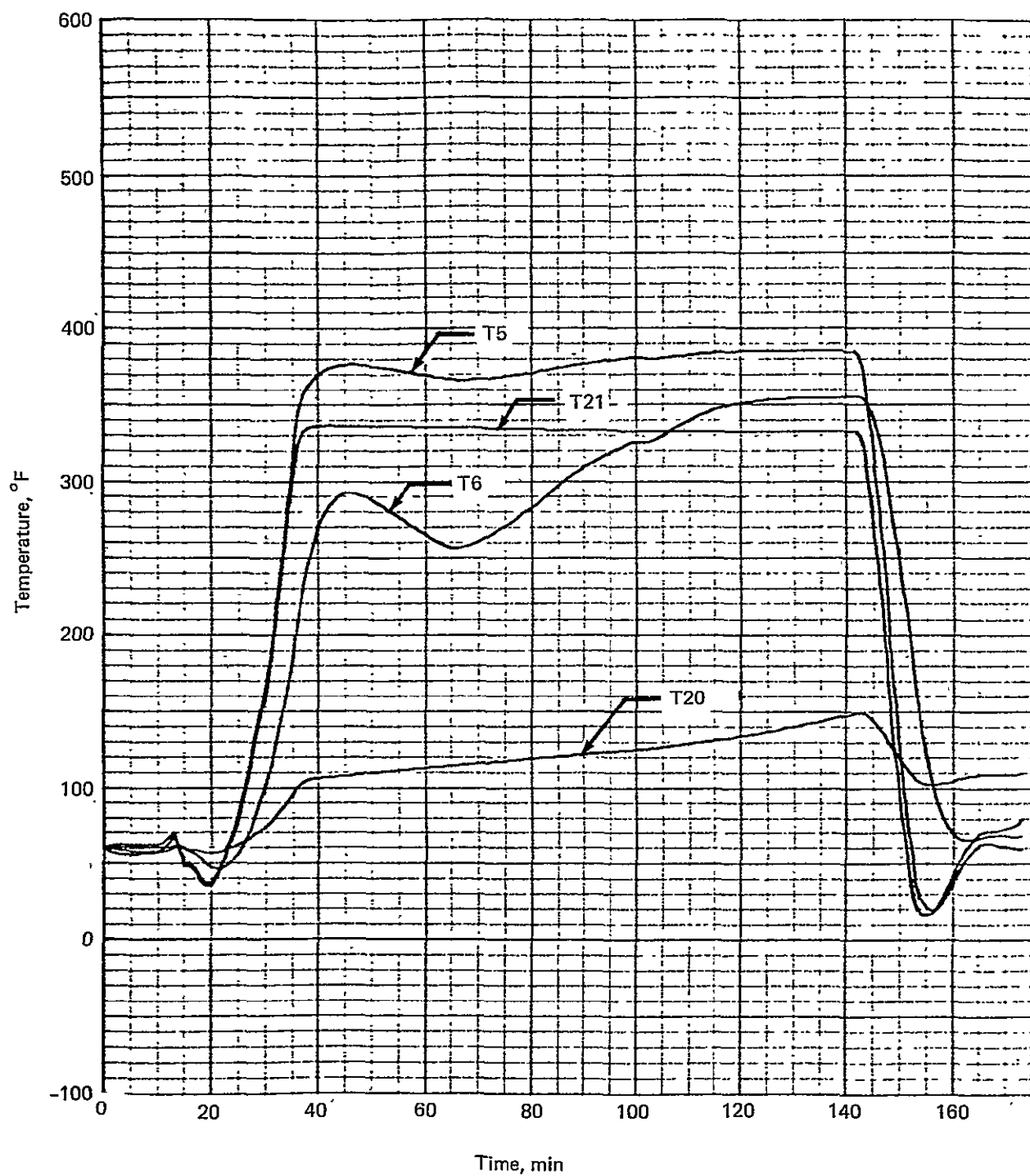


Figure 10-11.—Fuel Tank Temperatures, Light Gage, Wet Upper Panel: T5, T6, T20, T21

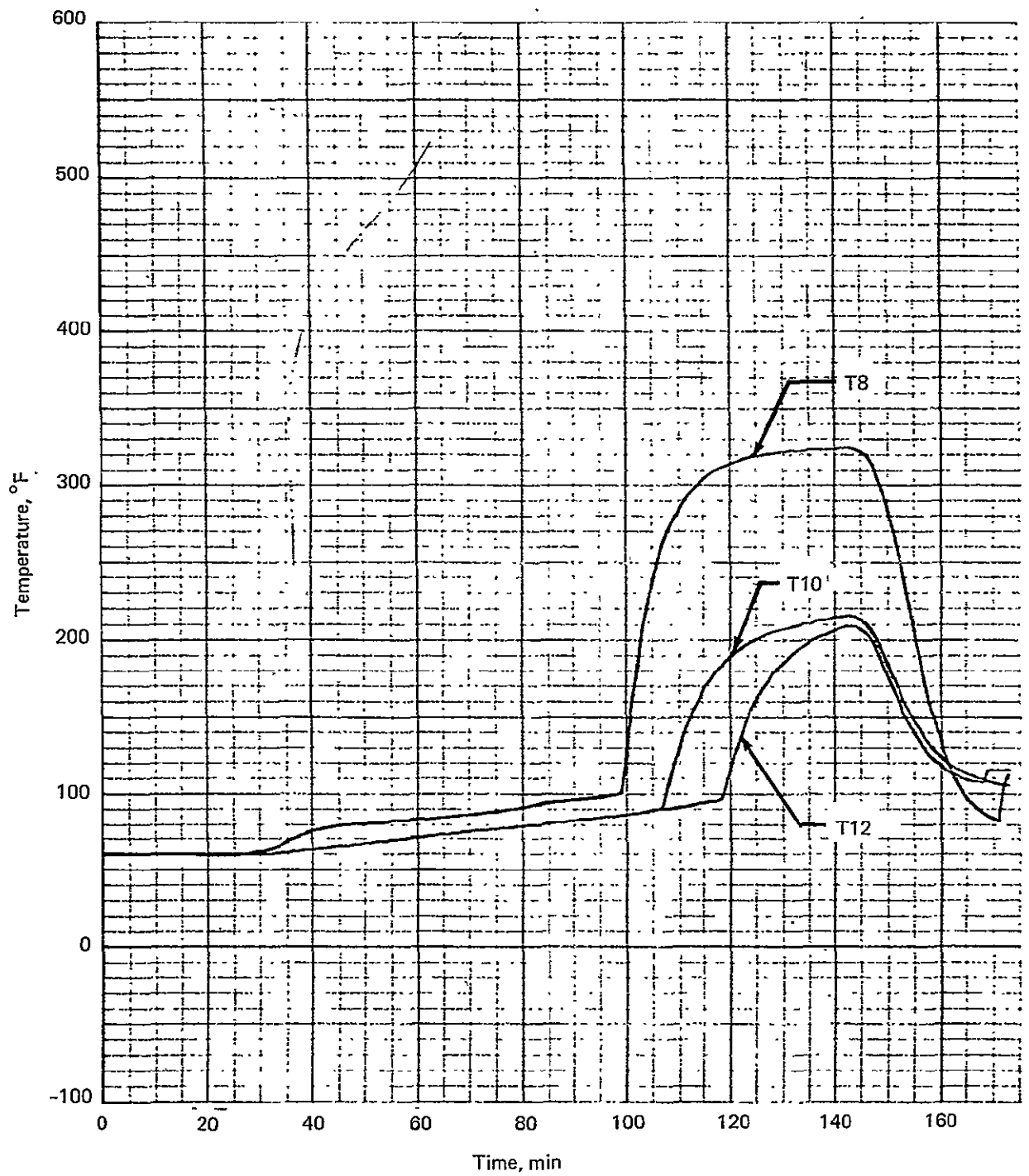


Figure 10-12.—Fuel Tank Temperatures, Light Gage, Wet Upper Panel: T8, T10, T12

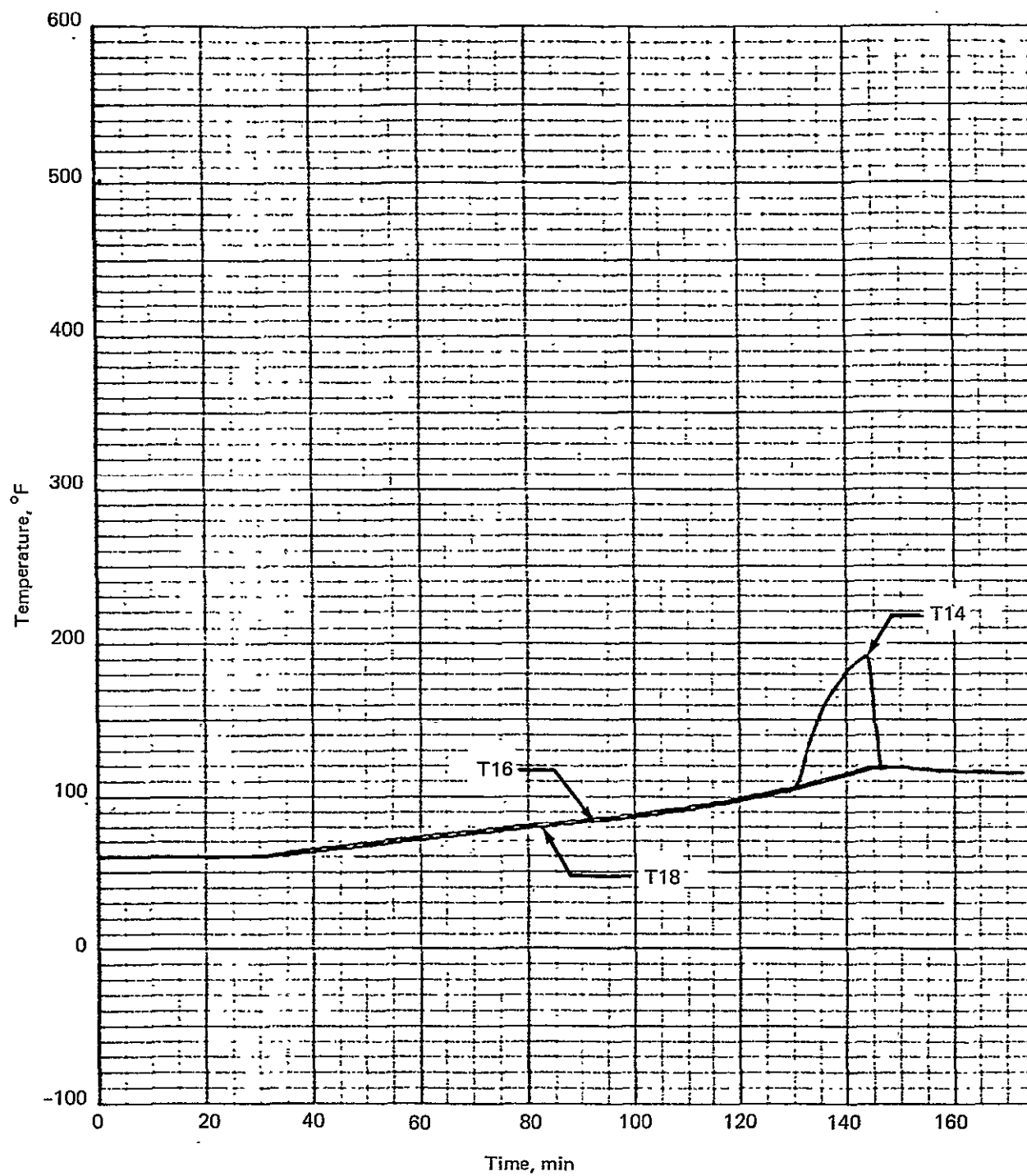


Figure 10-13.—Fuel Tank Temperatures, Light Gage, Wet Upper Panel: T14, T16, T18

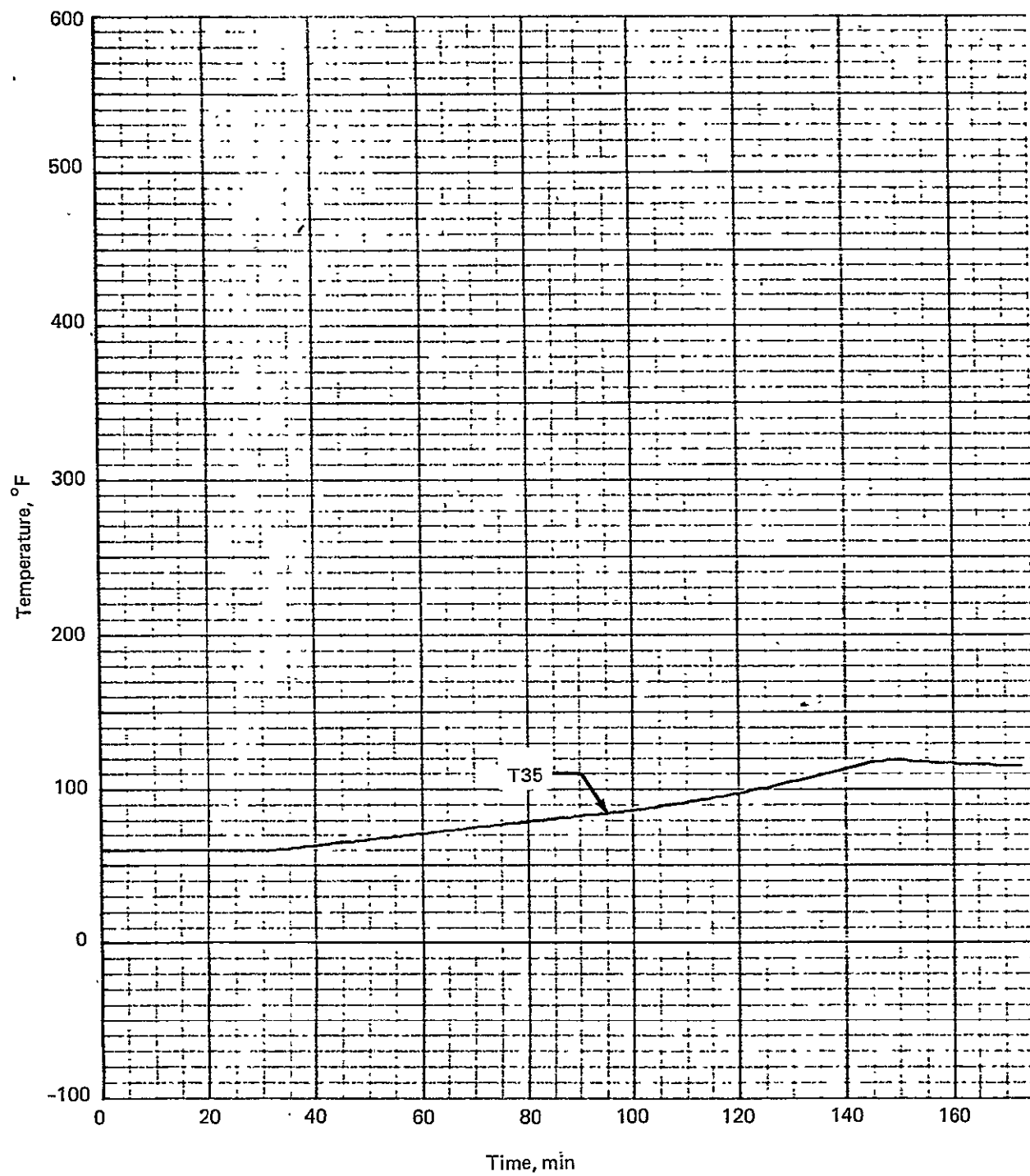


Figure 10-14.—Fuel Temperatures, Light Gage, Wet Upper Panel: T35

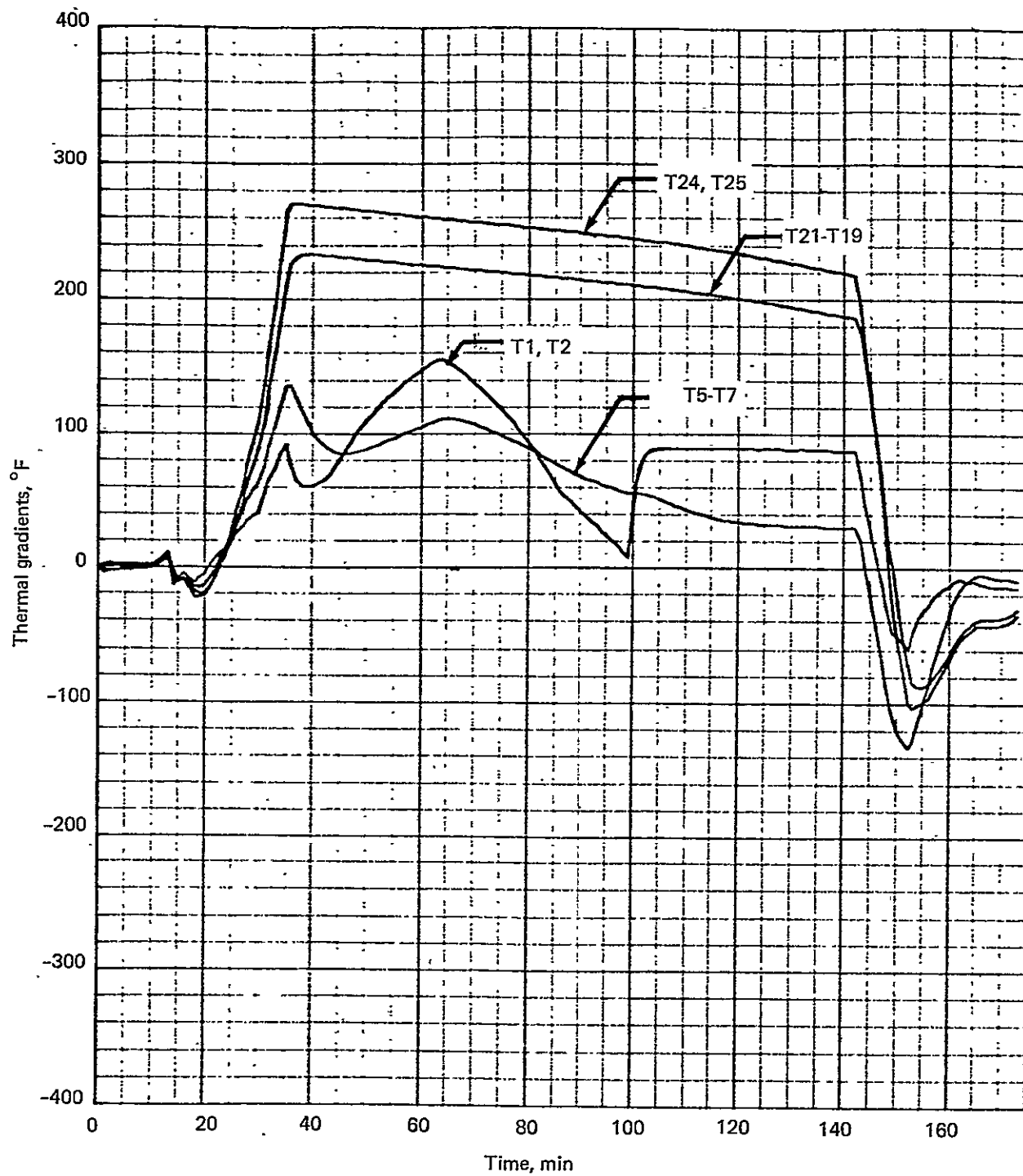


Figure 10-15.—Fuel Tank Thermal Gradients, Light Gage, Wet Upper Panel:
T1, T2; T5-T7, T21-T19; T24, T25

ORIGINAL PAGE IS
OF POOR QUALITY

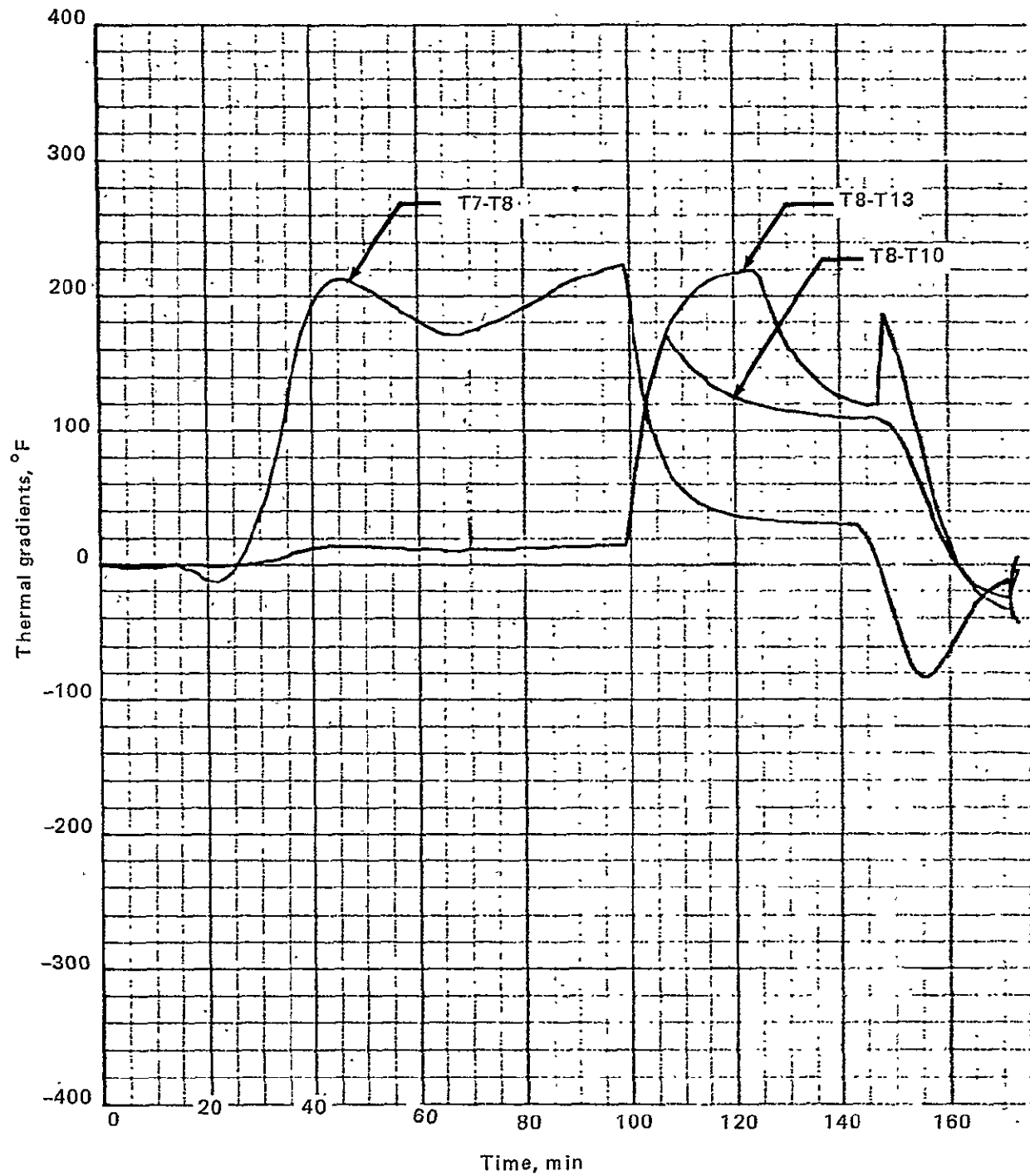


Figure 10-16.—Fuel Tank Thermal Gradients, Light Gage, Wet Upper Panel:
T7-T8; T8-T10; T8-T13

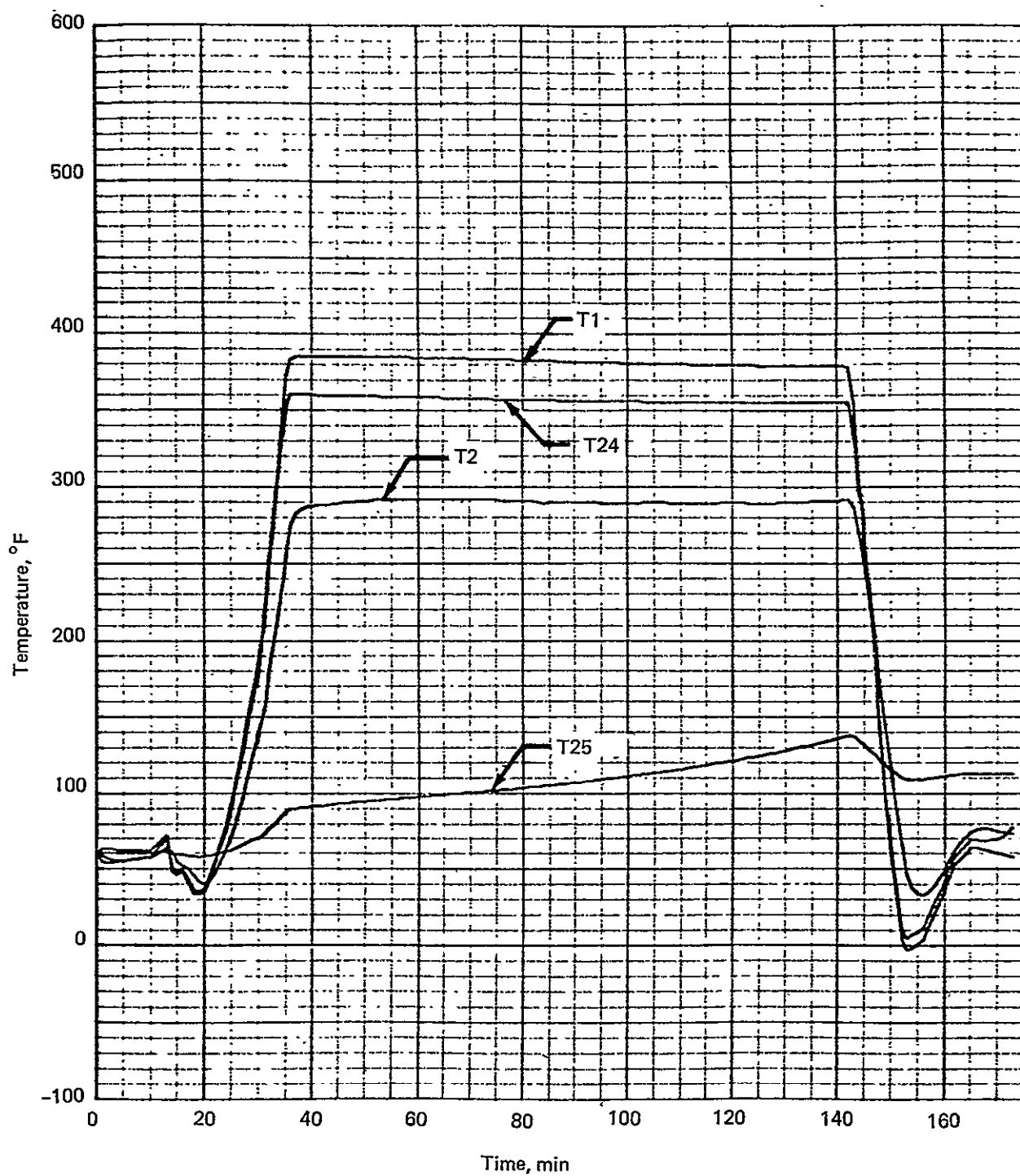


Figure 10-17.—Fuel Tank Temperatures, Light Gage, Dry Upper Panel: T1, T2, T24, T25

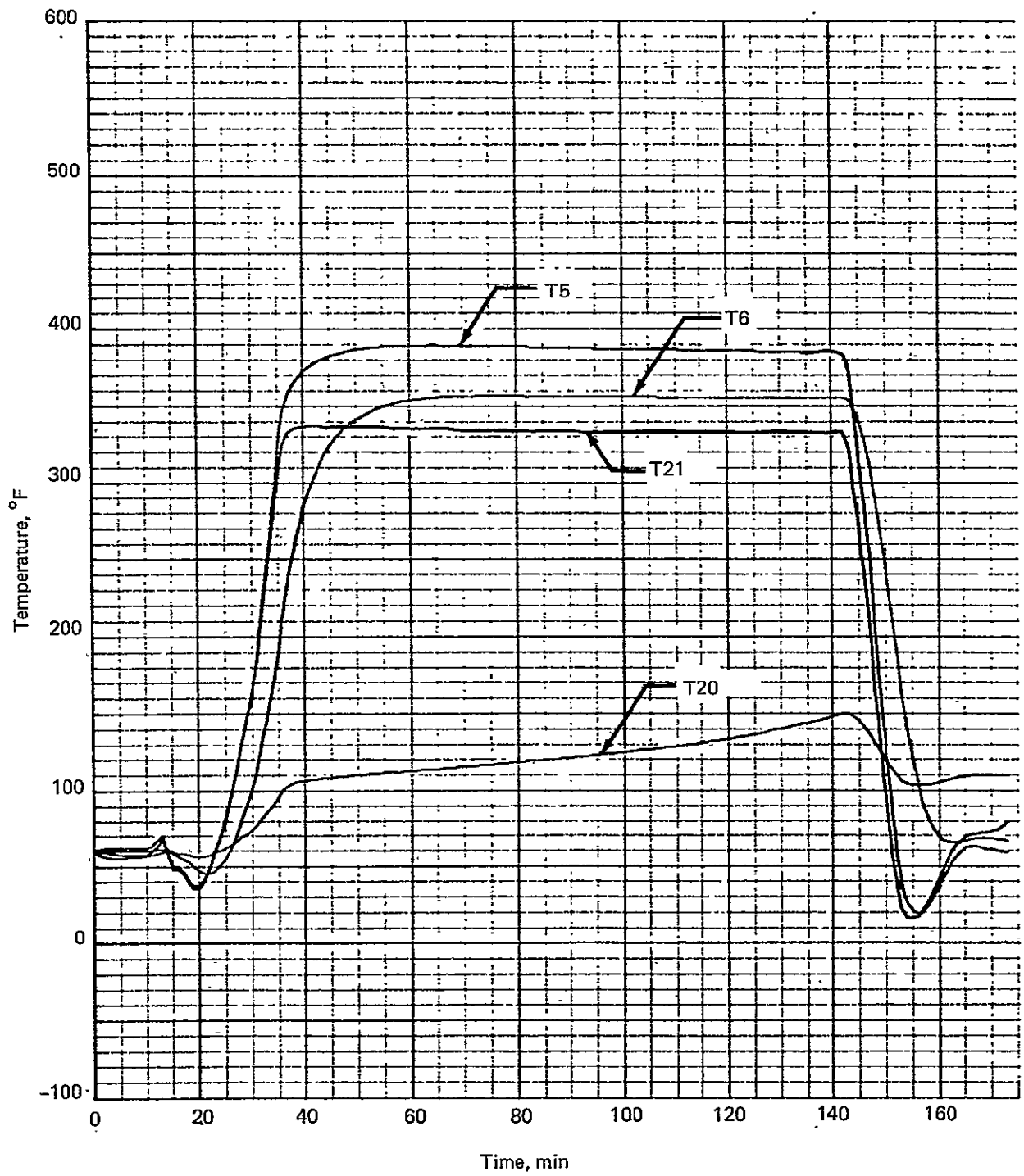


Figure 10-18.—Fuel Tank Temperatures, Light Gage, Dry Upper Panel: T5, T6, T20, T21

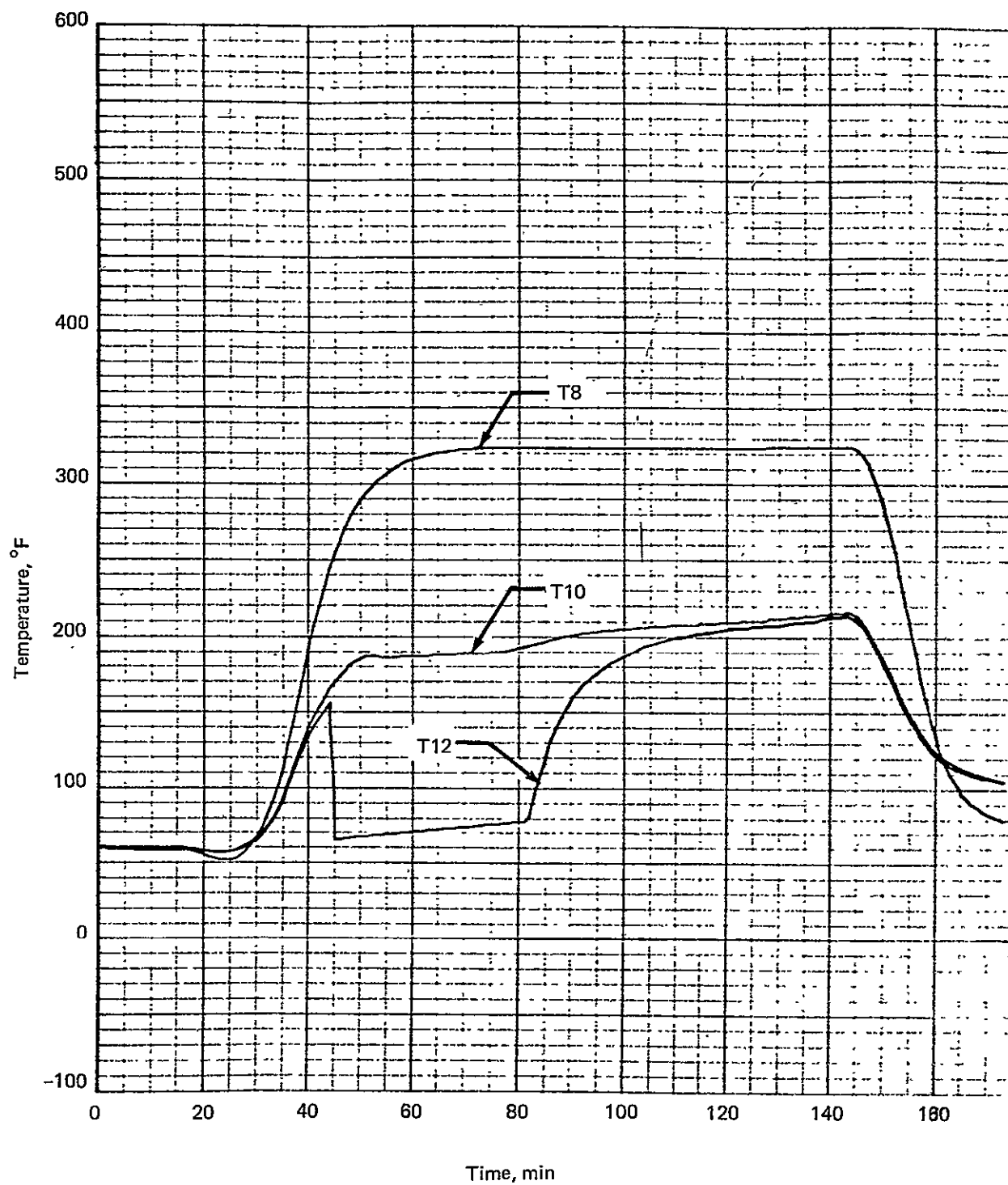


Figure 10-19.—Fuel Tank Temperatures, Light Gage, Dry Upper Panel: T8, T10, T12

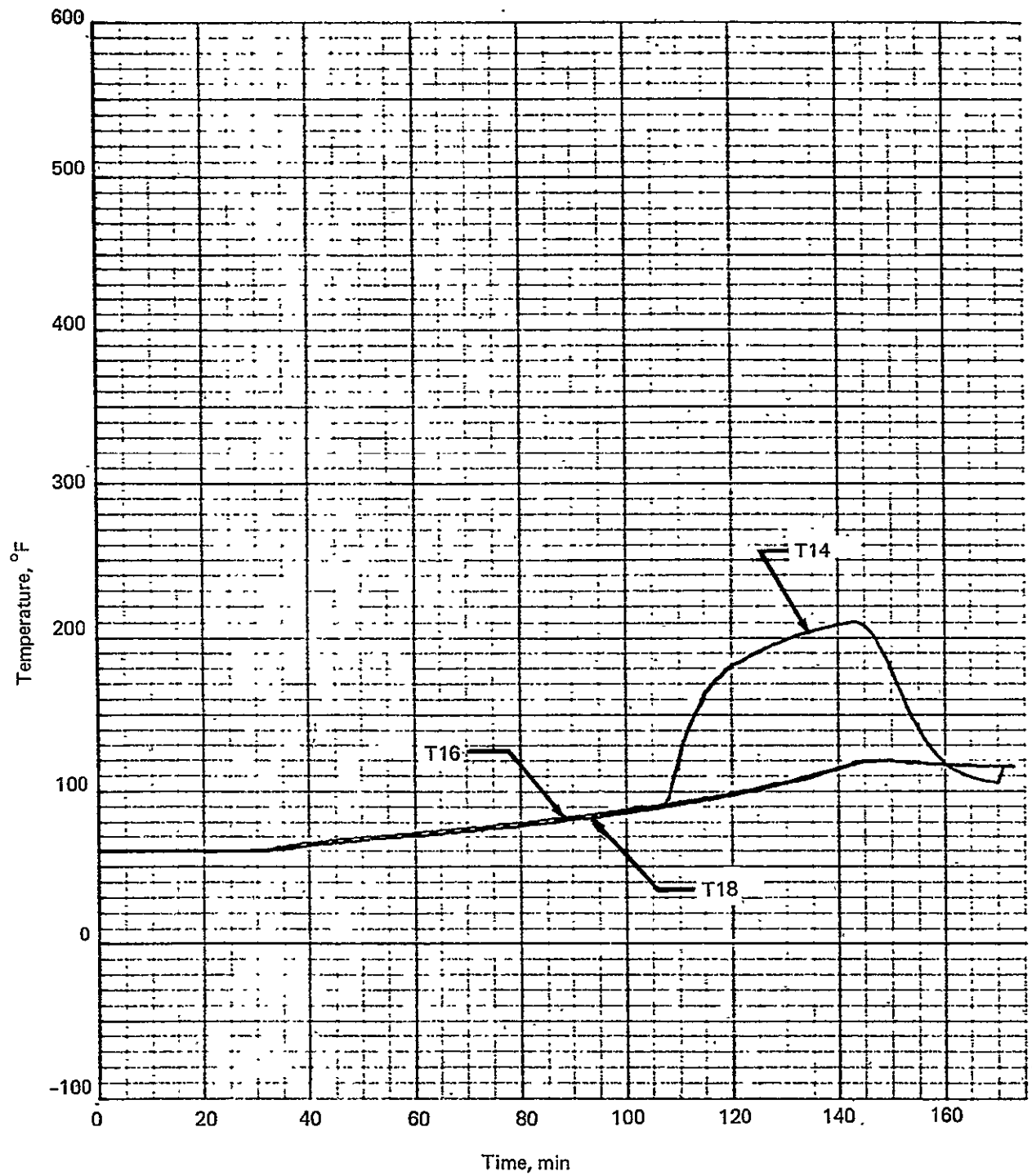


Figure 10-20.—Fuel Tank Temperatures, Light Gage, Dry Upper Panel:
T14, T16, T18

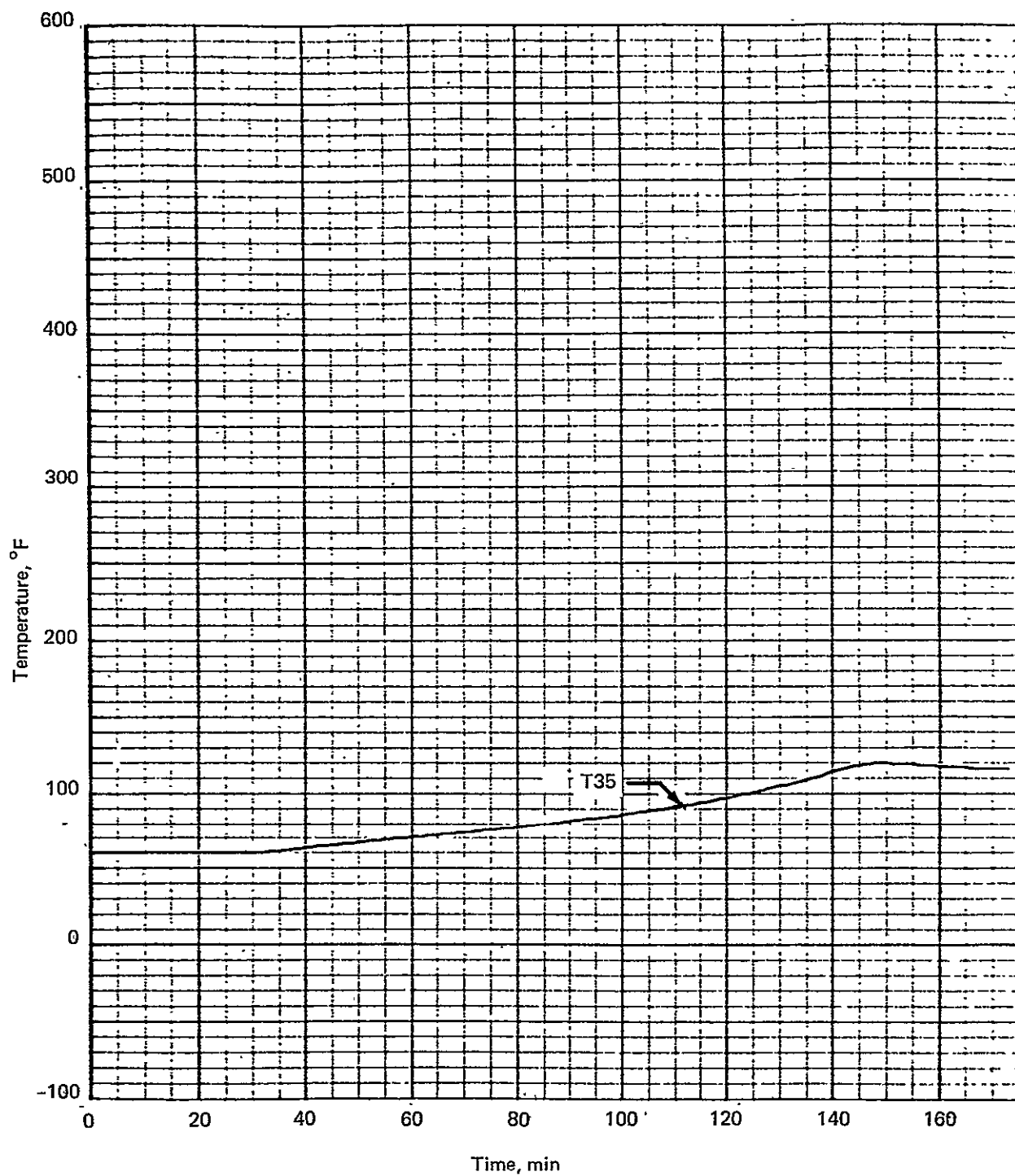


Figure 10-21.—Fuel Temperatures, Light Gage, Dry Upper Panel: T35

ORIGINAL PAGE IS
OF POOR QUALITY

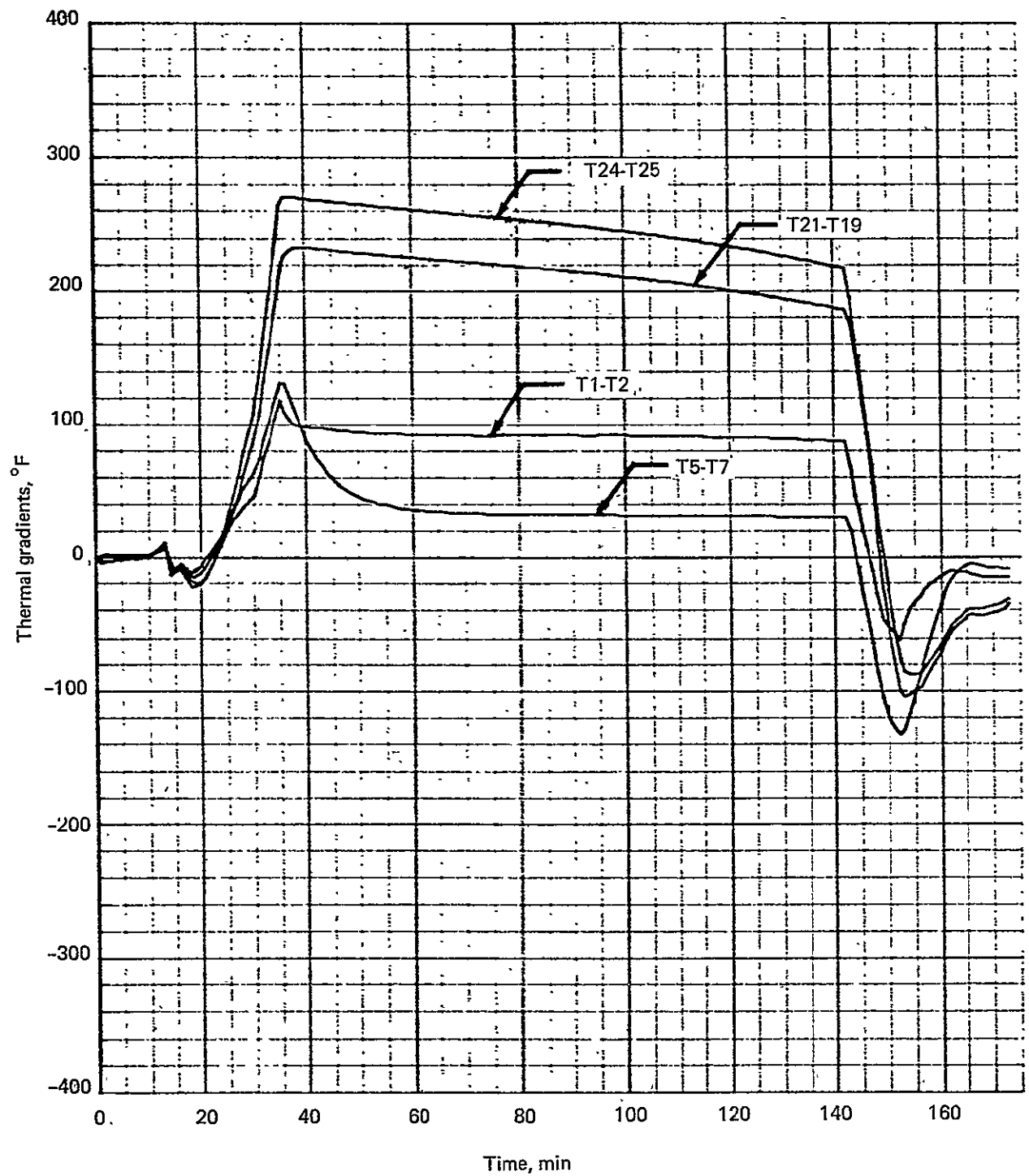


Figure 10-22.—Fuel Tank Thermal Gradients. Light Gage, Dry Upper Panel:
T1-T2; T5-T7; T21-T19; T24-T25

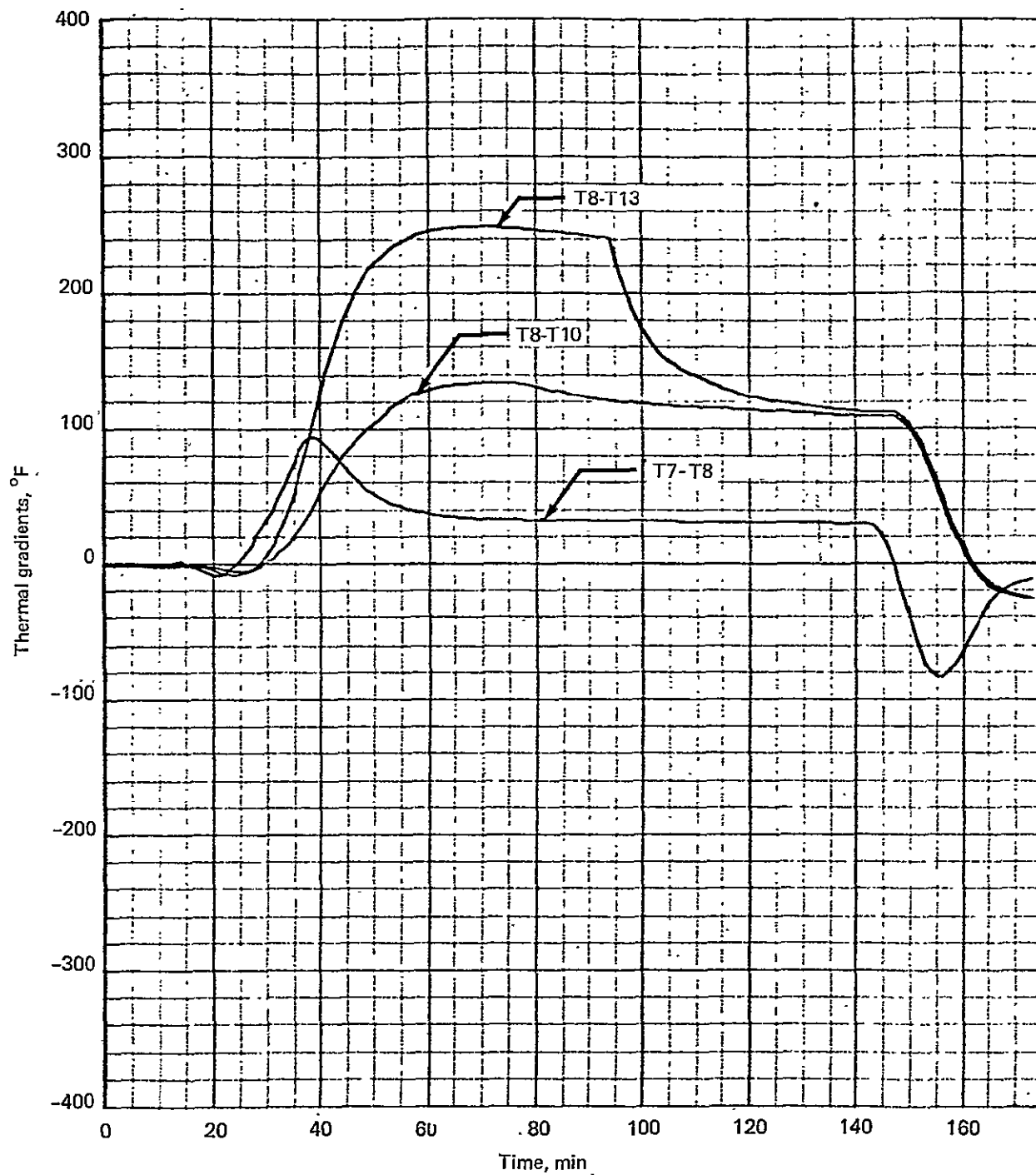


Figure 10-23.—Fuel Tank Thermal Gradients, Light Gage, Dry Upper Panel:
T7, T8; T8-T10; T8-T13

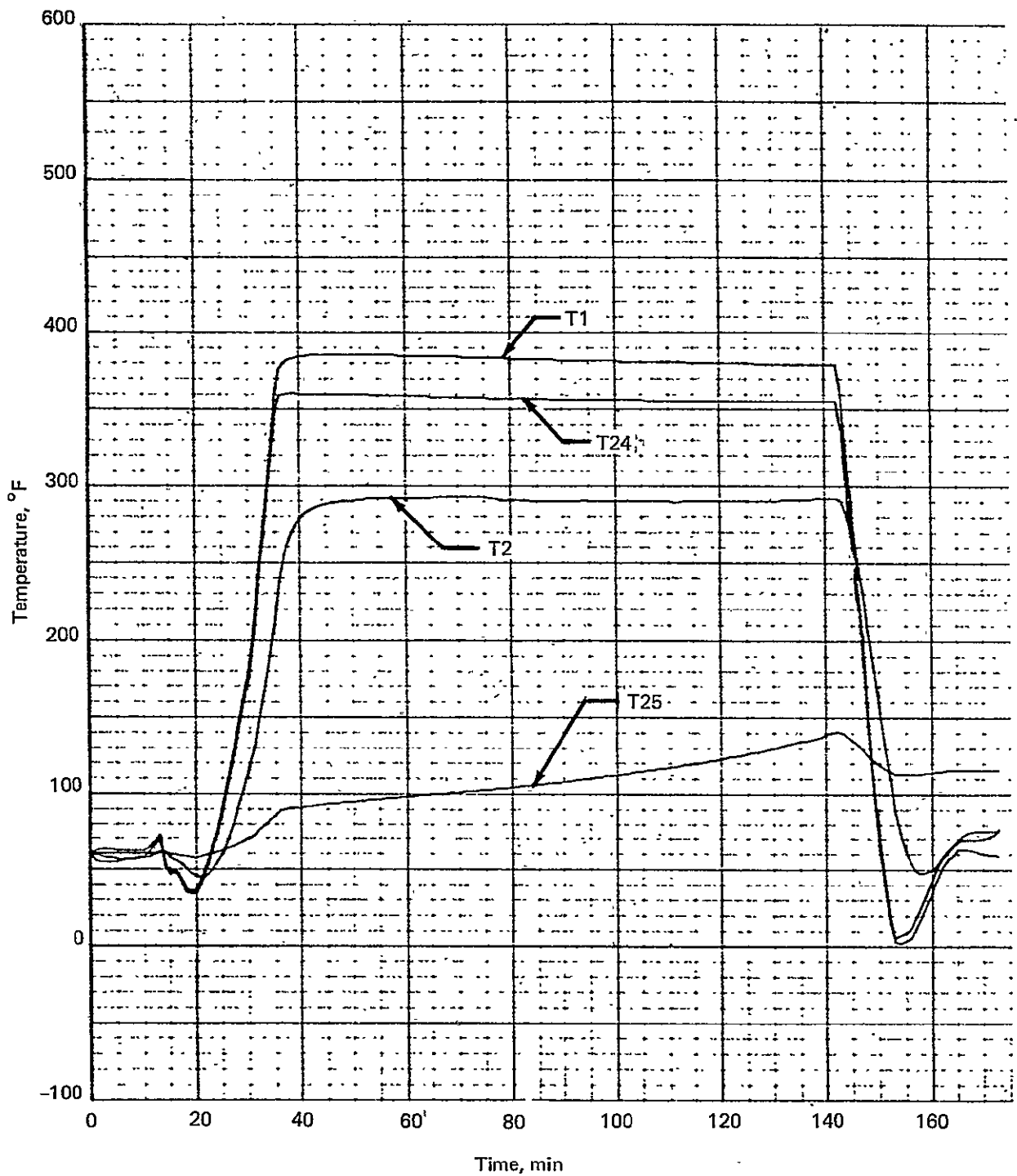


Figure 10-24.—Fuel Tank Temperatures, Heavy Gage, Dry Upper Panel: T1, T2, T24, T25

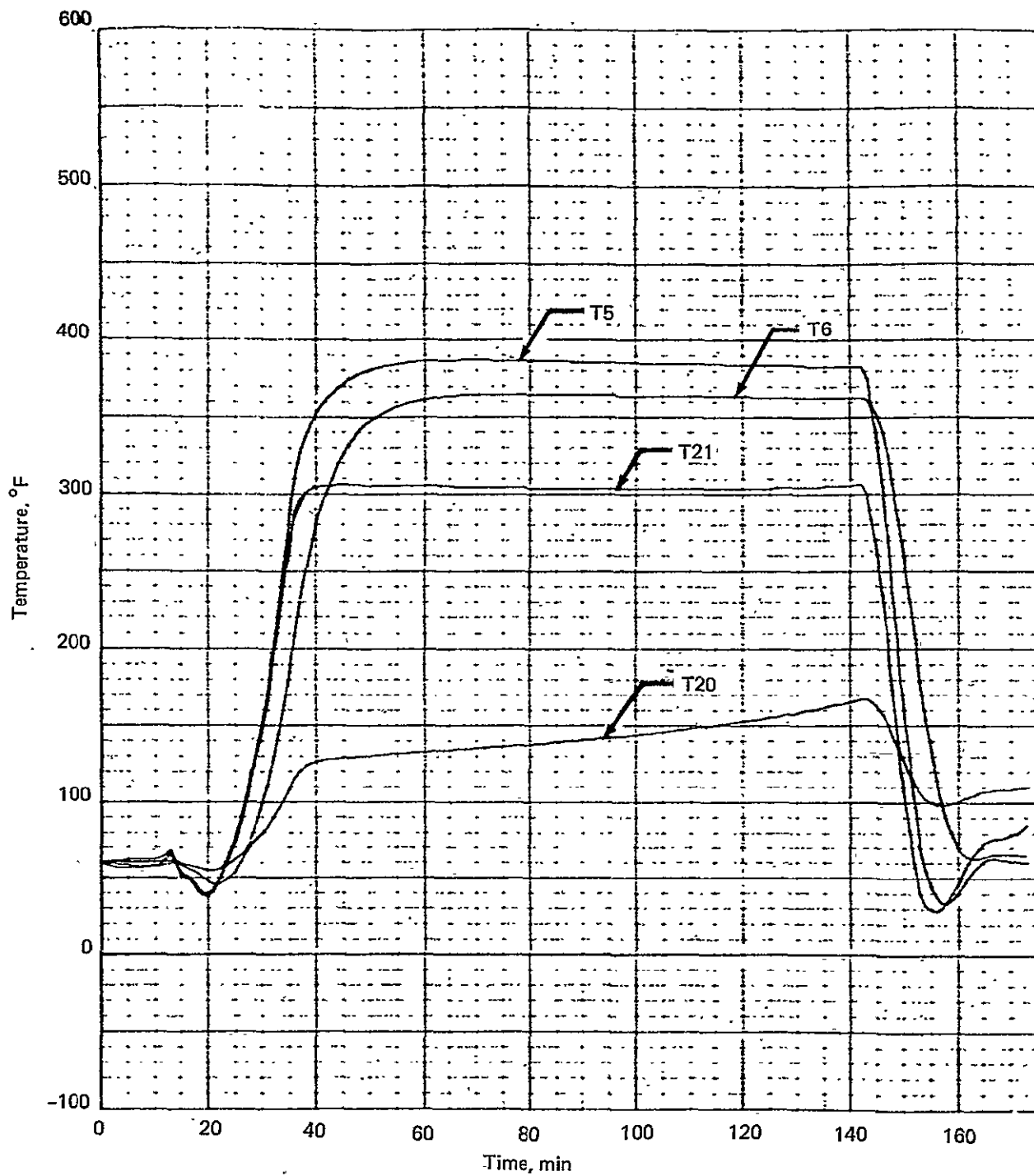


Figure 10-25.—Fuel Tank Temperatures, Heavy Gage, Dry Upper Panel: T5, T6, T20, T21

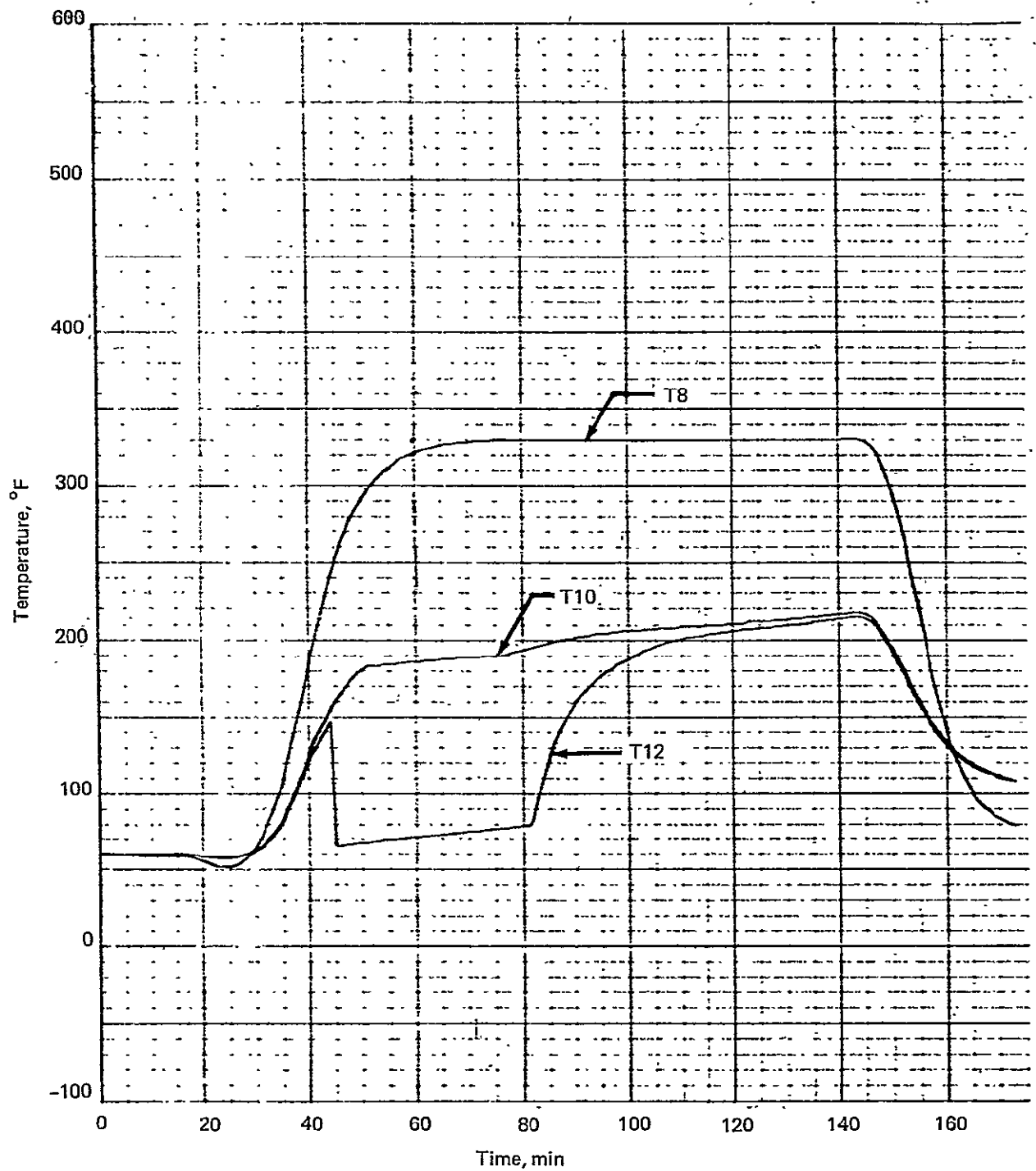


Figure 10-26.—Fuel Tank Temperatures, Heavy Gage, Dry Upper Panel: T14, T16, T18

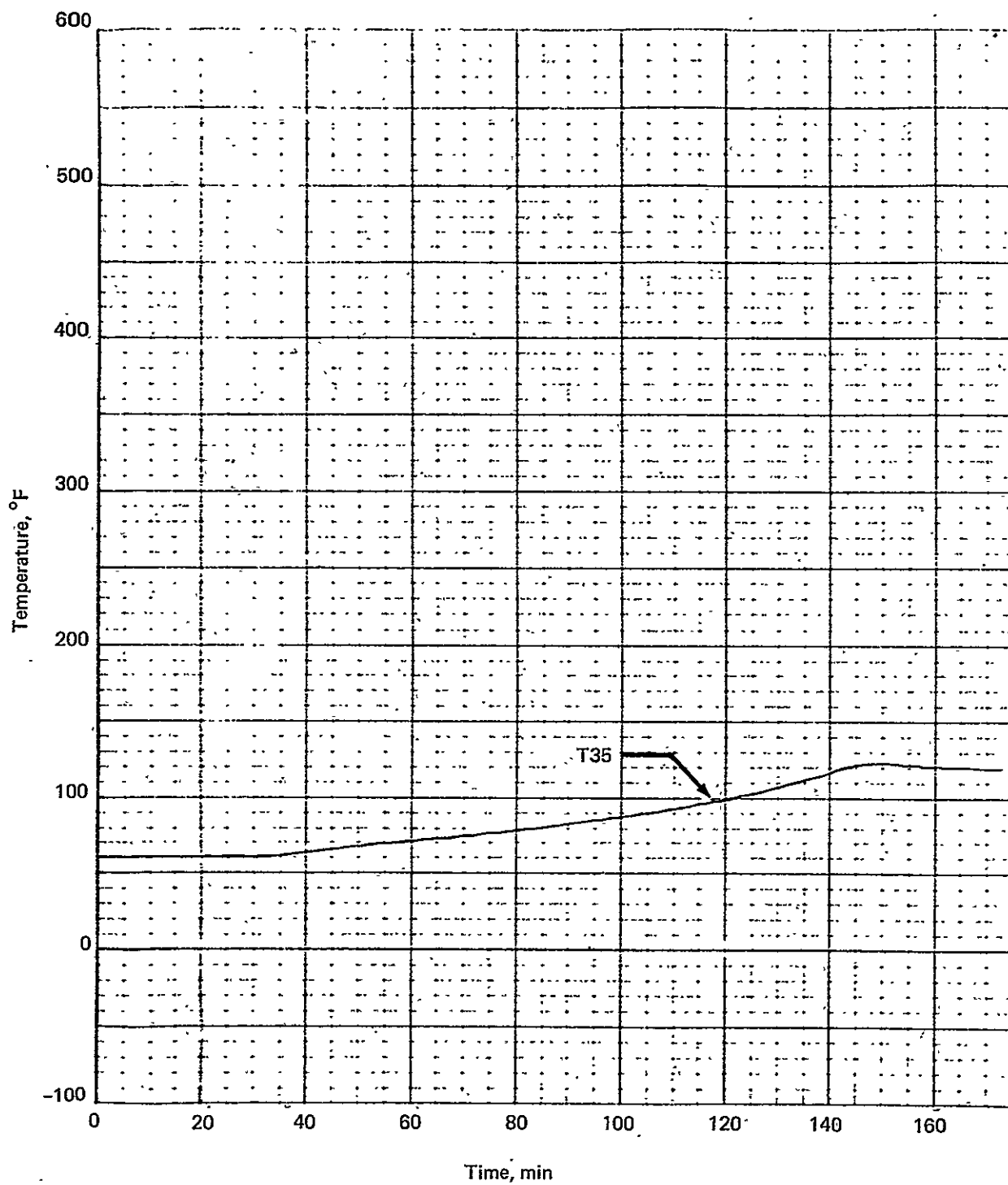


Figure 10-27.—Fuel Temperature, Heavy Gage, Dry Upper Panel: T35

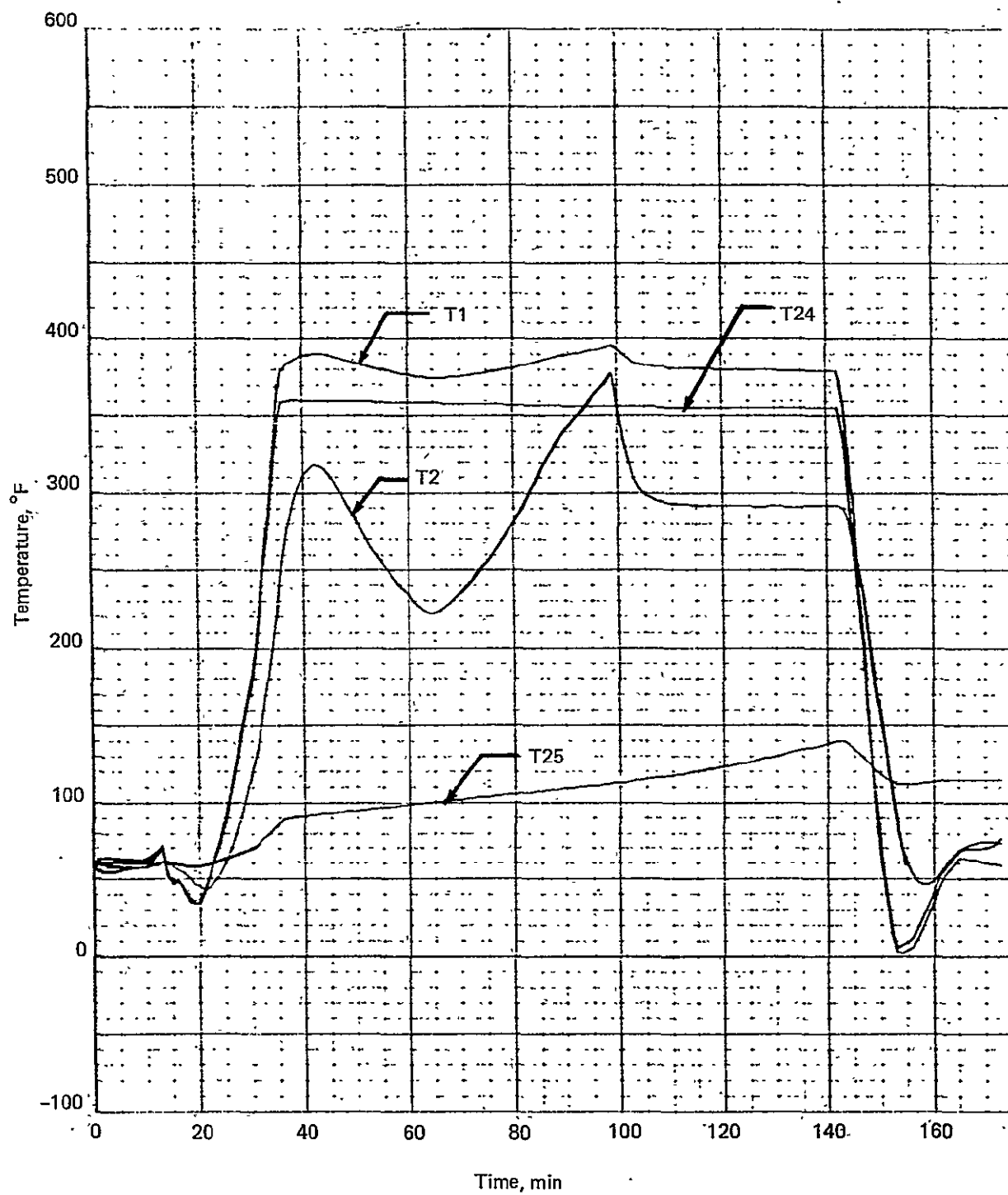


Figure 10-28.—Fuel Tank Temperatures, Heavy Gage, Wet Upper Panel: T1, T2, T24, T25

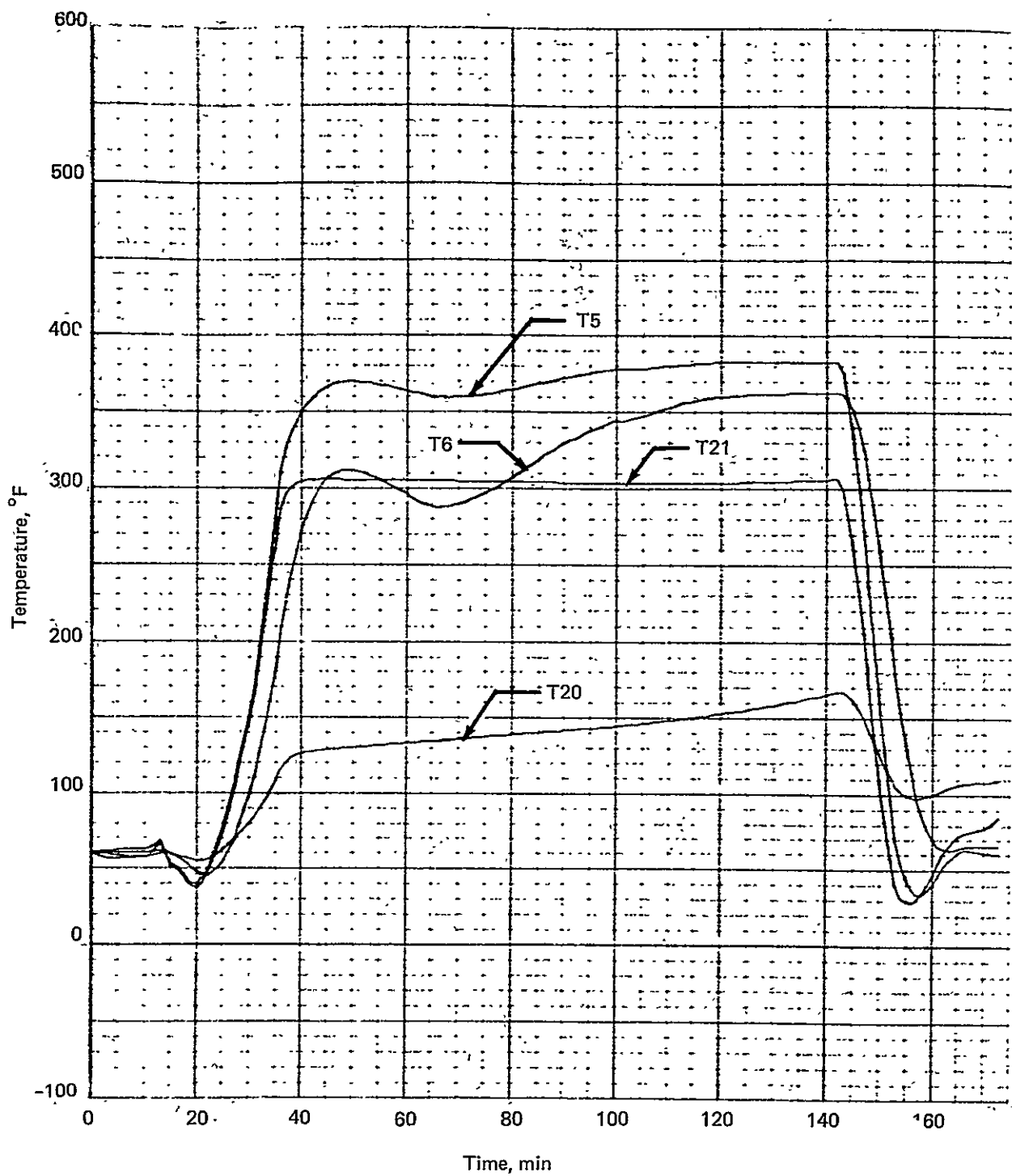


Figure 10-29.—Fuel Tank Temperatures, Heavy Gage, Wet Upper Panel: T5, T6, T20, T21

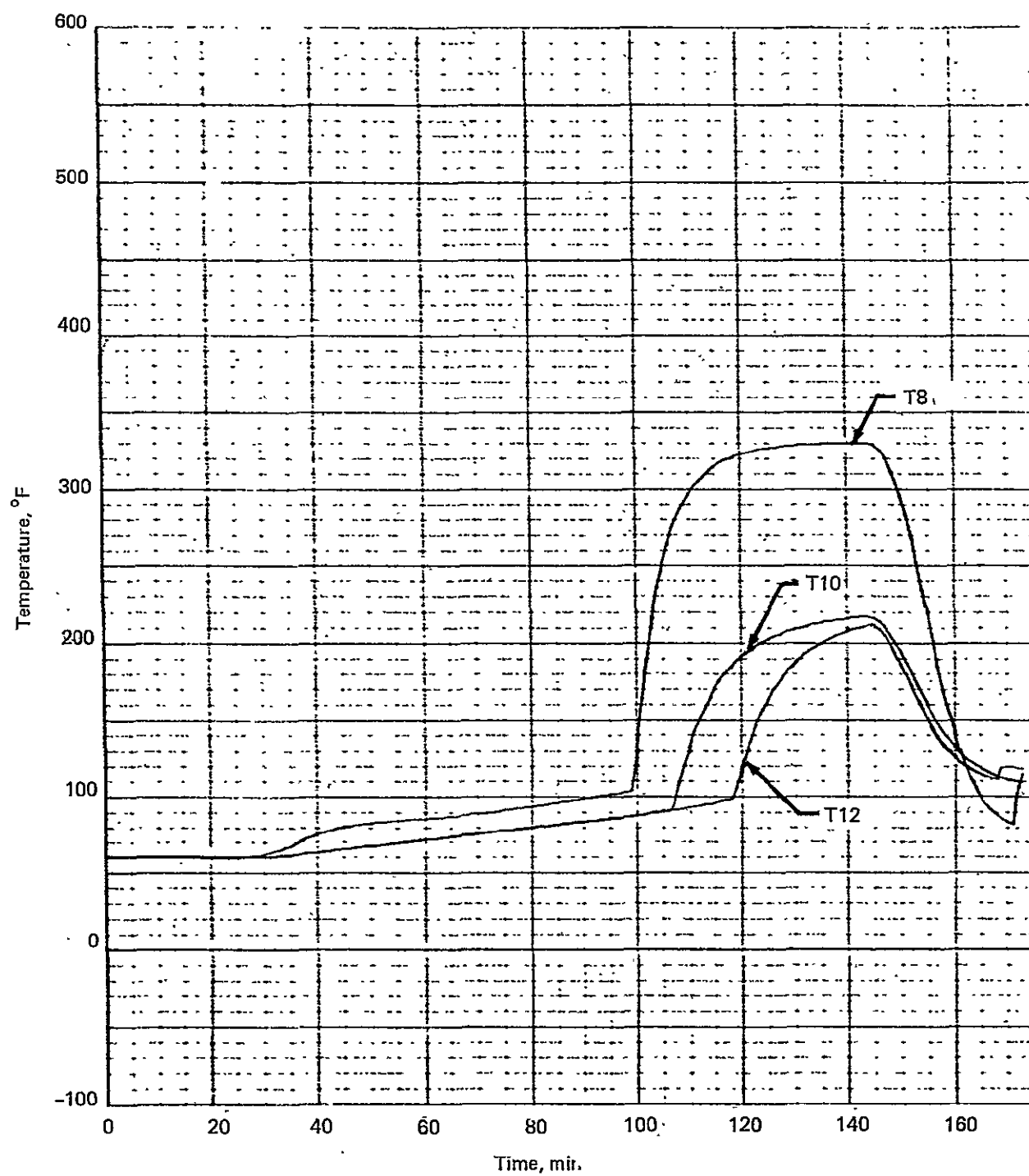


Figure 10-30.—Fuel Tank Temperatures, Heavy Gage, Wet Upper Panel: T8, T10, T12

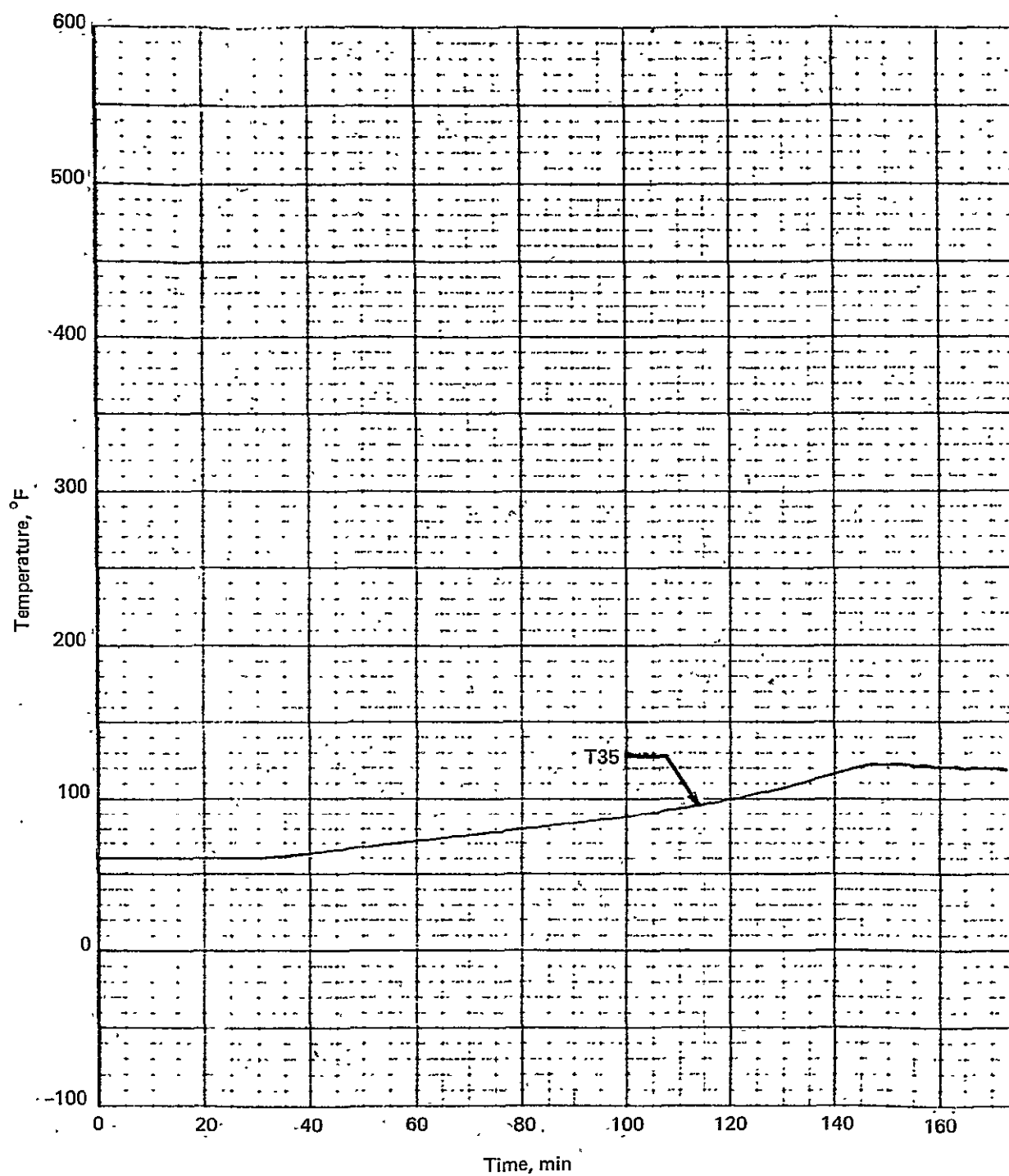


Figure 10-31.—Fuel Temperature, Heavy Gage, Wet Upper Panel: T35